Genomic analysis of the fresh water mollusc *Biomphalaria glabrata* to understand host: parasite interactions

A thesis submitted for the degree of Doctor of Philosophy

By

Edwin Chukwuemeka Odoemelam

Biosciences, School of Health Sciences and Social Care
Brunel University

September 2009

Abstract

The fresh water mollusc *Biomphalaria glabrata* is the intermediate host for the trematode parasite *Schistosoma mansoni*, this parasite is responsible for the human disease Schistosomiasis. The significance of *B. glabrata* in the transmission of schistosomiasis is such that it has been selected for complete genome sequencing.

The *Biomphalaria glabrata* embryonic cell line is an important resource for researchers investigating the interaction between the snail and parasite. The genome of the Bge cells was analysed at the chromosomal level, using DAPI karyotyping. The karyotype revealed extensive aneuploidy, whereby a modal chromosome complement of 63 and 67 was observed in two isolates of the Bge cells, which exceeds *B. glabrata*'s 2n=36 chromosome number. Indeed, in addition to characterising the Bge cell chromosomes, a method was established for mapping single copy *B. glabrata* genes onto the chromosomes from the Bge cells using fluorescence *in situ* hybridisation. Despite the Bge cell's inherent aneuploidy, the four genes mapped onto diploid homologous chromosomes. This methodology will be an important resource for the genome sequencing consortium.

The interphase nucleus is an organised organelle, whereby chromosomes and gene loci have been shown to be located non-randomly and hence it is hypothesised that the organisation of the interphase nucleus is pertinent to the function of the genome. Since there is no data on how the genes of the snail genome behaves in interphase, it was assessed in the Bge cells line. Again, this is important for the sequencing initiative, but also for evolutionary biology. Radially distributed chromosome territories were observed in the nuclei of the Bge cells. The territory position was organised according to territory size, with small chromosome territories positioned towards the interior and large territories intermediately located. In addition, four *B. glabrata* genes were positioned non-randomly in the interphase nuclei of the Bge cells, again emphasising organised positioning of the genome.

With co-culture of *S. mansoni* miracidia with the Bge cells there is up regulation of specific genes known to be involved in the host response to parasite. These genes are dramatically relocated within the interphase nuclei, implying that these are specific parasite induced nuclear events.

An analysis of the genomic distribution of specific histone modified chromatin in the interphase nuclei of *B. glabrata*, revealed different nuclear distribution of modified

chromatin. Indeed, a statistically significant difference in these patterns was observed between juvenile and adult snails, indicating developmental differences in the organisation of the snails' genome. These differences maybe relevant to the snails' resistance/susceptibility to the parasite.

Declaration

I hereby state that the work presented in this thesis has been performed by me unless stated otherwise.

Edwin C. Odoemelam

Acknowledgements

I would like to begin my acknowledgements by thanking Dr Joanna Bridger; my supervisor, colleague and friend, for her guidance throughout my PhD. Her scientific erudition as well as her unabated passion for academic research has permeated my life for the last 4 years and for that I am eternally indebted.

I would like to thank the following collaborators from the Biomedical research institute (BRI, USA). I would like to thank Dr Matty Knight, Dr Nithya Raghavan, Dr Fred Lewis and Andre Miller for supplying the *B. glabrata* snails, the Bge cells and the *B. glabrata* BAC genes. I'd especially like to thank Dr Matty Knight for her helpful advice and kind input. I'd like to extend the hand of gratitude to Dr Wannaporn Ittiprasert for her RT-PCR work on the *B. glabrata* ferritin and actin genes.

I would like to thank Prof. Wendy Bickmore and Dr Paul Perry for the 2D FISH erosion analysis script.

I express my gratitude to my colleagues from the Brunel institute for the environment (ife). I would like to express a particular thank you to Steve Pash and Alice Baynes for their helpful comments and assistance pertaining to snail husbandry.

I would like thank Dr David Tree (2nd supervisor), who has played an integral role in my development as a scientist.

For their assistance in microscopy, I would like to acknowledge Dr Ian Kill and Dr Julio Masabanda.

I reserve a special thank you to Ishita Mehta, Lauren Elcock, Dr Helen Foster and Dr Karen Meaburn for providing perspicacious insight, support and assistance throughout my PhD.

Finally, I would like to thank Stella Odoemelam, Stella-Jane Odoemelam, Sam Taffs, Peter Bingham, Inesa Bingham and Julia Giannetti. Thank you all for your dependable friendships!

Abbreviations

2D	Two- dimensional
3D	Three-dimensional
BB02	Non susceptible *B. glabrata* snail
Bp	Base pair
BSA	Bovine serum albumin
BrdU	Bromodeoxyuridine
BS90	Brazilian isolate resistant *B. glabrata* snail
CHO	Chinese hamster ovary cells
Cy3	Cyanine 3
DAPI	4, 6 di-amidino-2-phenylindole
DNA	Deoxyribonucleic acid
DOP-PCR	Degenerate oligonucleotide primed polymerase chain reaction
ES	Embryonic stem cells
EST	Expressed sequence tags
FISH	Fluorescence *in situ* hybridisation
FITC	Fluorescein isothiocyanate
FBS	Foetal bovine serum
FUrd	5-fluoro-2'-deoxyuridine
G0	Quiescence or senescence, exit from cell cycle
G1	Cell cycle gap 1
G2	Cell cycle gap 2
$H3Me_2K9$	Histone dimethylation modification to lysine 9
H3Me3K4	Histone trimethylation modification to lysine 4
$H4Me_3K20$	Histone trimethylation modification to lysine 20
HAT	Histone acetyltransferase
HCl	Hydrochloric acid
HDAC	Histone deacetylase
Hr	Hour
HSA	*Homo sapien* autosome
HU	Hydroxyurea

ICD	Interchromatin domain compartment
Kb	Kilobase (one thousand DNA base pairs)
Mb	Megabase (10^6 DNA base pairs)
MEF	Mouse embryonic fibroblast cells
MHC	Major histocompatibility complex
Min	Minute
mRNA	Messenger RNA
n	Sample size
NaCl	Sodium chloride
NBF	Neutral buffered formalin
NE	Nuclear envelope
NCS	New born calf serum
NMRI	Lab derived susceptible *B. glabrata* snail
NORs	Nucleolar organiser regions
PBS	Phosphate buffered saline
RNA	Ribonucleic acid
RNAi	RNA interference
ROS	Reactive oxygen species
RT	Room temperature
RT-PCR	Reverse transcription-polymerase chain reaction
S	Svedberg units
SSC	Saline sodium citrate
Sec	Second
SEM	Standard error of the mean (SD/square root of the sample size)
S-phase	DNA synthesis cell cycle stage
TBS	Tris-buffered saline solution
UV	Ultraviolet light
v/v	Volume/volume (ml of solution/100ml)
w/v	Weight/volume (g of substance/100ml)
Xa	Active chromosome X
Xi	Inactive chromosome X

Table of contents

Table of Figures

Table of Tables

Chapter 1:

Introduction

1. Introduction

1.1 Schistosomiasis

1.1.1 Public Health Importance

Digenetic trematode parasites are responsible for a number of debilitating human diseases these include *Paragonimiasis, Fascioliasis, Clonorchiasis and Schistosomiasis.* Of these diseases, schistosomiasis (also known as Bilharzia, after the german parasitologist, Theodor Bilharz, in *1851*) is the most widespread, infecting over 200 million people worldwide and has a mortality rate of 300,000 per year (Fitzpatrick et al., 2008, Steinmann et al., 2006). The disease is endemic in 74 tropical countries, (in regions of Africa, the Caribbean, the Middle East and South America) and causes mass devastation in terms of public health and socio-economic importance (LoVerde et al., 2004, Friedman et al., 2005).

The causative agents of schistosomiasis are schistosome parasites, whose pathological assaults on the human anatomy focus on the intravascular region (Isnard and Chevillard, 2008). The disease primarily affects those individuals who are exposed to freshwater in an endemic country. Hence in certain parts of the world, schistosomiasis is thought of as an occupational disease, relating to its prevalence among rural workers i.e. agriculture and fishing (LoVerde et al., 2004). These rural inhabitants are often integral members of the country's economic work-force, consequently the country's gross domestic product (GDP) suffers severely (as a result of the malaise the disease causes to the individual).

1.1.2 Trematode schistosome parasites

The schistosome parasites responsible for the key forms of schistosomiasis are listed in Table 1.1. Platyhelminth schistosome parasites are descended from a hermaphroditic ancestor (Fitzpatrick and Hoffmann, 2006). *Schistosoma* - when translated from greek

literally means ‘split body’, this refers to the dioecious anatomy of most species (Blanchard, 2004, Gryseels et al., 2006) . The females are clasped to the male in a long groove which extends across the entire length of the male. It is known as the ‘gynaecophoral canal’ (where copulation takes place). Significant sexual dimorphism exists within the *Schistosoma* genus. They are microscopic parasites with an average length and diameter of 20 mm x 0.6 mm respectively.

Table 1.1: Displaying human schistosomes, their host snails and relative regions of endemicity

Schistosome parasite	Snail Genera	Regions of endemicity
S. mansoni	*Biomphalaria*	Africa, Eastern Mediterranean, the Caribbean and South Asia.
S. mekongi	*Tricula*	Asia
S. intercalatum	*Bulinus*	Africa
S. japonicum	*Oncomelania*	Asia
S. haematobium	*Bulinus*	Africa and Eastern Mediterranean

The males tend to be of a stouter morphology than the females and the ventral oral sucker is located at the anterior end, near the acetabulum (Gryseels et al., 2006). Females suckers are weaker and of a less developed musculature than that of the males (Blanchard, 2004). The number of testes differs between species, ranging from 5-9 (Blanchard, 2004). The ovary can be located anteriorly or posteriorly to and at the centre of the body (Roberts and Janovy, 2000).

The schistosome worm pairs are found *in copulo* within the veins that drain specific organs of their definitive host, which include along with humans; dogs, cows, buffalo and rats. The adult worms that inhabit the mesenteric veins (surrounding the bowels) include *S. mansoni*, *S. japonicum*, *S. mekongi*, and *S. intercalatum*. The parasite *S. haematobium* on the other hand inhabits the veins of the vesical and pelvic plexuses (bladder and ureter) (Blanchard, 2004, Roberts and Janovy, 2000)

Humans are the definitive host for *S. mansoni* and as such, this species has been the subject of extensive research. It's proclivity of infection in the Western hemisphere over the other schistosomes is largely due to it's interaction with the intermediate host *Biomphalaria glabrata* (Miller et al., 1996). The origins of *S. mansoni* seem to lie within the Great lakes of central Africa (Gryseels et al., 2006). The parasite was broadly distributed throughout the World during the 17^{th} – 18^{th} centuries as a consequence of the slave trade (Roberts and Janovy, 2000).

1.1.3 Schistosome lifecycle

The lifecycle of the schistosome parasites is complex. The parasite undergoes considerable changes in it's anatomy as well as inducing changes to the organisms they inhabit. In the case of *S. mansoni*, the adult worm pairs prefer the portal venous plexus surrounding the bowels in humans (Blanchard, 2004). The females lay hundreds of eggs each day, these eggs slowly transverse the wall of the venule and eventually find their way into the lumen of the bowel, ready for expulsion from the host (Roberts and Janovy, 2000, DeMarco and Verjovski-Almeida, 2009). The eggs are hydro-sensitive, upon contact with water, the cilia of the miracidia (within the eggs) become active and oscillate furiously until an osmotically induced vent opens on the side of the egg (Isnard and Chevillard, 2008). The miracidia form of the schistosomes infects water snails. These snails form the intermediate

host within the lifecycle. *S. mansoni's* intermediate hosts are from the *Biomphalaria* genus (Isnard and Chevillard, 2008). In Africa, *S. mansoni* is mainly transmitted by *B.spp alexandrina*, *camerunensis* and *pfeifferi* (Knight et al., 2000). The majority of 'schisto-gastropoda' research has centred on the *B. spp* of the Western hemisphere that include *B. straminea*, *B. tenagophila* and *B. glabrata* (Knight et al., 2000). *Biomphalaria glabrata* as well as *S. mansoni* have been prioritized for complete genome sequencing (Knight et al., 2000). Indeed, the complete sequence is now available for *S. mansoni* and *S. japonicum* (Berriman et al., 2009).

Upon entry into the snail, the miracidia form primary (mother) sporocysts, which are located in the tentacles and head-foot of *Biomphalaria* snails (Lewis et al., 1986). The primary sporocyst grows and begets secondary (daughter) sporocysts, which are often situated in the hepato-pancreas of the snail (Lewis et al., 1986). The larval stage which is infective to humans, emerges from the snail a month after the initial infection (Richards, 1980). The furcocercous cercariae are highly motile and swim ceaselessly until they penetrate the skin of their definitive host (humans) (Blanchard, 2004). The cercariae lose their tails during the skin penetration process and transform into schistomules (Isnard and Chevillard, 2008). From the the skin, the schistomules enter the circulatory system and migrate in the blood to the liver (via the lungs). Maturation and mating of the young male and female *S. mansoni* worms takes place over a period of 4-6 weeks in the portal vein (Gryseels et al., 2006). Subsequently the paired worms migrate to the mesenteric venules of the bowel. The average lifespan of the worms in the human body is 3-5 years however they can live for upto 30 years. In theory a schistosome pair could potentially reproduce upto 600 billion schistosomes (Gryseels et al., 2006, Isnard and Chevillard, 2008).

Figure 1.1: Schistosome parasite life cycle

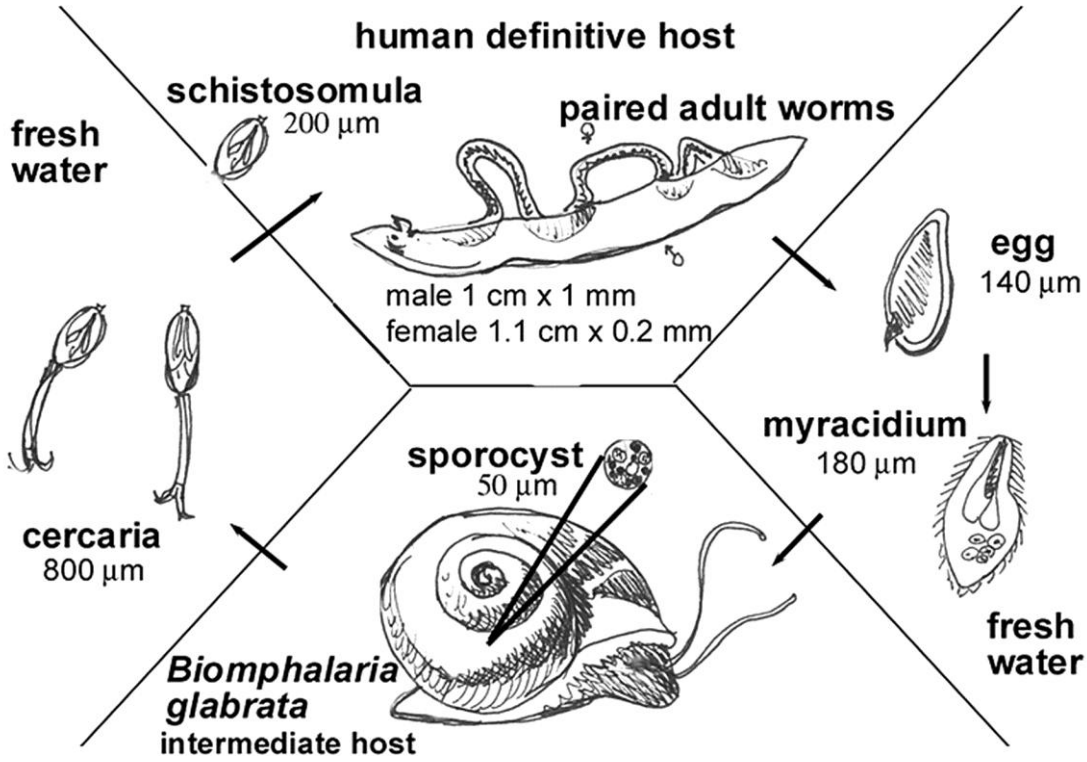

The schistosome lifecycle, showing the transitions from the primary snail host to secondary human host (Knudsen et al., 2005).

1.1.4 Human pathogenesis

Figure 1.1 shows the lifecycle of the *S. mansoni* parasite. Humans are the definitive host of the parasite and the parasite is released into fresh water with human faeces. As a consequence of this mode of parasite transmission, schistosomiasis is most prevalent amongst the impoverished (Blanchard, 2004, King). Families on the bottom rung of the 'social ladder' seldom have access to clean, transportable water; thus disease transmission is propagated due to the lack of viable excretion disposal systems (Blanchard, 2004, Wang et al., 2008).

Based on the knowledge of the schistosome lifecycle, a prescient conjecture upon pathology of the disease would point towards the invading worms and the mature schistomules. However, the aetiology is almost entirely 'egg related' and seldom involves the worms themselves (Cheever et al., 2002). The expulsion of *S. mansoni* eggs in the faeces of the human host is only partial. Approximately half of the eggs remain in the body. As mentioned previously, the eggs migrate through the lumen wall of the gut; the eggs are enveloped by granulomas which aids their migration (Cheever et al., 2002). The granuloma is composed primarily of macrophages, eosinophils and lymphocytes (Isnard and Chevillard, 2008). Some eggs, although still surrounded by a granuloma, do not transverse the lumen and hence remain behind, exuding schistosome antigens (Isnard and Chevillard, 2008). Consequently, there is a granulomatous reaction to schistosomal eggs (Roberts and Janovy, 2000). This type of reaction often takes several weeks to develop and is hence a delayed type hypersensitivity (DTH) response, which is symptomatic of a T helper1 and 2 (Th1 and Th2) cellular response (Cheever et al., 2002, Hirayama, 2004). Indeed, the dichotomy of the Th1/Th2 responses has been at the crux of *schistosoma* immunological research for many years.

Acute schistosomiasis (also known as Katayama fever) occurs 2-4 weeks in humans after exposure to *S. mansoni* (Ross et al., 2007). Such a period of time is enough for the host to initiate a humoral immunological response against the migrating schistomulae. Notably, there is a high level of Th1 instead of Th2 (Pearce et al., 2004). The result is a febrile reaction to the infection which is highlighted by malaise, headaches and abdominal tenderness (Ross et al., 2007). Subsequently, once the worms have serttled in the portal system, they start producing eggs (around four weeks post infection) (Isnard and Chevillard, 2008). The chronic pathology of schistosomiasis is concomitant with an increase in Th2 and is a reaction to the production of these eggs, which can become

trapped in tissue during peri-intestinal migration (Pearce and MacDonald, 2002, Gryseels et al., 2006). *S. mansoni* eggs migrating through the intestinal wall can elicit a granulomatous inflammatory reaction, microulcerations and bleeding (Gryseels et al., 2006). Symptoms in those suffering from chronic schistosomiasis can manifest as diarrhoea, bloody stools and a loss of appetite. *S. mansoni* eggs which are trapped in the periportal system of the liver can also provoke an inflammatory response (Isnard and Chevillard, 2008, Gryseels et al., 2006). Indeed, eggs which are trapped in the hepatic system are the main cause of hepatomegaly (enlarged liver) in schistosomiasis. As well as hepatomegaly, there is the formation fibrotic plaques, which can lead to liver congestion in periportal regions (known as Symmer's fibrosis) (Andrade, 2009).

1.1.5 Diagnosis and Treatment

The diagnosis of many platyhelminth spread diseases often involves the examination of excreta for eggs (Gryseels et al., 2006, Blanchard, 2004). In the case of schistosomiasis by *S. mansoni*, an effective diagnosis can be concluded from the identification of *S. mansoni* laterally spined eggs within the stools of the patient (Gryseels et al., 2006). These eggs can be viewed under a light microscope; faecal material is adsorbed onto a nylon screen through which it is filtered to remove larger fragments (Blanchard, 2004). The collected material is then placed between glass slides and analysed by a microscopist. This is known as the Kato-Katz method and used to assess the egg concentration from faecal samples ranging 20 – 50 mg in mass (Gryseels et al., 2006, Blanchard, 2004).

Diagnosis using serology utilises the host's production of antibodies against schistosomes as well as the detection of the antigens themselves (Gryseels et al., 2006). Before testing for antibodies, a number of caveats must be observed. Often infected individuals only display positive results after several weeks post infection (Blanchard, 2004). Indeed, the

same is true for patients who have been cured. It is also difficult to decipher which schistosome parasite caused the infection since the serology tests frequently cross react with other platyhelminth infections (Gryseels et al., 2006). However, analysing the schistosome antigens often negates the aforementioned problems. ELISA assays which utilise the *S. haematobium* soluble egg antigens (SEA) are cross reactive for most of the schistosome species (Blanchard, 2004).

The treatment of schistsosomiasis involves an oral dose of the dry Praziquantel (PZQ) (Pearce, 2003). PZQ kills most forms of schistosomiasis parasites and is also used to treat most platyhelminth diseases. PZQ disturbs Ca^{2+} cellular homeostasis and increases the membrane permeability of Ca^{2+} channels (Pearce, 2003, Jeziorski and Greenberg, 2006). The result is an influx of Ca^{2+} ions into schistosome worms, causing muscular contractions, paralysis, and eventual death (Jesiorski and Greenberg 2006). However, praziquantel does not prevent re-infection and parasites can develop resistance to the drug (Doenhoff et al., 2002, Fitzpatrick et al., 2007). Other drugs used to treat schistosomiasis include oxamiquine, metrifonate and the anti-malarial artemesinins (Blanchard, 2004, Pearce, 2003).

1.2 The role of *Biomphalaria glabrata* in the spread of *Schistosoma mansoni*

1.2.1 The Molluscan Phylum

The phylum mollusca, is a diverse group of triploblastic protozomes, renowned for their soft bodies and un-segmented anatomy (Brusca, 2005). The phylum itself ranks third to arthopoda and nematoda in terms of numbers of species (estimated at 130,000, which does not include the 35,000 fossilized species) (Runnegar and Pojeta, 1974). The first appearance of mollusca dates back to the earliest period of Cambrian (Tommotian) at the

beginning of the radiation of coelomate animals (animals with a true body cavity) (Brusca, 2005). Carbon dating of fossilized species estimated this took place 600 million years ago (Brusca, 2005, Marin et al., 2008). All molluscs have a body cavity filled with blood (Brusca, 2005). This unit is known as the 'haemocoel' and contains a blood analogue known as 'haemolymph' which surrounds all the cells in an open circulatory system (Barracco et al., 1993). In general, molluscs' internal organs consist of hearts, gonads and an organ that resembles a kidney (in terms of function) known as the metanephrida (Brusca, 2005).

1.2.2 Gastropoda

The class gastropoda emerged during a period of important evolutionary differentiation within the molluscan phylum. This period is known as the Ordovician, and it produced along with gastropoda, bivalvia and cephalopoda (Passamaneck et al., 2004). With over 80,000 species (living), the gastropods are a truly diverse class of molluscs. The subgroup classification of gastropods is based according to the anatomical layout of the respiratory system. The groups include opisthobranchia (gills in the front of the heart), prosobranchia (gill in the front of the heart) and pulmonata (lungs instead of gills) (Brusca, 2005). Of these three subclasses, pulmonata is considered to be the only one of monophyletic origin. Most pulmonates dwell in fresh water, with only a few found in terrestrial and marine habitats (Brusca, 2005).

The most extensively studied order of pulmonates is *Basommatophora* (basal eye-bearing stalk). More specifically, it is the genus Planorbidae and its subgenus *Biomphalaria* that has become the focus of researchers due to the integral role they play in the transmission of schistosomiasis.

1.2.3 *Biomphalaria glabrata*

The fresh water snail *B. glabrata* is the species most intimately associated with schistosomiasis in the Western hemisphere. It is easily maintained in the laboratory and is the best studied experimentally (Knight et al., 2002). *B. glabrata* natural habitats range from rivers and lakes to stream and transient ponds. Their diet consists of aquatic plants and the cyanobacterium, *nostoc* (found in soil and mud) (Lewis et al., 1986). The water plants are also used for oviposition in addition to acting as a shield against natural predators (birds and fish). Figure 1.2 shows a diagram of the genus *Biomphalaria*. The external shell of *B. glabrata* is composed of calcium carbonate over-laid with an organic membrane which defines the shell's colour (known as the periostracum). The shell fossilizes easily and hence provides an integral insight into the evolutionary processes of molluscs. The shells of *B. glabrata* have a counter clockwise spiral (known as sinistral coiling).

Figure 1.2: *Biomphalaria spp.*

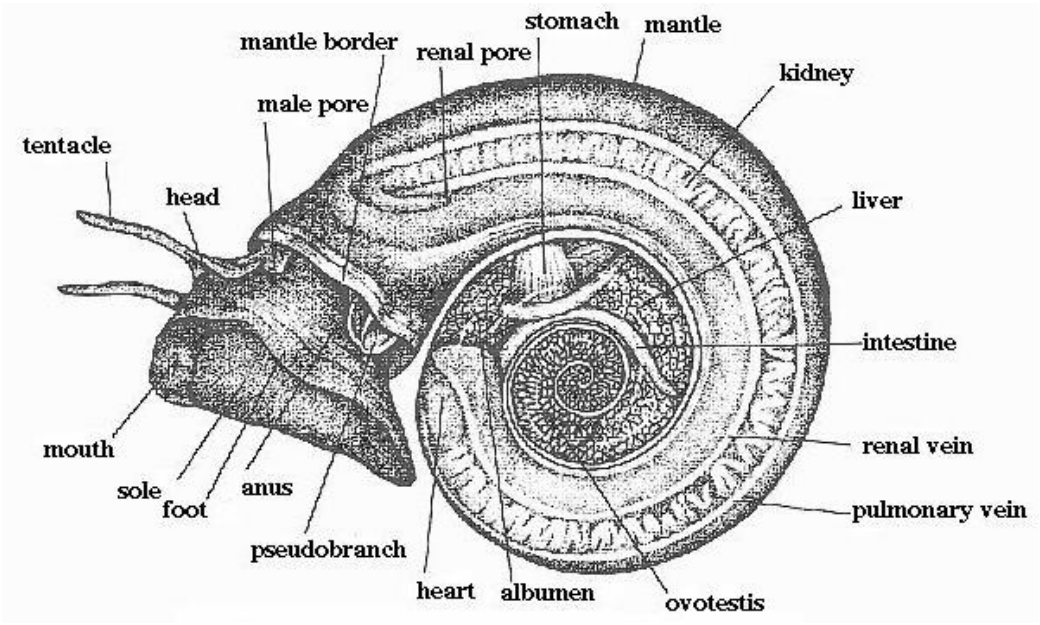

Anatomical diagram of the *Biomphalaria spp*, (courtesy of the Biomedical Research Institute, BRI, USA).

As the snail ages, the shell slowly increases in size from the apex (specifically the prontoconch) towards the aperture. The mantle is a line of skin which transcends the shell; to the mantle is attached a muscular fleshy foot (Brusca, 2005). The foot is often referred to as the 'head-foot' and as the name suggests, its duality allows it to function as a sensory organ (which has protruding tentacles, mouth and feeding structures) and provides locomotion.

The *Biomphalaria spp* (as well as all gastropods) undergo a process called torsion. This process entails the manipulation in position of the mantle cavity from a posterior to a more anterior position. As a consequence, the mantle cavity (as well as the anus) is prostrated over the head-foot. The heart is located in a pericardial chamber and contains a distinctive atria and ventricle.

B. glabrata snails are hermaphrodites with the ability to both self and cross fertilize, although they prefer to cross fertilize (Brumpt, 1941). They can exchange bundles of sperm to avoid self fertilization using an organ known as the ovo-testis. The ovum and mature sperm are conducted through respective ovi and sperm ducts. There is a typical 4-6 week egg-egg generation time. *B. glabrata* live for approximately 12 months, producing a succession of generations (Richards, 1984).

1.2.4 Susceptibility traits

The ability of *B. glabrata* to self fertilize has enabled genetists to examine the inherited traits of susceptibility to *S. mansoni*. Snails can be propagated through selfing over many generations allowing the selection of several characteristics, indeed recessive mutants may emerge in the F_1 generation (it is possible to produce 8 successive generations in 12 months) (Richards, 1975).

The studies of *B. glabrata* genetics were induced by the observation of W L. Newton upon the variations in compatibility between the snail and the parasite. Genetic susceptibility of *B. glabrata* to *S. mansoni* varied in different geographic areas, between indigenous areas and at different stages of development (Newton, 1953). The prescient supposition of Newton and his colleagues was that the interaction between *B. glabrata* and *S. mansoni* genes played a role in the proclivity of infection (Newton, 1953). Newton's pioneering methods of crossing snails established the foundations of analysing heritable characteristics of *B. glabrata* susceptibility to trematode infection (Newton, 1953, Newton, 1954, Newton, 1955).

The crux of Newton's research was the heritability of pigmentation in *B. glabrata* snails. He observed a correlation between the pigmentation of individual strains of *B. glabrata* and the propensity of schistosome infection (Richards, 1985). The fact that wild type pigmentation in *B. glabrata* follows a simple mendellian recessive pattern of inheritance enabled Newton to validate the success of crossing susceptible pigmented snails from Puerto Rico with albino non-susceptible snails. Upon exposure of the F_1 generation to *S. mansoni* miracidia, he noticed a proportion were susceptible to infection, however the snails of (albino) parental origin were not susceptible. Newton concluded that susceptibility to *S. mansoni* was indeed an inheritable trait. Consequently, he proceeded to self fertilize F_1 snails of albino parental origin. The F_2 progeny produced divergent patterns in infection, with some snails resistant and others highly susceptible, hence indicating a multi-factorial gene involvement (Newton, 1954, Newton, 1955, Knight et al., 2000).

Numerous strains of *B. glabrata* snails are used in laboratories all over the world. Many of these strains have definitive susceptibility phenotypes (based upon their susceptibility to the PR-I strain of *S. mansoni*) and are often derived from field isolates or produced via laboratory controlled crosses (Minchella and Loverde, 1983). The BS90 and BB02 stocks

of snails are natural field isolates from Brazil. BS90 is almost totally refractive to *S. mansoni*, BB02 on the other hand is very susceptible to *S. mansoni*. A laboratory derived line of snail known as NMRI is an albino and also susceptible to *S. mansoni* (Miller et al., 2001).

1.3 *Biomphalaria glabrata* embryonic (Bge) cell line

Early studies of trematode development *in vitro* and the divergent reactions of their molluscan host, was often hindered by the absence of dependable *in vitro* molluscan culture techniques. Hence, the development of a tissue culture system from the intermediate host of *S. mansoni* provided an important tool for studying the parasite's growth and development (Ivanchenko et al., 1999).

The work of Eder L. Hansen in establishing the *Biomphalaria glabrata* embryonic (Bge) cell line launched the efforts that led to most of what we currently know about the molecular genetic interactions between trematode and host (Hansen, 1976). Before the cell line, much of the work focused on maintaining molluscan organs *in vitro*. Primary explants from various parts of the snail were used to examine schistosome parasitological intra-molluscan development. The work of Benex in the 1960s, involved the use of *B. glabrata* tentacles maintained *in vitro* (Benex, 1961, Benex, 1965). The choice of organ was a thoughtful one, in that the motile, muscular contractible tentacles are often the site of *Schistosoma* miracidial penetration and primary schistosome development (Bayne, 1976). By using media that resembled that of the donor's internal medium (ionically, osmotically and in pH), Benex was able to maintain the tentacles for up to 4 weeks before de-differentiation. More importantly, Benex was able to assess the primary sporocyst development (mother sporocyst) to secondary sporocyst development and differentiation for 2 weeks (Benex, 1961, Benex, 1965, Heyneman, 1976). Hansen was also able to utilise

knowledge gained from insect tissue culture. Studies implementing insect tissue culture medium revealed that the recreation of invertebrate haemolymph composition was not a necessity, for the protein and various solutes could be substituted for invertebrate serum (Hansen, 1976).

Hansen decided upon the use of *B. glabrata* embryos from an albino mutant. These embryos were dissected from the egg sac when they were approximately 0.35 mm in diameter (from trochophore to the early stages of shell development). From their sacs, they were placed in physiological buffered saline and antibiotics. A suspension of cells was then prepared by homogenizing the embryos in a proteolytic enzyme solution containing trypsin with ethyldiaminetetraacetic acid (EDTA). This solution was then replaced by medium containing high levels of antibiotics. 100 embryos were used to seed a T25 flask, these cells within these flasks were grown at 25^{o}C, 27^{o}C or 30^{o}C in an atmosphere of air (Hansen, 1976).

Figure 1.3: The Bge cell line

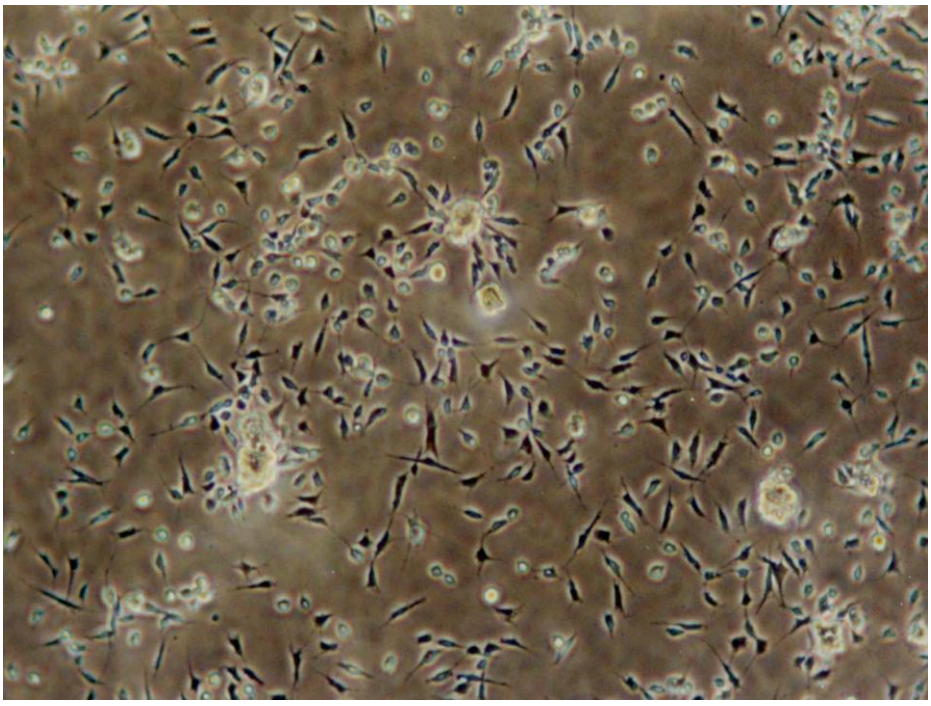

The Bge cell line, morphologically similar to human fibroblasts (image courtesy of Nithya Raghavan at the BRI, USA).

A primary culture which grew abundantly was given the Bge abbreviation (*Biomphalaria glabrata* embryo, Fig 1.3) to highlight its origin. Subcultures were created in accordance with density and growth rate. The medium used was designed to recreate the snail haemolymph amino acid composition. It was constructed from Schneider's *Drosophila* medium (diluted to attain the appropriate osmolarity, as well as incorporating galactose and lactalbumin hydrolysate). The Bge cell line originated from a subculture that grew at 27^{o}C. The cells appeared small (20µm in diameter when circular) with relatively large nuclei (9µm diameter). The cells differed in shape and formed protoplasmic extensions which gave the cells a fibroblast-like appearance. At 27^{o}C, the population doubling time was 18 hours (using an inoculum of 5 x 10^5 cells). The mitotic index ranged from 0.98-1.58% (Hansen 1976).

1.4 The Chromosomes of Pulmonate snails

The study of an organism genome at the chromosomal level can be used in differentiating one species from another, i.e. the analysis of chromosome numbers, size and centromere positions. Indeed, the characterisation of an organism's chromosomes is essential to constructing physical, cytogenetic maps of the genome, which can be achieved through the mapping of genes onto homologous metaphase chromosomes via the use of fluorescence *in situ* hybridization (FISH).

1.4.1 Snail cytogenetics

Early chromosomal studies of gastropods mainly involved the implementation of squash techniques (Thiriot-Quievreux, 2003). However, with the development of cytological methods such as KCl hypotonic treatment of tissue samples and pre-treatment with colchicine (as well as subsequent air drying techniques), came clearer deductions on

chromosome number and morphology (Thiriot-Quievreux, 2003). Most species differ in the aforementioned chromosome characteristics; such differences are often indicative of the extent of evolutionary divergence (Iannuzzi et al., 1990, Hamta et al., 2006). Karyotyping (organising chromosomes into groups in accordance with size and morphology) is a useful tool for studying taxonomic problems such as identifying species as unique from another within the same subgenus (Hamta et al., 2006). Research into gastropoda chromosomes has stagnated in recent years. A lot of the early work on the chromosomes of gastropods was in part initiated by Patterson and Burch (1967 and 1978). Much of their work focused on the pulmonata subclass of gastropoda, and involved a detailed analysis of chromosome numbers and morphology among different species. However, the development of various banding techniques such as silver-staining (Ag NOR), as well as C and G banding presented the biologist with a more elucidated description of pulmonate karyotypes (Goldman et al., 1983, Goldman et al., 1984). The pulmonates under scrutiny were *B. glabrata* and *Bulinus spp*; both of which are intermediate hosts of schistosome parasites (*Bulinus truncatus* being an obligate intermediate host for *Schistosoma haematobium*, a parasite responsible for urinary schistosomiasis). The basic chromosome number of planorbidae snail genera (which includes the aforementioned snails) is 2n=36, but numerous species of *Bulinus* exhibit as well as diploid, tetraploid, hexaploid and even octoploid levels of polyploidy (Goldman et al., 1984).

1.4.2 *Biomphalaria glabrata* chromosomes

All species of the *Biomphalaria* subgenus have been investigated and at present, *B. glabrata, B. pfeifferi, B. madagascariensis, B. sudanica, B. tanganyicensis* and *B. alexandrina* have a haploid chromosome complement of 18 (Burch, 1967). The

chromosomes are relatively small and monomorphic. Observations of these chromosomes have often entailed the use of embryonic squashes (Goldman et al., 1984), fixed chromosome preparations from the Bge cell line (Bayne et al., 1978) and meiotic preparations from the gonadal region (Raghunathan, 1976). Burch in the 1960s utilised preparations from the ovo-testis and reported a haploid complement of 18, however these results were deducted from the meiotic stage, where it was often difficult to identify each and every chromosome (Burch, 1967).

However, the research by Raghunathan (1976) on the mitotic metaphase chromosomes provided a much more elucidated observation of these chromosomes and a somewhat rudimentary karyotype (Raghunathan, 1976). Raghunathan utilised the embryos of *B. glabrata*, which are begat by the snails on a regular basis. The embryos are encased in a thick, gelatine-like sac, which is resistant to dehydration. These egg sacs were cleaned with alcohol and sterilised with penicillin–streptomycin and transferred to a petri dish containing Schneider's *Drosophila* medium (Hansen, 1976, Raghunathan, 1976). Approximately 15-20 embryos were dissected from their sacs, these were homogenised and subsequently centrifuged. The resultant pellet was then treated with colchicine and incubated at 27^{o}C for 45 mins. After this period, Raghunathan subjected the samples to KCl hypotonic and methanol-acetic acid fixation. Glass slides of dropped cellular suspensions were prepared for analysis. From these embryos of high mitotic activity, she deduced stages of prophase, metaphase and telophase (Raghunathan, 1976)

Such was the clarity of her results, she was able to organise these chromosomes into groups of metacentric, submetacentric, acrocentric and telocentric in accordance with centromere position as stipulated by Leven et al (1964) as well as confirm a diploid number of 36 (Levan et al., 1964). The karyotype constructed was basic, based entirely on centromere position and size. They were not differentially stained (i.e. C or G banded). In

total, there were 10 metacentric, 4 submetacentric, 2 acromentric and 2 telocentric chromosome pairs (Table 1.2). These were organised into six groups (Raghunathan, 1976). Of particular interest was chromosome pair 8 and 9. Pair 8 was telocentric and had a secondary constriction. Pair 9 had satellites at the end of their telomeres, she designated this pair as the nucleolus organizer. Raghunathan's results on the mitotic stages correlated with meiotic results she obtained from an ovo-testis preparation (Raghunathan, 1976).

Table 1.2: Karyotype of *B. glabrata* chromosomes according to size and centromeric position (Raghunathan, 1976)

Group	Size	Centromeric position	Chromosome pair number	Number in a diploid cell
A	Large Medium	Metacentric Metacentric	1 2, 3	6
B	Medium	Submetacentric	4-7	8
C	Medium Small	Telocentric Telocentric	8 9	4
D	Small	Metacentric	10-13	8
E	Small	Acrocentric	14, 15	4
F	Smallest	Metacentric	16-18	6
				Total 36

A later study by Goldman et al (1984) focused on the karyotype divergence within and among species of both *Biomphalaria* and *Bulinus*. Goldman et al (1984) analysed the karyotypes of numerous strains of *B. glabrata*; originating from various parts of the world (Dominican Republic, St Lucia and Brazil) as well as different *Biomphalaria* species i.e. *Biomphalaria traminea* (Goldman et al., 1984). The chromosome suspensions were prepared from dissected embryos of age 3-5 days. These embryos were treated with colchicine and fixed with methanol-acetic acid. Unlike the previous study by Raghunathan (1976), Goldman et al (1984) prepared G banded and Ag NOR stained (to reveal nucleolar organizer regions) slides of metaphase spreads (Fig 1.4) (Goldman et al., 1984). The chromosomes were arranged according to size and centromere position. The individual chromosomes were measured (arbitrary units). The lengths of the chromosomes were subsequently converted to a percentage of the total haploid chromosome length (Goldman et al., 1984).

The *B. glabrata* chromosomes in this study were organised into 9 distinct groups (Table 1.3). Of particular interest was group 6 which contained a chromosome pair with a lightly staining arm. A previous study by Goldman et al (1983) identified the P arm of the lightly staining pair as positive for a nucleolar organizer region. The procedure of Ag-NOR banding was performed on four strains of *B. glabrata*, all of which stained positively (upon the LSA) (Goldman et al., 1983). Interestingly, Goldman et al (1983) also reported the NORs in *Bulinus* spp as being located in group VI, which perhaps indicates a degree of evolutionary conservatism amongst these planorbidae snails (Goldman et al., 1983). The positive staining for Ag NORs reveals nucleolar organizer regions that were actively synthesising rRNA during the previous interphase (Kalmarova et al., 2007). However, it should be noted that Ag NOR staining has its limitations, in that it does not take into consideration cellular transcriptional variation. Although this method was adequate during

the 1980s, a more sensitive technique for identifying this region would be the utilisation of FISH. FISH has shown huge potential in the characterisation of chromosomes of various species (Pascoe et al., 1996). Perhaps the use of labelled *Biomphalaria* rDNA probes in the future will provide an even clearer picture of the NORs on the *B. glabrata* chromosomes (Goldman et al., 1983).

Figure 1.4: A metaphase spread of the *B. glabrata* chromosomes

B. glabrata chromosomes from the Goldman et al (1984) publication. The metaphase spread was prepared from the embryos and stained with R66 Giemsa in Gurr's buffer (Goldman et al., 1984).

An intermediate host for the parasite *S. haematobium*, the *Bulinus* spp has also been the focus of attention. The karyotypes within this subgenus have presented cytogenetists and evolutionary biologists with a conundrum of significant interest. In the 1960s, Burch deduced a haploid number of 18 chromosomes in *Bul. tropicus, Bul. beccarii, Bul. senegalensis, Bul. tangolensis, Bul. ferkalli, Bul. globosis, Bul. guernei, Bul. jousseaumei,*

Bul. recticulus, *Bul. zanzibaricus* and *Bul. natalensis* (Burch, 1967). However *Bul. truncatus* was identified as having 36 pairs of chromosomes. Further studies on *B. truncatus* revealed several polyploidy levels including diploid (n=18), tetraploid (n=36),

Table 1.3: Karyotype 2 of *B. glabrata* chromosomes according to size and centromeric position by Goldman et al (1984).

Group	Size	Centromeric position	Chromosome pair number
1	large	metacentric	1
2	large	metacentric	2,3
3	large	metacentric	4,5,6
4	large	subtelocentric	7
5	medium	metacentric	8,9,10
6	large	no mention (LSA)	11
7	medium	telocentric	12,13,14,15
8	medium	submentacentric	16
9	smallest	metacentric	17,18

hexaploids (n=54) and octaploids (n=72) (Burch, 1967). Subsequently the *Bulinus* subgenus was organised into two species groups, the *tropicus* group of 18 pairs of chromosome which is mainly found in Southern Africa and *truncatus*, which is generally found in Kenya, Ethiopia, the Eastern African great lakes and parts of West Africa (Brown et al., 1996, Goldman and LoVerde, 1983).

The *Bul. tropicus/truncatus* complex of snails, not only differ in their chromosome complement but also in their susceptibility to *S. haematobium*. The *B. truncatus* species group are capable of transmitting schistosomiasis, indeed the tetraploid snails are significant hosts in nature. However the *tropicus* group has been shown to be refractive to infection with *S. haematobium* (with a few exceptions). The *Bul. tropicus* chromosomes were organised into 10 groups based on morphology and chromosome size. The *Bul. truncatus* chromosomes were also grouped in a similar fashion, with most groups having twice the chromosome complement as *tropicus*. Goldman et al (1980) proposed that the tetraploid *Bul. truncatus* arose via species hybridization of karyotypically distinct taxa (Goldman and LoVerde, 1983, Goldman et al., 1980).

1.5 Molecular analysis of *B. glabrata* responses to trematode parasites

The goal of most molecular biology laboratories researching schistosomiasis is the identification of genes involved in the intermediate snail's resistance to trematode infection. This is often achieved via the analysis of modulated transcriptomes upon infection of the snail (Melo et al., 2006).

1.5.1 Innate immunity

The genetic phenotypes of susceptibility to *S. mansoni* differ among the numerous strains of *B. glabrata*. In resistant strains such as the previously mentioned BS90, there exists an innate ability to destroy invading trematodes (echinostomes as well as schistosomes). The mechanism is mediated by ameobocytic haemocytes (produced from the ameobocytic producing organ APO) which are dispersed throughout the haemolymph and binds to digean sporocysts, encapsulating them and subsequently destroying them (Knight and Raghavan, 2006). Pulmonate snails such as *Planorbarious corneus, Lymnaea stagnalis* and

B. glabrata usually have two types of haemocytes; granulocytes and hyalinocytes (however it is granulocyte cells which are apparent effector cells) (Humphries and Yoshino, 2003). The haemocytes *in vivo* circulate the haemolymph freely and are akin to phagocytic leukocytes in as much as they will aggregate and phagocytose alien molecules (Knight and Raghavan, 2006). These cells participate in several internal defense associated actions, such as bacterial and microbial phagocytosis (Humphries and Yoshino, 2003). Indeed, experiments utilising *B. glabrata* haemocytes and the Bge cell line have shown the haemocytes have the ability to phagocytose heat treated *E. coli* (Humphries and Yoshino, 2003). The cellular signalling of the haemocytes involve cell surface receptors such as integrin and lectin like proteins, and receptors capable of binding peptide hormones, cytokines and growth factors (Humphries and Yoshino, 2003). In susceptible snails, the ability of the haemocytes to destroy the invading trematodes seems to have been effectively nullified by the parasite (Humphries and Yoshino, 2003).

1.5.2 Parasite destruction

The involvement of reactive oxygen species (ROS) in the cell-mediated killing of trematode parasites was displayed by Adema et al (1994). The study utilised the avian schistosome *Trichobilharzia ocellata* and the haemocytes of its intermediate host *Lymnaea stagnalis* (Adema et al., 1994). By inhibiting the production of ROS by the haemocytes they reduced the ability of the haemocytes to eradicate the schistosome parasite (Bayne et al., 2001, Adema et al., 1994).

The production of ROS in phagocytic cells is achieved via the NADPH oxidase complex within the phagocyte plasma membrane. O_2^- produced by catalytic enzyme complexes is the first in a production belt of free radicals. Super oxide dismutase (SOD) converts O_2^- to hydrogen peroxide (H_2O_2), and in the presence of chloride ions H_2O_2 is converted to

hypochlorous acid (HOCL) by the enzyme myelinoperoxidase (MPO). HOCL can subsequently produce $^{\cdot}OH$ and a singlet O_2. Also a majority of phagocytic cells have an inducible nitric oxide synthase (INOS) which can create nitric oxide (NO) from O_2 and L-arginine. Hence, in order to establish which reactive oxidants were involved in mediated haemocyte destruction of *S. mansoni* Bayne et al (2001) employed an *in vitro* assay of killing the sporocysts of *S. mansoni* by haemocytes from a resistant strain of *B. glabrata*. Enzyme inhibitors and oxidant scavengers were utilised, such as hypotaurine for HOCL and $^{\cdot}OH$, and SOD for O_2^{-}. The addition of these components did reduce the killing capability of the haemocytes. However, when catalase was added (which converts H_2O_2 to harmless H_2O and an oxygen molecule), there was a significant reduction in destructive capabilities of the haemocytes. It was thus deduced that H_2O_2 is the pertinent ROS involved in sporocysts termination (Bayne et al., 2001, Bixler et al., 2001, Bender et al., 2002). A subsequent study by Hahn et al (2001) showed NO (as well as H_2O_2) plays a role in the killing of sporocysts by haemocytes (Bayne et al., 2001).

A study by Bender et al (2005) found that haemocytes from resistant strains of *B. glabrata* produce more H_2O_2 than that of those from susceptible snails (Bender et al., 2005). The study implicated copper zinc (Cu/Zn SOD) enzyme activity as having a critical role in haemocytes ability to destroy schistosome parasites (Bender et al., 2005). This research prompted Goodall et al (2006) to investigate the role the *SOD1* gene plays in resistance and susceptibility. The study by Goodall et al (2006) identified alleles of genes coding for *SOD1*. Indeed, one allele identified was associated with resistance to schistosome infection and another with susceptibility (Goodall et al., 2006). A later study by Bayne and colleagues focused upon analysing the *SOD1* transcript level from haemocytes obtained from genotyped *B. glabrata* snails (Bender et al., 2007). The haemocytes from the snails with the resistance associated allele previously documented in Goodall et al (2006)

produced significantly higher levels of the *SOD 1* transcript than those snails which lacked this allele (Bender et al., 2007). These results substantiated the supposition of *SOD1's* contributory role in *B. glabrata's* susceptibility/resistance to *S. mansoni* (Bender et al., 2007).

1.5.3 *B. glabrata* transcriptome modulation in response to *S. mansoni*

Raghavan et al (2003) used a method of expressed sequence tag (EST) analysis to assess the modulation in transcription in haemocytes from resistant snails, pre and post exposure to *S. mansoni*. The EST sequences were processed through GenBank and SwissProt. Raghavan et al (2003) identified a number of genes with a close similarity to housekeeping genes and reverse transcriptases (RT) (Raghavan et al., 2003). By implementing RT-PCR, Raghavan et al (2003) deduced that the RT transcripts were expressed in unexposed susceptible snails as well as those snails which had been exposed to miracidia and cells from the Bge cell line. One of the RTs identified was homologous to the C-terminal cysteine knot signature, and located in the haemocytin (a lectin involved in humoral defense) of the silk moth (Raghavan et al., 2003). Subsequently RT-PCR assays of pre- and post-infected resistant and susceptible snails were carried out utilising protein extracts from the tissue of head-foot and posterior tissue snail regions. Prior to infection, the RT activity was greater in the posterior region in both resistant and susceptible snails, however the RT activity was more prominent in the head-foot post infection of resistant *B. glabrata* snails (Raghavan et al., 2003).

An article by Knight et al (2009) identified an antioxidant enzyme peroxiredoxin (*BgPrx4*, homologous to human peroxiredoxin). Quantitative real-time PCR analysis of the *BgPrx4* transcriptome levels in resistant and susceptible snails exposed to *S. mansoni* revealed that the *Bgprx4* transcript level was up-regulated in resistant snails during the early phase of the

exposure (5 hr post exposure). In contrast, the *Bgprx4* levels were down regulated in the susceptible snails during this phase. Interestingly, an increase in the *Bgprx4* transcription level was observed 48 hr post exposure in the susceptible snail, somewhat indicative of a delayed reaction to the parasite. The *Bgprx4* peroxiredoxin enzyme is postulated to function in the scavenging of aforesaid harmful ROS produced by *B. glabrata* in response to parasitic invasion (Knight et al., 2009). However, the role of peroxiredoxin in susceptibility/resistance in *B. glabrata* has yet to be determined (Knight et al., 2009).

Another study by Knight and colleagues has focused upon the stress response in juvenile susceptible (NMRI), resistant (BS90) and non susceptible (LAC2, derived from NMRI snails which were refractory to miracidial infection) *B. glabrata* snails (Ittiprasert et al., 2009). They investigated the induction (transcriptional up-regulation) of heat shock protein 70 (*Hsp70*), a gene which had previously been shown to be transcriptionally activated upon thermal stress (Laursen et al., 1997). *Hsp70* was shown to be concurrently up-regulated with the *B. glabrata* non-LTR retrotranspon, *Nimbus* (Raghavan et al., 2007), early in the post- exposure phase to *S. mansoni* miracidia in juvenile NMRI susceptible snails. The resistant BS90 and non-susceptible LAC2 snails in contrast displayed less elevated levels of both of the aforesaid transcripts as well as a temporally delayed transcriptional occurrence (Ittiprasert et al., 2009). Ittiprasert et al (2009) hypothesise that both *Hsp70* and *Nimbus* are transcriptionally induced via the same molecular pathway, they also speculate that the difference in *Hsp70* and *Nimbus* expression between susceptible snails and the resistant/ non susceptible counterparts may reflect differences in molecular responses to parasitic infection (Ittiprasert et al., 2009).

1.5.4 Fibrinogen related proteins (FREPs)

The molecular characterisation of proteins produced within the haemolymph upon trematode infection is another avenue for studying molecules involved in *B. glabrata* resistance to trematode infection (Loker and Bayne, 2001). Research by Eric S. Loker and colleagues has focused on a haemolymph lectin which is up regulated upon exposure of *Lymnaea stagnalis* and *B. glabrata* to respective trematodes *Echinostoma paraensei* and *S. mansoni* (Adema et al., 1994). The lectins discovered have a homology with fibrinogen and have consequently been called Fibrinogen-related proteins (FREPs). They are composed of a C-terminal domain which are similar to fibrinogen and an N-terminal domain which is similar the V-type loops of immunoglobulin superfamily (Jiang et al., 2006, Loker and Bayne, 2001). It is thought that FREPs play an important role in identifying trematode products (antigen recognition). Currently eleven FREP encoding sequences have been discovered, two of which have been completely sequenced and known as *FREP2* and *FREP4* (Leonard et al., 2001). A later study by Hertel et al (2005) utilising quantitative PCR found that *FREP*2 and *FREP4* were up regulated in the resistant BS90 strain of the *B. glabrata* upon its exposure to *S. mansoni* (Hertel et al., 2005*).*

1.6 Genome sequencing of *Biomphalaria glabrata*

According to the World Health Organisation (WHO) an estimated 600 million people are at risk from infection by schistosomiasis ((WHO), 1997). During the 1980s, the WHO expert committee on the control of schistosomiasis suggested a plan of action for morbidity control, with mass chemotherapy as the main method of curtailing the spread of infection ((WHO), 1997). This was a deviation from previous control strategies which often involved the application of molluscicides to eradicate snail intermediate hosts. Concomitant with chemotherapy is the implementation of adequate sanitation and health education both of which have reduced the spread of the disease (Utzinger et al., 2003). The

application of PZQ has been a success in the reduction of schistosomiasis transmission in some regions (Savioli et al., 2004). However PZQ isn't a 'magic bullet', the treatment often has to be repeated, since immature schistosome worms are immune to PZQ (indeed, strains of schistosome worms have been developed in the lab which are resistant to PZQ) and the application of PZQ does not prevent re-infection. Undeniably, a protective vaccine against the parasite would be a great success for researchers, yet efforts to develop a vaccine have been up to now unsucessful (research into this is often slightly hindered by the schism between promoters of the vaccine and those whom still favour molluscicides and mass chemotherapy). Vaccination targets have included schistosome antigens such as Glutathione S-transferase (p28/GST), paramyosin (Sm97), triose phosphate (TPI), myosin heavy chain protein (IrV-5) and a fatty binding protein (Sm14). These antigens were implemented in mouse model studies with *S. mansoni* however, the results were disappointing (Pearce, 2003, DeMarco and Verjovski-Almeida, 2009). Progress into a vaccination against *S. hematobium* on the otherhand has been more promising, with phase I and II human clinical trials in progress using *S. hematobium* glutathione S-transferase (ShGST) (DeMarco and Verjovski-Almeida, 2009). Hence, without a vaccine or a full understanding of host/parasite interaction, there appears to have been only a small degree of progression in the schistosomiasis field of research (Bergquist et al., 2002, Pearce, 2003).

Recent ideas on the long term prevention of the spread of schistosomiasis have focused on the intermediate host of schistosome parasites. Ever since the pioneering work of Newton and Richards on the heritability of snail resistance to *S. mansoni,* ideas of prevention have included the displacement of snails susceptible to schistosomiasis for those snails that are resistant to the parasite i.e. the BS90 strain of *B. glabrata* (Newton 1953; 1954; 1955; and Richards. 1962; 1967; 1973; 1975). Newton and Richards hypothesized that by identifying

the genes involved in the snail's resistance to schistosomiasis, we might able to take advantage of this and perhaps create methods of nullifying schistosome propagation. The advent of modern molecular biology methods, such as genome sequencing have provided schistosomiasis scientists with a new avenue of investigation. With the availability of the sequence of two of the three organisms relevant to the spread of schistosomiasis i.e. *Homo sapiens* (Venter et al., 2001) and *S. mansoni* (Berriman et al., 2009), it has become imperative to attain the sequence of *B. glabrata* (Raghavan and Knight, 2006).

The genome size of *B. glabrata* is approximately 931 MB and is based on the analysis of haemocyte samples which also gave a GC content of 46% (Gregory, 2003). The *B. glabrata* genome is three times smaller than that of the 3000 MB human genome (Venter et al., 2001) and three times larger than that of the 363 MB *S. mansoni* genome (Berriman et al., 2009). Yet in comparison to other molluscs, the genome is relatively small, i.e. *Aplysia californica* at 1800 MB, and *Lymnaea stagnalis* at 1195 MB (Knight and Raghavan, 2006). Currently, on the NCBI databases there are 55,766 nucleotide sequences (54,309 EST) and 650 protein entries that have been deposited. To date, numerous gene libraries have been constructed e.g. cosmid, genomic, cDNA and BAC; at the moment there exists a fully sequenced *B. glabrata* mitochondrial genome of 13,670 nucleotides (Knight and Raghavan, 2006).

As a consequence of proposals for a snail genome project put forward at the American Society for Parasitologists meeting in New Mexico 2001, a snail genome consortium was formed. Subsequently, a scheme for the construction of a BAC library was accepted by the National Human Genome Research Institute (NHGRI) and a library was created from the susceptible BB02 line of *B. glabrata* at the Arizona Genomics Institute (insert size 144 kb, genome coverage ~9.5).

The positive applications of the BAC library were followed by the submission of a proposition for complete sequencing of the *B. glabrata* genome. This was put forward to NHGRI in 2004 (Adema et al., 2002). The Genome Sequencing Centre in Washington now organises the sequencing of the genome.

1.7 Genome organisation in the interphase nucleus

This section of the introduction sheds light on the importance of nuclear organisation heeding particular interest to the control of gene expression.

1.7.1 Chromosome territories

The cell nucleus is an ordered organelle in which genomes are housed. Not only does it encompass the genetic material of the organism, but it is the site of DNA repair, DNA replication, RNA processing, interactions between transcription factories and regulating sequences, ribosome biogenesis and chromatin remodelling (Foster and Bridger, 2005, Parada et al., 2004). The orchestration of genomic control is present with regards to the organisation of chromosomes in the interphase nucleus. Chromosomes occupy distinct, regional positions in interphase nuclei and differ in the spatial volumes they occupy within the nucleus. These designated regions are known as chromosome territories and are a conserved feature of higher order nuclear organisation (Meaburn et al., 2007, Soutoglou and Misteli, 2008). The position of these territories is demonstrably non-random in higher order eukaryotes (Croft et al., 1999, Boyle et al., 2001, Foster et al., 2005, Meaburn et al., 2008, Cremer et al., 2001). In terms of chromosome structure observed during metaphase, the chromosomes are decondensed and composed of higher order chromatin fibre exceeding 10 nm (Pombo and Branco, 2007) as well as expansive channels that provide a conduit for inhibitors and gene activators to genomic sequences (Meaburn et al., 2007).

Contemporary models concerning the spatial relation between chromosome territories proposes that they are separated by interchromatin domains (ICD) saturated with the nuclear machinery necessary for nucleic acid metabolism (Branco and Pombo, 2006).

Most of the existing data on the morphology and spatial organisation of chromosome territories has been derived through the deployment of the FISH technique, whereby fluorescently labelled sequences (genes and whole chromosomes) are hybridized to homologous sequences in the interphase nucleus, thereby allowing the identification of pertinent regions of the genome. Another method of visualising chromosome territories is the use of pulse labelling the genome with a thymidine analog such Bromo-deoxy-uridine (BrdU) (Ferreira et al., 1997, Zink et al., 1998, Alexandrova et al., 2003). The incorporation of BrdU into the genome during DNA synthesis results in sister chromatid labelling (Fig 1.5). The labelled and unlabelled chromatids are randomly distributed into the daughter cells after subsequent divisions. After 5-10 cell cycles, the interphase nuclei can be observed with single chromosome territories (Fig 1.6).

The spatial and morphological organisation of chromosome territories in the interphase nucleus has been shown to vary between different organisms. The Rabl pattern of chromosome organisation is adopted by wheat, rye, barley, oat (Dong and Jiang, 1998) and *Drosophila* (Hochstrasser and Sedat, 1987). The chromosomes are polarized in their orientation within the nucleus, whereby the centromere and telomere are on opposite sides of the nucleus. Initially observed by Rabl (1885) in the salivary glands of salamanders (Rabl, 1885); the conformation is the result of chromosome segregation during anaphase, in which the separated sister chromatids or homologous chromosomes are drawn with spindle fibres microtubules to the poles, with the sister centromeres pulled in one direction trailed by the telomeres (Santos and Shaw, 2004).

Figure 1.5: Schematic diagram detailing the labelling of genomic regions with a pulse of the thymidine analog BrdU**.**

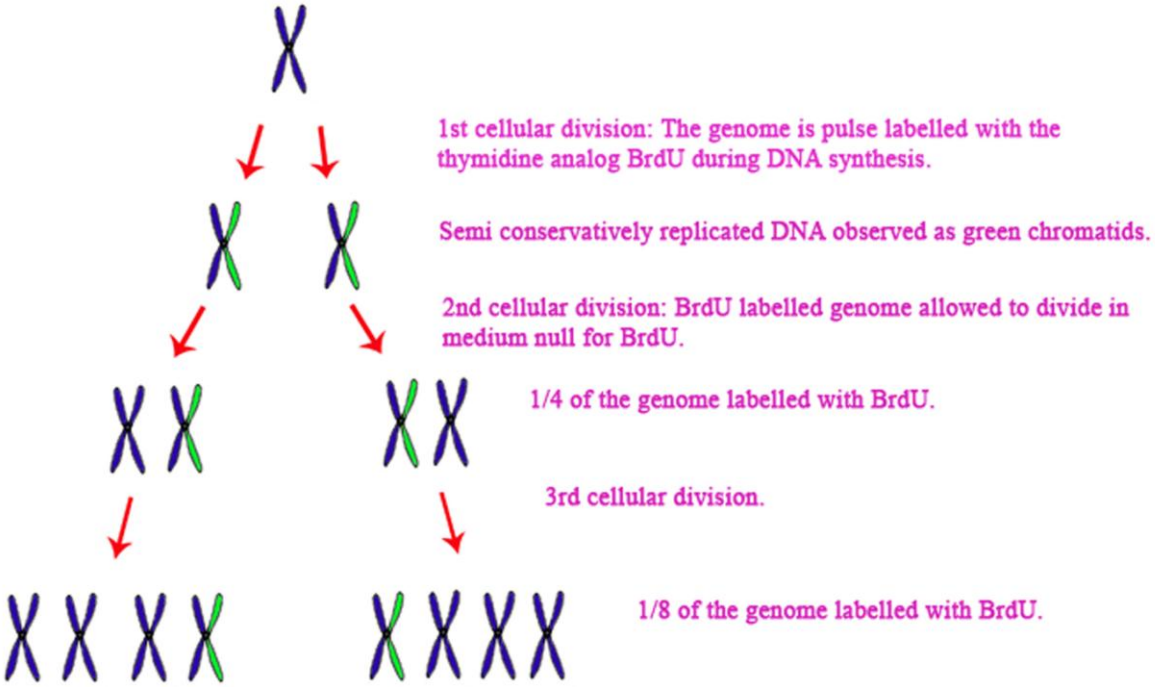

The cells are pulse labelled with BrdU and allowed to divide, in the absence of new BrdU.

Figure 1.6: BrdU labelled chromosome territories in the interphase nuclei of the Bge cells.

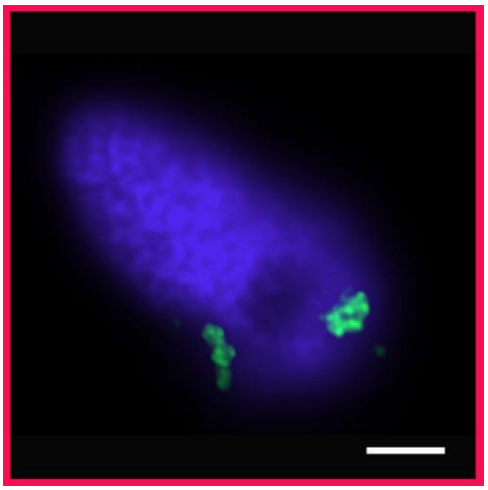

Bge cells pulse labelled with BrdU were allowed to divide over approximately 5 cell cycles and display chromosome territories in the interphase nuclei (fluorescein isothiocyanate, FITC, green). The chromosome territories were identified with antibodies against BrdU. The nuclei were counterstained with 4, 6 – diamidino-2-phenylindole (DAPI, blue). Bar, 5 µm.

The persistence of this orientation through the subsequent interphase is postulated to be manifested by interplay between chromosomes and proteins of the nuclear envelope, candidates being nuclear lamins (Cowan et al., 2001). In terms of functionality of the configuration, there is a correlation between Rabl configuration and organisms with large metaphase chromosomes (Cowan et al., 2001). Consequently, it has been postulated that the aforesaid configuration is a necessity of organisms with large chromosomes (Cowan et al., 2001).

The distribution of chromosome territories in eukaryotic organism such as mammals differs from Rabl, in that the chromosomes are distributed radially across the nucleus. In some organisms such as mammals, these territories have a high probability of being located in particular regions within the interphase nucleus i.e. internally, intermediately or towards the nuclear periphery (Croft et al., 1999, Pombo and Branco, 2007). Indeed, such probabilistic patterns of chromosome nuclear positioning are observed with chromosomes containing tandem repeats of ribosomal DNA (rDNA) known as nucleolar organizer regions (Bridger et al., 1998). Human chromosomes 13, 14, 15, 21 and 22 bearing these sequences have been found embedded in the nucleus (Bridger et al., 1998, Kalmarova et al., 2008). With regards to non random positioning of chromosome territories relative to one another, it has been shown that in the nuclei of mouse lymphocytes a single chromosome homologue from the diploid chromosomes of 12, 14 and 15 are found clustered together (Parada and Misteli, 2002). Studies correlating specific chromosomes with different regional radial locations in the interphase nucleus resulted in the development of two contrasting theories known as the size and the gene density interphase chromosome positioning theories.

1.7.2 The size theory of chromosome positioning in the interphase nucleus

Exponents of the positioning of chromosome territories according to chromosome size (Fig 1.7), propose that chromosomes are organised in the interphase nucleus in a manner whereby small chromosomes are positioned towards the interior and large chromosomes towards the periphery of the nucleus (Sun et al., 2000, Habermann et al., 2001, Bolzer et al., 2005, Rens et al., 2003). Research data supporting this theory was first presented by Sun et al (2000) in an investigation concerning human chromosomes. Sun et al, (2000) utilised nine unique subtelomeric probes for different q arms and positioned these probes in the interphase nuclei using FISH. They deduced that the q arms of the smaller chromosomes of 19 and 21 were preferentially positioned towards the interior and the q arm of the larger chromosome 1 and 2 occupied peripheral positions (Sun et al., 2000). Yokota and colleagues provided two theories explaining these observations. The first theory known as the volume exclusion model is predicated on the diversity in volume among the chromosome territories, it proposes that any particular chromosome territory is experiencing steric hinderance from another chromosome territory and because of the finite size of the chromosome territory it is limited in its ability to co-occupy the main domain of another chromosome (Sun et al., 2000).

The second size theory purports that the non-random organisation of chromosome territories in interphase nuclei is the result of the persistence the metaphase plate orientation from cellular division through to the G1 of interphase. The centromeres aggregate inside the mitotic rosette in such a manner that the larger arms of the chromosomes are positioned towards the periphery and the smaller arms towards the interior. Theoretical sustainment of this pattern into G1 would result in the consequent substantiation of this size theory (Sun et al., 2000, Bolzer et al., 2005).

Figure 1.7: A schematic diagram illustrating the organisation of chromosome territories in interphase nuclei according to the size theory.

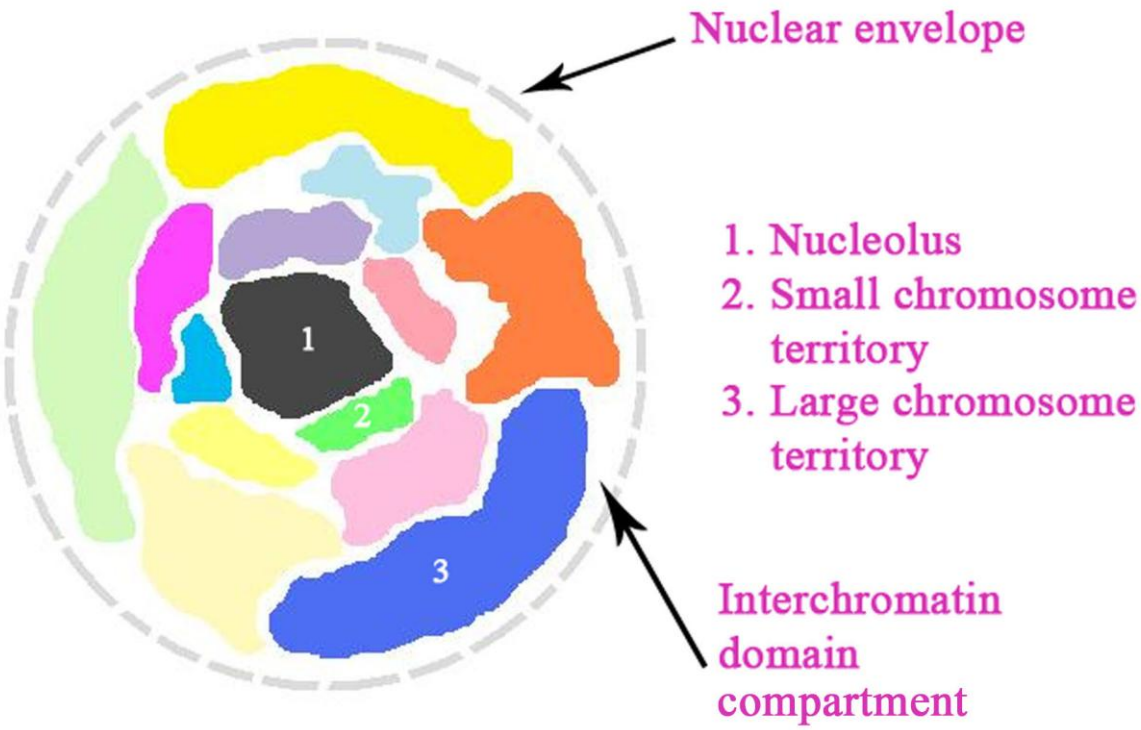

The diagram displays the nuclear envelope in grey, nucleolus in black surrounded by chromosome territories (various colours). The small chromosome territories are positioned in the interior of the nucleus (example shown with the green territory labelled 2). The large chromosome territories are positioned toward the periphery of the nucleus (example shown in blue, labelled 3). The chromosome territories are separated by the interchromatin domain compartment.

Supportive evidence for the size theory has been adduced in a number of research articles (Rens et al., 2003, Sun et al., 2000, Bolzer et al., 2005, Habermann et al., 2001). An interesting study by Cremer and colleagues focused on analysing human chromosomes in the nuclei of fibroblasts in three dimenstion. By utilising 3D FISH, Bolzer et al (2005) observed in both human fibroblasts and amniotic cells a correlation with chromosome size and interphase nuclear position, concurring with results reported by Sun et al (2000) in which small chromosomes were located towards the nuclear interior and large

chromosomes towards the nuclear periphery. In addition to Sun et al (2000) and Bolzer et al (2005) a study in 2001 by Solovei and colleagues extended the size theory to chickens. The availability of whole chromosome painting probes for macro and micro-chromosomes of the chicken nucleus aided the multi coloured 3D FISH on the non proliferative neurons and the proliferative embryonic fibroblasts from the chicken (Sun et al., 2000, Bolzer et al., 2005, Habermann et al., 2001, Rens et al., 2003). Habermann et al, (2005) deduced a size-correlated distribution of chromosomes in both the aforesaid cell types, with the macro chromosomes positioned at the nuclear periphery and the micro chromosomes positioned in the nuclear interior. In addition to size correlated positioning in chickens, another organism which adheres to this form of nuclear spatial organisation is the marsupial, *Potorous tridactylus* (Rens et al., 2003). Rens et al (2003) used syntenic whole chromosome painting probes from the rat kangaroo, *Aepyprymnus rufescens* to perform 3D FISH analysis on *P. tridactlylus*. Indeed, Rens et al (2003) observed a size dependent positioning of the *P. tridactylus* chromosomes in the interphase nuclei.

1.7.3 The gene density theory of chromosome positioning in the interphase nucleus

In opposition to the size theory, is the gene density theory (Fig 1.8). Proponents of the gene density theory have shown a correlation between the gene density of a chromosome and interphase chromosome territory position (Croft et al., 1999, Boyle et al., 2001, Neusser et al., 2007, Cremer et al., 2003, Bridger et al., 2000). This was first demonstrated by Croft et al (1999) using lymphoblast and proliferating human dermal fibroblasts. Human chromosomes 18 and 19 presented Croft et al (1999) with an apt candidate of genetic content disparity in human chromosomes whereby chromosome 19 is very gene rich and chromosome 18 is gene poor (Croft et al., 1999). Bickmore and colleagues used 2D and 3D FISH to position the aforesaid chromosomes in the interphase nuclei and found

chromosome 19 adopted an internal position and chromosome 18 a peripheral position (Croft et al., 1999). These results were subsequently substantiated in a publication by Boyle et al (2001), in which the position of all the human chromosomes in diploid lymphoblasts and primary fibroblasts were positioned (Boyle et al., 2001). They observed that the majority of the gene rich chromosomes were located in the interior of the nucleus and the gene poor chromosomes towards the periphery.

Figure 1.8: A schematic diagram illustrating the organisation of chromosome territories in interphase nuclei according to the gene density theory.

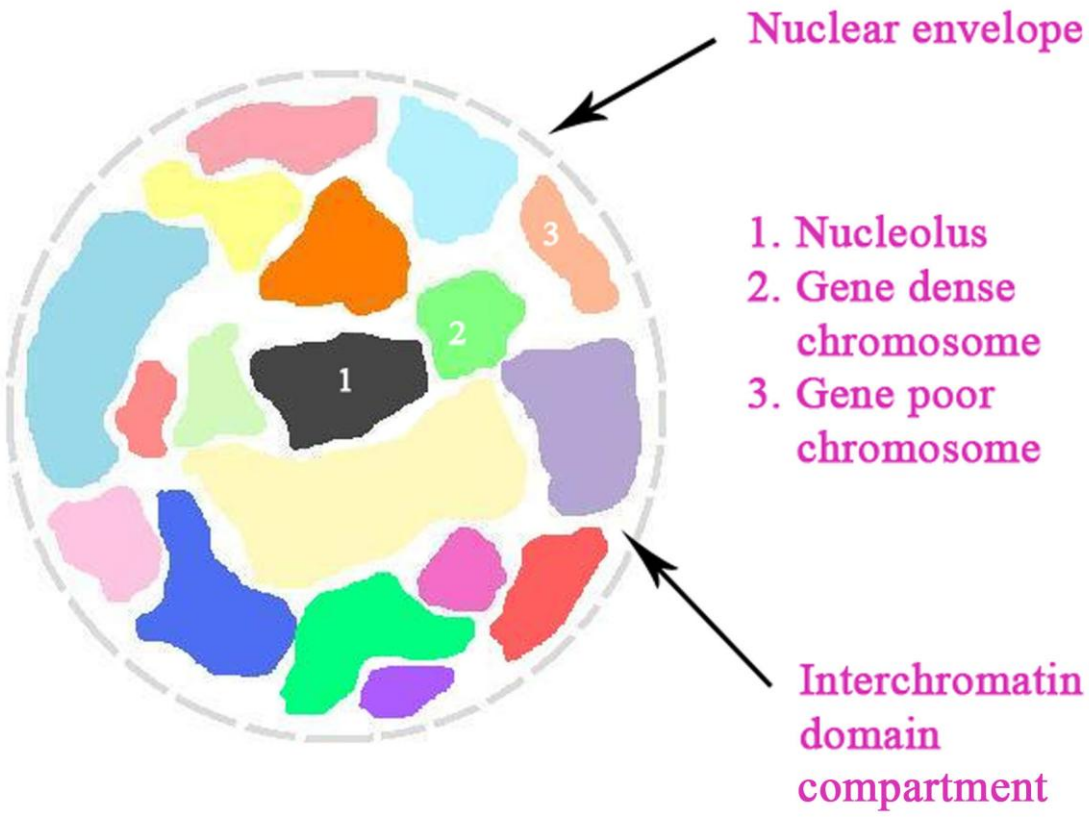

The diagram displays the nuclear envelope in grey, the nucleolus in black with the surrounding chromosome territories (various colours). The gene dense chromosomes are positioned in the nuclear interior (example shown in green, labelled 2) and the gene poor chromosomes are positioned towards the periphery (example shown in pink, labelled 3). The chromosome territories are separated by the interchromatin domain compartment.

In accordance with the results from Boyle et al (2001) and Croft et al (1999) was a 2003 study by Cremer et al (2003) which investigated the positioning of human chromosomes 18 and 19 in six normal cell types and in eight tumour cell lines. As well as finding corroborative gene density positioning results, they also observed altered positioning, with an increased number of nuclei from the malignant cells exhibiting more internal positions for chromosome 18 relative to that of chromosome 19 (Cremer et al., 2003).

1.7.4 Alterations in spatial genome organisation

The exact mechanisms which govern the spatial organisation of the genome within the interphase nucleus have yet to be fully elucidated. It might be the case that the aforementioned competing theories of size and gene density dependent chromosome territory positioning are not mutually exclusive or indeed that they work in tandem with an additional variable (Meaburn et al., 2008). Evidence which substantiates this view has been adduced with regards to alterations in chromosome territory position during cellular differentiation (Foster et al., 2005). The study by Foster et al (2005) investigated the positioning of chromosomes in porcine sperm nuclei using 2D FISH and deduced alterations in the nuclear position of the X and Y chromosomes during spermatogenesis (Foster et al., 2005). During differentiation, changes in chromosome positioning during disease has also been demonstrated (Meaburn et al., 2007). This study investigated interphase chromosome positioning in proliferating cells with mutations to A-type lamins (an integral protein of the nuclear lamina); the mutation is associated with a disease of tissue mutations and premature aging in humans (termed laminopathies). Meaburn et al (2007) found that proliferating laminopathy fibroblast displayed altered nuclear positioning of chromosomes 18 and 13 (Meaburn et al., 2007).

The organisation of the interphase nucleus extends to the position of gene loci. Indeed, there is evidence correlating the spatial positioning of genomic loci with gene expression (Ragoczy et al., 2003, Williams et al., 2006, Ballabio et al., 2009, Szczerbal et al., 2009). A study by Bridger and colleagues revealed specific porcine gene loci radiating from specific chromosome territories upon transcription activation during adipogenesis (Szczerbal et al., 2009). In fact, loops of chromatin have been exhibited emanating away from particular chromosome territories (Volpi et al., 2000, Williams et al., 2006). However, correlation does not precipitate cause and it has yet to be established whether these changes in gene location are a consequence of transcriptional activation or whether they have a contributory role.

1.7.5 Chromatin organisation and histone proteins

The foundation of chromatin is the nucleosome which is formed from histone octomers and includes H2A, H2B, H3 and H4 (Rice et al., 2003, Lachner and Jenuwein, 2002). These histone octomers are surrounded by two 146 bp super-helical turns of DNA (Lachner and Jenuwein, 2002). The nucleosome units are connected by histone linker protein 1 (Strahl and Allis, 2000). The structural state of chromatin can be dynamically altered; such alterations can be transitorily reflected in gene expression (Huang et al., 2007). Indeed, these structural states are classified accordingly: euchromatin is enriched with actively transcribed genes such as housekeeping genes (in humans, actin and GADPH), which are early replicating and are typified by decondensed (open state) chromatin (Peters et al., 2002, Skalnikova et al., 2007). Heterochromatin consists predominantly of inactive, late replicating genes and has a condensed chromatin state. Heterochromatin can be subcategorised into facultative heterochromatin whereby the chromatin state differs between different cell types and is often developmentally regulated

e.g. the inactive X_i chromosome in female mammals can vary between different cell types and has a condensed heterochromatic morphology and replicates late in DNA synthesis (Boggs et al., 2002, Skalnikova et al., 2007, Peters et al., 2002). In contrast, constitutive heterochromatin is found in specific regions such as the centromere, pericentric locations, nucleolar organizer regions and telomeres (Lachner and Jenuwein, 2002).

Covalent post-translational modification to histone amino acid termini are thought to function in chromatin organisation (Fuks, 2005). These modifications can manifest in the form of methylation, acetylation, ubiquitination, phosphorylation, sumoylation, citrullination and ADP-ribosylation (Strahl and Allis, 2000). The histone-histone and histone-DNA interactions are postulated to influence gene expression by altering the accessibility of the DNA to activators and inhibitors of transcription (Fuks, 2005).

Histone modifications serve as transcriptionally active and repressive markers. Of particular interest is the methylation of lysine residues on histones 3 and 4 (H3 and H4). Indeed, modifications associated with transcriptional activation include methylation to lysine 4, 36 and 79 of H3 (Schotta et al., 2004); whereas methylation to the lysine residues of H3K9 (Schotta et al., 2004, Soppe et al., 2002) and H4K20 (Regha et al., 2007, Shi and Dawe, 2006) have been correlated with transcriptional inactivation and repressive chromatin conformations. These modifications to histone proteins can be visualised fluorescently in interphase nuclei using antibodies raised against specifically modified histones proteins (Strasak et al., 2009, Skalnikova et al., 2007, Bartova et al., 2005). Indeed, the modified histone proteins can be observed as specific patterns of foci distribution in the interphase nucleus, often correlating with regions of heterochromatin and euchromatin (Bartova et al., 2005). Global alterations and differences in chromatin composition and nuclear histone modification patterns have been correlated with changes from proliferating to non-proliferating cells (Baxter et al., 2004), embryonic to

differentiated cells (Wen et al., 2009), oncogenesis (Kondo et al., 2008, Wiencke et al., 2008) and random X chromosome inactivation in mammals (Mermoud et al., 2002, Boggs et al., 2002).

1.8. Summary

The snail *Biomphalaria glabrata* is the intermediate host to the parasite *Schistosoma mansoni*. This parasite is responsible for the human disease schistosomiasis, which is prevalent in many parts of the world. Current research into schistosomiasis has focused on preventing the spread of the disease via the development of vaccines and methods to halt the transmission of the schistosome parasite from the intermediate host to the definitive human host. *S. mansoni's* new world host *Biomphalaria glabrata* presents itself as topic of study in preventing the spread of schistosomiasis. The existence of different strains of *B. glabrata* with different susceptibility traits to the *S. mansoni* parasite has provided a point for molecular study i.e. investigating the up/down modulation of genes post exposure to the parasite. Moreover, the existence of an immortal cell line derived from the embryos of *B. glabrata* (Bge cell line, the only molluscan cell line in existence) has provided a suitable *in vitro* model for host-parasite studies.

Changes to the expression of genes in *B. glabrata* upon exposure to the *S. mansoni* intimates that the parasite has the ability to manipulate the genome of *B. glabrata*. The genome in terms of the interphase nucleus is highly organised. The chromosomes occupy discreet contained locations within the interphase nucleus known as chromosome territories. These territories have been demonstrated to be radially located probabilistically in different regions of the nucleus according to size and gene density. Indeed, the organisation and control of the genome extends to the location of gene loci and chromatin proteins known as histones which can post-translationally alter gene expression.

This thesis will focus upon investigating the genome organisation of *B. glabrata in vitro* and *ex vivo.* In addition, an analysis of how the host-parasite interaction impacts upon the *B. glabrata's* genome will be undertaken.

Chapter 2:
Characterisation of the *Biomphalaria glabrata* embryonic cell line

2. Characterisation of the *Biomphalaria glabrata* embryonic cell line

2.1 Introduction

2.1.1 Classical molluscan cytogenetics and the Bge cell line

The work of Hansen (1976) in establishing the *B. glabrata* embryonic (Bge) cell line aided the efforts that led to most of what we currently know today about the molecular genetic interactions between trematode and the intermediate snail host *in vitro* (as reviewed in chapter 1). Before the cell line was established, much of the work focused on maintaining molluscan organs *in vitro* (Benex, 1961, Benex, 1965). Development of cell lines from other molluscs, such as the oyster *Crassostrea gigas* and the hard clam, *Meretrix lusoria*, have been attempted and primary cultures were successfully maintained for only up to 5 months (Chen and Wang, 1999), thus making the Bge cells the only established cell line from molluscs. Despite this overall advantage, these cells are an underutilized resource. The Bge cells' competence as a model for the *in vitro* development of *S. mansoni* was demonstrated when in the presence of these cells, miracidia were able to transform and most significantly, complete the intramolluscan cycle from miracidium to cercaria (Ivanchenko et al., 1999, Coustau and Yoshino, 2000). By co-culturing these cells with the helminth parasites, it has been possible to examine the *in vitro* response to parasitic antigens and excretory–secretory (ES) products (Coustau and Yoshino, 2000). Indeed, some have shown that ES products from *S. mansoni* can stimulate the p38 signalling pathway of Bge cells, a response that is associated with stress factors, such as UV light, osmotic changes and heat shock (Sano et al., 2005, Humphries and Yoshino, 2006).

Patterson and Burch (1978) performed the pioneering work in the field *B. glabrata* chromosome analysis. They identified the basic chromosome number of planorbidae snail genera (which includes *B. glabrata*) as 2n = 36. Another important schistosome

intermediate host, genus *Bulinus* exhibits diploid, tetraploid, hexaploid and even octoploid levels of polyploidy (Goldman et al., 1984). Raghunathan (1976) described the karyotype of *B. glabrata* by organising chromosomes into groups of metacentric, submetacentric, acrocentric and telocentric (in accordance with centromere position as stipulated by Levan et al. (1964), as well as confirming a diploid number of 36 chromosomes (Levan et al., 1964). Subsequently, Goldman et al. (1984) produced another karyotype of *B. glabrata*. As reviewed in section 1, both karyotypes were derived from the snail and not the Bge cell line.

The laboratory in which Hansen established the Bge cell line also pursued research using the mosquito cells from *Aedes albopictus*. Consequently, there was some concern regarding the contamination in the Bge cells from those of *Aede albopictus*. Bayne et al. (1978) performed a detailed analysis of the Bge cell line developed by Hansen (1976) with respect to its' antigenic determinants, behavioural, enzyme characteristics and karyotype, prior to depositing the cells at the American Type Culture Collection (ATCC, Manassas, USA). With regards to antigenic comparisons, Bayne et al (1978) utilised micro-Ouchterlony double diffusion gels to confirm that the antigens from *Aedes albopictus* do not cross react with those from anti-*B. glabrata* serum and that antigens from extracts of the Bge cells are homologous to those from those of *B. glabrata*. Furthermore, the analysis of enzymes from the Bge cells and *B. glabrata* extracts via poly-acrylamide gels revealed single eletrophoretic loci for gluco-6-phosphate dehydrogenase and malic dehydrogenase, underpinning the Bge cells origin from *B. glabrata*. The cytogenetic characterisation of the Bge cell line was performed by comparing the chromosomes from the Bge cell line with those from the karyotypes of Raghunathan, (1976) and Burch (1960).

The Bge cells that were deposited by Dr. C. Bayne are currently available from ATCC (Catalog No. CRL-1494TM) where they are described as only being loosely adherent, which is in contrast to their original morphology, described as monolayer forming fibroblast like cells (Hansen, 1976, Bayne et al., 1978). Bayne et al (1976) produced chromosomes from the Bge cells by arresting the Bge cells in metaphase using colcemid and employing Hanks' buffered saline (HBS) solution as a hypotonic agent. The metaphase spreads produced on microscope slides were stained with Giemsa. Bayne et al (1976) identified 36 chromosomes in accordance with the diploid number observed in *B. glabrata* by Burch (1960), Raghunathan (1976) and substantiating the chromosome complement observed in the Bge cells by Hansen (1976). It was documented in the Bayne et al (1976) publication that there were no discernable differences in the chromosomes from the Bge cells and those from the embryos of *B. glabrata* (Raghunathan, 1976). In contrast to Raghunathan (1976), the chromosomes were classified into six groups as oppose to five.

2.1.2 Aneuploidy and cell lines

Aneuploidy defines the situation whereby the chromosome complement of a daughter cell differs from the exact multiple of the haploid number (Shi and King, 2005). The terms aneuploidy and polyploidy (although sometimes used interchangeably) define different genetic situation in the cell (cells with polyploidy possess an excess of two complements of homologous chromosomes). Aneuploidy has been documented in many different organisms such as humans (Boormans et al., 2009), mice (Rao et al., 2009) and oyster (Bouilly et al., 2007, Bouilly et al., 2006). The aberrant chromosome number in aneuploidy might be due to the duplication or absence of one or more chromosomes. Mechanistically, aneuploidy is the result of non-disjunction, which is the failure of homologous

chromosome separation during anaphase, resulting in the deposition of duplicated chromosomes into the same cell (Shi and King, 2005). It was postulated by Shi and King (2005) that non-disjunction is not the primary causative mechanism behind aneuploidy, but rather acts to produce tetraploid (4n) cells which after several cell cycles become aneuploidy (Shi and King, 2005). If this is case, then other forms of tetraploidy production could give rise to aneuploidy cells, for example cellular fusion, which can occur naturally in human cells (Ogle et al., 2005). Another initiator of tetraploidization has been hypothesised by Shi and King (2005), which theorises that non-disjunction may result in chromatin being trapped in the cytokinetic furrow (the cellular indentation which proceeds cytokinesis). This may encourage the regression of the cleavage furrow (termed cleavage furrow regression) thereby negating cellular division, leaving the cell tetraploid.

Aneuploidy and polyploidy has been documented in transformed cell cultures from mouse embryonic fibroblasts (Hagos et al., 2009), Chinese hamster ovary cells (Cantero et al., 2006) and immortalized human mesenchymal stem cells (Takeuchi et al., 2009). A definitive answer as to the reason for the propagation of aneuploidy cells over normal diploid cells remains elusive. Some have hypothesised that the cells with increased chromosome complements are imbued with a buffering mechanism against cell cycle arrest elements which are normally initiated as a result of DNA damage and breakage (Ganem et al., 2007). One may expand on this hypothesis in such manner; the presence of an excess of normal chromosomes may increase the proliferative capacity of cells with damaged DNA by perturbing the effects of cell cycle dependent proteins such as p53 (Ganem et al., 2007).

2.1.3 Characterising the Bge cell chromosomes

The Bge cells are an important resource to the parasitological and molluscan field of research. Since the Bge cell line development in the 1970s, there has been one published

study on the chromosomes of the cell line (Bayne et al., 1978). As an important *in vitro* resource to those investigating the host-parasite relationship between *B. glabrata* and *S. mansoni,* it is important that the genome of the Bge cells is characterised.

Methodology concerning the cytogenetic analysis of the chromosomes from *B. glabrata* is not comparable to those for mouse and human chromosomes. The *B. glabrata* chromosomes are small and good spreading of metaphase chromosomes has been essential to recognising specific chromosomes (Odoemelam et al., 2009). This chapter will firstly describe the establishment of a suitable hypotonic method for producing identifiable, well spread metaphases. Secondly, this chapter will describe the attempt at producing G-banded chromosomes from the Bge cell line. Finally, a description of the analysis of the DAPI stained chromosomes of the Bge cell lines from two different sources, named here as Bge 1 (E.S. Loker Laboratory) and Bge 2 (C. Bayne Laboratory). This analysis led to the construction of a revised karyotype that reveals extensive aneuploidy in the cell line isolates (Odoemelam et al., 2009).

2.2 Materials and Methods

During the past several years, different vials of Bge cells have been independently purchased from the ATCC and to date have failed to propagate in the Laboratory of Nuclear and Genomic health at Brunel University and in that of collaborators from the BRI (Biomedical Research Institute, Rockville, USA). Personal communication with the technical support at the ATCC indicated that the cells are currently not being actively propagated due to lack of demand and also low availability of their stocks. Because of the failed attempts to propagate commercially purchased Bge cells from the ATCC, the Bge cells were obtained from two different sources, the original ATCC depositor Dr. C. Bayne (Oregon State University, Corvallis, USA), and Dr. E.S. Loker (University of New

Mexico, Albuquerque, USA). The interest was to characterize the isolates from these two different sources prior to using them for any molecular analysis, since slight differences were observed in their physical characteristics, for example in their ability to adhere, form monolayers and in their generation time.

2.2.1 Bge cell culture

Bge cells used in this study were obtained from the laboratories of Dr. E.S. Loker (Bge 1) and Dr. C. Bayne (Bge 2). Both cultures were derived from Hansen's original Bge cell line (Hansen, 1976) and were grown in the absence of carbon dioxide, at 26^{o}C in medium that comprised of 22% Schneider's *Drosophila* medium (Invitrogen, Paisley, UK), 0.13% galactose (Invitrogen, Paisley, UK), 0.45% lactalbumin hydrolysate (Invitrogen, Paisley, UK) and 14.1 µM phenol red. The medium was sterilised using a 0.22 µm pore filter (Fisher Scientific UK Ltd., Loughborough, UK) and the antibiotic gentamicin (Invitrogen, Paisley, UK) was added post-filtration at a concentration of 20µg/ml. The Bge medium was made complete by adding 10% FBS (v/v, Hyclone, Cramlington, UK) which had previously been inactivated at 56^{o}C for 30 min. The Bge cells were passaged when their confluence had reached approximately 80% and then reseeded at a 1:12 dilution. Since trypsinization of either cell line isolates over 10–15 passages resulted in the loss of viability of the cells and ultimately led to cell death, the cells were released using either a cell scraper (Falcon, Becton Dickinson Labware, Franklin Lakes, NJ) or by firm tapping motion.

2.2.2 Bge cellular fixation and established hypotonic concentration and incubation time

The Bge cells were arrested in metaphase using the mitotic inhibitor colcemid. 200 µl of Colcemid (10 µg/ml) dissolved in Hank's balanced salt solution (Invitrogen, Paisley, UK)

was added to T75 flasks (Fisher Scientific UK Ltd., Loughborough, UK) of Bge cells (at the stage of 70–80% confluence). Five different flasks containing the Bge 1 cells were incubated with the colcemid for duration of 1.5 hr at 26^{o}C. The cells were subsequently dislodged and then centrifuged at 400g at 15^{o}C. The cell pellets were resuspended by vigorously tapping the tube, followed by the addition of hypotonic potassium chloride solution (0.05 M) and subsequent fixation with methanol and acetic acid (3:1 v/v).

2.2.3 Slide preparation

Twenty microliters of the Bge cellular suspension was then applied onto a glass slide using a Gilson pipette at an angle of 45^{o} to achieve metaphase chromosome spreads. Glass slides of fixed Bge cellular suspensions were stained with the DNA intercalator DAPI (4′,6-diamidino-2-phenylindole). Ten microliters of 2 μg/ml DAPI in Vectorshield anti-fade mountant (Vector Laboratories, Peterborough, UK) was applied to the slide and covered with a 22 x 50 mm coverslip.

2.2.4 G- banding the Bge cell chromosomes

The attempts to G-band the Bge cell chromosomes involved the use of the following two protocols:

Protocol A was derived and modified from trypsin G-banding method in Human cytogenetics: constitutional analysis; practical approach (Rooney, 2001). The aforementioned method has been utilised and cited in other publications (Vanagaite et al., 2006, Murthy et al., 2008, Trimborn et al., 2004).

Protocol B was adapted from Goldman et al (1983) and has been cited in Goldman et al (1984) as a method used to G-band planorbid genera snails such as *Bulinus* and our putative *Biomphalaria*.

2.2.4.1 Protocol A

Protocol A was modified in order to optimize the banding in *B. glabrata* chromosomes. This optimization involved two phases. Phase 1, involved giemsa staining and was an assessment of the optimum trypsin concentration and incubation time. Phase 2, followed on from Phase 1, and was an assessment of the optimum incubation time in giemsa solution.

Slide preparation

By utilising the established optimum concentration of hypotonic KCl solution of 0.05M, the Bge cells were cultured and glass slides of fixed Bge cellular suspension prepared as previously explained in section 2.2.1. The slides were aged in the laboratory at room temperature for 5 days before G-banding.

Phase 1

The aged slides were subjected to trypsin G-banding which involves the main steps of the trypsinization and subsequent staining with giemsa solution. The trypsin solutions were prepared from 1:250 trypsin (Gibco, Invitrogen). Trypsin solutions of 0.0125, 0.025 and 0.05% (w/v) were prepared. The five day aged slides were incubated in the aforementioned different concentrations of trypsin. For each trypsin concentration, different incubation times were examined, these were 20, 30 and 40 sec. Following the trypsinization, the slides were washed thoroughly in ice cold 1X PBS (137 mM NaCl, 2.7 mM KCl, 10mM

Na_2HPO_4 and 2mM KH_2PO_4 in ddH_2O) for 1 min. They were subsequently stained for 3 min in 5.5 % giemsa modified stain (Sigma Adrich) in phosphate buffer consisting of 0.025M KH_2PO_4 in ddH_2O (v/v), titrated to pH 6.8 with 10% NaOH (v/v). Finally, the slides were rinsed briefly in ddH_2O and air-died. 20µl of DPX mountant (Biotech Sciences Ltd) and a 22 x 50 mm coverslips was added to the slides.

Phase 2

As consequence of the results from phase 1; metaphase spreads were aged 5 days and trypsinized with 0.025% of trypsin for 30 sec. The slides were then washed in same way as in phase 1. These slides were incubated in 5.5 % Giemsa modified stain solution for different durations of 1, 2, 3, 4 and 5 min. They were subsequently washed and mounted as in the aforementioned phase 1.

2.2.4.2 Protocol B

Slide preparation

The slides of metaphases spreads were prepared as described in sections 2.2.4.1. However, as opposed to aging the slides for 5 days at room temperature, the slides were aged in a drying oven at 60^oC for 24 hr before implementing the subsequent protocol.

Following the oven incubation, the metaphase spreads were allowed to cool to room temperature before an incubation in coplin jars contain 2X sodium salt citrate (SSC) (0.3M NaCl, 0.03M tri-sodium citrate; pH 7.0) at 60^oC. Two different incubation times of 60 and 90 min were used. The slides were rinsed thrice in ddH_2O before staining in 2% (v/v) Gurrs' giemsa stain improved R66 (BDH chemicals, VWR). After an incubation of 12 min,

the slides were washed five times in ddH_2O and then dried at room temperature. The slides were mounted and visualised as described in sections 2.2.4.1.

2.2.5 Slide preparation for DAPI karyotyping

Glass slides of Bge cellular suspensions fixed with methanol and acetic acid were stained with the DNA intercalator DAPI. Ten microliters of 2 µg/ml DAPI in Vectorshield anti-fade mountant (Vector Laboratories, Peterborough, UK) was applied to the slide and sealed with a 22 x 50 mm coverslips.

2.2.6 Image capture of G-banded and DAPI stained chromosomes

The brightfield images of the G-banded chromosomes were captured with Zeiss EC Epiplan Neofluar objective. The chromosomes were visualised using an epifluorescence microscope and X100 oil immersion objective (Zeiss, Axioplan 2). The images were captured using a charged coupled device (CCD) camera (RS Photometrics Sensys camera model KAF1401E G2) and the program Smart capture 3.00 (Digital Scientific). The greyscale images of the chromosomes were inverted using IPLab software (Scanalytics, BD Biosciences, San Jose, CA). The images were subsequently saved as TIFF files and visualised using the program Adobe Photoshop 5.0.2.

For the DAPI karyotyping, the chromosomes were digitally isolated and arranged initially according to size and then centromere position. Fifty images for both the Bge 1 and 2 cell line isolates were analysed in total. The chromosomes were organised into groups of large metacentric (group A), large submetacentric (group B), large acrocentric (group C), medium metacentric (group D), medium submetacentric (group E) and small acrocentric (group F). They were then grouped with other homologous chromosomes. Single chromosomes without a designated homologous copy were grouped as ‘unassigned’.

2.3 Results

2.3.1 Establishing a protocol for producing metaphase chromosomes from Bge cells

Figure 2.1: Representative images of DAPI stained Bge cell metaphase spreads prepared with different incubation times in and different concentrations of hypotonic KCl solution.

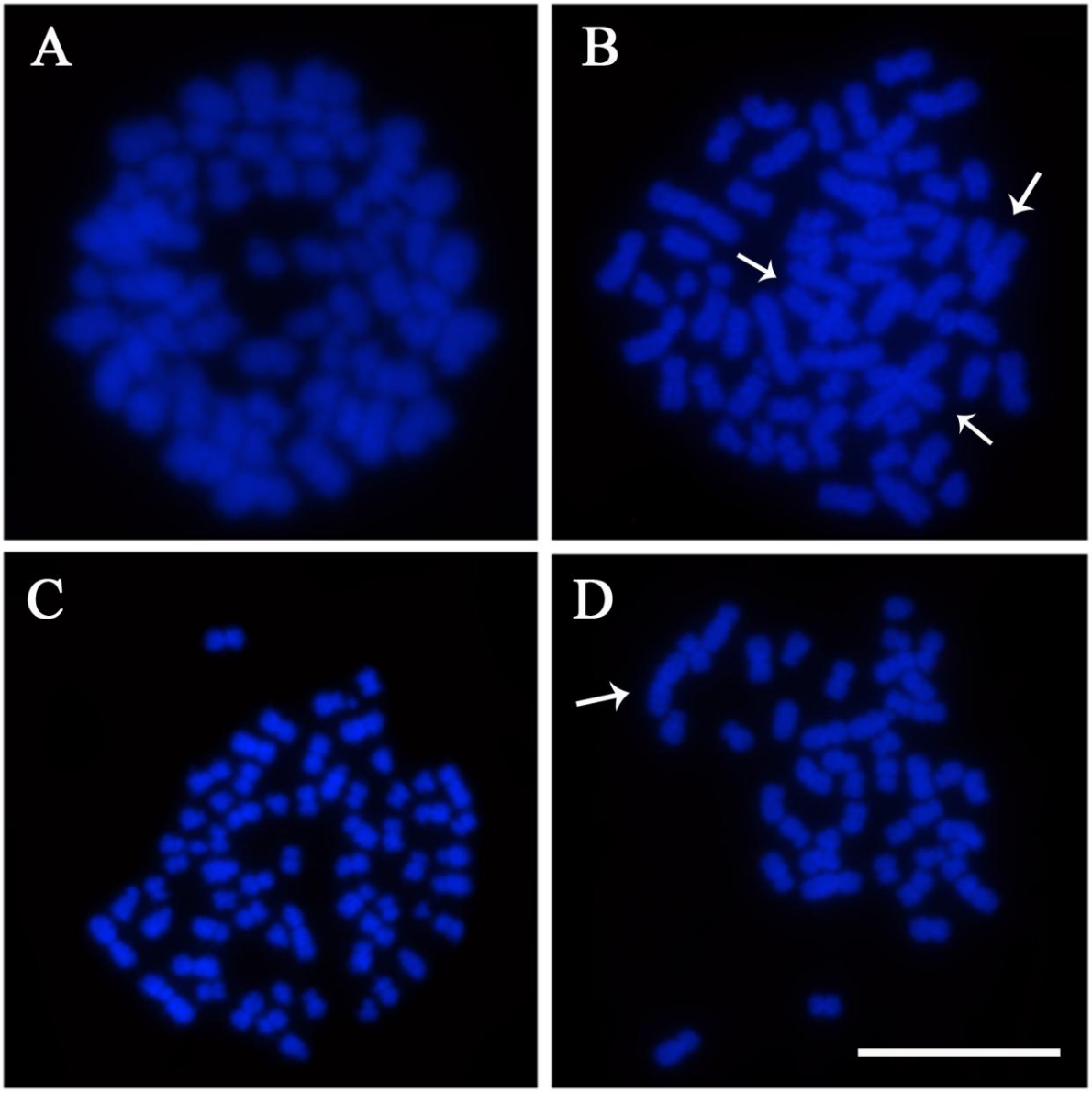

Representative images of DAPI stained Bge cell metaphase spreads prepared with different concentrations of hypotonic KCl solution. The metaphase spreads in Images (A) and (B) were prepared with 0.075 M of KCl and were incubated for 15 and 20 min respectively. Images (C) and

(D) were prepared with 0.05 M of KCL and were incubated for 15 and 20 min respectively. Bar = 10 μm.

The deployment of cytogenetic techniques is the base and starting point to understanding an organisms' genome. For organisms like *B. glabrata*; an organism whose genome is comparatively under-researched with respect to that of humans, a lot of the established cytogenetic techniques need to be manipulated in order for them to be successful in aiding proper and constructive analysis. Indeed, the field of analysis of chromosomes from *B. glabrata* to date remains under-researched and as a consequence we have had to establish protocols to produce chromosomes of an appropriate standard for analysis. Hypotonic solution is routinely used in the fixation of cells. The solution via osmosis, swells the cells to an extent where cell membrane becomes fragile and when subjected to force, such as the impact onto a glass slide and the surface tension, results in spread metaphase chromosomes. The crux of this techniques lies with the concentration and the incubation time of the hypotonic KCl solution with the cells. If the incubation time is too short or the concentration is too high, then the metaphases produced will be under spread. In opposition; a longer incubation time or a low concentration may lead to over-spread chromosomes. Indeed, these were parameters utilised to attain well spread chromosomes.

Fig 2.1 displays a selection of representative images from the use of different concentrations of hypotonic solution and incubation times. Fig. 2.1 A shows a very under spread metaphase, which was prepared using 0.075 M of KCl with an incubation time of 15 min. The chromosomes are very hard to distinguish from one another, in particular the smaller chromosomes which are very close to each other another. Fig 2.1 B was prepared with the same concentration of hypotonic solution but with an extended incubation of 20 min. The chromosomes are more spread with a clear separation between the different chromosomes. Yet, even with this longer incubation time, there were quite few over-

lapping chromosomes (as denoted by the white arrows). These over-lapping chromosomes make it very difficult to analyse the individual chromosomes and consequently, pair homologues (especially if the overlapping occurs across the centromere). Fig 2.1 C and D display the representative images of the use of a lower concentration of 0.05 M of KCl and incubation times of 15 and 20 min respectively. The chromosomes in both images are very well spread, with absence of over-lapping aiding cytological analysis. Although the chromosomes in Fig 2.1 D appear well spread; the metaphase itself is incomplete. There are chromosomes missing from the spread, such as a homologue for the largest chromosome (as denoted by the white arrow). The metaphase is overly spread and missing some chromosomes; indeed these mssing chromosomes have been dispersed across the slide and have formed what is known in cytological terms as 'chromosome soup'. This renders the chromosomes in this metaphase inadequate for analysis. However, the chromosomes in Fig 2.1 C are well spread with the chromosomes not being too far apart from each other.

Hence, although both the concentrations of 0.075M and 0.050M can be used to attain metaphase spreads from the Bge cells, it the incubation time of 15 min with 0.05M which produced well spread chromosomes, without overlapping or missing chromosomes. This method can consequently be utilised to produce *B. glabrata* chromosomes for karyotyping, gene mapping and further genome analysis.

2.3.2 G-banding the Bge cell chromosomes

The results obtained using the giemsa banding protocols were quite variable and yielded bands of poor standard despite efforts at experimental optimisation.

Protocol A was based on the protease denaturation of the chromosomes with trypsin. Fig 2.2 shows Phase 1: G-banding of the *B. glabrata* chromosomes using variable

concentrations and incubation times in trypsin solution, whilst maintaining a constant incubation time in giemsa stain of 3 min.

Figure 2.2: Representative brightfield images of G-banding in Bge cell chromosomes using different trypsin concentrations and incubation times.

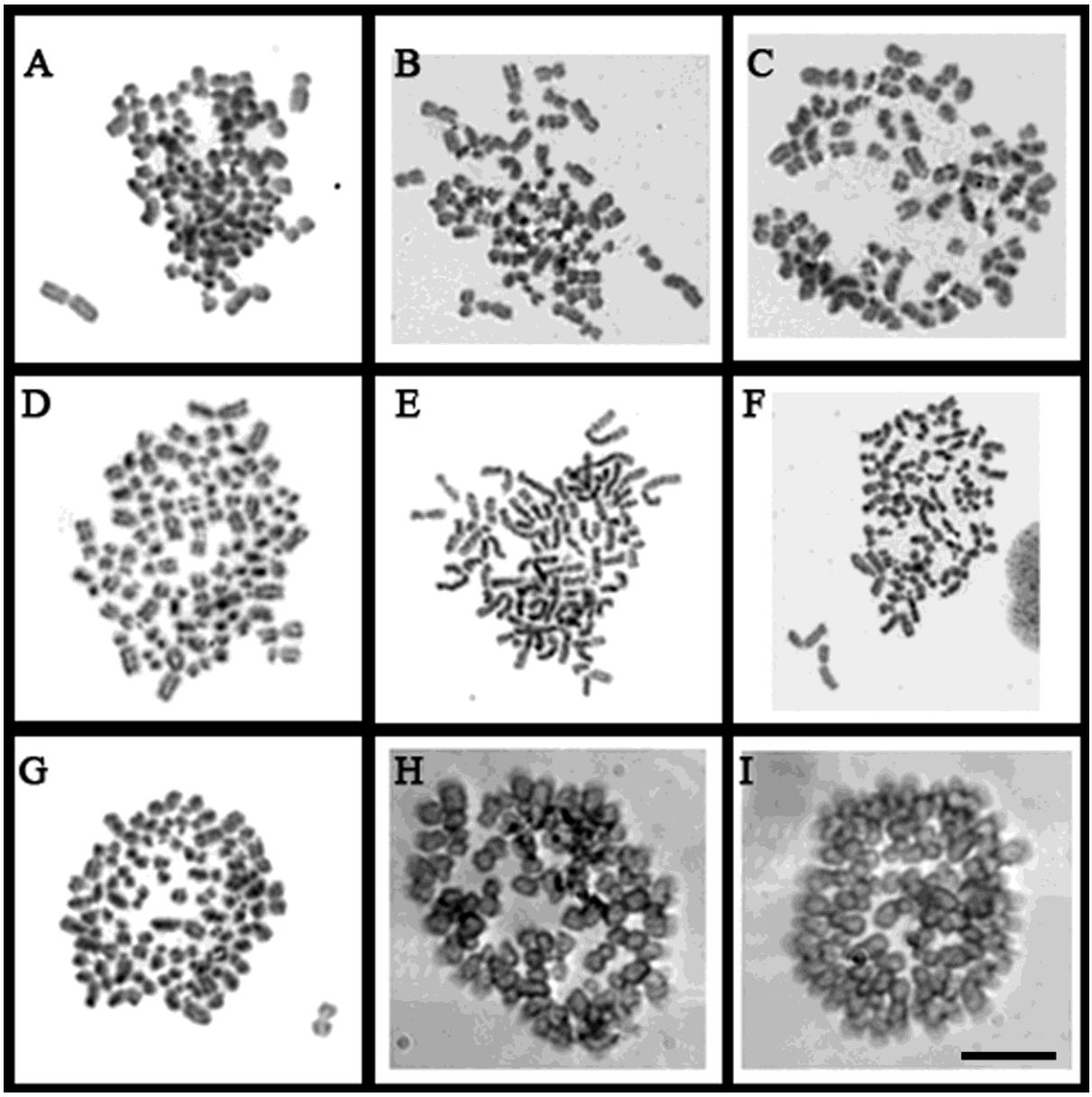

Representative brightfield images of G-banding in Bge cell chromosomes using different trypsin incubation times and concentrations. Images A-C represents the respective 20, 30 and 40 seconds incubation in 0.0125% of trypsin. Images D-F represents the respective 20, 30 and 40 seconds incubation in 0.0025% of trypsin. Images G-I represent the respective 20, 30 and 40 seconds incubation in 0.005% of trypsin. Following trypsinization, the chromosomes were stained with giemsa stain for 3 min. Bar = 10 µm.

At the lowest concentration trypsin of 0.0125%, (Fig 2.2, A-C), the morphology of the chromosomes is unaltered by the protease. Fig 2.2 A and B show that at the incubation times 20 and 30 secs, there are few dark giemsa staining regions, with the chromosomes mainly homogenously stained with no demarcation between dark and light bands. However, at 40 sec, Fig 2.2 C, the dark regions appear more defined. Fig 2.2 D-F reveals the effects of doubling the above stated trypsin concentration to 0.025%. The incubation times 20, 30 and 40 seconds at this concentration produced more definable bands than was observed at half the trypsin concentration. As well as producing bands, the effect of the protease didn't impinge too greatly upon chromosomal morphology.

The subsequent doubling of the trypsin concentration to 0.05%, shows the over trypsinization (Fig 2.2 G-I). Fig 2.2 G at 20 sec shows the first signs of an unravelling of chromosomal architecture, as the chromosomes appear plump and swollen; although there are still some dark regions. Fig 2.2 H and I, shows extensive denaturation, the morphology of most of the chromosomes has altered majorly and they appear very large and pale.

The deduction from these experiments was that the trypsin concentration of 0.025% was the optimum band resolution for the *B. glabrata* chromosomes. At this concentration, an incubation time of 30 sec revealed the most bands (Fig 2.2 E).

As a consequence, the next step was optimizing the G-banding by adjusting the incubation time in giemsa staining solution (Phase 2) using the aforestated trypsin concentration and incubation time (Fig 2.2 E). Fig 2.3 A-C, respectively display the results from the shortest incubation times of 0.5, 1 and 2 min in giemsa stain. At 0.5 min (Fig 2.3 A) the chromosomes appeared paler than previously observed in Fig 2.2 E, with a few dark regions. Fig 2.3 B and C are slightly darker and with a few bands. The incubation of 3 min in giemsa staining solution (as utilised in Phase 1) reveals more bands (Fig 2.3 D). The bands also appear darker and more distinct. The longer incubation times of 4 and 5 min,

resulted in less bands and more homogenously stained chromosomes. Fig 2.3 E shows many dark regions, yet the bands are not as obvious as those observed in Fig 2.3 D. Fig 2.3 F shows the longest incubation in giemsa staining solution and displays no visible bands.

Figure 2.3: Representative brightfield images of trypsinized Bge cell chromosomes stained for different durations of time in giemsa solution

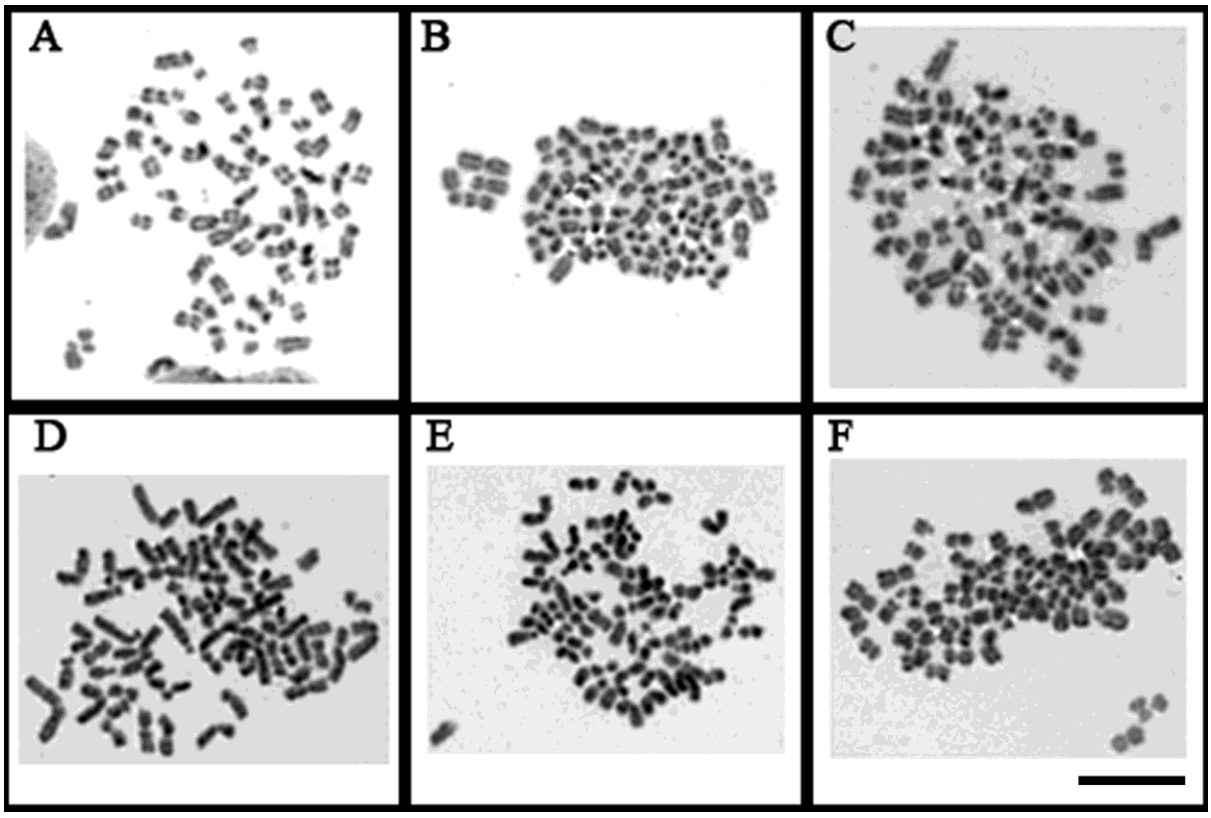

Representative brightfield images of trypsinized Bge cell chromosomes stained for different durations in giemsa solution. Images A-F corresponds with the giemsa staining times of 0.5, 1, 2, 3, 5, and 6 min respectively. The trypsin solution concentration of 0.025% was the same for all experiments. Bar = 10µm.

The G-banding protocol B utilised hot saline solution as a means of denaturing the chromosomes to reveal the bands. The incubation time was varied in this experiment and the giemsa staining time of 12 min kept constant. Fig 2.4 A and B, represent respective 60

and 90 min incubations in Gurr's giemsa staining solution. The Bge cell chromosomes at both 60 and 90 min, display some dark regions with a few indistinct bands.

Figure 2.4: Representative brightfield images of G-banded Bge cell chromosomes prepared using protocol B

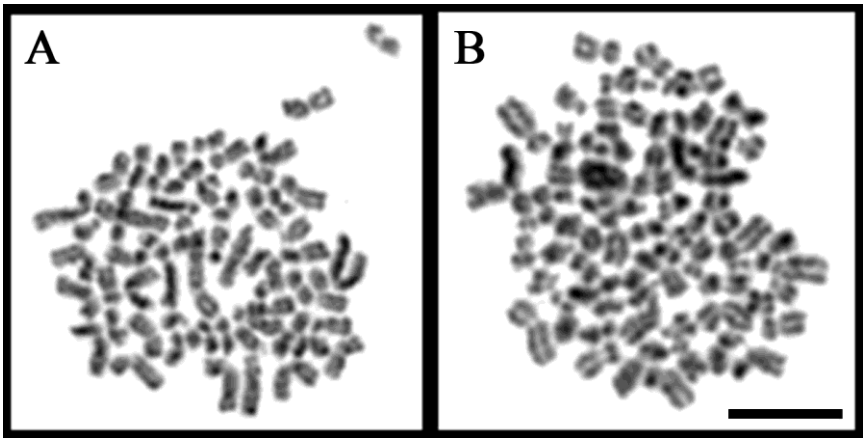

Representative brightfield images of G-banded Bge cell chromosomes prepared using protocol B. The Bge cell chromosomes were incubated for 60 and 90 min (images A and B respectively) in 2XSSC at 60^{o}C. They were subsequently stained for 12 min in Gurr's giemsa stain. Bar = 10μm

Both G-banding protocols yielded results of an incomparable standard to that observed in other routinely karyotyped organisms such as humans and mice. Although protocol A produced a few banded chromosomes, it was often the case, that the bands which were present were too indistinct and of a poor resolution. It was deduced from protocol A that an incubation time of 30 sec in 0.025% of trypsin solution was the optimum condition. However, the results from these conditions still provided insufficient bands of a defined nature to aid pairing of homologous chromosomes. Protocol B proved just as unsatisfactory as protocol A, with there being fewer distinct bands.

2.3.3 A revised karyotype for the Bge cells that reveals extensive aneuploidy in the cell line isolates

DAPI banding was chosen since G-banding proved to be unsatisfactory for these chromosomes.

Biomphalaria glabrata in vivo has a mitotic chromosome complement of 2n = 36. The results observed in this study reveal extensive aneuploidy in the Bge cell line. Both Bge 1 and 2 have a mean chromosome complement that vastly exceeds 36. Fig. 2.5 shows representative karyotypes for both Bge 1 cell line isolate (Fig. 2.5 A) and Bge 2 (Fig. 2.5 B) cell line isolate (representative from a total of 50 metaphase spreads of each cell line isolate). The modal total number of chromosomes in metaphases was 63 and 67 for Bge 1 and 2, respectively (see Table 2.1). These numbers surpass both *B. glabrata's* natural diploid number of 36 and a theoretical triploid number of 54. Yet, both modal complements are lower than the theoretical tetraploid number of 72. These results indicate there is a non-uniform duplication of chromosomes within these cell line isolates. Table 2.1 displays both the chromosomal mean and mode for each group within the karyotypes. The modal numbers between the groups is identical for groups A–C (6, 10 and 6, respectively). However, they deviate in groups D and E. The Bge 2 cell line isolate has 21 and 17 chromosomes for the groups D and E respectively, which exceeds Bge 1's groups D and E, respectively. The modal chromosome numbers for groups F and G (unassigned) are the same. Fig. 2.6 shows the frequency distribution graphs for groups A–G for both Bge cells 1 and 2. Compared with groups D and E, groups A, B, C, F and G display moderate distribution with integer ranges not exceeding 10. Groups D and E, however, show a more marked distribution, with chromosome integer ranges of 14–26 and 8–20, respectively. Hence, although there are duplications in the larger chromosomes, the duplications appear to be more pronounced in the medium-sized chromosomes.

Figure 2.5: Representative DAPI karyotype images of Bge cell line isolates.

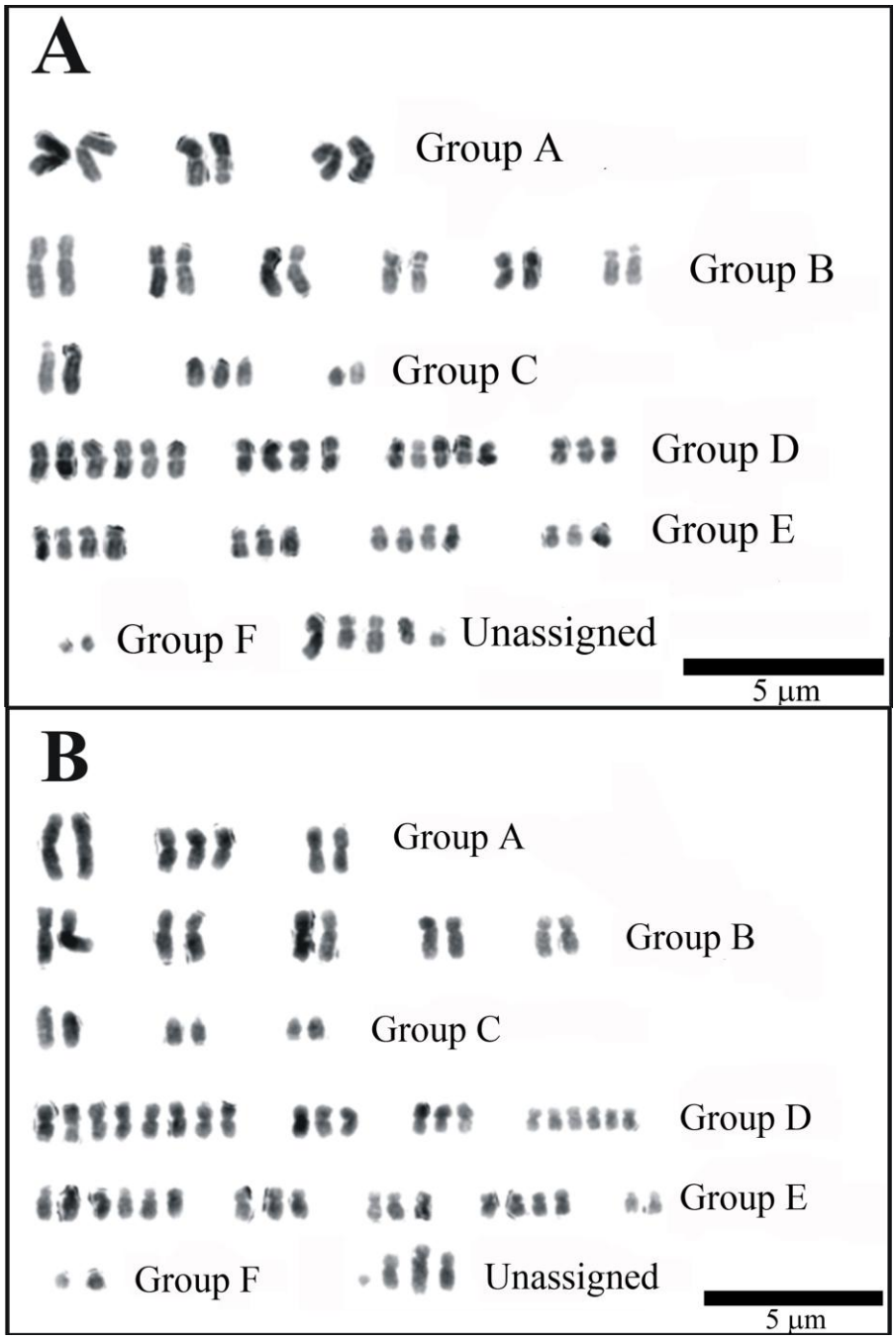

DAPI karyotype images of Bge cell line isolates. Chromosomes from Bge 1 (A) and Bge 2 (B) cell line isolates were stained with DAPI and then converted into grey scale image with subsequent inversion. There were variations between karyotypes for different metaphase spreads from the same isolate. The chromosomes were organised into groups according to size and centromere position (as indicated with notations). The unassigned group contains chromosomes which, given their unique morphology, were without a suitable homologue. Bar = 5 µm (Odoemelam et al., 2009).

Table 2.1: The group mean and modal numbers of chromosomes in Bge cell lines 1 and 2

	Bge 1		Bge 2	
Groups	**Mean**	**Mode**	**Mean**	**Mode**
A	**6.18**	**6**	**6.4**	**6**
B	**10.36**	**10**	**11.04**	**10**
C	**6.12**	**6**	**6.8**	**6**
D	**19.42**	**18**	**20.58**	**21**
E	**13.36**	**16**	**14.54**	**17**
F	**2.8**	**2**	**2.14**	**2**
G	**4.04**	**5**	**3.7**	**5**
TOTAL	**62.3**	**63**	**65.2**	**67**

Table 2.1: The mean and mode for each chromosomal group was calculated based on 50 reads for each of the Bge cell lines, Bge 1 and 2. The mean and modal numbers for groups A–G (unassigned) for two cell lines, Bge 1 and Bge 2 are shown. The mean and modal total chromosomal numbers derived from the groups for each isolate, Bge 1 and 2 are shown at the bottom of the table (Odoemelam et al., 2009).

Figure 2.6: Frequency distribution of chromosomal groups for both Bge 1 and 2 cell lines.

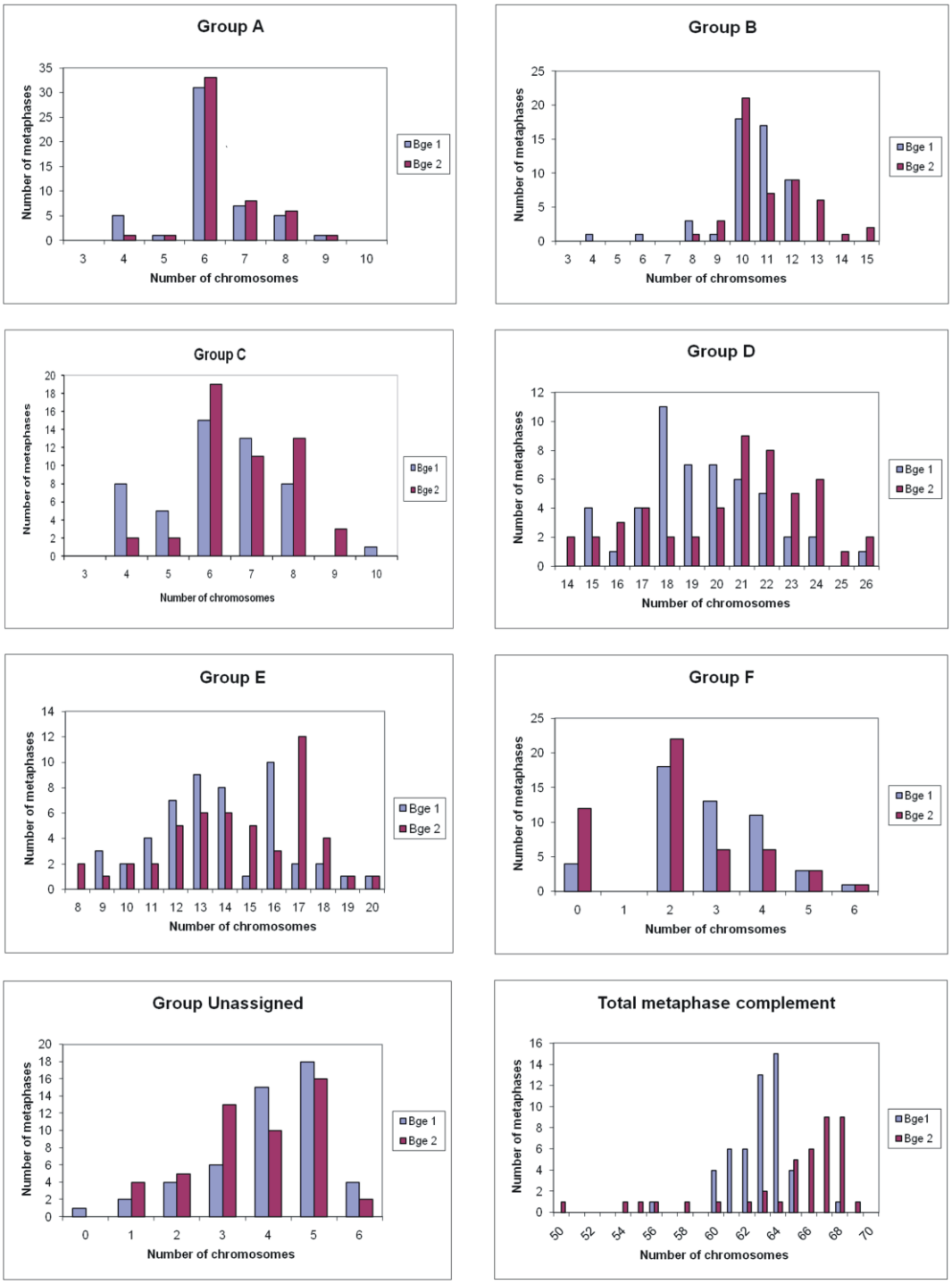

Frequency distribution of chromosomal groups in Bge cell line. Chromosome groups A–F, the unassigned group and total metaphase complement for both Bge 1 and 2 cell lines. For groups A–F the chromosomes from 100 metaphases (50 each for Bge 1 and 2) were grouped according to size and centromere position (Odoemelam et al., 2009).

The morphology of these chromosomes can be described in relation to other organisms such as *Homo sapiens*, as being comparatively small and monomorphic. Thus the size of these chromosomes restricted the clarity of banding that one would observe in human chromosomes. When compared to chromosome grouping from the two cell line isolates to that originally reported by Bayne et al. (1978), it was observed that only a loose similarity to the original chromosomal grouping exists for cell line isolates 1 and 2. These differences may be due to morphological changes that might have resulted from the extensive polyploidy/aneuploidy in the current cell line isolates that was not present when the original karyotype of the Bge cell line was reported (Hansen, 1976; Bayne et al., 1978). Also, the resolution of previously published *ex vivo* karyotypes by Raghunathan (1976) and Goldman (1984) (both karyotypes were produced from snail tissue) were not of a quality that could be used as a comparison. However, it was possible to relate some other designated groups for these Bge cells back to that of Raghunathan's karyotype. Indeed, certain chromosomes from Raghunathan's published karyotype were easily identifiable, such as the largest chromosomes in groups A and C, which are chromosomes 1 and 8 in Raghunathan's (1976) publication.

2.4 Discussion

Interest in the mollusc *B. glabrata* has increased greatly during the past few years with it being chosen as a model organism for whole genome sequencing (Raghavan and Knight, 2006). Thus, it is not only parasitologists who will champion this era of modern genomics biology of this lochotrophozoan but other investigators as well, especially those interested in comparative genomics and genome evolution. The existence of a cell line from *B. glabrata*, indeed the only established molluscan cell line (Hansen, 1976, Bayne et al., 1978, Bayne, 1998), has been a useful tool for parasitologists and has been used for many

in vitro experiments. Since the original Bge cells that were purchased commercially from the ATCC could not be propagated in the Nuclear and Genomic health laboratory at Brunel University, Bge cells were obtained from two different sources as mentioned earlier. As differences were observed between the cell line isolates, we analysed the karyotype of these cells to determine if any differences occurred at the chromosomal level compared with the original Bge cell line (Hansen, 1976, Bayne et al., 1978).

Based on the analysis in this chapter, it was deduced that the Bge cell line has undergone significant cytological changes since Hansen first established it in the 1970s. Therefore, those designing experiments assuming normal gene dosage and expression may be misled without accounting for these changes. The natural diploid number of chromosomes for *B. glabrata* is 36. The changes in two Bge cell line isolates are such that there is considerable aneuploidy amongst the cells, to the effect that a chromosome count of 100 metaphase plates produces modal chromosome complements of 63 and 67. It is intriguing that two supposedly identical cell lines, which have been cultured separately in different laboratories, have such disparate numbers of chromosomes. These findings will need to be taken into account when designing *in vitro* experiments that hope to extrapolate to the *in vivo* situation, as there may well be extra copies of genes and alterations to transcriptional profiles. To achieve construction of the karyotypes from these cell line isolates with such divergent modal counts, it has been difficult arranging these chromosomes into groups as previously performed from the snail itself by Raghunathan (1976) and Goldman et al. (1984). Difficulties were encounterd when identifying these chromosomes from those of the aforementioned previously published karyotypes. However, certain chromosomes, such as the largest chromosomes in groups A and C, were very distinct and were easily identifiable in Raghunathan's (1976) and Goldman et al. (1984) karyotypes (Raghunathan designated these chromosomes as 1 and 8, respectively).

A simple case of triploidy as observed in the human cervical cancer cell line, HeLa (Ghosh and Ghosh, 1975) was initially hypothesised. However, such theories were negated not only by the modal numbers of 63 and 67 chromosomes in the Bge 1 and 2 cell line isolates, but also by the presence of diploid pairs of homologous chromosomes (see Fig 2.5). Hence, the results presented here indicate an uneven duplication of chromosomes. Such duplications exist most prominently in the chromosomes deemed medium metacentric and medium submetacentric. As mentioned previously, aneuploidy is common in many cancer cell lines such as that of HeLa cells (Ghosh and Ghosh, 1975). In mammalian cells it can arise via irregular mitotic division or indeed by the knockout of DNA repair genes such as Breast cancer susceptibility genes BRCA1 and BRCA2 (Tutt et al., 1999, Weaver et al., 2002). The Bge cell line's immortality was apparently due to a spontaneous transformation. One could postulate that the spontaneous transformation of the Bge cells as observed and noted by Hansen in 1976, may have given certain aberrant cells a selective advantage over other cells within the culture. Such a transformation may have been a mutation of a gene controlling mitotic checkpoint signalling and silencing. Or it may have occurred through chromosome mis-segregation via the presence of multipolar spindles (Kops et al., 2005). We can only speculate that the changes that took place in these cells favoured the duplication of the medium metacentric and submetacentric chromosomes. Thus, researchers using the Bge cell line will have to consider their experiments carefully if genes of interest are found to be located on these medium-sized grouped chromosomes. While one can also speculate that the extra chromosomes could be derived from another organism (the laboratory in which the original Bge cell line was established also cultured cells from the mosquito *Aedes albopictus*), it was unequivocally shown, however, by serology and antigen-based analysis that the Bge cell line was not contaminated (Bayne et al., 1978, Odoemelam et al., 2009).

Chapter 3:

The physical mapping of non-repetitive *B. glabrata* single copy genes onto the homologous chromosomes of the Bge cell line

3. The physical mapping of non-repetitive *B. glabrata* single copy genes onto the homologous chromosomes of the Bge cell line

3.1 Introduction

3.1.1 Fluorescence *in situ* hybridisation (FISH) of genetic sequences onto metaphase chromosomes

The mapping of genetic sequences onto their chromosomes of origin is an important tool in genomic analysis and the construction of physical maps and often leads to a better understanding of the structure and organisation of an organisms' genome. The technique of fluorescence *in situ* hybridization (FISH) is used routinely to identify locus specific unique sequences (Odoemelam et al., 2009), repetitive sequences (Knight et al., 2007, Valentim et al., 2008) and whole chromosomes (Taguchi et al., 2007). Metaphase (as well as prometaphase), prophase, interphase and meiotic pachytene chromosomes can be used as hybridization templates for FISH (Trask, 1991). However, the construction of genomic physical maps often utilises mitotic metaphase chromosomes, the chromosomes at this stage in the cell cycle are highly condensed and visibly identifiable from one another by size and by analysing the position of the centromere on the chromosome. The location of the mapped gene is defined by its location on the p or q arm of the chromosome and in its relation to its distance from the centromere (Rooney, 2001, Trask, 1991).

3.1.2 FISH probes

The gene probes used for FISH can be prepared from DNA libraries with large inserts of DNA sequences. Artificial chromosome cloning systems are usually used to house these

large genetic inserts and they include Bacterial (BAC), yeast (YAC), and bacteriophage P1 (PAC) clones. The clones with insert sequences pertaining to the gene in question can be used as probes in FISH. The BAC is the preferred system of cloning vector system and is based on the F factor of *E. Coli* and can be used to stably propagate DNA inserts (Shizuya et al., 1992). The maximum insert size is approximately 300 kb, but BAC libraries normally have an average insert size of 100-150 kb. BAC libraries have been prepared from BB02 (Adema et al., 2006) and BS90 (Raghavan et al., 2007) *B. glabrata* snails. Indeed, a BAC library has also been prepared from the *S. mansoni* parasite (Le Paslier et al., 2000).

The probes can be directly labelled with fluorochromes such as fluorescein isothiocyanate (FITC) and cyanine-3 or indirectly with a hapten molecule such as biotin or digoxigenin and followed by a reporter molecule such as steptavidin or anti-digoxigenin conjugated with a fluorochrome. Indeed, commercially available probes can be utilised for human and murine chromosomes (Cambio Ltd, Cambridge). The mapping resolution of FISH onto metaphase chromosomes is 5 -10 Mb (Trask, 1991); and can often be dependent on the condensation state of chromosome i.e. the resolution is greater on uncondensed chromosomes.

The technique is frequently used in animals such as humans (Lichter et al., 1988, Cremer et al., 1988), dogs (Kukekova et al., 2009, Soller et al., 2008), cats (Szczerbal and Michalak, 2003), birds (Masabanda et al., 2004, Skinner et al., 2009) and plants (Brown et al., 1999). The initial vanguards of this technique such Lichter et al (1988) utilised the technique to identify numerical and structural chromosome aberrations, such as those to HSA 21 and the diagnosis of its phenotypical consequence, Down's syndrome (Lichter et al., 1988). The technique has also been used to identify un-karyotyped chromosomes, such as the creation of whole chromosome probes via microdissection and degenerate oligonucleotide

primed PCR (DOP-PCR) for the microchromosomes of chicken (Masabanda et al., 2004). This technique involved the isolation of microchromosome chicken chromosomes from a metaphase spread stained with giemsa (Masabanda et al., 2004). The isolated chromosome or chromosome fragment is subsequently amplified by DOP-PCR which utilises degenerate primers (Telenius et al., 1992). Indeed, this technique was also utilised by Taguchi et al (2007) to identify chromosomes 5, 6 and 7 of *S. mansoni* (Taguchi et al., 2007). In addition to microdissection, whole chromosome painting probes can also be attained via flow cytometry. This technique is used to separate individual chromosomes by using a laser to analyse the chromosome binding properties of fluorescent dyes such as Hoechst 33258 (affinity for A/T regions) and chromomycin A3 (affinity for G/C regions) (Sambrook and Russel, 2001). The technique has been employed to analyse the sex chromosomes of monotremes such as platypus and echidna (Rens et al., 2007, Rens et al., 2004).

The use of FISH to construct physical maps is under-utilised in gastropods. Previous studies using FISH in gastropods have shown the mapping of 18S-28S rDNA, 5S rDNA and $TTAGGG_n$ telomeric repeats in periwinkle *Melarhaphe neritoides*, *Cantareus aspersus* and *C. mazzullii* (Vitturi et al., 2005). FISH with *B. glabrata* genes has been demonstrated with the mapping of a repetitive non-Long Terminal Repeat (LTR)-retrotransposons onto the chromosomes from the Bge cells (Knight et al., 2007). The study by Knight et al (2007) identified the aforesaid retrotransposon (named *nimbus*, *BgI*) from a BAC clone which was cross hybridized with probes from a previously investigated reverse-tansscriptase (RT) identified from a cDNA library prepared from the haemocytes of the snail. BAC DNA containing the *BgI* sequence was used as a probe for FISH onto the Bge cell chromosomes (Knight et al., 2007). The *BgI* sequence was shown to hybridize onto most of the chromosomes at centromeric and juxtaposed-centromeric positions (Knight et

al., 2007). This was the first chromosomal mapping of genetic sequences onto chromosomes from the Bge cells and hence an important step forward in the field of *B. glabrata* cytogenetic studies. The authors also highlight the importance of investigations into the *nimbus's* (*BgI*) role as a mobile genetic element (MGE) and the possibility of horizontal transfer in *S. mansoni* (Knight et al., 2007). The FISH mapping retrotransponson sequences also extends to *S. mansoni*; BAC clones containing an LTR (named *Boudicca*) and a non-LTR (*Perere* 03) were used as probes and successfully mapped onto *S. mansoni* sporocyst chromosomes (*Perere* 03 mapped onto euchromatic regions of chromosome 2 and *Boudicca* mapped onto euchromatic regions of chromosome 2 and the sex chromosome Z) (Valentim et al., 2008).

3.1.3 Optimizing the FISH procedure

It is often the case when performing FISH for the first time on an organism that the methodology needs to be established or manipulated to attain clear signals on the two chromatid arms. There are many crucial components in FISH which can affect hybridisation, such the pH of the buffers used, formamide concentration, probe concentration, competitor/suppressive DNA concentration and the denaturation temperature. The latter two can vary from organism to organism and can be a source of difficulty when trying to effectively map genes with clear signals onto a chromosome with a conserved morphology. Thus, it is critical that the protocols utilised are suitable for the organism. This chapter describes the methodology for the chromosomal mapping of non-repetitive (single-copy) genes of the snail *Biomphalaria glabrata* onto metaphase chromosomes derived from the Bge cell line. The techniques described in this chapter were developed for the *Biomphalaria glabrata* genome sequencing project through trouble-shooting experimental procedures established for other organisms, so that both the

optimum resolution of metaphase chromosomes and the effective hybridisation of genes was achieved. This chapter demonstrates for the first time, the mapping of non-repetitive (single- copy) *B. glabrata* genes onto homologous chromosomes isolated from Bge cells.

3.2 Materials and Methods

3.2.1 Bge cellular fixation and slide preparation for establishing an optimum denaturation time for the Bge cell metaphase chromosomes

The Bge cells from isolate 1 were cultured and fixed as described in chapter 2. The 20µl of cellular suspension was dropped onto the slides to achieve metaphase spreads. These slides were aged at room temperature for 2 days.

3.2.2 Establishing the chromosome denaturation time

The metaphase spreads were then dehydrated through a series of ethanol solutions of 70%, 90% and 100% (5 min each). The slides were subsequently denatured in a solution of 70% formamide and 2 X saline sodium citrate (SSC) at 70^{o}C. The denaturation was assessed for different durations of 0.75, 1, 1.25, 1.5, 1.75 and 2 min. Immediately after denaturation, the slides were immersed in ice cold 70% ethanol for 5 min before an additional 90% and 100% ethanol cycle. The slides were allowed to dry on a hot block (37^{o}C) before addition of 10 µl of 2 µg/ml DAPI in Vectorshield anti-fade mountant (Vector Laboratories, Peterborough, UK) was applied to the slide and sealed with a 22 x 50 mm coverslips.

3.2.3 Preparation of Bge cell genomic DNA for suppressing repetitive sequences

The Bge cells were cultured as described in chapter 2. The cells were collected after centrifugation (400g) at 15^{o}C, incubated with a digestion buffer containing 100 mM Tris (pH 8.0), 5 mM EDTA, 200 mM NaCl and 0.2% SDS for 16 hr and centrifuged at 10,000g

for 5 min. The supernatant collected was subsequently precipitated with ethanol at -80^{o}C. The DNA was dissolved for 24 hr in 500 µl of sterile deionised distilled water. This solution was then sonicated until the size of the DNA was between 200 and 500 bp. The concentration of DNA was measured using the High Sensitivity (HS) Qubit machine (Invitrogen, Paisley, UK).

3.2.4 Slide preparation for the analysis of the optimum quantity of genomic DNA in the FISH experiment

The slides of Bge metaphase spreads were aged for 2 days at room temperature. They were then dehydrated through a series of ethanol solutions of 70%, 90% and 100% (5 min each). The slides were subsequently denatured in a solution of 70% formamide and 2 X SSC at 70^{o}C for 1.5 min. Immediately after denaturation, the slides were immersed in ice cold 70% ethanol for 5 min before an additional 90% and 100% ethanol cycle. The slides were allowed to dry on a hot block (37^{o}C) before the addition of the probe.

3.2.5 Probe preparation for the analysis of the optimum quantity of genomic DNA in the FISH experiment

DNA was isolated from BAC clones attained from the *B. glabrata* (BS90) BAC DNA library as previously described (Raghavan et al., 2007). The actin BAC DNA was stably propagated in *E. coli* cultures. The *E. coli* was grown in super broth solution of 0.14M NaCl, 20g yeast extract, 35g Bactotryptone and 1ml of 5M NaOH. The DNA was extracted using a Qiagen midi kit (Qiagen, UK). The BAC clone containing the house keeping gene for *B. glabrata* actin was labelled with Biotin-14 – dATP via nick translation (Langer et al., 1981). A nick translation kit (BioNickTM, Invitrogen, Paisley, UK) was used for DNA labelling and products analysed on a 1% agarose gel. Probes ranging from 200 to 500 bp in

size were used in the experiment. 500 ng of the labelled actin probe and 3 µg of herring sperm DNA (as a carrier) were combined with different quantities of sonicated Bge genomic DNA: 10, 20 and 40 µg. A control actin probe without genomic DNA was also prepared. These constituents were ethanol precipitated together at -80^{o}C for 30 min. The DNA was subsequently dissolved in 12 µl of hybridisation buffer (50% formamide, 10% dextran sulphate, 2 X SSC and 1% Tween 20) at room temperature for 24 hr. The probes were denatured at 75^{o}C for 5 min and then incubated at 37^{o}C between 30 and 120 min.

3.2.6 Hybridisation, washing and counterstaining

Eight microliters of the biotin-labelled probe was placed onto the slide, covered with a 24 x 40 mm coverslip and sealed with rubber cement. The denatured slides and probes were hybridised overnight (12–16 hr) in a humidified chamber at 37^{o}C. Following hybridisation, the rubber cement and coverslips were removed and the slides were washed three times for 5 min in a neutral buffered solution of 50% formamide and 2 X SSC at 45^{o}C. Subsequently, the slides were transferred to coplin jars containing pre-warmed 0.1 X SSC at 60^{o}C. These coplin jars were then transferred to a 45^{o}C water bath. The slides were washed three times with 0.1 X SSC for 5 min. Subsequently, the slides were placed in a solution of 4 X SSC at room temperature for 10 min. This was followed by the addition of 100 µl of blocking solution to each slide (4% Bovine serum albumin, BSA, in 4 X SSC). A 22 x 50 mm coverslip was placed on the slide and these were left for 10 min at room temperature. The coverslips were then removed and 100 µl of streptavidin conjugated to cyanine 3 in 1% BSA/4 X SSC (1:200 dilution) was added to each slide and a coverslip applied. The slides were incubated at 37^{o}C for 30 min in the dark. After this incubation, the slides were washed three times for 5 min in 4 X SSC with 0.1% Tween 20 (v/v) at 42^{o}C in the dark. A brief rinse in deionised distilled water was followed by the addition of the

counterstain. The slides were counterstained with DAPI in Vectorshield anti-fade mountant (Vectorlabs).

3.2.7 The effective mapping of non-repetitive *B. glabrata* genes onto the Bge cell chromosomes

The FISH experiments were performed as described previously in sections 3.2.3-3.2.6 with a chromosome denaturation time of 1.5 min and 40 µg of sonicated Bge cell genomic DNA. As well as the previously mentioned *B. glabrata* actin gene probe (which was used to assess the optimum amount of genomic DNA); three more BACs probes were used. These were *B. glabrata* peroxiredoxin (*BgPrx4*), the P-element induced wimpy testis (*piwi*) and ferritin. The probes of these gene loci were prepared in the same manner as previously described for actin in section 3.2.5.

3.2.8 Image capture and analysis

The denatured metaphase chromosomes and metaphase chromosomes with hybridized probes were viewed using an epifluorescence microscope and X100 oil immersion objective (Zeiss, Axioplan 2). The images were captured using a charged coupled device (CCD) camera (RS Photometrics Sensys camera model KAF1401E G2) and the program Smart capture 3.00 (Digital Scientific).

3.3 Results

3.3.1 Establishing the optimum denaturation time for the metaphase chromosomes of the Bge cells

Figure 3.1: Denatured Bge cell metaphase spreads

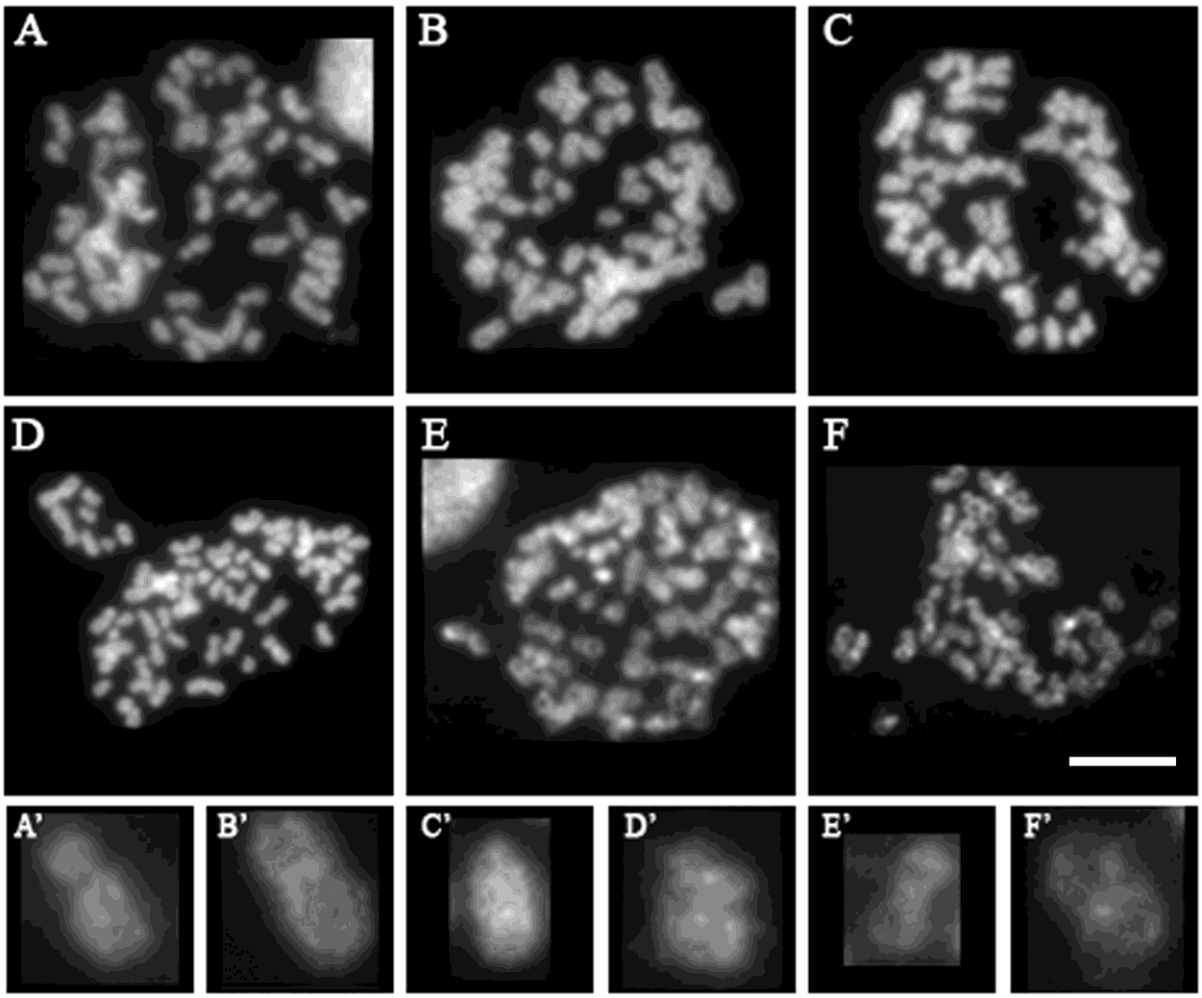

Denatured Bge cell line 1 metaphase spreads. The Bge 1 cells were denatured in 70% formamide for different durations of time. A-F corresponds to 0.75, 1, 1.25, 1.5, 1.75 and 2 min. Bar 10 µm.

The denaturation of the target double stranded DNA of chromosomes is a crucial stage in FISH. The chromosomes must be denatured sufficiently to allow the probe to access the single stranded complementary sequences without too much hindrance. Hence, the duration and temperature to which the chromosomes are exposed can alter the experiment drastically. Under-denatured chromosomes may preclude probe and chromosome hybridisation. Conversely overly denatured chromosomes can lead to a completely distorted morphology and unrecognisable chromosomes, thus negating the accuracy of metaphase gene mapping. Hence, an optimum time needs to be established to achieve both

sufficiently denatured chromosomes as well as a conserved morphology. Fig. 3.1 displays the results from a time-lapse experiment, whereby the *B. glabrata* chromosomes were denatured in 70% formamide at 70^{o}C for different time lengths. Fig 3.1 A-D shows the chromosomes after 0.75, 1, 1.25 and 1.5 min of denaturation respectively. Although the chromosomes are denatured, the morphology wasn't too distorted. At the longer denaturation times of 1.75 and 2 min (Fig 3.1 E and F respectively), the chromosome morphology becomes progressively altered. The representative images are shown in Fig 3.1 E and F, the chromosomes appear indistinct, hazy in outline and swollen, with fragments missing on some chromosomes.

The denaturation method used these experiments is routinely employed in FISH. Indeed, a similar method was used in (Meaburn et al., 2007). This published protocol was based on FISH performed on human chromosomes, where the denaturation time was 2 min. One could hypothesize that due to the diminutive nature of the *B. glabrata* chromosomes in comparison to that of humans, they are less likely to with stand equivalent denaturation times. Indeed, it was deduced from these results that a denaturation time of more than 1.5 min was too long for the *B. glabrata* chromosomes. Therefore, the duration of 1.5 min was the selected optimum denaturation time for *B. glabrata* chromosomes; and can be utilised in FISH experiments to map *B. glabrata* genes.

3.3.2 Optimization of FISH by suppressing repetitive sequences

This section describes the experimental use of different quantities of *B. glabrata* genomic DNA (derived from the Bge cell line) in an effort to suppress the repetitive sequences in the Bge cell genome and consequently reduce non-specific binding of the gene probe. FISH probes contain regions of repetitive DNA that anneal to homologous regions found throughout the genome. In mammalian FISH studies a fraction of species specific C_0t-1

DNA is used to suppress the repetitive elements that would then create signal all over the chromosomal preparation (Lichter et al., 1988). As the results show, a C_0t-1 DNA fraction was not used for suppression however, an excess of genomic sequences that contain within them the repetitive sequences was used. By performing a short reannealing step after denaturation of the probe mixture, including the genomic DNA, the repetitive sequences are suppressed. The re-association/ hybridization kinetics of the unique probe sequences results in it re-annealling at a slower rate than the repetitive sequences. Hence, although the probe sequence is also suppressed concomitantly with the repetitive sequences, the unique probe sequence will have a relatively longer period to hybridize with its homologous chromosome region. The genomic DNA used in this method was prepared from the Bge cells.

Figure 3.2 shows the suppressive effect of using different quantities of genomic DNA in the FISH experiment. The probe used in the experiment was derived from a BAC clone containing *B. glabrata* gene actin. Figure 3.2 A shows the use of no genomic DNA. In this image the probe has hybridized ubiquitously throughout the *B. glabrata* genome. There are many signals and as such, it's impossible to delineate the gene signal to its chromosome of origin. The use of 10 µg of genomic DNA in Figure 3.2 B shows a reduction in the non-specific hybridisation of probe and as a consequence it is possible to identify the strongest signals, as that on a large acrocentric chromosome (as denoted by the white arrows). These signals appear on two homologous chromosomes. However, the genomic DNA was not suppressing all the repetitive sequence as there is still quite a lot of non-specific hybridisation. The next step was to double the quantity of genomic DNA content to 20 µg. This quantity resulted again in a reduction of background signal (Figure 3.2 C).

Figure 3.2: Representative 2-dimensional FISH images of hybridization of non-repetitive (single-copy) genes of *Biomphalaria glabrata* onto chromosomes from the Bge cells using different quantities of genomic DNA for suppression of repetitive sequences.

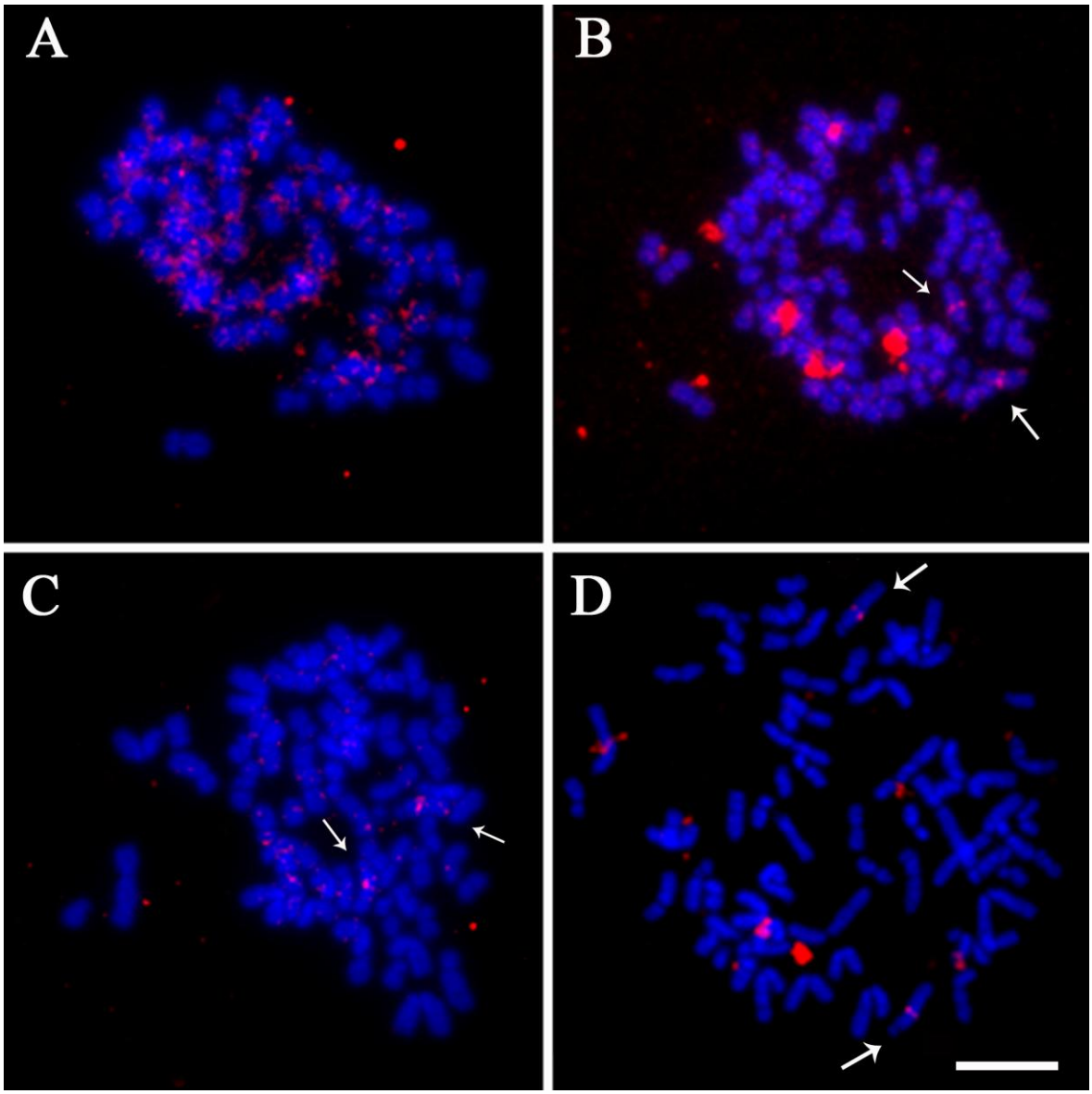

Representative 2-dimensional FISH images of hybridization of non-repetitive (single-copy) genes of *Biomphalaria glabrata* onto Bge cell homologous chromosomes. The chromosomes were fixed, hybridized with DNA from bacterial artificial chromosome (BAC) clones corresponding to the gene for *B. glabrata* actin (seen as red fluorescence). The images A-D correspond respectively to the quantities of 0, 10, 20, and 40µg of suppressive genomic DNA. The chromosomes were counterstained with DAPI. The arrows indicate the location of the actin genes on the chromosome arms. Scale bar = 10 µm.

The strong signals which were present in Figure 3.2 B are still apparent. Yet, there are some slight speckles of non-specific signals dispersed widely amongst the chromosomes (although, these signals are not as bright those on the large acrocentric chromosomes). A subsequent doubling of genomic DNA to 40 µg in Figure 3.2 D, presents an almost complete elimination of the background signals. The probe signals appear bright and very apparent on the two homologues without the cluster of non-specific signals.

The effectiveness of genomic DNA in this experiment is demonstrated by the clear mapping of the actin gene to the large acrocentric chromosome. Yet, the caveat still exists for its effectiveness in comparison to that of C_0t-1 DNA; since not only are the repetitive signals suppressed with the implementation of genomic DNA, but also the unique sequences of the probe (even if to a lesser extent). Perhaps the use of a C_0t-1 equivalent may lead to brighter signals however, it is impossible to make any deductions in this respect.

3.3.3 The physical mapping of non-repetitive single copy genes onto the homologous chromosomes of *Biomphalaria glabrata* isolated from Bge cells

The effective mapping of the gens was performed by utilising the results attained in section 3.3.1 and 3.3.2. The FISH experiments were performed with a denaturation time of 1.5 min and 40 µg of suppressive sonicated Bge genomic DNA. In addition to the *B. glabrata* actin gene probe; three more BACs probes were used. These were *B. glabrata* peroxiredoxin (*BgPrx4*), the P-element induced wimpy testis (*piwi*) and ferritin.

Figure 3.3 displays images from the mapping of four BACs gene probes onto homologous chromosomes. Each probe mapped onto a homologue of two chromosomes. The denaturation time of 1.5 min resulted in a conserved chromosome morphology.

Figure 3.3: Representative 2-dimensional fluorescence *in situ* hybridization (FISH) images of the hybridisation of non-repetitive (single-copy) genes of *Biomphalaria glabrata* onto two homologous chromosomes from the Bge cell line.

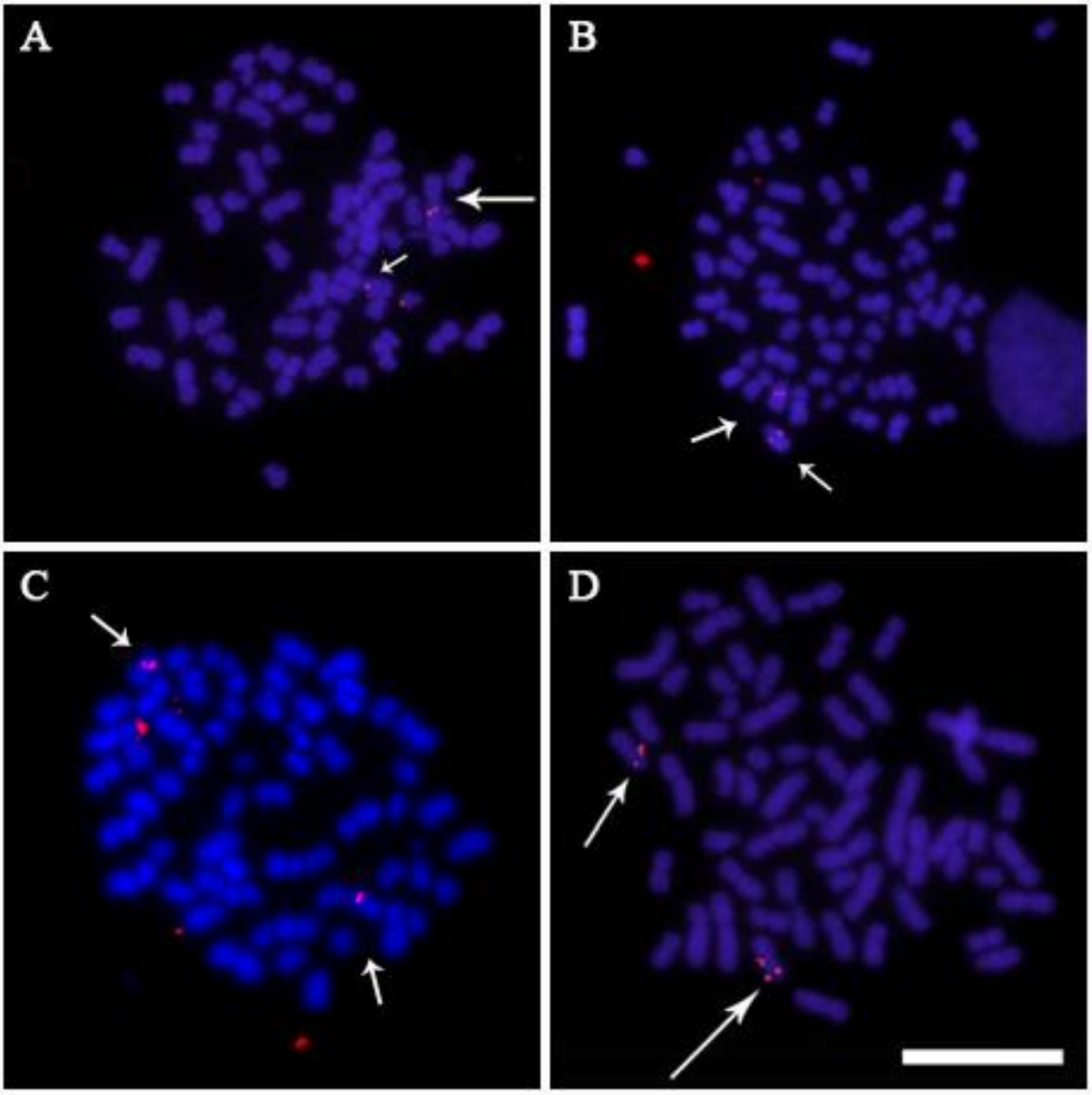

Representative 2-dimensional FISH images of hybridization of non-repetitive (single-copy) genes of *Biomphalaria glabrata* onto two homologous chromosomes from the Bge cells. The chromosomes were fixed, hybridized with DNA from bacterial artificial chromosome (BAC) clones corresponding to genes for *B. glabrata* (seen as red fluorescence). (A) peroxiredoxin, *BgPrx4*, (B) actin (C) ferritin and (D) P-element induced wimpy testis, *piwi*. The chromosomes were counterstained with DAPI (seen as blue fluorescence). The arrows indicate the location of the genes on the chromosome arms. Scale bar = 10 μm.

The established optimum genomic DNA quantity of 40 µg resulted in clear FISH signals. Figure 3.3 A shows the mapping of the *BgPrx4* gene onto the largest metacentric chromosome 1. The probe was mapped proximally onto a pair of homologous chromosomes. *BgPrx4* was located proximally from the centromere. Figure 3.4 B shows the previously mapped actin gene (utilised in section 3.3.2) mapped onto the largest acrocentric chromosome. The gene is mapped on the q arm, proximal from the centromere. The ferritin gene mapped onto the second largest metacentric chromosome from the revised Bge cell karyotype group A (Figure 3.3 C). Finally, the *piwi* gene was located distally from the centromere of the smallest metacentric chromosome in the revised Bge cell karyotype group A (Figure. 3.3 D).

3.4 Discussion

The main reason for investigating the genomic content of these Bge cell line isolates was to assess how relevant and important they would be as a resource for the molluscan genome sequencing project. They would be a useful tool to perform physical mapping upon and develop protocols required for performing FISH on snail chromosomes. Thus, the Bge cell line has been used to develop a methodology for physical mapping of BACs by FISH for *Biomphalaria*.

It has been discussed by interested parties in the *B. glabrata* genome sequencing consortium that the Bge cell line would be a useful tool for mapping genes since it is easier to prepare DNA and chromosomes from a cultured cell line than from whole organisms. Thus, it was imperative to re-evaluate its karyotype and develop protocols for physical mapping of genes by FISH that can be implemented for the future mapping of *ex vivo* chromosomes. Further, as previously mentioned in chapter 2, the chromosomes from the Bge cells are mono-morphic, with only the larger chromosomes being very distinctive.

Hence, mapping of genes onto homologues allows these chromosomes to be characterized more thoroughly and provides an identifying probe. The task itself was not simple and the final results were the culmination of experiments to establish methodology. A suitable denaturation time was to be identified for these small, mono-morphic chromosomes. The 1.5 min duration was found to be the optimal time to denature the chromosomes whilst maintaining chromosome morphology. The *B. glabrata* genome is highly repetitive and it was found that robust FISH methods, where no suppression of repetitive DNA is required, were not suitable for this organism; although they have been successful when assessing the distribution of repetitive elements such as the *B. glabrata* gene *Nimbus* by FISH (Knight et al., 2007). These problems were overcome by the incorporation of unlabelled *B. glabrata* genomic DNA, to prevent the probe from hybridising onto repetitive sequences in the genome. I found 40 µg was an optimum amount of DNA to suppress the repetitive sequences in the *B. glabrata* genome and to give clear signals on two chromatids of both homologues. The development of the aforesaid techniques also enabled the correct delineation of genes to chromosomes from the revised Bge cell karyotype (chapter 2). It is hoped that the mapping will now go some way to establishing chromosome specific gene libraries.

Despite having surmised that there is aneuploidy (Odoemelam et al. 2009) and possibly unrecognisable translocations in these cells, this study shows that FISH mapping experiments with the first non-repetitive (single-copy) BACs that hybridisation was observed on two homologous chromosomes. This was true for four genes actin, ferritin, *piwi* and *Bgprx4* and is an important step forward because it shows that despite its imperfections, the Bge cell line is still a useful first line reagent for developing standardized protocols. Hopefully this will eventually be used to perform similar physical mapping experiments by FISH with non-repetitive probes on *ex vivo* chromosomes.

3.4.1 The future use of FISH on chromosomes derived from *B. glabrata*

The development of whole chromosome paints for the Bge cells and *B. glabrata* is an exciting prospect. Not only will they add more depth to the characterisation of these chromosomes, but they may allow for some comparative analysis with other syntenic organisms. The work by Burch (Burch, 1960a, Burch, 1960b, Burch, 1967) and Goldman and colleagues (Goldman et al., 1984, Goldman et al., 1983), have demonstrated the homology between the chromosomes from *B. glabrata* and the *Bulinus* snail (2n:36). It is conceivably that whole chromosome paints attained from the Bge cell line will hybridise onto some of the chromosomes or chromosome regions from the *Bulinus* snail. Indeed, alongside *B. glabrata*, *Bulinus* is another medically important snail in terms of its role as a host for schistosome parasites. It would be interesting to analyse which *Bulinus* chromosomes/chromosome regions hybridise with the whole chromosome paints.

Raghunathan (1976) has demonstrated that *B. glabrata* chromosomes can be extracted from the embryos as well as the ovo-testis tissue (Raghunathan, 1976). Hence, FISH mapping using the technique described in this chapter on chromosomes from the embryos or ovo-testis is perhaps the next step forward. As a caveat, future researchers pursuing this avenue of study must bear in mind the amount of metaphases needed for a FISH experiment. To maximise the success of the FISH, many metaphase spreads must be present on slide, which can normally be achieved with immortalised cell lines. One may find it difficult to attain as many metaphases from the snail tissue. Perhaps the initiation of another cell line from *B. glabrata* might be the way forward.

In addition to these four mapped genes, there are more genes from the BS90 *B. glabrata* BAC library (Raghavan et al., 2007) to be mapped, they include, L32 ribosomal protein, Myoglobin, Heat shock protein 70 (*Hsp70*), Superoxide dismutase 1 (*SOD1*), Cathepsin B and Fibrinogen related protein 4 (*FREP4*).

Indeed, with the FISH technique now firmly established for metaphase chromosomes of the Bge cell line, the technique described in this chapter can be employed to study the *B. glabrata* genome further, such as the analysis of gene organisation in the interphase nuclei of the Bge cells.

Chapter 4:

Nuclear and genome organisation of the Bge cells

4. Nuclear and genome organisation of the Bge cells

4.1 Introduction

The interphase nucleus is a highly organised, compartmentalized organelle. Structurally, it is dynamic, and is the site of the orchestration of genomic replication, DNA repair, interactions between transcription factors and regulatory sequences, ribosome biogenesis, RNA processing and chromatin remodelling via epigenetic mechanisms such as histone methylation and acetylation (Parada et al., 2004, Foster and Bridger, 2005). Indeed, as well as accommodating these functions, it has an ordered architecture of compartments such as nucleoli, PML bodies, splicing factor domains, nuclear envelope and chromosome territories (Parada *et al*., 2004). The degree of organisation in the latter compartment may influence the regulation of genomic function.

4.1.1 Nuclear organisation in terms of genomic replication

The replication of genomic regions during S-phase has been documented widely in metazoan organisms (Alexandrova et al., 2003, Kill et al., 1991, O'Keefe et al., 1992). In humans, the procession of DNA replication is temporally and spatially co-ordinated (O'Keefe et al., 1992). Individual replication foci (replicons) are distributed throughout the nucleus and are activated at different times during S-phase. The replication foci are temporally organised in a non-random manner i.e. the arrangement of chromatin in the nucleus pertains to the replication of different regions of the genome (O'Keefe et al., 1992, Kill et al., 1991). Genes which are expressed tend to be replicated early in S-phase and conversely, inactive genes tend to be replicated late in S-phase (Foster and Bridger, 2005, Alexandrova et al., 2003, Ferreira et al., 1997). Many research groups have documented

the correlation between the spatial organisation of replication foci and different temporal stages during S-phase (Kill et al., 1991, Ferreira et al., 1997, O'Keefe et al., 1992). Early replicating DNA is dispersed ubiquitously in a granular pattern throughout the nucleus in small foci, mid replicating DNA foci are observed distributed in a perinuclear pattern and late replicating DNA is organised as sparsely distributed large foci (O'Keefe et al., 1992, Kill et al., 1991, Alexandrova et al., 2003).

4.1.2 Interphase chromosome territories

In eukaryotes, the chromosomes in the interphase nucleus occupy defined, decondensed regions known as chromosome territories (Croft et al., 1999, Cremer et al., 1988). In contrast to the compact, X-shaped chromosomes observed during metaphase, the conformation of the interphase chromosomes is more unravelled, yet still demarcated within the nucleus. Indeed, regions of heterochromatin can be observed as the denser regions and eurochromatin as the less dense region (Cremer et al., 2006, Meaburn and Misteli, 2007). The chromosome territories are imbued with branched networked channels which provide conduits for factors which inhibit or activate gene expression. The morphology and positioning of chromosome territories can vary in eukaryotes. In lower eukaryotes, the chromosome territories take on a Rabl conformation. As a consequence of sister centromere segregating in opposite direction during anaphase, the chromosomes become polarized in their orientation (Meaburn and Misteli, 2007). Subsequently, if this orientation is conserved through to interphase, the resultant chromosomes are organised with the telomere and the centromere positioned on opposite sides of the nucleus. The Rabl conformation is found in *Drosophila melanogaster* (Hochstrasser and Sedat, 1987) and plant species such as *Arabidopsis thaliana* and cereals species such as wheats, barley and oats (Santos and Shaw, 2004, Dong and Jiang, 1998). In higher eukaryotic cells such as

those of mammals, the chromosome territories within the interphase nucleus, are organised radially and in some organisms, preferentially positioned internally, intermediately and at the periphery of the nucleus (Bridger and Bickmore, 1998).

The positional patterns of the chromosome territories, has been shown to be non- random in higher eukaryotic organisms. An examples of this is exhibited in mammalian nuclei in which the chromosomes containing rDNA sequences known as Nucleolar organising region (NOR) are positioned in the nucleolus of the nucleus (Soutoglou and Misteli, 2008). In human cells, the tandem repeats of rDNA are found on the chromosomes 13, 14, 15, 21 and 22 and their respective territories are embedded in the nucleolus (Kalmarova et al., 2008, Bridger et al., 1998). The spatial organization of the nucleus in some organisms may function as a regulatory mechanism for gene expression and genome stability, for example in some tumour cell lines chromosomes exhibit altered nuclear position to normal HSA cells (Cremer et al., 2003).

As described previously in section 1.7, there are two theories with regards to the positioning of chromosome territories in the interphase nucleus; they are the size theory and the gene density theory. In terms of evolutionary conservation, the size theory of nuclear organisation has been adduced in organisms such as humans through to chicken and marsupial (Sun et al., 2000, Habermann et al., 2001, Rens et al., 2003).

However, the evidence for the evolutionary branching of the gene density theory is alot stronger, indeed data supporting gene density organisation has been found in humans, apes, Old and New world monkeys. Indeed, it maybe evolutionarily conserved amongst these primate lineages (Tanabe et al., 2002, Neusser et al., 2007). The gene density theory has even been expounded in the nuclei of mice (Mayer et al., 2005), amphibians and reptiles (Federico et al., 2006). The evolutionary conservation indicates a functional relevance i.e.

the compartmentalization of active and inactive genomic regions, the nuclear interior being a transcriptionally active region, with early replicating genes and the nuclear periphery a site for late replicating, inactive regions of the genome (Meaburn and Misteli, 2007, Meaburn et al., 2008). Bickmore and colleagues have provided evidence to this theory by suppressing the expression of human genes via tethering specific chromosomes onto the inner nuclear membrane (Finlan et al., 2008). Indeed, even in lower organism such as yeast, the nuclear periphery in budding yeast is the site for transcriptional repression and is occupied by silent chromatin (Andrulis et al., 1998, Ebrahimi and Donaldson, 2008).

4.1.3 Gene positioning

The non-randon spatial organisation of the genome is not limited to chromosome territories and includes gene loci, indeed there is evidence for the preferential positioning of genes in the interphase nucleus. Such preferentially positioning has been linked with function and gene activity. As mentioned previously, the NOR gene loci cluster around the nucleolus in mammalian nuclei and in yeast the tRNA genes have been shown to aggregate around the nucleolus (Thompson et al., 2003). The relationship between eukaryotic gene loci and its chromosome territory is dynamic, studies into gene positioning have demonstrated genes 'looping' out from the chromosome territory (Volpi et al., 2000, Mahy et al., 2002a). Volpi et al. (2000) found that the major histocompatibility complex on human chromosome 6, extended away from the territory in large chromatin loops of several megabases (Volpi et al., 2000). They correlated this re-organisation of the MHC locus into loops with the up regulated transcriptional activity of the genes in that region. Indeed, the evidence indicates that chromatin loops are a functional consequence of increased gene activity (Volpi et al., 2000). It has been suggested by Bickmore and colleagues that it is the overall gene density and transcription which influences the organisation of chromatin as oppose to individual

genes. This was demonstrated by analysing human 11p15.5, a chromosomal region which is gene dense, with genes expressed at different levels. Chromatin from this region was shown to loop out and extend away from the chromosome territory (Mahy et al., 2002a).

4.1.4 Summary

The eukaryotic nucleus is a dynamic, highly organised organelle in which chromosomes can occupy discrete territories in interphase. The spatial organisation of these territories and their gene loci may function to control gene expression. *B. glabrata* has a large potential for attaining new genetic data because of its vast evolutionary distance from humans. This chapter seeks to address the question as to how the nuclear genome of *B. glabrata* is organised using the Bge cells as an *in vitro* model. This chapter focuses on DNA replication in the Bge cells, the identification of chromosome territories and an analysis of their spatial organisation and finally the radially positioning of *B. glabrata* gene loci in Bge cell nuclei.

4.2 Materials and Methods

4.2.1. Pulse-chase labelling of the Bge cell genome with Bromodeoxyuridine (BrdU) for S-phase analysis

The DAPI karyotyped Bge cells from cell line isolate 1 (chapter 2) (Odoemelam et al., 2009) were utilised for this experiment. These cells were grown on sterile 13 mm diameter circular coverslips placed in 90 mm diameter petri dishes. The petri dish was seeded at a density of 2.5 x 10^5 and the cells were grown in complete Bge medium overnight as described in Chapter 2, before the addition of the thymidine analogs. The Bge cells were subsequently supplemented with 0.1% BrdU and 5-fluoro-2'-deoxyuridine (FUrd) (both from Sigma-Aldrich). These were prepared as 3mg/ml in H_2O and then sterilised using a

0.22 µm pore syringe filter (Fisher) (stored at 4^{o}C until use). The cells were incubated with the BrdU and FUrd for 4 hours before fixation.

4.2.2 Pulse-chase labelling with BrdU to establish a Bge cell cycle time

The Bge cell isolates 1 and 2 were grown on coverslips and were both supplemented with 0.1% BrdU and FUrd as mentioned above. They were incubated with the thymidine analogs for 24 and 48 hours before cellular fixation.

4.2.3 Pulse-chase labelling with BrdU for chromosome territory analysis

The Bge cell line isolate 1 was grown on coverslips and supplemented with BrdU and FUrd as described in 4.2.1 and 4.2.2. The Bge cells were incubated with the thymidine analogs for 48 hrs after which the medium containing the BrdU and FUrd was removed and replaced with complete Bge medium. The Bge cells were subsequently allowed to grow for 10 days in complete Bge (devoid of BrdU and FUrd) before fixation.

4.2.4 Fixation of BrdU pulse-chase labelled Bge cells

The Bge medium with the thymidine analogs was removed from the dish and the cells washed thrice with 1 x PBS. The cells were then fixed with 10 ml of ice cold 1:1 acetone and methanol (v/v) for 4 min. Subsequently, the fixative was removed and the coverslips washed thrice in 1 X PBS. The coverslips were kept in ice cold 1 X PBS before the subsequent indirect immunofluorescence.

4.2.5 Indirect immunofluorescence

Immunological detection of BrdU incorporation requires the pre-treatment of the Bge cells with acid. The coverslips were washed with 10 ml of 2N HCl for 30 min. The acid was then removed and slides washed 10 times in 1 X PBS so as to eliminate any latent acid.

After this wash, the excess 1 X PBS was drained from the coverslips and these were transferred into a square numbered humidified chamber. The primary mouse monoclonal antibody of anti-BrdU (Beckton and Dickenson) was prepared diluted 1:100 in 1% New born calf serum (NCS) in 1 % PBS (v/v). The coverslips were incubated with the anti-BrdU antibody for 1 hour at room temperature. These coverslips were then washed thrice in 1 X PBS before the addition of the secondary antibody. The donkey anti-mouse fluorescein isothiocyanate (FITC, Jackson laboratory) was prepared as a 1/80 dilute with 1% NCS in 1 X PBS. The cells on the coverslips were incubated in the dark with this antibody for 1 hour at room temperature. The antibody was removed by washing the coverslips thrice in 1 X PBS before a brief rinse in ddH_2O. The excess water was drained from the coverslips before counterstaining and mounting with Vectorshield anti-fade mountant containing DAPI (vectorlabs). The coverslips were placed onto 22 X 50 mm slides.

4.2.6 2D FISH of *B. glabrata* genes onto the interphase nuclei of the Bge cells

The FISH was performed as described in chapter 3 on the Bge cells from isolate 1 using the BAC genes actin, ferritin, peroxiredoxin (*BgPrx4*) and the P-element induced wimpy testis (*piwi*).

4.2.7 Image capture and analysis

Images of Bge cells with the anti-BrdU antibody (for S-phase and chromosome territory analysis) and the 2D FISH Bge cells were captured as described in chapters 2 and 3. For the Bge cell cycle time analysis, up to 1000 nuclei from both Bge cell line isolates 1 and 2 were counted and the nuclei positive for BrdU genome incorporation determined.

The chromosome territories were categorised into large and small. 50-60 images of BrdU labelled chromosome territories and the hybridized *B. glabrata* genes in interphase nuclei

of the Bge cell line isolate 1 were analysed using an erosion analysis script developed by Dr Paul Perry in IPLab software (Croft et al., 1999) and was kind gift from Prof. Wendy Bickmore (MRC HGU, Edinburgh). The interphase positioning of both the BrdU labelled chromosome territories and the mapped *B. glabarata* genes was analysed by partitioning DAPI image of the nuclei into five concentric shells of equal area from the nuclear periphery to the centre and the background removed from the BrdU and FISH signal by subtracting the mean pixel intensity of the nuclei. The fraction of DAPI to BrdU signal/ FITC probe signal was determined and normalised by division with the DNA content of each cell.

4.3 Results

4.3.1 Nuclear organisation during DNA synthesis in the Bge cells

The Bge cells were pulse-chase labelled with BrdU for 4 hr. This period of time allowed the fraction of cells cycling through S-phase and hence replicating their genomes to take up the thymidine analog and incorporate it into the Bge cell genome. These cells were cycling asynchronously and as such were at different stages of the cell cycle and indeed at different stages of DNA synthesis. Fig 4.1 displays the representative images of Bge nuclei with BrdU incorporated into the genome. These S-phase positive cells display unique patterns of small and large punctate foci (green) distributed around the nucleus. Fig.4.1 A represents a pattern observed amongst the Bge cell nuclei whereby the DNA replication foci are distributed around the nucleus, with no bias towards any region. The foci in the nuclei with this pattern were similar in size and as such displayed a granular pattern. Fig 4.1 B is representative image of the nuclei with the second pattern, which was observed as preferentially BrdU labelling towards the periphery of the nucleus. The punctate foci size is similar to that observed in the nuclei with pattern 1 (represented by Fig 4.1 A). The final

pattern observed in the Bge nuclei is represented in Fig 4.1 C; the nuclei had a BrdU pattern dissimilar from that observed in pattern 1 and 2 (Fig 4.1 A and B). The labelled DNA foci are considerable larger and are dispersed sparsely throughout the nucleus.

Figure 4.1: Representative images of chromatin organisation during S-phase in Bge and Human cells

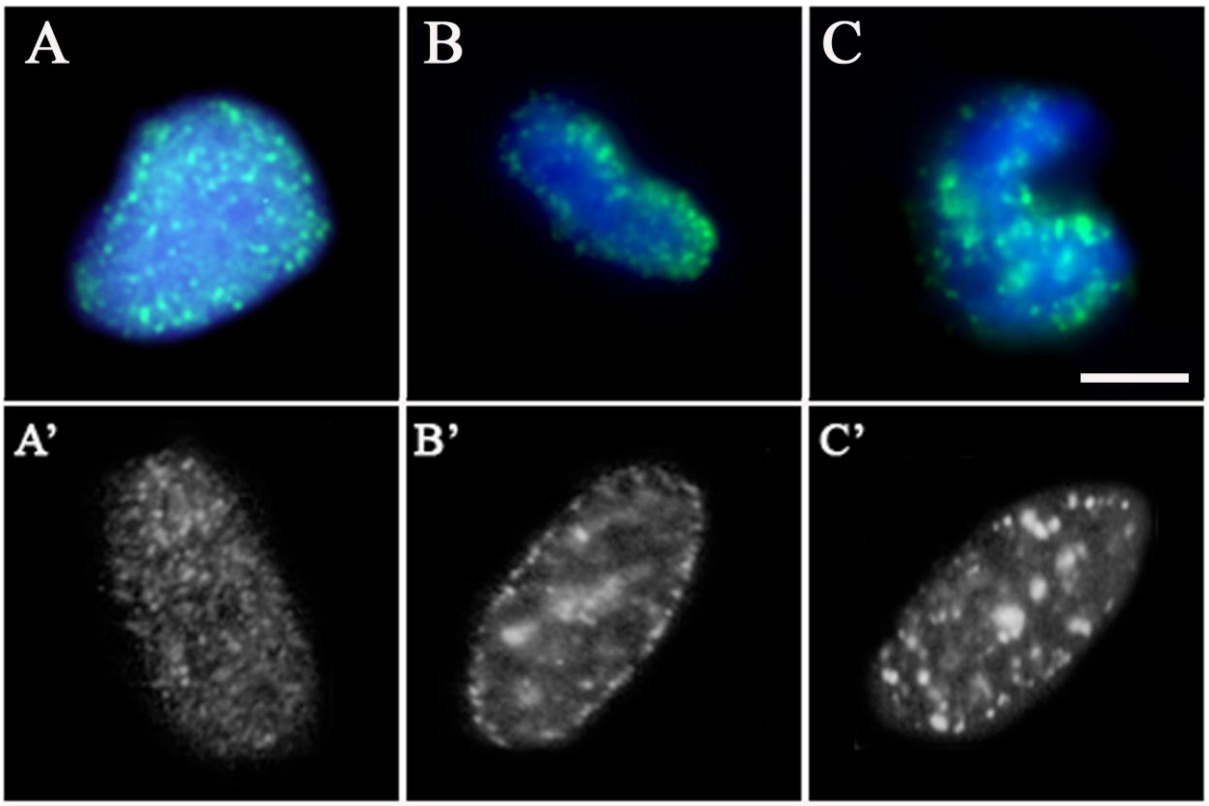

The Bge cells from isolate 1 were grown in petri dishes and pulse-chase labelled with BrdU for 4 hrs before cellular fixation. Three patterns were observed amongst the labelled Bge cell nuclei; (A) ubiquitous granular pattern, (B) Perinuclear distribution of DNA foci and (C) Sparsely distributed large and small DNA foci. Similar to the temporal patterns DNA replication foci observed in human interphase nuclei, (A') early S-phase, (B') mid S-phase and (C') late S-phase (Kill et al., 1991). Bar = 5 µm.

4.3.2 The radial positioning of large and small chromosome territories in the interphase nuclei of *B. glabrata*

4.3.2.1 The Bge cell cycle time

By culturing the Bge cells with the thymidine analog BrdU, it was possible to identify the fraction of cycling cells which have undergone or are undergoing DNA synthesis. Hence by assessing the fraction of such cells over a period of time (48 hrs), it's possible to identify the time at which the maximum amount of cells were positive for BrdU.

Figure 4.2: A graph showing the percentage of BrdU positive Bge cell line 1 and 2 after 24 and 48 hr pulse with BrdU

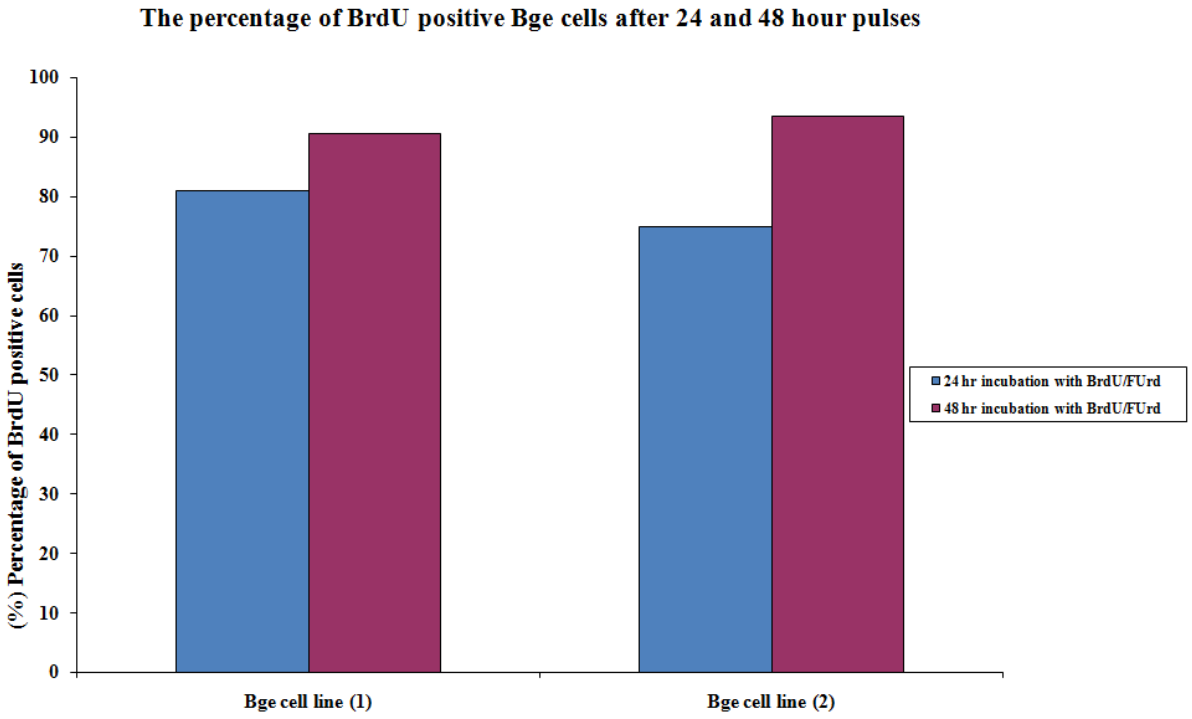

A graph displaying the percentage of BrdU positive Bge cell line 1 and 2 after 24 and 48 hr pulses. The cells from both Bge cell lines 1 and 2 were incubated with BrdU for 24 and 48 hr in order ascertain an approximate cell cycle length. Blue bars are for 24 hrs and the purple bars are for the 48 hrs.

Fig 4.2 shows the percentage of BrdU positive Bge cells after 24 and 48 hrs incubation. For the Bge cells 1 and 2, 80.9 and 74.9 respectively was the percentage of BrdU positive cells after 24 hours. After 48 hours, this percentage rose to 90.6 and 93.5 respectively. Hence, although the duration of BrdU incubation was doubled from 24 to 48 hours, the percentage of BrdU positive cells remained below 100%. This might be attributed to cells dying within that period of time and those that failed to take up the thymidine analog. Therefore, 90.6 and 93.5% were considered the maximum percentage of cells that have been through the cell cycle. Thus the Bge cells cycle time must be between 24 and 48 hours.

4.3.2.2 Large and small chromosome territories in the Bge cell nuclei

Having established that the Bge cell cycle time was ≤ 48; an incubation with BrdU for 48 hr would be sufficient time for the uptake and incorporation of the thymidine analog into the genome of the Bge cells. Hence, by allowing the cells to divide in the absence of BrdU (post- BrdU removal from the Bge medium) for 10 days, would allow for a minimum of 5 divisions during the 10 days. The semi conservative division of labelled and unlabelled sister chromatids resulted in their random segregation into the daughter cells. As a consequence, the number of labelled chromatids in the nuclei was inversely proportional to the number cell divisions undergone i.e. increasing numbers of cell divisions resulted in the reduction in the number of BrdU labelled chromatids. Indeed, the duration of 10 days in culture medium without BrdU yielded Bge cell nuclei with both labelled and unlabelled chromosome territories. The chromosome territories of the Bge cells varied in size, shape and position within the nucleus. The chromosome territories were distinct and were distributed radially around the nucleus, occupying peripheral and internal positions. The variation in size between the chromosome territories was discernible; hence by analysing

over 100 images, the chromosome territories were categorised into groups of large (diameter ≥ 2.5 μm) and small (diameter < 2.5μm) *B. glabrata* chromosome territories.

Figure 4.3: Representative images of large and small interphase chromosome territories in the nuclei of the Bge cells.

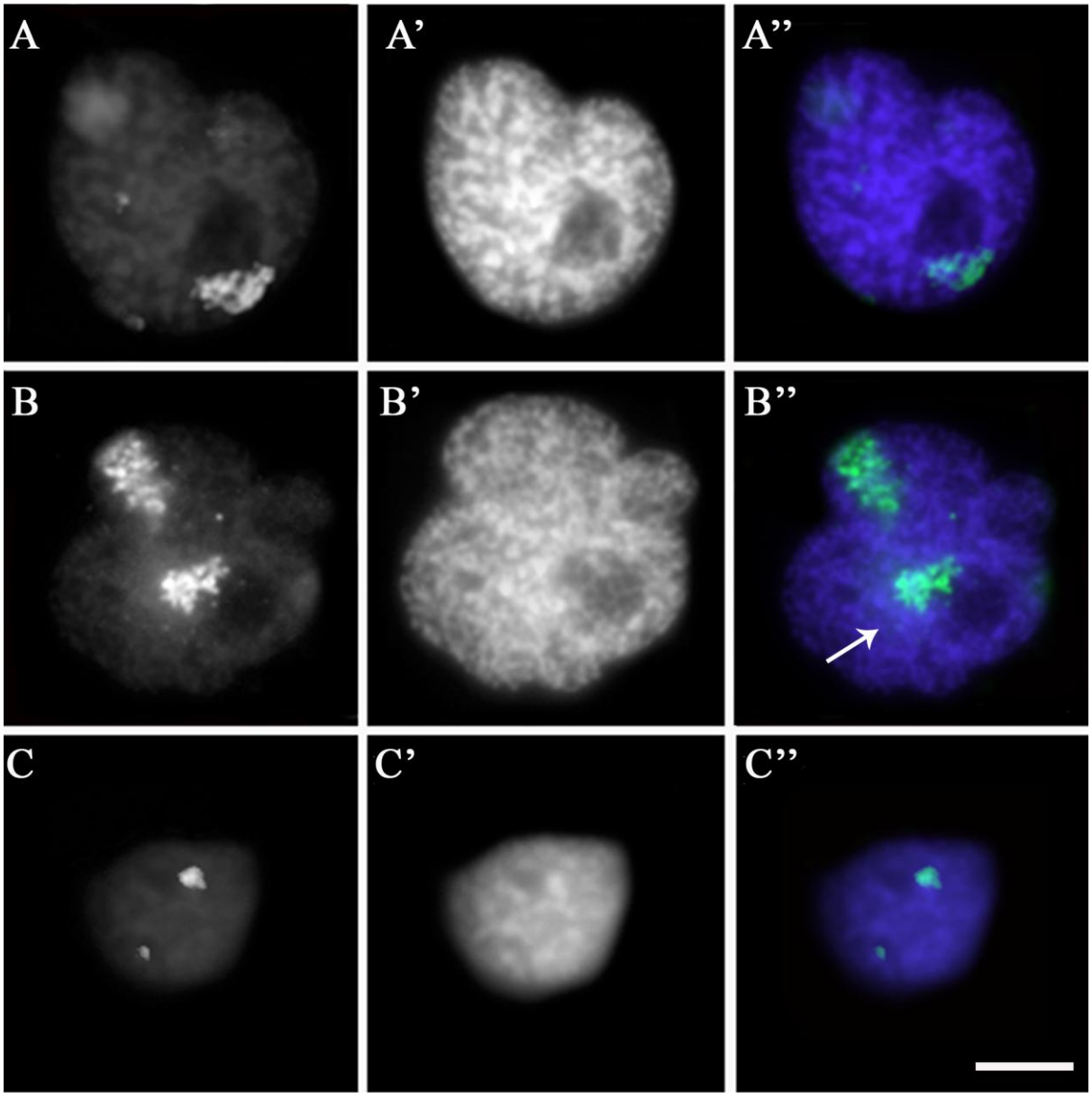

Representative images of large and small interphase chromosome territories in the nuclei of *B. glabrata.* The Bge cells were incubated with thymidine analog BrdU and allowed to divide post-BrdU incubation for 10 days. Chromosome territories were labelled with BrdU and were detected immunologically with anti-BrdU. The territories are shown in green as fitc and nuclei were counterstained with DAPI in blue. Images A and B, display nuclei with large chromosome

territories and Image C displays nuclei with small chromosome territories. The arrow in Image B'' indicates a chromosome territory in close proximity to the nucleolus. (A) Fitc signal, (A') grey scale DAPI signal, (A'' FITC and DAPI), (B) Fitc signal, (B') grey scale DAPI signal, (B'' FITC and DAPI), (C) Fitc signal, (C') grey scale DAPI signal, (C'' FITC and DAPI). Bar = 5 μm.

Fig. 4.3 displays the representative images of *B. glabrata* chromosome territories. Fig 4.3 A, shows a large chromosome territory, which occupies a position abutting the nuclear periphery subjacent to the nucleolus in the nucleus. Such a position may indicate that this chromosome territory contains NOR ribosomal gene sequences (rDNA) and is involved in the reformation of the nucleolus after mitosis (Kalmarova et al., 2008). Structurally, the territory appears elongated and the chromatin is diffuse. Indeed, the nuclear chromatin around the periphery of the nucleus appears less condensed than that of the chromatin in the interior, which is stained brightly with DAPI in Fig 4.3 A'. Fig. 4.3 B shows a representative image of two large chromosome territories in the nucleus of a Bge cell. These chromosome territories are elongated like that of territory in Fig.4.3 A. The chromatin of both territories is quite diffuse and has a similar compaction of the chromosome territory observed in Fig.4.3 A. However, in Fig 4.3 B their positions within the nucleus differ in that they occupy peripheral and internal positions. Indeed, this is true of the two small chromosome territories in Fig. 4.3 C. Both territories have denser chromatin, than that of the larger chromosome territories. This difference in chromatin density and shape between large and small chromosome territories suggests these territories are composed of different chromatin or the action of different chromatin modifiers.

4.3.2.3 The position of large and small chromosome territories in the interphase nuclei of the Bge cells

The BrdU labelled chromosome territory images were subsequently analysed to determine the average nuclear position of large and small territories. 50-60 images of nuclei with large and small territories (as represented in Fig. 4.3) were analysed using an erosion analysis script (Croft et al., 1999); the results gathered from this are displayed in Fig 4.4 and 4.5. The images of the nuclei were partitioned into five concentric shells of equal area. The intensity of the fluorescent signal from the DAPI and the FITC probe of the chromosome territory were measured for each shell. The signal was normalised by division with the DNA content of each shell. Fig 4.4 and 4.5 show the histograms displaying the proportion of normalised probe signal in shells 1 -5, whereby 1 is the nuclear periphery and 5 is the nuclear interior (with standard error of mean bars). Fig 4.4 and 4.5 show that chromosome territories of *B. glabrata* are organised in a non-random manner. Fig 4.4 shows the data from positioning the large chromosome territories. The large chromosome territories occupy an intermediate position in the Bge cell interphase nuclei. The largest proportion of chromosome territory signal is observed in shell 3, the intermediate shell, this is followed by the interior shell 4. The peripheral shells 1, 2 and internal 5 have similar proportions of probe signal. The histogram in Fig 4.5 shows a skewed radial distribution of probe intensity to the nuclear periphery (left), with the distribution peak to the interior (right), signifying that the small chromosome territories are positioned in the interior of the interphase Bge cell nuclei. Indeed, shell 5 has the largest proportion of probe signal intensity, which declines towards the peripheral shell 1.

Figure 4.4: A histogram showing the radial positioning of large interphase chromosome territories in the nuclei of the Bge cells.

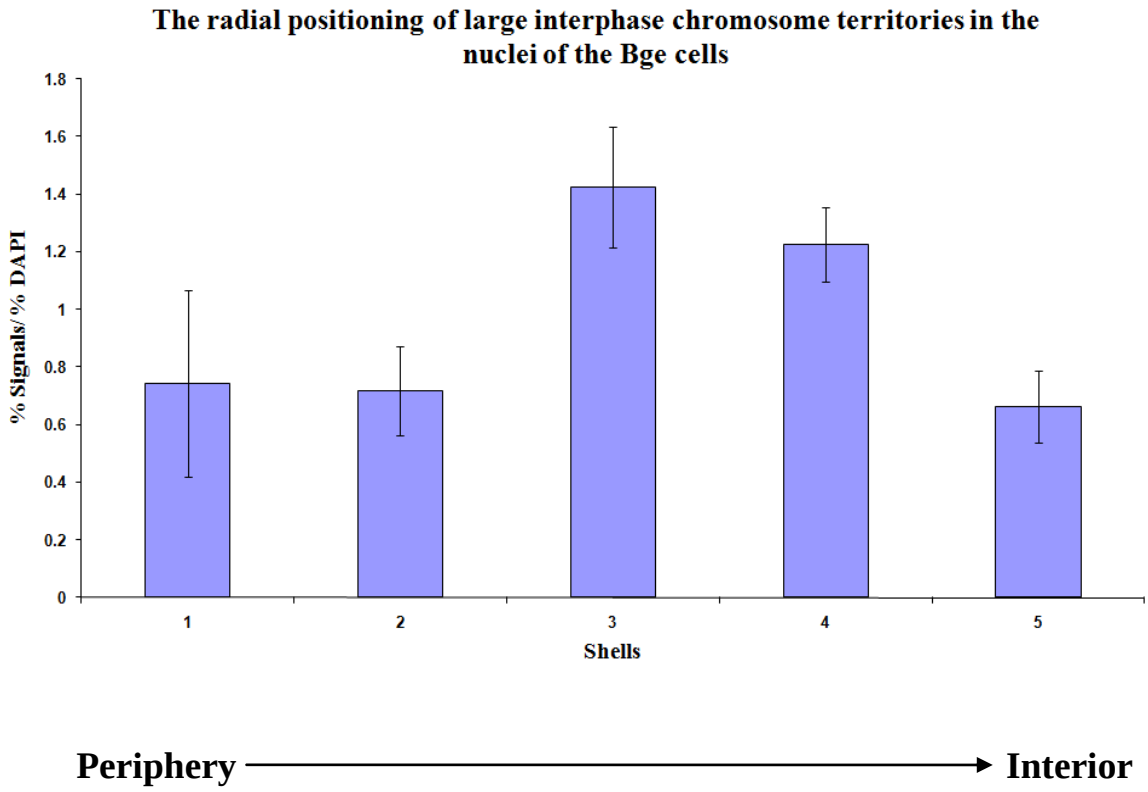

A histogram showing the radial positioning of large interphase chromosome territories in the nuclei of the Bge cell line. The histogram was prepared by using an erosion analysis script which partitions the nucleus into five concentric shells of equal area (x axis), periphery shell 1 to interior shell 5 (Croft et al., 1999). The intensity of the fluorescence signals from the BrdU labelled territories was measured for each shell and normalised by division of the DNA content of each shell (Y axis, with 0.2 increments).

Figure 4.5: A histogram showing the radial positioning of small interphase chromosome territories in the nuclei of the Bge cells.

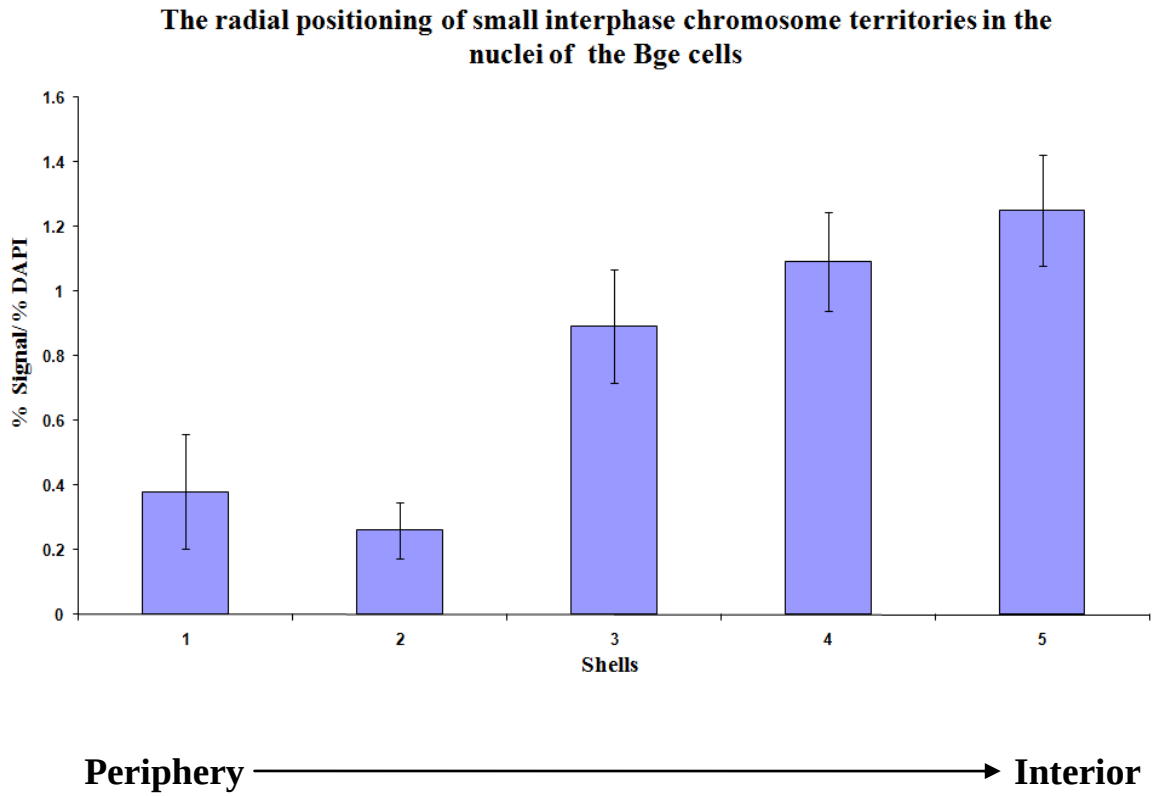

A histogram showing the radial positioning of small interphase chromosome territories in the nuclei of the Bge cell line. The histogram was prepared by using an erosion analysis script which partitions the nucleus into five concentric shells of equal area (x axis), periphery shell 1 to interior shell 5 (Croft et al., 1999). The intensity of the fluorescence signals from the BrdU labelled territories was measured for each shell and normalised by division of the DNA content of each shell (Y axis, with 0.2 increments).

4.3.3 Gene loci positioning in the interphase nuclei of the Bge cells

Figure 4.6: Representative images of hybridised *B. glabrata* genes in the interphase nuclei of the Bge cells via 2 D FISH

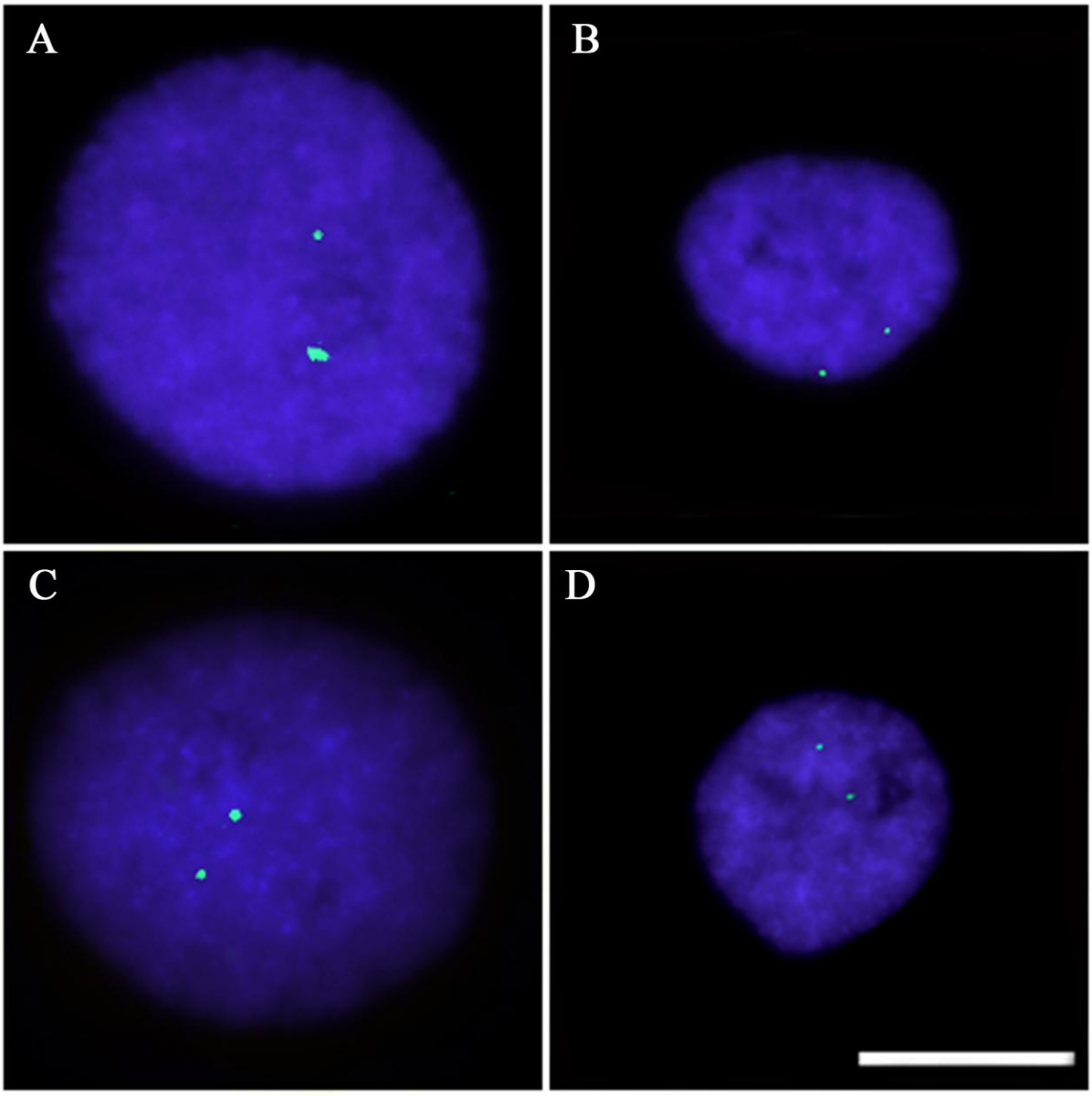

Representative images of 2D FISH hybridized *B. glabrata* genes in the interphase nuclei of the Bge cells. The images show the nuclei stained with DAPI (blue) and the gene loci for (A) actin, (B) ferritin, (C) *piwi* and (D) *BgPrx4*. Bar 10µm.

The data in section 4.3.2 shows that with regards to chromosome territories in the interphase nuclei of the Bge cells, a level of organisation exists; the chromosomes form defined territories of different size positions and are not positioned randomly. The

organisation extends to the genetic sequences of *B. glabrata*, which are positioned non-randomly in the Bge cell interphase nucleus. *B. glabrata* genes that have been mapped on metaphase chromosomes in chapter 2 (Odoemelam et al., 2009) were hybridized onto the Bge cell interphase nuclei using FISH and positioned. 50-60 2D FISH images of the *B. glabrata* genes actin, ferritin, *piwi* and *BgPrx4* (as represented in Fig 4.6) were hybridized onto Bge cell interphase nuclei and analysed using the previously mentioned erosion analysis script (Croft et al., 1999). The images of the nuclei were partitioned into five concentric shells of equal area. The intensity of the fluorescent signal from the DAPI and the FITC of the gene probe were measured for each shell. The signal was normalised by division with the DNA content of each shell. As previously shown in chapter 2, the genes selected for this study mapped onto homologous, diploid chromosomes and as such, two dots of gene loci were observed in the interphase nuclei (Fig 4.6). Fig 4.6 A is representative image of the hybridised actin genes located in an interior position. Fig 4.6 B is a representative image of the ferritin genes which occupied a very peripheral position. The *piwi* genes shown in Fig 4.6 C are positioned internally and *BgPrx4* genes displayed in Fig. 4.6 D are located in internal and intermediate nuclear positions.

The histograms presented in Fig 4.7, show the radial distribution of the aforementioned *B. glabrata* genes in the interphase nuclei of the Bge cells. The actin gene in histogram A shows that it is moderately positioned towards the nuclear interior, with a large proportion of probe signal intensity found in shell 4. The radial positioning of the ferritin gene in histogram B has a right skewed distribution of normalised probe signal intensity. The ferritin gene is positioned peripherally in the interphase nucleus, with a large proportion of signal intensity in peripheral shell 1. The *BgPrx4* gene in histogram C shows an opposite radial distribution and is positioned internally, more so than the actin gene in histogram A. Finally, the *piwi* gene in histogram D is positioned more to the nuclear interior.

Figure 4.7: Histograms displaying the radial positioning of *B. glabrata* genes in the interphase nuclei of Bge cells.

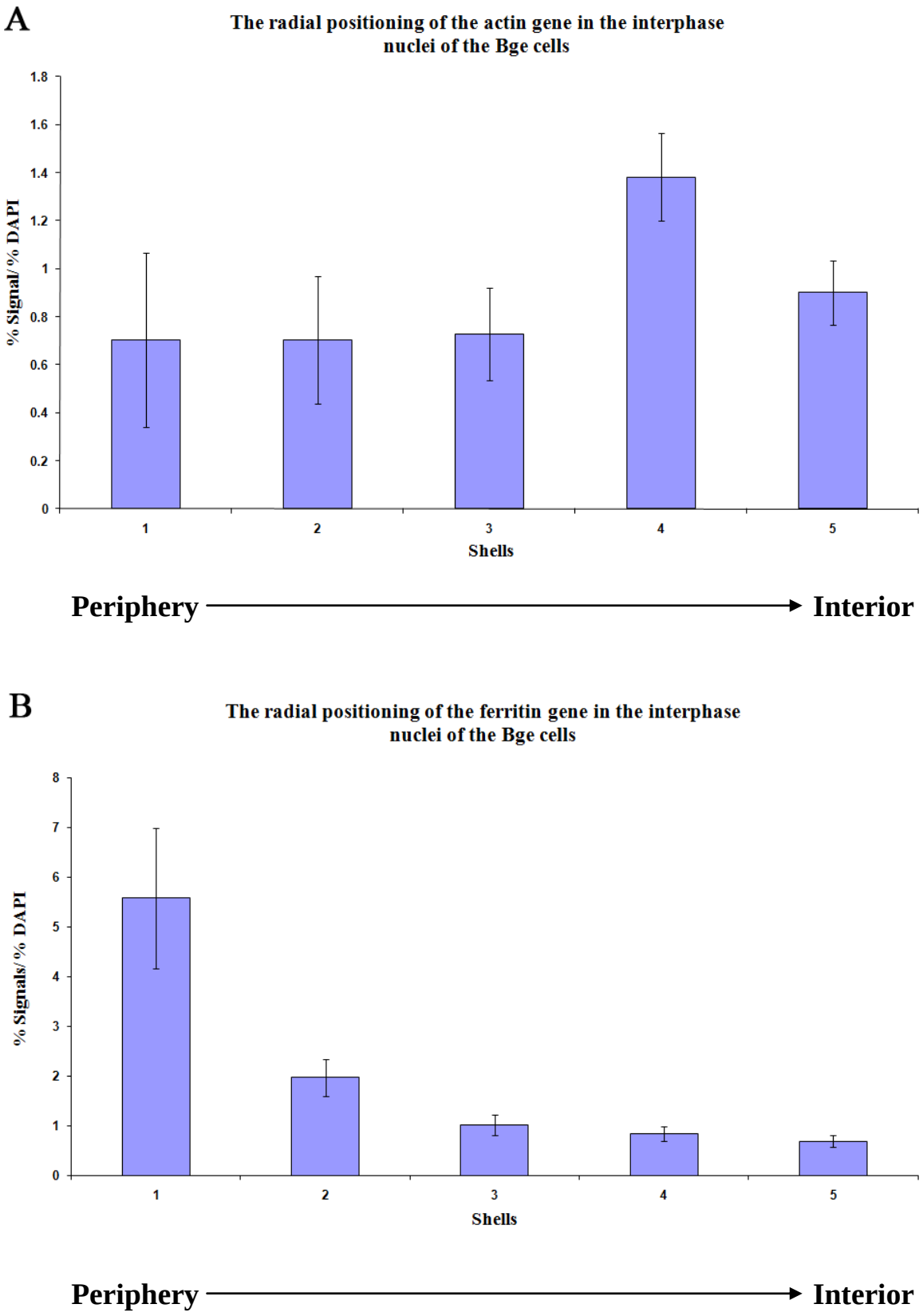

C

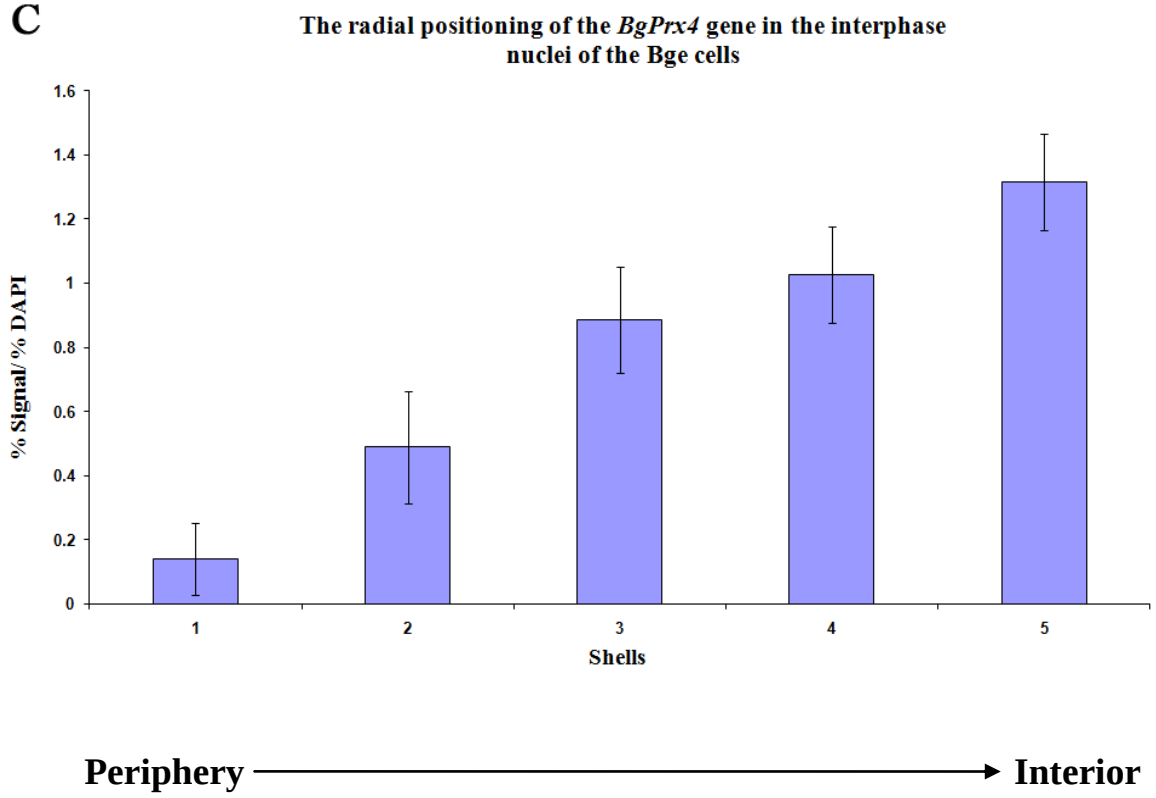

Periphery ⟶ Interior

D

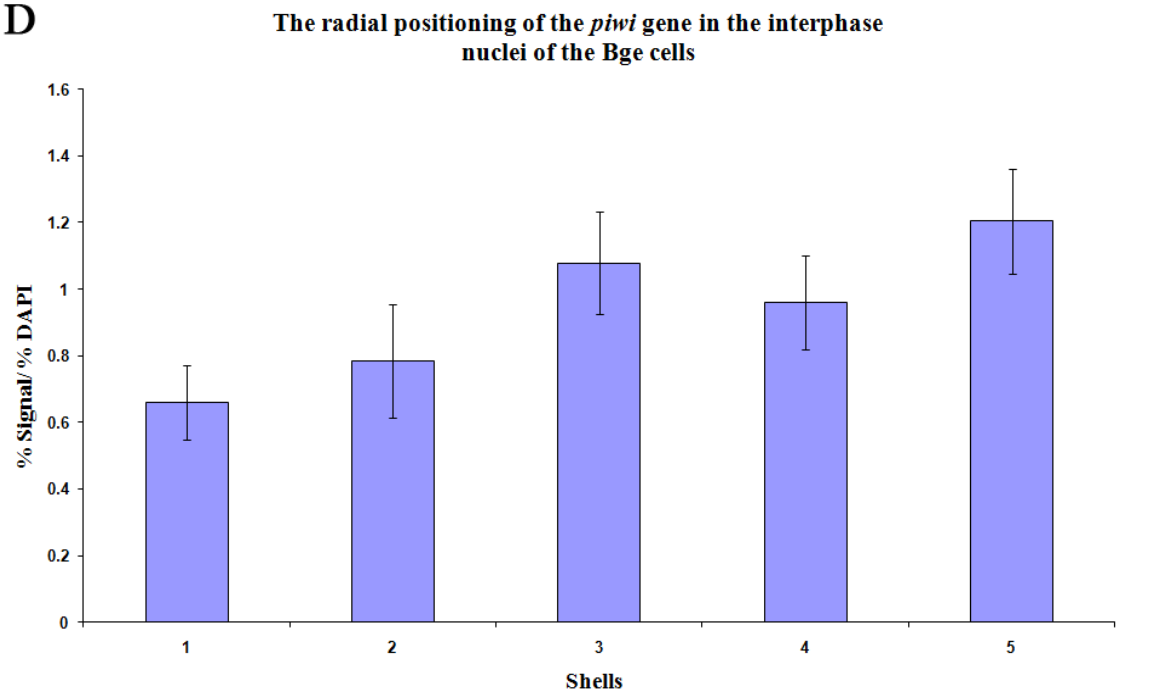

Periphery ⟶ Interior

Histograms showing the radial positioning of *B. glabrata* genes in the interphase nuclei of the Bge cells. The histogram was prepared by using an erosion analysis script which partitions the nucleus into five concentric shells of equal area (x axis), periphery shell 1 to interior shell 5 (Croft et al., 1999). The intensity of the fluorescence signals from the gene probes of actin, ferritin, *BgPrx4* and *piwi* was measured for each shell and normalised by division of the DNA content of each shell (Y axis, with 0.2 increments).

4.4 Discussion

4.4.1 DNA replication and foci distribution in Bge cell nuclei

Documented studies of mammalian DNA replication during the DNA synthesis phase of the cell cycle have shown that this temporal process proceeds in a non-stochastic manner (O'Keefe et al., 1992, Kill et al., 1991, Leonhardt et al., 2000, Manders et al., 1999). The nuclear organisation of replication follows a pattern such that synthesis begins in clustered DNA foci spread uniformly throughout the nucleus and in regions rich in euchromatic DNA. As DNA synthesis progresses, the location of DNA foci becomes peripheral and is subsequently positioned in regions of the nucleus which are predominately heterochromatic (Alexandrova et al., 2003, Rens et al., 2003, Bolzer et al., 2005).

The organisation of DNA synthesis seems to be a conserved feature of mammalian cells, in fact there is evidence this level of organisation is an evolutionary conservation of higher order organisms which belong to phyla segregated from mammalia by almost 600 million years (Alexandrova *et al*. 2003). Before this study, knowledge of DNA replication in molluscan organisms was sparse. It is hoped that *B. glabrata* will become a paragon of research into molluscan nuclear organisation and referred to in much the same way as mouse and humans are in mammalian studies. The significance of the chromatin distribution observed in Fig 4.1 suggests that the patterns observed in mammals are conserved in *B. glabrata.* The representative images in Fig. 4.1 A, B, and C, shows that the

spatial distribution of DNA replication foci differ in the Bge cells and correlate with those observed temporally in human nuclei (Kill et al., 1991). In humans, early replicating DNA has similar granular distribution of DNA foci depicted in Fig 4.1 A, mid replicating regions of the genome are observed distributed in a perinuclear manner, similar to Fig. 4.1 B and late heterochromatic regions of the genome, with late replicating genes forming large, sparse clusters of replication foci, not dissimilar to the pattern in Fig 4.1 C (Kill et al., 1991, O'Keefe et al., 1992).

Further analysis of DNA replication in *B. glabrata* could proceed focusing on the temporal replication of the genome. The Bge cells cycle asynchronously and hence a synchronizing agent such as the anti-mitotic agent Hydroxyurea (HU) could be deployed to synchronise the cells before pulse-chase labelling with BrdU. The fixation of the cells at different time intervals, will allow the procession of DNA synthesis to be observed via the changes in replication patterns. Indeed, it would be possible to estimate the length of S-phase and deduce how long the different regions of the genome take to be replicated.

4.4.2 Radially distributed chromosome territories in the interphase nuclei of the Bge cells

The visualisation of interphase chromosome territories in mammals such as humans (Boyle et al., 2001), pigs (Foster et al., 2005), mice (Mayer et al., 2005) can be performed by hybridising fluorescently labelled whole chromosome paints onto homologous chromosomes. One method of attaining whole chromosome paints for FISH is flow sorting. This method allows the isolation of chromosomes based on DNA content and AT/GC ratio and requires the presence of a substantial fraction of cells in the metaphase stage. This can be achieved using various cytogenetic techniques. The Bge cells were flow sorted on four occasions, all of which have yielded no whole chromosomes. The flow

sorting was performed by Wellcome Trust Sanger Institute (WTSI) at Cambridge University. Another method of chromosome isolation for the production of whole chromosome paints is Microdissection. Indeed, this method was also deployed on chromosomes from the Bge cells. The method involved the isolation of a whole chromosomes or chromosome fragments from a metaphase spread via a Borosilicate glass needle, controlled by an electronic micromanipulator. The isolated chromosome is subsequently transferred to a PCR tube and the DNA amplified using degenerate primers (Degenerate oligonucleotide primed PCR, DOP-PCR) (Telenius et al., 1992). FISH on chromosomes from the Bge cells using probes prepared using the microdissection and DOP-PCR method yielded no results.

Interphase chromosome territories can be identified by semi-conservative replication labelling of an organisms' genome with a thymidine analog such as BrdU and subsequently allowing successive cell divisions in the absence of BrdU (Zink et al., 1998, Alexandrova et al., 2003). This latter technique was utilised to provide data for the existence of defined territories of chromosomes in the interphase nucleus of the Bge cells.

To the best of my knowledge, this is the first time that chromosome territories have been identified and visualised in the interphase nucleus of molluscs. In terms of evolution, the presence of chromosome territories appears to be a conserved feature of functional genome organisation in higher organisms (Foster and Bridger, 2005). Indeed, the field of interphase chromosome territory research encompasses species such as humans (Boyle et al., 2001), primates and old world monkeys (Neusser et al., 2007), pig (Foster et al., 2005), chicken (Habermann et al., 2001), mice (Mayer et al., 2005), *Drosophila* (Hochstrasser and Sedat, 1987), parasites such *Trypansoma brucei* (Ogbadoyi et al., 2000), *Hydra* (Alexandrova et al., 2003), yeast (Bystricky et al., 2005) and plants (Lysak et al., 2001). Indeed, considering this wide spectrum of species studied, the addition of *B. glabrata* to the

aforementioned list of organisms may provide a model molluscan or gastropoda organism in this field of research. Unlike the Rabl conformation of chromosome territories seen in *Drosophila*, yeast and cereal species (Santos and Shaw, 2004, Cowan et al., 2001), this study has shown that these territories are distributed radially around the nucleus (Fig 4.3), a type of spatial organization prevalent in mammalian, chicken and rodent nuclei (Boyle et al., 2001, Habermann et al., 2001, Mayer et al., 2005).

4.4.3 Bge cell interphase chromosome organisation by size

As displayed in Fig 4.3, the chromosome territories localised in both interior and peripheral regions. Fig 4.3 B shows a large chromosome territory in an internal position adjacent to the nucleolus of the Bge cell nucleus. In humans, the rDNA sequences are found on the acrocentric chromosomes 13, 14, 15, 21, and 22. The presence of NOR regions on *B. glabrata* chromosomes has been demonstrated by Goldman et al (1983) and Kawano et al (1987) and they located the NOR region on a relatively small acrocentric chromosome (Goldman et al. 1983, Kawano et al. 1987). This is contrary to the large size of territories observed in Fig 4.3 A and B, and perhaps implies that the aforementioned chromosome territories did not contain rDNA sequences. Indeed, it has been shown in human nuclei, that large blocks of heterochromatin and arms of chromosomes without rDNA sequences can preferentially locate within the nucleolus (Bridger et al., 2000, Bridger et al., 1998). However, the position of these chromosome territories and their functional relevance with respect to involvement in nucleolus formation after cell division cannot be extrapolated from this study.

The burgeoning field research into genome organisation has provided a considerable amount of evidence that the compartmentalized chromosome territories occupy regions within the interphase nucleus in accordance to the genomic characteristic of the

chromosome, i.e. the volume and gene density of the chromosome. The purpose of this study was to investigate the role of chromosome size in interphase nuclear organization. With regards to spatial organisation in *B. glabrata*, the results in section 4.3.2.3 indicate that the size of the chromosome territory may play role in the position of the territory in the interphase nucleus. Fig 4.4 and 4.5 display the histograms for the radial distribution of large and small chromosome territories respectively. The large chromosome territories displayed an intermediate nuclear distribution with a slight bias towards the interior, whereas the small chromosome territories occupied an internal position. Hence, Bge cell interphase nuclei chromosome positions adheres to the size-dependent positioning only partially; inasmuch as it is only the position of the small chromosomes which correlates with the preferential positioning to the interior. Nonetheless, these results may indicate a different form of spatial organisation present in *B. glabrata* and perhaps other gastropods or molluscan organisms. However, considering the gene density of the chromosomes in the Bge cells remains unknown and without a fully sequenced syntenic organism, it is impossible to disregard the role of gene density in genome organisation in the Bge cells. Further characterisations of Bge cell and *B. glabrata* genomes in the forms of gene mapping and sequencing; and the possible future utilisation of whole chromosome paints may go some way to providing conclusive evidence to fully qualify or negate the two theories of size and gene density with regards the Bge cell interphase nuclei. It might be the case that the spatial organisation of chromosome territories in the interphase nucleus of Bge cells fits both the size and gene density theory. Indeed, studies into chicken and porcine genome have added credence to both theories (Habermann et al., 2001, Foster et al., 2005).

4.4.4 Gene positioning in the Bge cell nuclei

The visualisation and positioning of chromosome territories (as demonstrated in section 4.3.2) in the Bge nucleus, has shown that the genome is highly organised. Studies into the positioning of gene loci in mammalian interphase nuclei have determined that genes occupy non random locations, which sometimes differ from the location of chromosome territory of origin (Volpi et al., 2000, Mahy et al., 2002a). This study was focused on the organisation of the Bge cell genome with respect to the position of *B. glabrata* gene loci. The genes analysed were all found to be distributed in a non-random manner. Fig. 4.7 A shows the actin was distributed intermediately in the nucleus with a slight bias towards the interior. This distribution was in contrast to the ferritin gene which was positioned in a very peripheral position (Fig 4.7 B). The genes *Bgprx4* and *piwi* both occupied internal positions. These genes mapped onto relatively large metaphase chromosomes (chapter 3). According to the size theory of spatial organisation in the interphase nucleus, these chromosomes should be positioned towards the periphery of the nucleus (Sun et al., 2000). Indeed, if these genes were used as a marker for chromosome positions, then only the peripheral position of the ferritin gene (located on a large chromosome) would adhere to the size theory. However, the results from the radial positioning of the large and small chromosome territories demonstrated that the *B. glabrata* chromosomes do not fully adhere to the size theory, with large chromosomes occupying intermediate positions with a slight bias toward the interior (Fig 4.4). However, as a caveat, gene loci have been shown in many studies to be very dynamic, with loops of chromatin looping out from the chromosome territories, often as a consequence of the transcription activity of the gene(s) (Mahy et al., 2002a). Perhaps the internal position of the actin, *Bgprx4* and *piwi* is a reflection upon the transcriptional activity of the genes? These genes may be expressed at a higher level than that of ferritin and consequently adopt an internal position. Or indeed, the

periphery of the nucleus in the Bge cells may function (as in yeast and humans) as a region of gene repression. Further studies analysing gene expression would elucidate this hypothesis.

4.4.5 Conclusion

The nuclear genome of *B. glabrata* is highly organised in terms of genomic replication, chromosome territories and gene loci. During replication in *B. glabrata*, clusters of DNA foci form in the nucleus, in patterns very similar to those observed in humans. The *B. glabrata* interphase chromosomes occupy discrete territories which are distributed radially around the nucleus with a possible correlation between chromosome size and location. Finally, the genes are organised in a non-random manner occupying both internal and peripheral positions. It is hoped that these studies will provide a platform for future research into genome organisation in *B. glabrata* and related organisms from the phylum mollusca. Further research into the gene density of the *B. glabrata* chromosomes and expression studies upon the genes may help to elucidate some of the caveats placed upon the data gathered from this study. However, at present the research presented here demonstrates that genome organisation of *B. glabrata* is not dissimilar from that of higher organisms such as humans.

Chapter 5:

An *in vitro* analysis of the Bge cell genome organisation upon parasitic invasion

5. An *in vitro* analysis of the Bge cell genome organisation upon parasitic invasion

5. 1. Introduction

5.1.1 Exposure of the Bge cells to *S. mansoni*

The host parasite interaction between *B. glabrata* and *S. mansoni* is initiated when the trematode in its form as miracidium enters the snail via the surface epithelium and consequently develops into a primary sporocyst (Miller et al., 2001). Naturally, the field of research into this relationship has focused on the genetic factors and potential markers which lead to parasite elimination in some snails and not in others. *S. mansoni's* specificity for *Biomphalaria* species; (*B. glabrata, B. alexandrina, B. tenagophila, B. pfefferi*) points towards a structured genomic communication between host and parasite and perhaps to some extent, co-evolution (Miller et al., 2001, Raghavan et al., 2003). The internal defense system of the snail is structured around immunological cells known as haemocytes (Hahn et al., 2001). In snails which are resistant to the parasite, the innate immunity manifests itself via the migration of the haemocytes into the snails open circulatory system, where they bind and encapsulate primary sporocysts (Raghavan et al., 2003). Phagocytic destruction of the parasite is achieved via the production of reactive oxygen species (ROS) such as hydrogen peroxide and nitric oxide (Goodall et al., 2006, Hahn et al., 2001). Other factors contributing to the snail's defense system include soluble carbohydrate-binding proteins known as fibrinogen related proteins (FREPs) and cytokine like components (Loker and Bayne, 2001, Miller et al., 2001).

An elucidation of the genetic factors which influence resistance and susceptibility in the snail host has come from research investigating the transcriptional modulation of genes in the snail upon and post invasion from the parasite (Hertel et al., 2005, Miller et al., 2001).

Investigations into *B. glabrata's* relationship with *S. mansoni* have been aided by the development of an *in vitro* model for the intramolluscan sporocyst stage of *S. mansoni*. Such a model exists in the Bge cell line (Hansen, 1976). The immortalized Bge cell line has demonstrated its ability to maintain primary sporocysts and produce secondary sporocyst via co-culturing with miracidia (Coustau et al., 1997). A later study by Ivanchenko (1999) exhibited the continuous *in vitro* propagation and differentiation of *S. mansoni* in cultures of the Bge cells (Ivanchenko et al., 1999). Cultivation of *S. japonicum* and *Echinostoma caproni* with Bge cells has been successfully observed (Coustau et al., 1997, Coustau et al., 2003). Indeed, the utility of the Bge cells in terms of parasite culture, extends to the deer liver fluke, *Fascioloides magna* (Laursen and Yoshino, 1999).

Changes in gene expression upon co-culturing the Bge cells with miracidia from *S. mansoni* or *E. paraensei* have been documented (Humphries and Yoshino, 2006, Coustau et al., 2003). Humphries and Yoshino (2006) conducted one such study in which they utilised the excretory and secretory products from *S. mansoni* miracidia to stimulate the p38 signalling pathway in the Bge cells (Humphries and Yoshino, 2006). They observed the activation/phosphorylation of p38 mitogen-activated protein kinase after a 5 min incubation with larval excretory and secretory products from *S. mansoni* (Humphries and Yoshino, 2006). The significance of these result stems from the associated role of mitogen-activated protein kinases in inflammatory signalling and cellular stress response (Humphries and Yoshino, 2006); perhaps this signalling pathway plays a part in immune response to parasitic invasion? A similar experiment by Coustau et al (2003) using excretory and secretory products from *S. mansoni* miracidia and *E. paraensei* observed the modulation of 4 gene transcripts in the Bge cells with homology to cytochrome C, methyl binding proteins, glutamine synthetases and a protease inhibitor from the Kunitz family (Coustau et al., 2003). The Bge cells are often used in experiments concomitantly with the

B. glabrata snail and this provides a means of examining the snails' response to the parasite *in vitro* and *in vivo*. One such experiment using the aforementioned paradigm investigated the *in vivo* and *in vitro* knockdown of *FREP2* gene expression in *B. glabrata* (Jiang et al., 2006). The *FREP2* gene is part of the FREP gene family, which encode a group of immunological proteins with an immunoglobulin super family domain (IgSF) and a highly conserved fibrinogen region (Loker and Bayne, 2001). These proteins have been shown to bind *S. mansoni* sporocysts and precipitate soluble trematode antigens. Using doubled stranded RNA for specific regions of the *FREP2*, Jiang et al (2005) were able to suppress the *FREP2* gene expression in the Bge cells upon exposure to *E. paraensei* miracidia and resistant BS90 *B. glabrata* snails upon exposure to *S. mansoni* miracidia (Jiang et al., 2006). The implication of this data bodes well for future studies investigating the role candidate genes of resistance and susceptibility play during parasitic invasion.

Indeed, in terms of gene expression, it is not just the host-parasite relationship which has been investigated in Bge cells. Research by Laursen et al (1997) focused on the stress response of the Bge cells to sub-lethal levels of heat (Laursen et al., 1997). The heat-shock to the cells resulted in the induction of *HSP70*. This assay was subsequently used by Yoshino (1998) in combination with the transfection of the Bge cells with a DNA construct consisting of an inducible HSP promoter and a luciferase reporter gene (Yoshino et al., 1998). Yoshino (1998) was able to activate the expression of the luciferase reporter gene via HSP promoter induction. The data from this research will hopefully aid future studies transfecting the Bge cells with genes pertinent to parasitic infection (Yoshino et al., 1998, Laursen et al., 1997).

5.1.2 Chromatin remodelling during transcriptional activation

The highly compartmentalized structure of the eukaryotic cell nucleus and the dynamic organisation of chromosome territories and chromatin fiber has been shown to play an integral role in controlling gene expression (Kumaran et al., 2008). The extent to which the nuclear organisation of the aforementioned nuclear entities play in genomic function have yet to be fully defined. However, a number of studies using mammalian models have correlated regional positions in the nucleus with levels of gene expression (Volpi et al., 2000, Mahy et al., 2002b, Williams et al., 2006, Finlan et al., 2008, Meaburn and Misteli, 2008, Ballabio et al., 2009, Szczerbal et al., 2009). The nuclear periphery has been demonstrated to be a location correlating with silent heterochromatin (Andrulis et al., 1998, Ebrahimi and Donaldson, 2008). In budding yeast *Saccharomyces cerevisae*, the peripheral anchoring of chromatin results in transcriptional silencing; this anchoring of chromatin to the periphery is facilitated by the localisation of telomeres with the telomere binding complex Ku (Ku70 and Ku80) at the nuclear envelope (Ebrahimi and Donaldson, 2008). In addition to Ku, proteins such as Sir4 (silent information regulator) and ESC (establishes silent chromatin) also function in transcriptional silencing and occupy perinuclear positions (Ebrahimi and Donaldson, 2008, Finlan et al., 2008). The nuclear periphery in mammalian nuclei has also been shown to function in transcriptional repression. Bickmore and colleagues were able to anchor two different human chromosomes to the nuclear periphery (Finlan et al., 2008). They conducted this experiment utilising the interaction between lac repressor (Lac I) combined with an inner nuclear membrane protein Lap2ß and human chromosomes tagged with *E .coli* Lac operator (Lac O) arrays. This re-localisation resulted in the down regulation of genes proximal to the Lac O sites. Additionally, the transcriptional suppression was reversible via the abrogation of the Lac O- Lac I interaction or the activity of HDAC (histone

deacetylases) (Finlan et al., 2008). This study demonstrated the causative role of nuclear organization upon transcription activation. A similar study by Reddy et al (2008) using the Lac O – Lac I interaction, involved the re-localisation of an integrated reporter gene from the interior of mammalian nuclei to the periphery (via anchoring to the inner nuclear membrane) (Reddy et al., 2008). Reddy et al (2008) found that recruitment to the periphery can induce transcriptional repression of the aforementioned gene (Reddy et al., 2008). However, as a caveat towards the dogma of the nuclear periphery being an exclusive region of gene suppression, Bickmore and colleagues noted that although located at the nuclear periphery, some genes were still actively transcribed (Finlan et al., 2008). Indeed in yeast, transcriptionally active genes have been found located around the nuclear pore complex (Brown and Silver, 2007).

On the other-hand, repositioning of genes to the nuclear interior from the periphery has been correlated with transcriptional activation (Williams et al., 2006, Szczerbal et al., 2009). During embryogenesis, a vital transcription factor Mash (AsII), is required for the production of neuronal precursor cells (Williams et al., 2006). In embryonic stem cells, the *Mash 1* gene is transcriptional repressed, however during neuronal differentiation it is preferentially repositioned from the nuclear periphery to the nuclear interior and is transcriptional up-regulated by more than 100 fold (Williams et al., 2006). Not only was the *Mash 1 gene* loci shown to alter nuclear position upon an increase in transcriptional activity, but also the time in which it replicates during S-phase; which altered from late replicating (in association with inactive genes and heterochromatin) in undifferentiated cells to early replicating (in association with active genes and euchromatic regions of the genome) in differentiated cells (Perry et al., 2004). Such changes in the replication time maybe indicative of global re-organisation of chromatin. Indeed, the impact of cellular differentiation upon specific gene loci repositioning and transcriptional activation has also

been reported in porcine mesenchymal stem cells (Szczerbal et al., 2009). Seven genes involved in adipogenesis were found to adopt a more internal position upon the induction of adipogenesis and transcriptional up-regulation (Szczerbal et al., 2009). The genomic re-organisation also extended to whole chromosome territories containing the adipogenesis gene loci moving to the nuclear interior (Szczerbal et al., 2009). This study was able to demonstrate gene loci looping away from chromosome territories as extensions of chromatin fiber; indeed the localization of gene loci away from specific chromosome territories have been documented in numerous studies (Volpi et al., 2000, Mahy et al., 2002b, Williams et al., 2006, Szczerbal et al., 2009).

The decondensation of chromatin away from the surface of chromosome territories has been shown to extend several megabases and it is postulated to be dependent on transcriptional activity and gene density of the chromatin fiber as opposed to the transcriptional activity of individual genes (Mahy et al., 2002b). The up-regulation of genes and the movement of gene loci may correlate with the location of transcription factories (Osborne et al., 2004, Osborne et al., 2007). It has been shown by Osborne et al (2007) that genes can occupy the same transcription factory and may migrate to different transcription factories as a function of transcription activity. Through studying the intermediate early (IE) gene induction in mouse B lymphocyte, Osbourne et al (2007) showed that the *Myc* proto oncogene on chromosome 15, relocated and occupied a mutual transcription factory of the transcriptionally active *Igh* gene located on chromosome 12 (Osborne et al., 2007). This study suggests that genes may relocate to pre-assembled transcription factories and adds more credence to the dynamic nature of the nucleus (Osborne et al., 2007, Osborne et al., 2004).

In summary, *B. glabrata* genes have been documented to alter their transcriptional activity upon parasitic invasion. Indeed, in other organisms, changes in transcriptional activity have

been correlated with the spatial re-organisation of gene loci in the interphase nuclei, with the interior correlating with transcriptional activity and the periphery correlating with transcriptional down-regulation. This chapter seeks to address the role *S. mansoni* infection plays in genome re-organisation in *B. glabrata in vitro*, by investigating the spatial organisation of the *B. glabrata* gene loci in the interphase nuclei of the Bge cells post exposure to *S. mansoni* and comparing this to the expression of the genes.

5.2. Materials and Methods

5.2.1 Bge cell culture

Bge cell line isolate 1 was utilised for this experiment. The Bge cells were grown and cultured by collaborators at the BRI laboratory (Biomedical Research Institute, Rockville, USA) in the same manner described in chapter 2.

5.2.2 Exposure to *S. mansoni* miracidia

The Bge cells in T75 flasks were exposed to five *S. mansoni* miracidia. The exposure was for different durations of time (0.5, 2, 5, 24 hr). After the specified period of time, the cells were subsequently dislodged from the flasks via the application of either a cell scraper (Falcon, Becton Dickinson Labware, Franklin Lakes, NJ) or by firmly tapping the flask. The cells were then centrifuged at 400g at 15^{o}C. The cell pellets were resuspended by vigorously tapping the tube, followed by the addition of hypotonic potassium chloride solution (0.05 M) and subsequently fixed with methanol and acetic acid (3:1 v/v).

5.2.3 Fluorescence *in-situ* hybridisation (FISH) of the ferritin and actin gene loci onto Bge cell interphase nuclei

The ferritin and actin gene loci probes used in chapter 3 for FISH onto metaphase chromosomes were employed in this study for gene hybridisation onto interphase nuclei from the Bge cells exposure to the miracidia for the aforementioned different time periods. The FISH procedure was the same as that used in chapter 3. Briefly, the probe was composed of 500 ng of the nick translated labelled BAC DNA, 3 µg of herring sperm DNA as carrier and 40 µg of sonicated Bge genomic DNA dissolved in 12 µl of hybridization mixture. Following probe and nuclei denaturation, 8µl of the biotin labelled probe was placed onto a slide containing Bge interphase nuclei (aged for 2 days at room temperature), and hybridized overnight in a humidified chamber. The slides with the interphase nuclei and hybridised probe, were washed and subsequently blocked with 4% bovine serum albumin, BSA, in 4 X SSC. After blocking, the probe was immunologically detected by incubating the interphase nuclei on the slide with streptavidin conjugated to cyanine 3. The slides were washed, counterstained with DAPI in Vectorshield mountant (Vectorlabs) and mounted with a 22 x 50 mm coverslip.

5.2.4 Image capture and analysis

The interphase nuclei with hybridised gene loci were visualised using an epifluorescence microscope and X100 oil immersion objective (Zeiss, Axioplan 2). The images were captured using a charged coupled device (CCD) camera (RS Photometrics Sensys camera model KAF1401E G2) and the program Smart capture 3.00 (Digital Scientific). The hybridized *B. glabrata* ferritin and actin genes in interphase nuclei of the Bge cell line isolate 1 were analysed using an erosion analysis script developed by Dr Paul Perry in IPLab software (Croft *et al*., 1999) and was kind gift from Prof. Wendy Bickmore (MRC HGU, Edinburgh). The interphase positioning of the hybridised *B. glabrata* genes were analysed by partitioning DAPI images of the nuclei into five concentric shells of equal area

from the nuclear periphery to the centre and the background removed from the FISH signal by subtracting the mean pixel intensity of the nuclei. The fraction of DAPI to probe signal was determined and normalised by division with the DNA content of each cell.

5.2.5 Real time RT-PCR analysis of Bge cell ferritin and actin transcripts

The experiment was performed by collaborators from the BRI laboratory to accurately analyse the quantitative differences in the induction level of ferritin and actin transcript following exposure to *S. mansoni* miracidia for different durations (0, 0.25, 0.5, 2, 5 and 24 hr). The Real time PCR was performed using the Applied Biosystems 7300 Real Time PCR System (Applied Biosystem, Foster City, CA). Reactions were performed in a one step format with total Bge cell RNA (80 ng). Synthesis of first strand cDNA and amplification by PCR were performed sequentially in a single tube using Full velocity SYBR Green QRT-PCR Master mix according to the manufacturers' instructions (Stratagene). Reactions (25µl final volume) contained the following; 200nM of specific *B. glabrata* primers for ferritin (F: 5'-CTCTCCCACACTGTACCTATC-3'; R: 5'-CGGTCTGCATCTCGTTTTC-3'), actin (F: 5'-GGAGGAGAGAGAACATGC-3'; R: 5'-CACCAATCTGCTTGATGGAC-3'). A parallel reaction was performed with the stably expressed myoglobin gene (50 nM of *B. glabrata* specific myoglobin primers F: 5'-GATGTTCGCCAATGTTCCC-3'; R: 5'AGCGATCAAGTTTCCCCAG-3') to assess the comparability of samples and confirm that template cDNA was used in equivalent amounts for each amplification reaction. All reactions contained 300 nM of reference dye, 1X of Full Velocity SYBR Green QRT-PCR master mix containing RT-PCR buffer, SYBR green I dye, $MgCl_2$, and nucleotides. The amplification protocol included an initial incubation at 48^oC for 45 min for cDNA synthesis and a 95^oC initial denaturation for 10 sec, and annealing/ amplification at 58^oC for 1 min. Detection of the fluorescent product was carried out at the end of the amplification period. All amplifications were run in triplicate

and the fluorescence threshold value (Ct) was determined using the 7300 System v1.3.1 SDS software (Applied Biosystems). Comparison of the expression of the ferritin and actin genes between pre and post exposure Bge cells was determined using delta-delta (ΔΔ) Ct.

Results were transformed into 'fold increase' according to the following formula:

Fold change = $2^{-\Delta\Delta Ct}$

= 2^{-} [$^{(Ct}$Actin or Ferritin, exposed^{-Ct}myoglobin, exposed$^{)-(Ct}$Actin or Ferritin, unexposed^{-Ct}myoglobin, unexposed$^{)}$]

In order to determine the significance of differences ($P< 0.01$) and ($P < 0.05$) in gene expression for the different time points the *P*-value was calculated by comparing delta Ct values using the Student's *t*-test between the exposed and unexposed Bge cells.

5.3. Results

5.3.1 The radial positioning of the ferritin gene in the interphase nuclei of the Bge cells post exposure to miracidia

As demonstrated in chapter 3, the *B. glabrata* gene ferritin mapped onto diploid homologous metaphase chromosomes and in chapter 4, this gene was shown to be located non-randomly in the interphase nuclei of the Bge cells. Using FISH, the ferritin gene was hybridised onto interphase nuclei derived from Bge cells exposed to miracidia. The cells were co-cultured with the parasite for different durations of time; 0.5, 2, 5, and 24 hr. Fig 5.1 displays a selection of representative images of the FISH performed on these cells using the ferritin probe. Fig 5.1 A, is a representative image of a nucleus from the cells exposed 0.5 hr to miracidia, the two ferritin signals are positioned at the centre of the nucleus. The image of the nucleus from 2 hr exposed cells (Fig 5.1 B) shows a condensed chromatin structure, dispersed with brighter regions of punctate foci. The ferritin signals

are located towards the interior of the nucleus. The representative image of the 5 hr exposure in Fig 5.1 C shows the ferritin signals positioned internally. Fig 5.1 D shows the representative image of the nuclei from the 24 hr exposed Bge cells; the ferritin signal is less internal than the previous 0.5, 2 and 5 hr nuclei.

Figure 5.1: Representative images of 2D FISH of *B. glabrata* ferritin gene onto interphase nuclei from Bge cells exposed to *S. mansoni* miracidia.

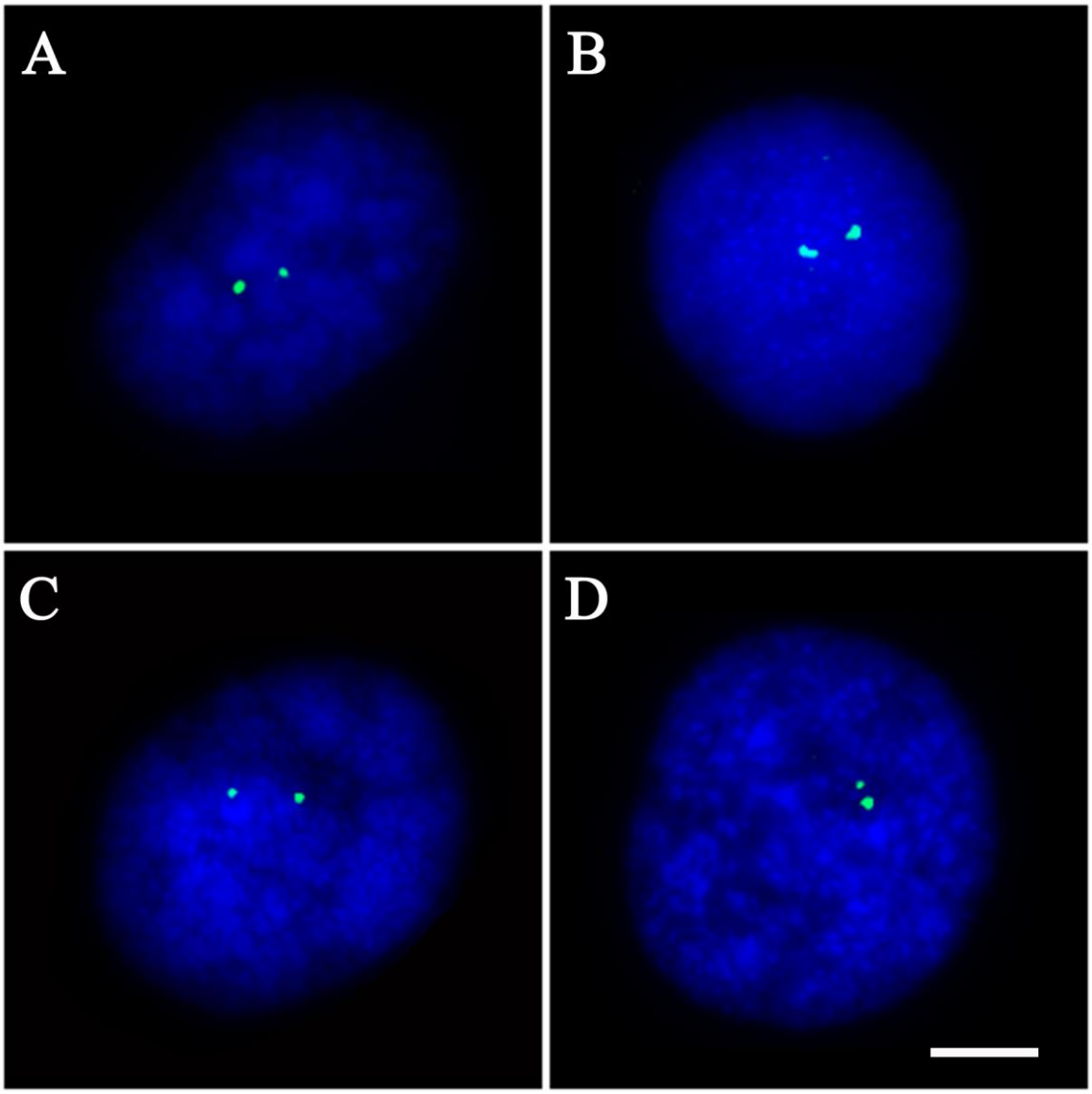

Representative images of 2D FISH hybridized *B. glabrata* gene ferritin in the interphase nuclei of *B. glabrata*. The images show the DAPI (blue) and the gene loci (green). The nuclei are derived

from Bge cells post exposure to the *S. mansoni* miracidia (A) 0.5 hr (B) 2 hr, (C) 5 hr and (D) 24 hr. Bar 5 µm.

The ferritin gene was visualised non-randomly in the interphase nuclei of the Bge cells exposed to miracidia. 50-60 2D FISH images of the *B. glabrata* gene ferritin (as represented in Fig 5.1) were hybridized onto Bge cell interphase nuclei and analysed using the previously mentioned erosion analysis script (Croft et al., 1999). The images of the nuclei were partitioned into five concentric shells of equal area. The intensity of the fluorescent signal from the DAPI and the Cy3 (observed as a green signal) of the gene probe were measured for each shell. The signal was normalised by division with the DNA content of each shell. This analysis was performed on Bge nuclei from the 0.5, 2, 5 and 24 hr exposures to miracidia. Fig 5.2 displays the results from the positioning of the ferritin pre and post exposure to miracidia. Fig 5.2 A is the histogram for the ferritin gene before exposure to miracidia. The ferritin gene is positioned peripherally and the histogram is skewed greatly to the right. Upon exposure to miracidia, the ferritin changes nuclear position and is located more to the interior in Fig 5.2 B at 0.5 hr. The histogram displayed in Fig 5.2 B contrasts greatly with Fig 5.2 A inasmuch as the largest proportion of probe signal is found in shell 5 (interior) rather than shell 1 (periphery) as in Fig 5.1. A. The ferritin gene remains positioned internally at 2 hrs post exposure to miracidia (Fig 5.2 C); the distribution of the probe signal in the nucleus is similar to the nuclei of the 0.5 hr exposure, with shell 5 having the largest proportional of ferritin signal. However, the ferritin gene can be considered to occupy a more internal position since Fig 5.2 C shows there is a larger distribution of gene signal in shell 4 when compared with Fig 5.2 B. At 5 hrs post exposure to miracidia, the ferritin gene is still in an interior position with the histogram in Fig 5.2 D skewed to the right. However, at 5 hrs post exposure, more of the ferritin gene signal is found in shell 4 than in shell 5 as observed at 0.5 and 2 hr post

exposure to miracidia; which shows a slight shift in position of the ferritin gene away from the interior. After 24 hrs post exposure to the miracidia, the position of the ferritin gene in the interphase nuclei of the Bge cells remains radically altered from the position pre exposure to miracidia. The histogram in Fig 5.2 E, displays the ferritin positioned towards the interior; the ferritin gene has shifted to a more internal position than was observed at 5 hrs post exposure with largest proportion of ferritin gene signal found in shell 5 than shell 4.

Figure 5.2: Histograms displaying the radial distribution of the *B. glabrata* ferritin gene interphase nuclei of the Bge cells pre and post exposure to *S. mansoni* miracidia

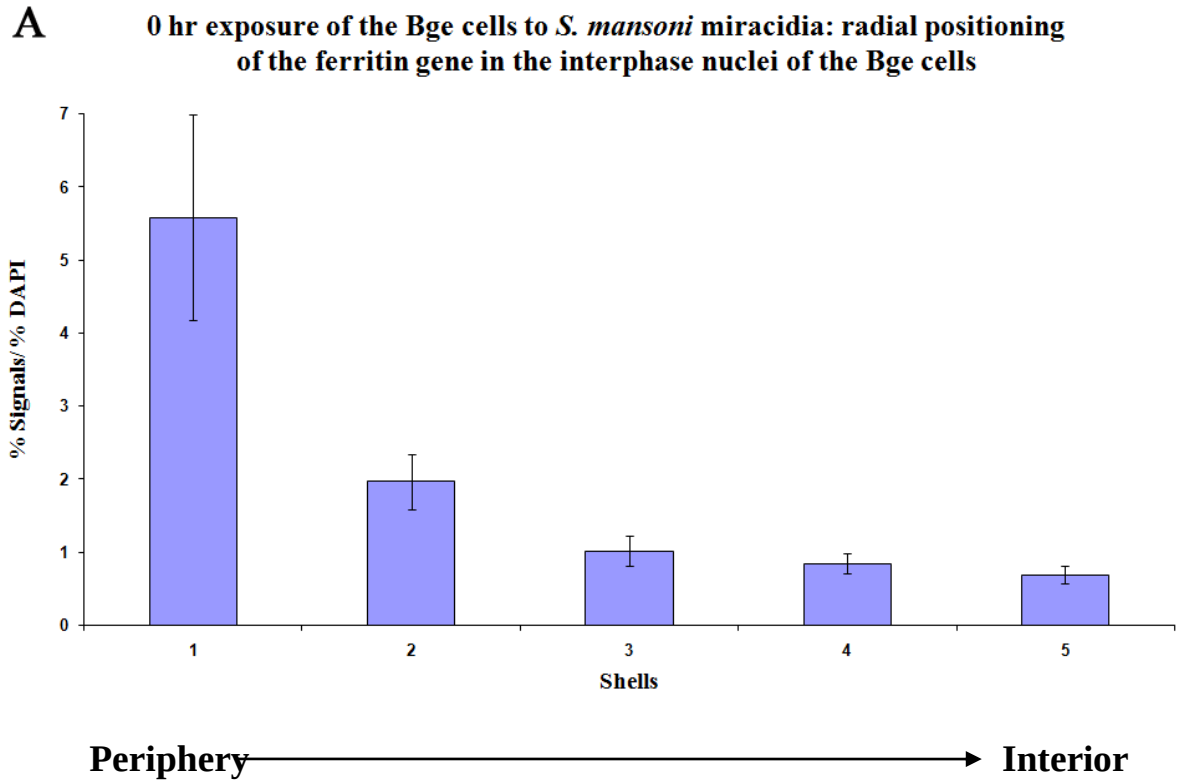

Histogram A, previously shown in chapter 4, showing the radial positioning of *B. glabrata* ferritin gene in the interphase nuclei of the unexposed Bge cells. The histogram was prepared by using an erosion analysis script which partitions the nucleus into five concentric shells of equal area (x axis), periphery shell 1 to interior shell 5 (Croft et al., 1999). The intensity of the fluorescence signals from the gene probes ferritin was measured for each shell and normalised by division of the DNA

content of each shell (Y axis). The position of the ferritin gene was analysed for the different exposure times of nuclei to miracidia.

B **0.5 hr exposure of Bge cells to *S. mansoni* miracidia: radial positioning of the ferritin gene in the interphase nuclei of the Bge cells**

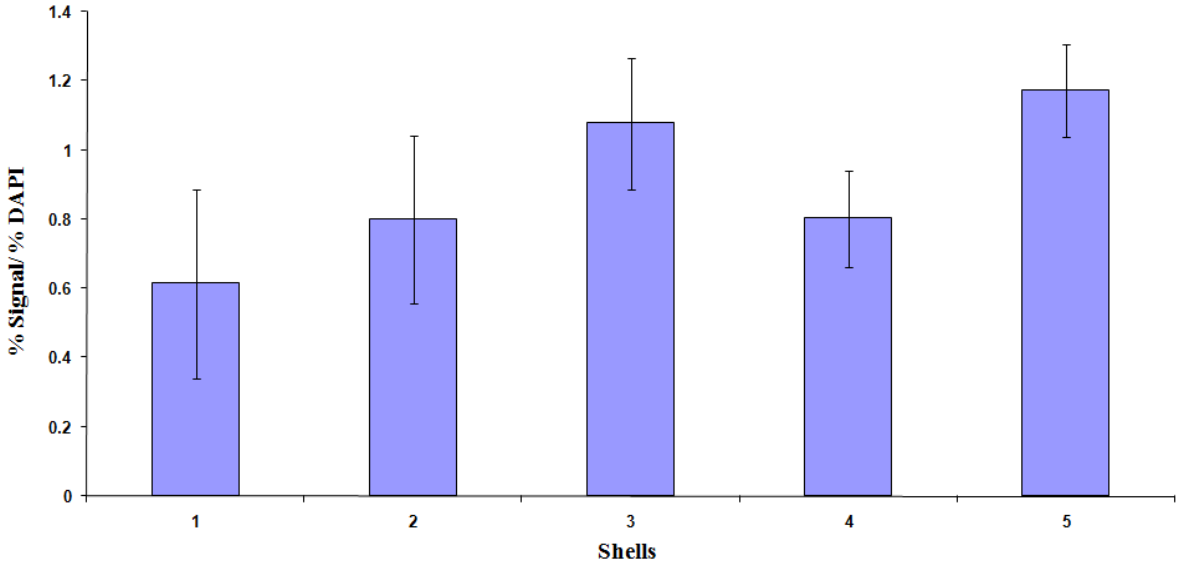

Periphery ⟶ **Interior**

C **2 hr exposure of the Bge cells to *S. mansoni* miracidia: radial positioning of the ferritin gene in the interphase nuclei of the Bge cells**

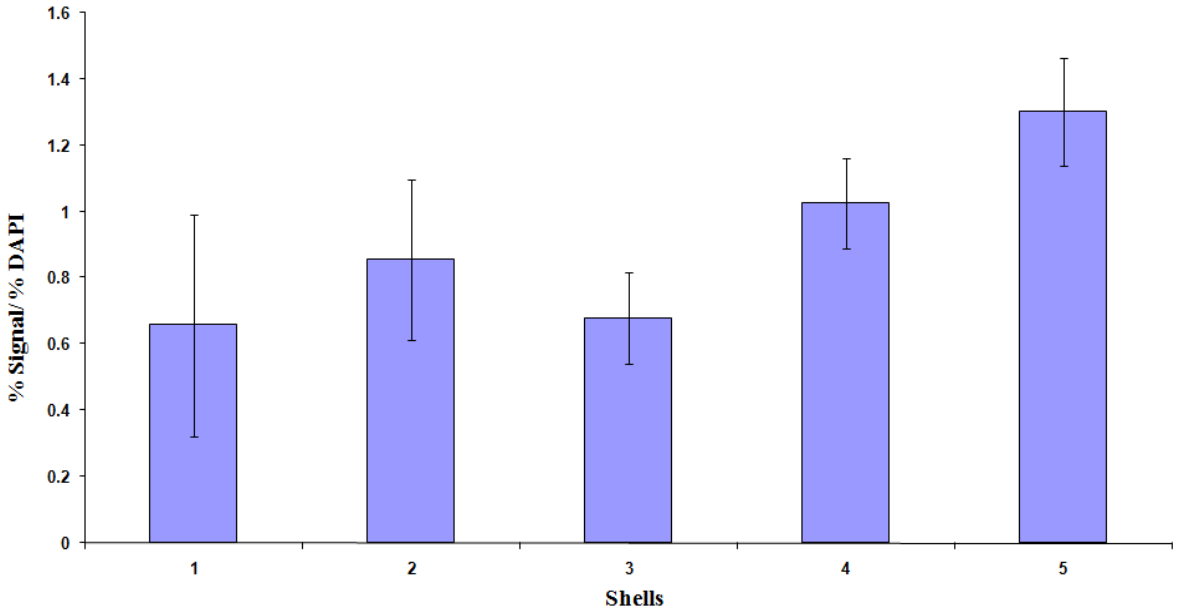

Periphery ⟶ **Interior**

D

5 hr exposure of the Bge cells to *S. mansoni* miracidia : radial positioning of the ferritin gene in the interphase nuclei of the Bge cells

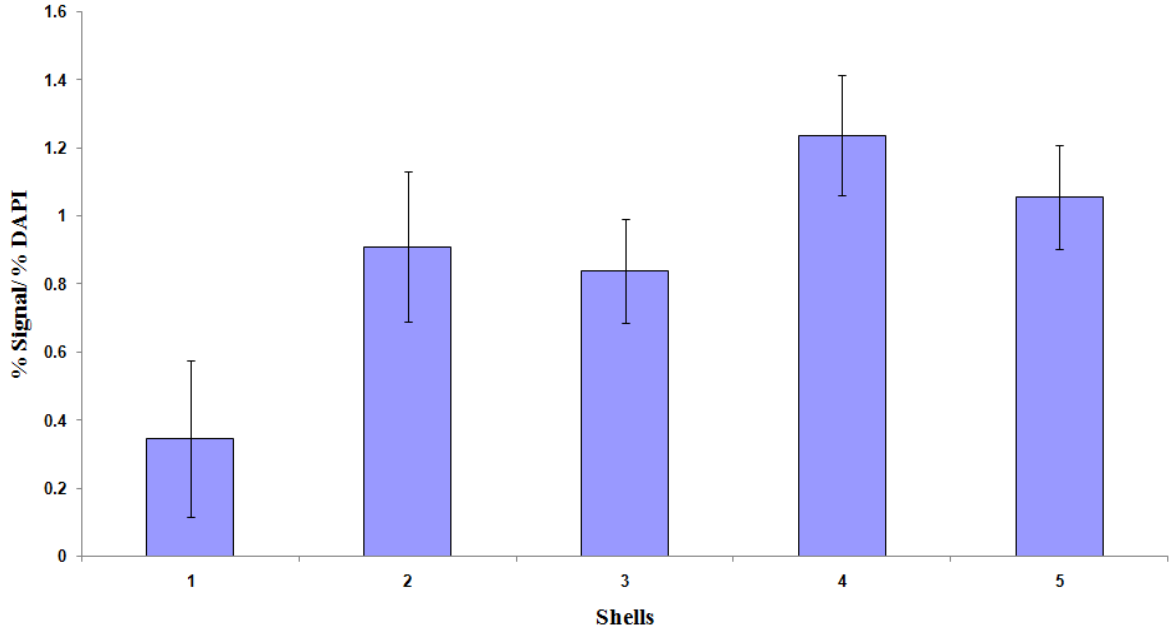

Periphery ⟶ **Interior**

E

24 hr exposure of the Bge cells to *S. mansoni* miracidia : radial positioning of the ferritin gene in the interphase nuclei of Bge cells

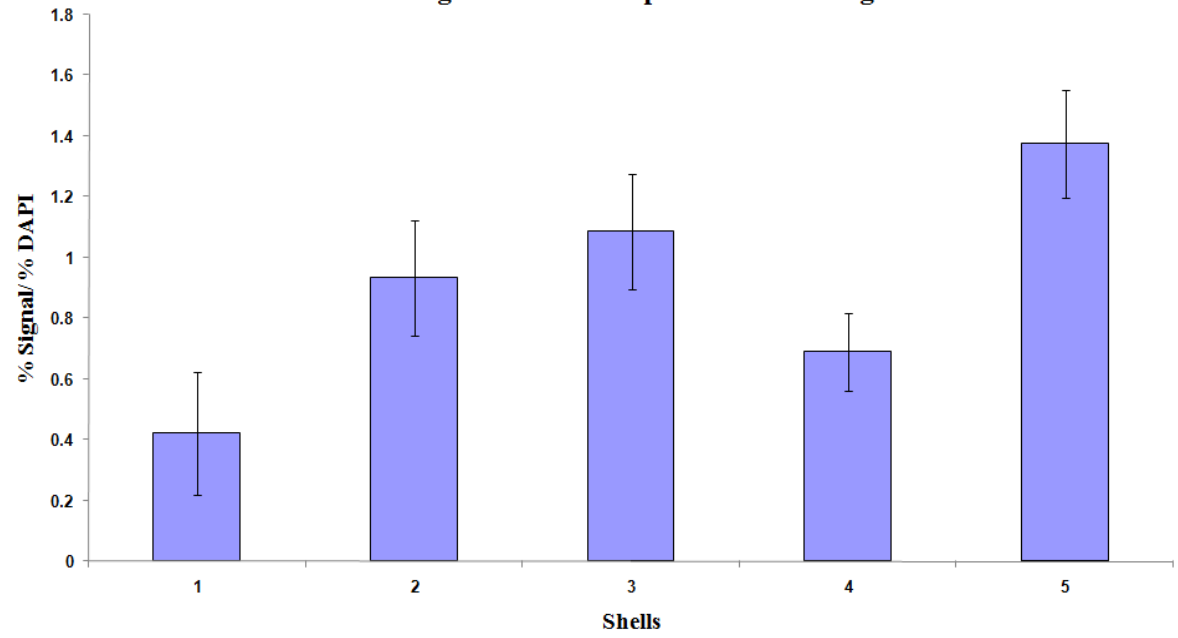

Periphery ⟶ **Interior**

Histograms showing the radial positioning of *B. glabrata* ferritin gene in the interphase nuclei of the Bge cells. The histograms were prepared by using an erosion analysis script which partitions the nucleus into five concentric shells of equal area (x axis), periphery shell 1 to interior shell 5 (Croft et al., 1999). The intensity of the fluorescence signals from the gene probes ferritin was measured for each shell and normalised by division of the DNA content of each shell (Y axis). The position of the ferritin gene was analysed for the different exposure times of nuclei to miracidia (B) 0.5 hr, (C) 2 hr (D) 5 hr (E) 24 hr.

5.3.2 Real time RT-PCR reveals temporal modulation of ferritin gene expression in Bge cells upon exposure to miracidia

In order to analyse the quantitative difference in ferritin transcripts from the Bge cells post exposure to miracidia, RNA from the Bge cells was isolated before and after exposure and examined by real-time RT-PCR. This experiment was performed by collaborators from the BRI laboratory in Washington (Rockville, USA). The real-time Q-RT-PCR was performed twice using the methods stipulated in section 5.2. The first real-time RT-PCR experiment (Fig 5.3 A) analysed the transcript levels of ferritin from Bge cells at 0 hr and those exposed to miracidia for 0.25, 1, 5 and 24 hr. As displayed in Fig 5.3 A, after 0.25 hr there is a significant 8.1 fold increase in transcript level (from the basal level of 1 before exposure to miracidia). The transcript falls from 8.1 to 1.6 fold 1 hr post exposure. Subsequently, the transcript level is more than doubled for 5 and 24 hr with significant fold increases of 2.4 and 2.6 respectively. In contrast, the second real-time RT-PCR experiment (Fig 5.3 B) examined the ferritin transcript levels from Bge cells at 0 hr and those exposed to miracidia for 0.25, 0.5, 1, 2, 5, and 24 hr. The transcript level at 0.25 hr increases significantly by 4.6 fold however, this is considerable less than the 8.1 fold increase observed in the first real-time RT-PCR. Interestingly, in both real-time RT-PCR experiments, the ferritin gene transcripts are at the highest levels at 0.25 hr post exposure to miracidia. At 0.5 hr, the ferritin transcript level drops to near basal level at 0.9 fold. The

following post exposure hours of 1, 2, 5 and 24 show an up and down fluctuation around the basal level with the respective transcript levels altering at 1.6, 0.8, 1.2 and 1.6 fold.

5.3.3 Correlating the temporal modulation of ferritin gene expression with the position of the ferritin gene in the interphase nuclei of the Bge cells

The results in Fig 5.2 and Fig 5.3 clearly show *S. mansoni's* induction of transcription of ferritin correlated with genome reorganisation in Bge cell interphase nuclei in terms ferritin gene position and the induction of the ferritin encoding transcript. The ferritin gene shifts from occupying a peripheral position in the interphase nuclei of Bge cells before exposure to *S. mansoni* to an interior position post exposure to *S. mansoni*. As described in section 5.1.2, published studies into gene positions in the interphase nucleus have correlated specific regions of the nucleus with transcriptional activity; the periphery being a region of transcriptional suppression and the interior a site a transcriptional activation (Finlan et al., 2008). At 0.5 and 2 hr (Fig 5.3 B), the ferritin gene is located towards the interior of the Bge cell interphase nucleus however, the respective transcript levels of 0.9 and 0.8 fold remain close to the basal level of 1. However, the ferritin transcript level increases to 2.4 and 2.6 fold for 5 and 24 hr respectively in Fig 5.3 A. Indeed, the ferritin gene occupies an internal position at the 5 and 24 hr post exposure stage. In addition, the ferritin gene position shifts to a more internal position from the 5 to the 24 hr post exposure (Fig 5.2 D and E). This movement to an internal position may correlate with the slight increase in transcript level of 2.4 to 2.6 observed at 5 and 24 hr post exposure (Fig 5.3 A). However, the transcription level at 5 and 24 hr in the second real-time PCR (Fig 5.3 B) show that there is no significant increase in ferritin transcript level.

Figure 5.3: The temporal modulation in gene expression of ferritin gene in the Bge cells upon exposure to *S. mansoni* miracidia

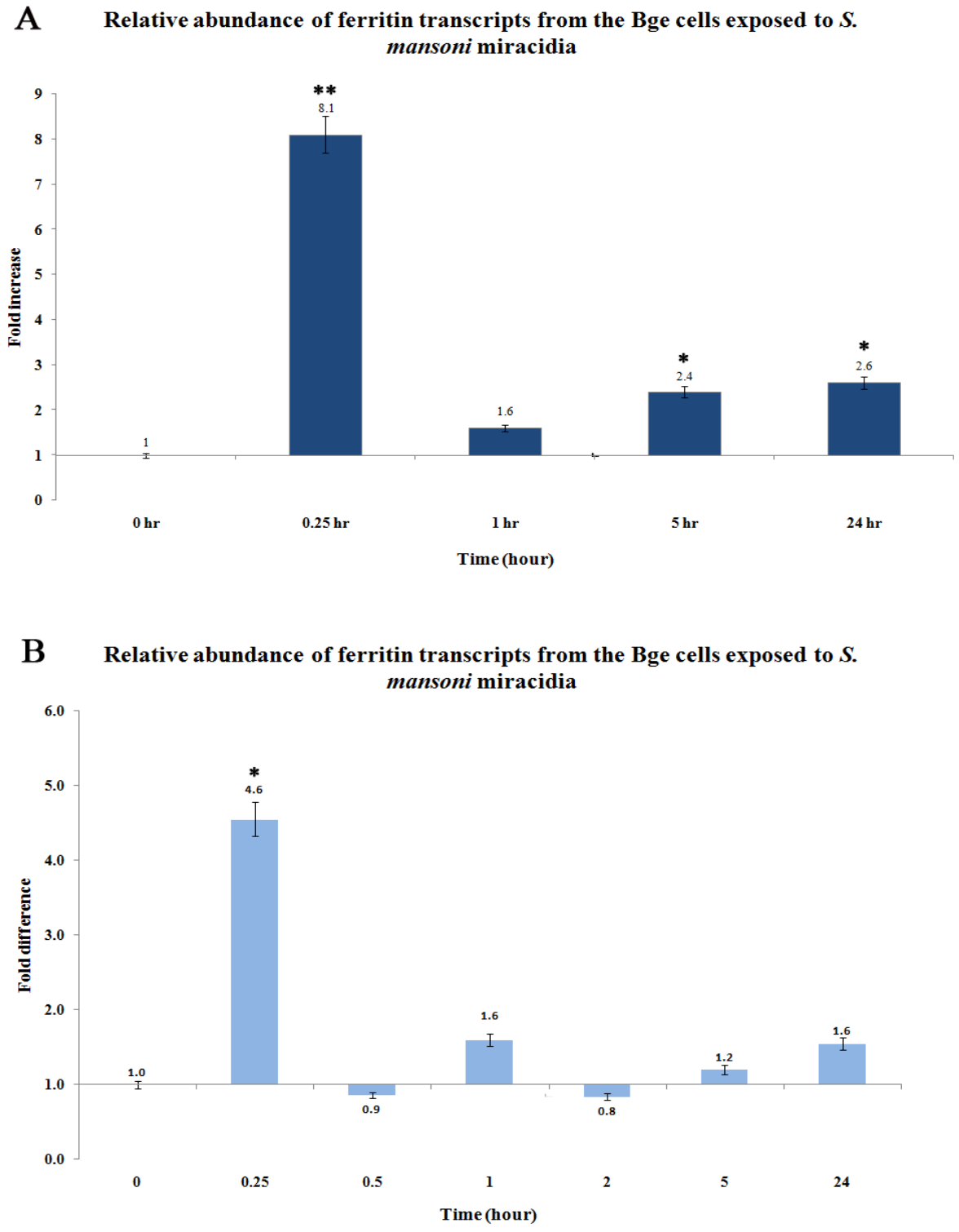

The differential expression of the ferritin transcripts by real-time Q-RT-PCR in Bge cells following exposure to *S. mansoni* miracidia for no exposure (0 hr) or exposure for 0.25 , 0.5, 1, 2, 5 and 24

hr. The fold change of expression of transcript was determined by comparing the unexposed and exposed Bge cells by comparative Ct method and the formula (as described in section 5.2) with the normalised basal level of expression in unexposed Bge cells as 1.0. Error bar= S.D. The significant *P*-value < 0.01 are indicated by ** and the significant P-value < 0.05 are indicated by * at the top of each bar.

5.3.4 The radial positioning of actin gene loci in the interphase nuclei of the Bge cells post exposure to miracidia

Figure 5.4: Representative images of 2D FISH of *B. glabrata* actin gene onto interphase nuclei from Bge cells exposed to *S. mansoni* miracidia

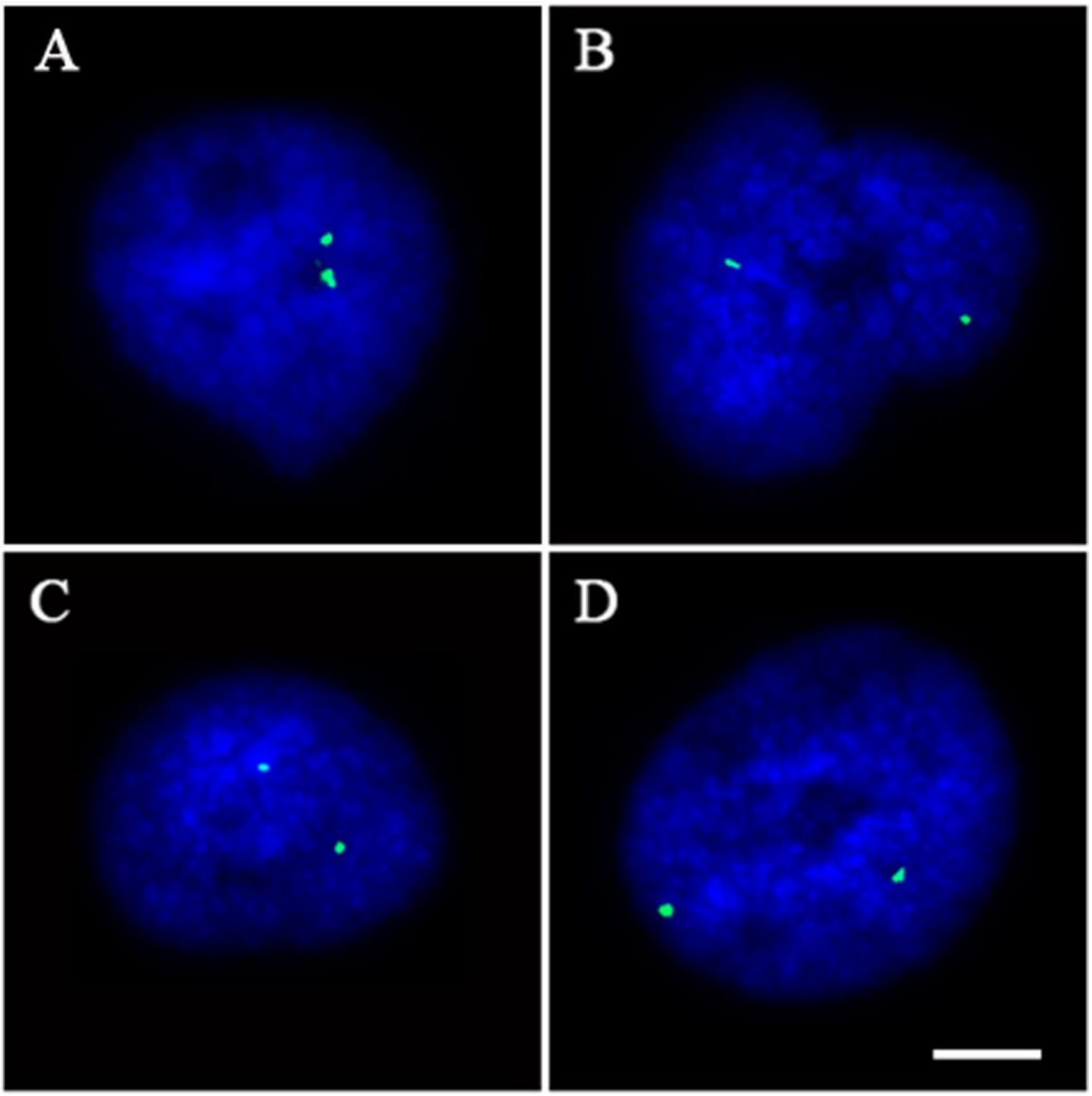

Representative images of 2D FISH hybridized *B. glabrata* gene actin in the interphase nuclei of the Bge cells. The images show the DAPI (blue) and the gene loci (green). The nuclei were derived from Bge cells post exposure to the *S. mansoni* miracidia (A) 0.5 hr (B) 2 hr, (C) 5 hr and (D) 24 hr. Bar 5 µm.

Using FISH, the actin gene probe was shown to map on two homologous metaphase chromosomes from the Bge cell line in chapter 3 and two gene signals were observed to be non-randomly positioned in the Bge cell interphase nuclei in chapter 4. The Bge cell nuclei used in this study were derived from cells exposed to *S. mansoni* miracidia for different durations of time; 0.5, 2, 5 and 24 hr. The actin gene probe was hybridised onto the interphase nuclei using FISH, the representative images (from a population of the nuclei) are presented in Fig 5.4. The actin gene signals in Fig 5.4 A for the 0.5 hr exposure are located in close proximity of each other towards the interior of the nucleus. The actin genes observed in Fig 5.4 B for the 2 hr post exposure are further apart and occupy positions in the nucleus towards the periphery. Fig 5.4 C and D, display the representative images of the actin gene signals in Bge cell nuclei from the 5 and 24 hr post exposure. Actin gene signals at 5 hr occupy interior and intermediate positions (Fig 5.1 C) in contrast to the 24 hr exposure nuclei in which the signals are intermediate and peripheral (Fig D).

As described previously for the ferritin gene, the actin gene loci were positioned radially in the interphase nuclei of the Bge cells exposed to miracidia. 50-60 2D FISH images of the *B. glabrata* gene actin gene (as represented in Fig 5.5) were hybridized onto Bge cell interphase nuclei and analysed using the previously mentioned erosion analysis script (Croft et al., 1999). The images of the nuclei were partitioned into five concentric shells of equal area. The intensity of the fluorescent signal from the DAPI and Cy3 (in green) of the gene probe were measured for each shell.

Figure 5.5: Histograms displaying the radial distribution of the *B. glabrata* actin gene in the interphase nuclei of the Bge cells pre and post exposure to *S. mansoni* miracidia

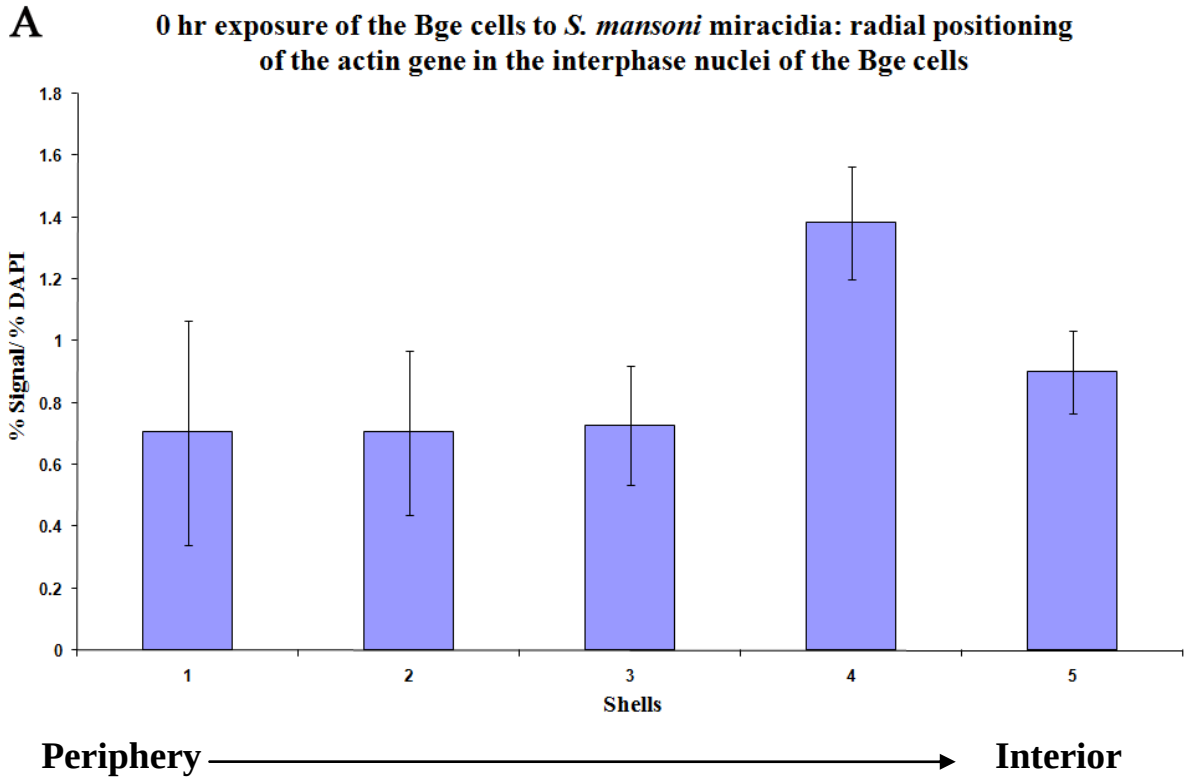

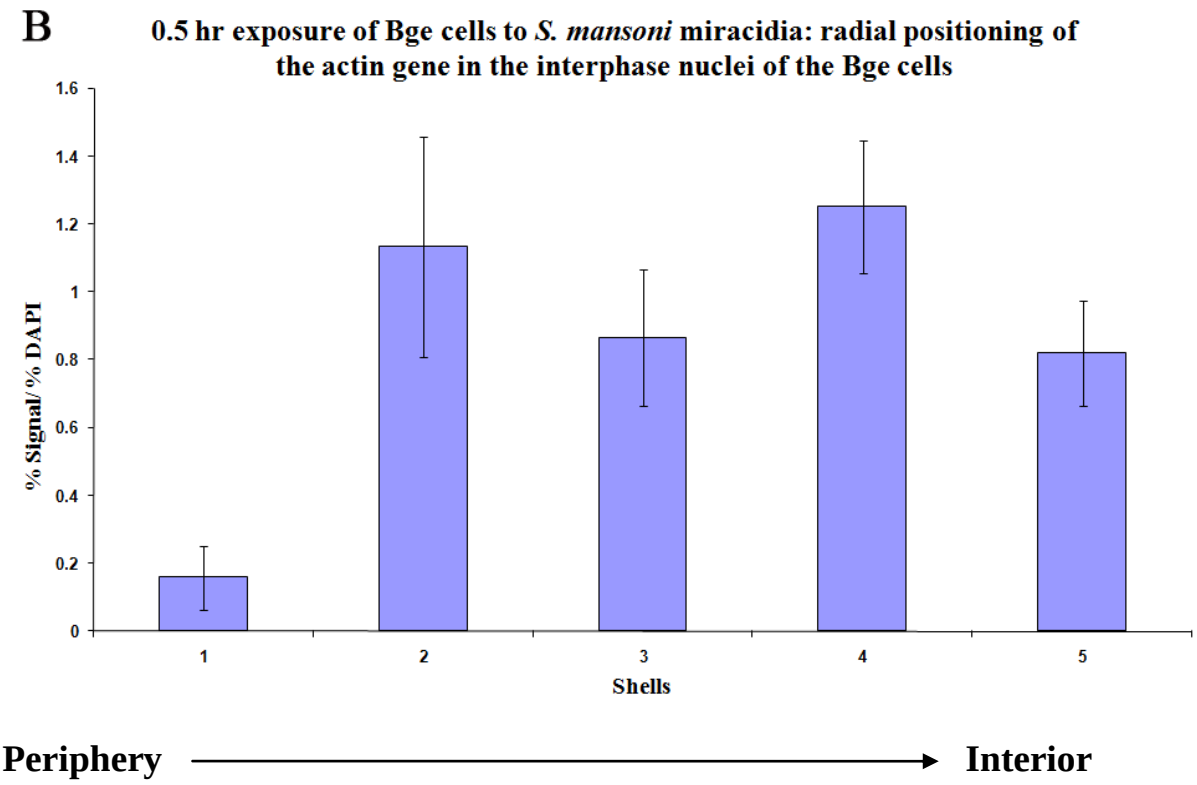

C

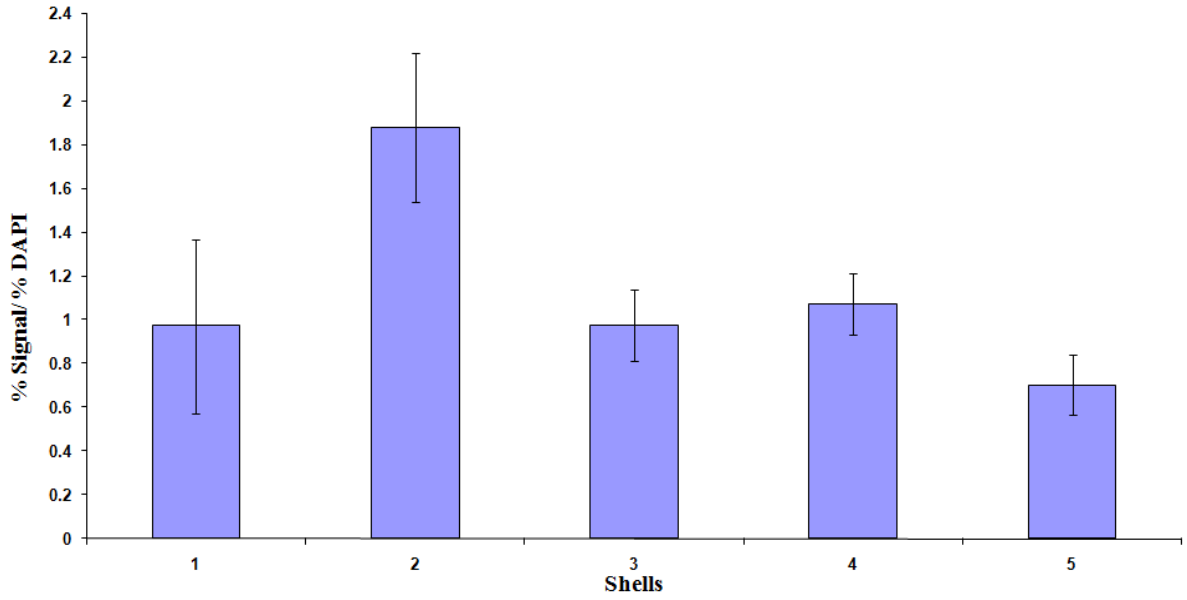

Periphery ⟶ **Interior**

D

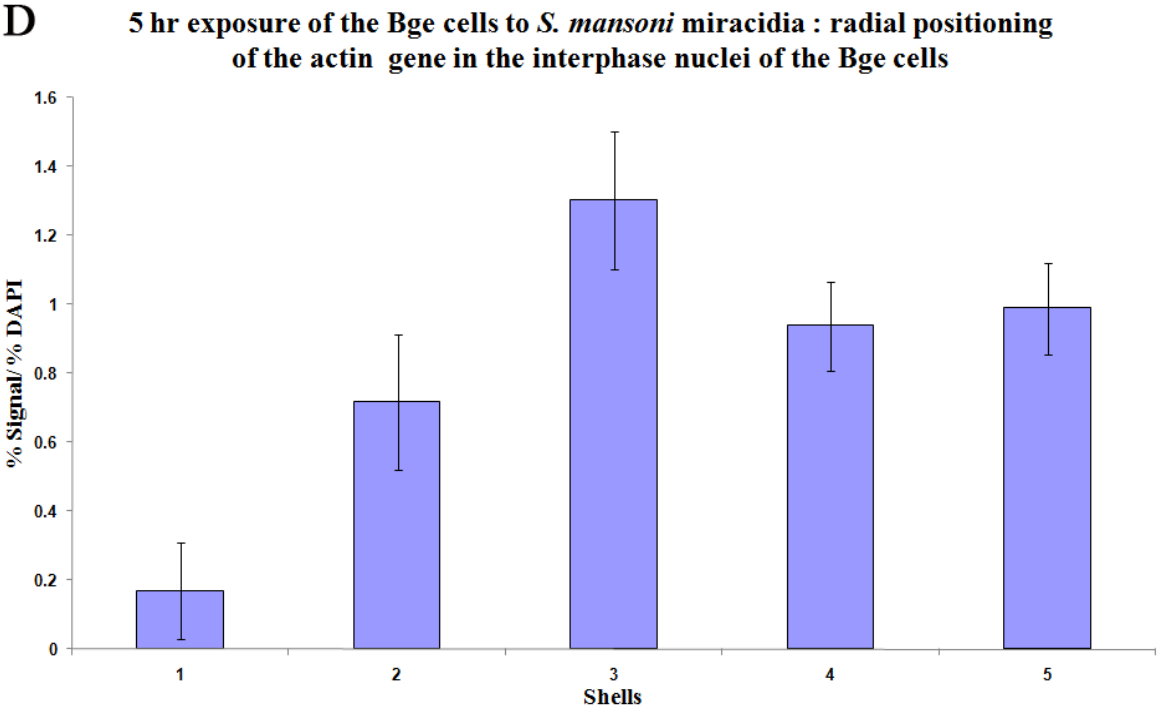

Periphery ⟶ **Interior**

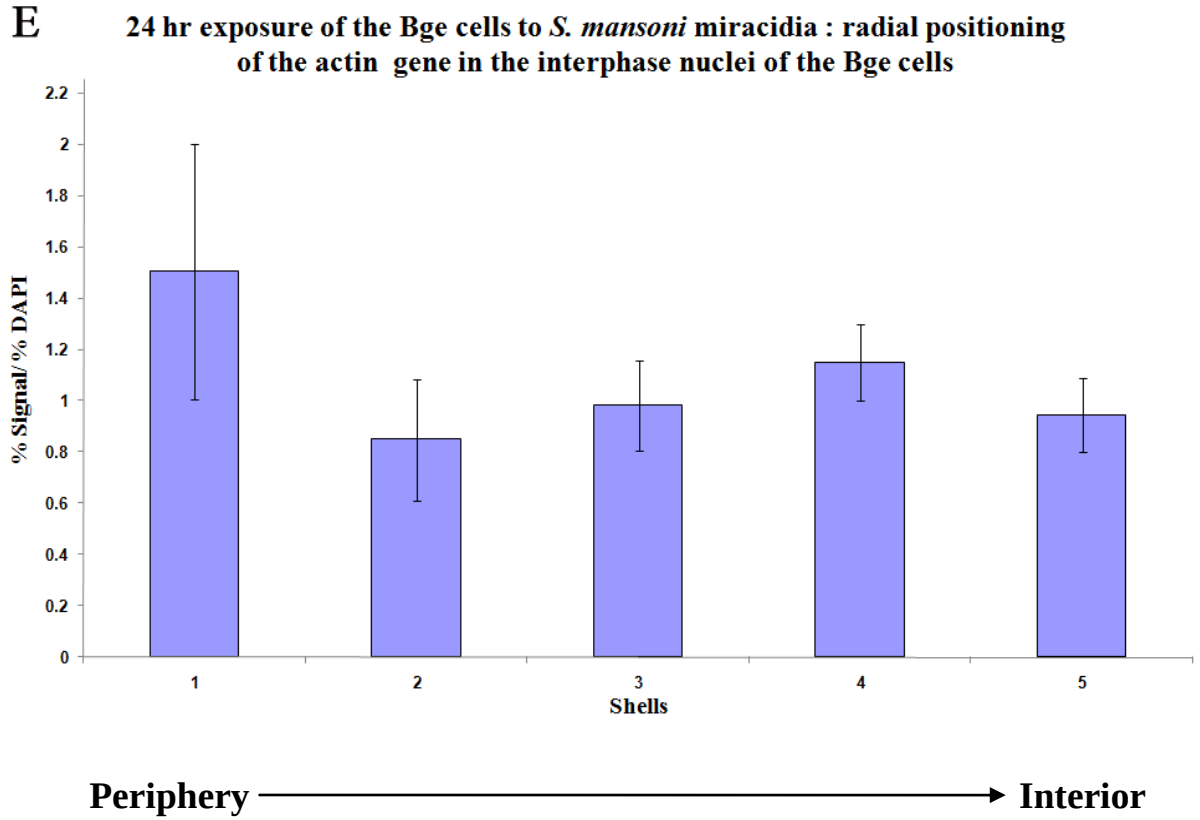

Histograms showing the radial positioning of *B. glabrata* actin gene in the interphase nuclei of the Bge cells. The histograms were prepared by using an erosion analysis script which partitions the nucleus into five concentric shells of equal area (x axis), periphery shell 1 to interior shell 5 (Croft et al., 1999). The intensity of the fluorescence signals from the gene probes actin was measured for each shell and normalised by division of the DNA content of each shell (Y axis). The position of the actin gene was analysed for the different exposure times of nuclei to miracidia (A) pre exposure 0 hr- previously shown in chapter 4, (B) 0.5 hr, (C) 2 hr (D) 5 hr (E) 24 hr.

The signal was normalised by division with the DNA content of each shell. This analysis was performed on Bge nuclei from the 0.5, 2, 5 and 24 hr post exposure to miracidia. Histograms showing the radial distribution of the actin gene pre-exposure to miracidia (shown previously in chapter 4) are displayed in Fig 5.5 alongside histograms for the aforementioned exposure times to miracidia. At 0 hr (Fig 5.5 A) the actin gene is located in an intermediate position with a slight bias toward the interior of the nucleus, however the actin gene position is altered as observed after 0.5 hr exposure in which the histogram in Fig 5.5 B displays a bimodal distribution with slight bias toward the interior of the nucleus.

Fig 5.5 C presents a histogram whereby the actin gene is positioned towards the periphery, with the largest proportion of gene signal located in shell 2. The histogram for the 5 hr exposure (Fig 5.5 D) shows the actin located in an intermediate position with slight bias towards the interior, shell 3 having the largest proportion of actin gene signal followed by shell 5 and 4. At 24 hr post exposure to miracidia, actin again alters position and is located towards the periphery, with shell 1 having the largest proportion actin gene signal.

5.3.5 Real time RT-PCR reveals temporal modulation of the actin gene expression in Bge cells upon exposure to miracidia

As explained previously for the analysis of the modulation in the level of the ferritin transcript, RNA from the Bge cells before exposure to miracidia and post exposure to miracidia was isolated and analysed by real-time RT-PCR. The experiment was performed twice by collaborators from the BRI laboratory (Rockville, USA) using the methods described in section 5.2. The results from the first real-time RT-PCR experiment are displayed in Fig 5.6 A and shows the induction of the actin gene expression begins at 0.25 hr whereby the transcript level increases significantly to 7.5 fold. Thereafter, the transcript level falls to just above basal level at 1.4 fold for both 1 and 5 hr post exposure. At 24 hr post exposure, the transcript increases significantly to 3.0 fold. In contrast, the second real-time RT-PCR experiment shows the induction of the actin gene begins at 0.25 hr, however the increase is almost half of that observed in Fig 5.6 A at 3.0 fold. The transcript drops to near basal level at 0.8 and 1.4 fold for 0.5 and 1 hr respectively. The transcript level of actin increases significantly by 4.8 fold at 2 hr post exposure, but subsequently drops to 0.5 fold at 5 hr. The transcript level increases to 1.7 fold at the 24 hr post exposure stage.

Figure 5.6: The temporal modulation in gene expression of the *B. glabrata* actin gene in the Bge cells upon exposure to *S. mansoni* miracidia

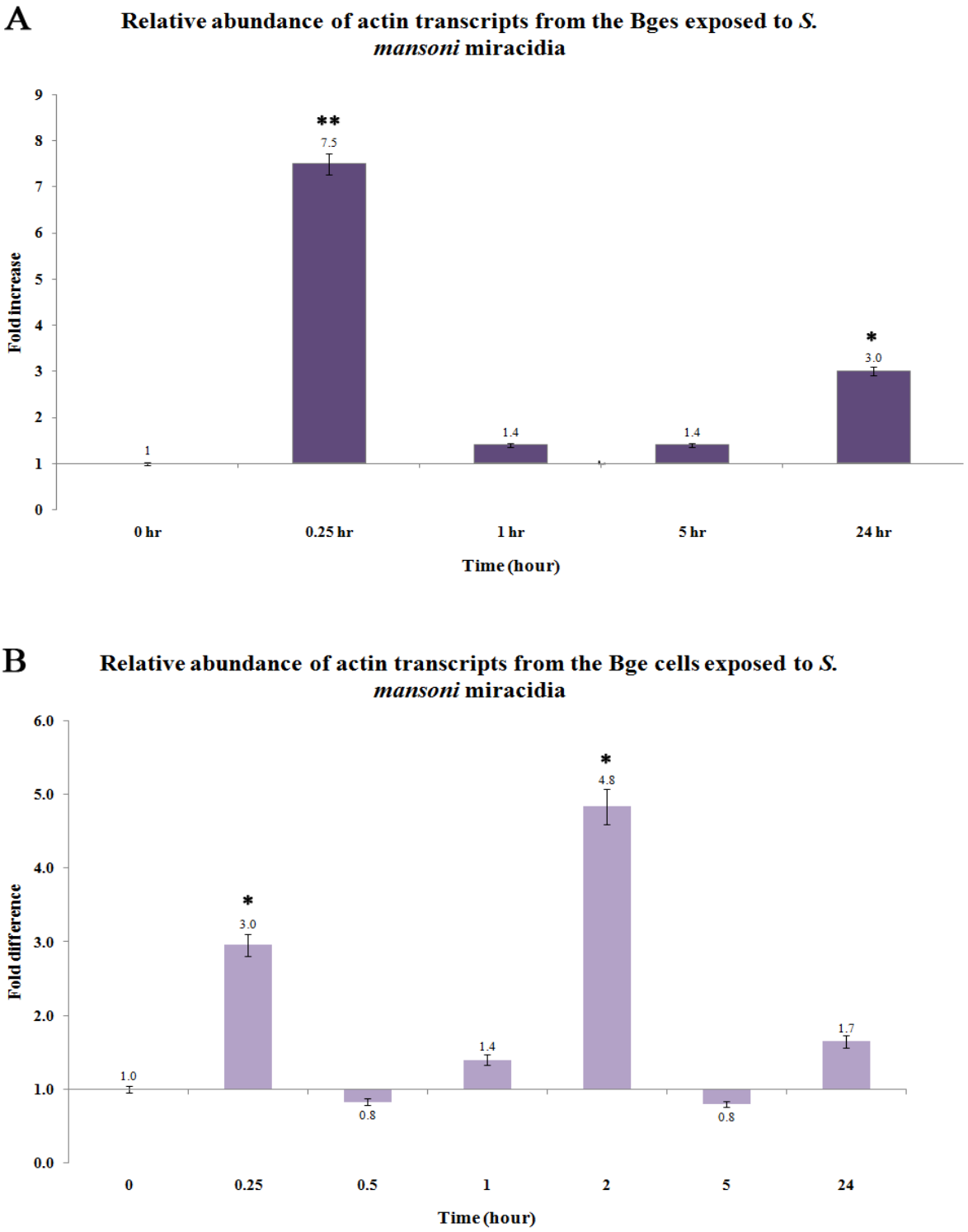

The differential expression of the actin transcripts by real-time Q-RT-PCR in Bge cells following exposure to *S. mansoni* miracidia for no exposure (0 hr) or exposure for 0.25 , 0.5, 1, 2, 5 and 24 hr. The fold change of expression of transcript was determined by comparing the unexposed and

exposed Bge cells by comparative Ct method and the formula (as described in section 5.2) with the normalised basal level of expression in unexposed Bge cells as 1.0. Error bar= S.D. The significant *P*-value < 0.01 are indicated by ** and the significant P-value < 0.05 are indicated by * at the top of each bar.

5.3.6 Correlating the temporal modulation of actin gene expression and the position of the actin gene in the interphase nuclei of the Bge cells

As mentioned previously the location of genes in the interphase nucleus may reflect the expression of the gene; with the nuclear periphery often correlating with transcriptional repression and the nuclear interior with transcriptional activation and up-regulation. The actin gene upon exposure to the miracidia alters it position in the interphase nucleus of the Bge cells; however unlike the movement of the ferritin gene which moved from a peripheral position (pre exposure) to the interior (post exposure), the actin position continues to alter position post exposure to miracidia. The actin is located towards the interior pre exposure; at 0.5 hr post exposure the histogram distribution of the actin gene in Fig 5.5 B is bimodal with a slight bias towards the interior. The actin transcript level at this point is 0.8 fold (Fig 5.6 B), which is very close to the basal level of 1. Considering the actin gene remains more to the interior at 0.5 hr, perhaps the bimodal distribution of the actin gene in Fig 5.5 B is reflected in the decrease to 0.8 fold? However, at the 2 hr post exposure the actin gene is positioned towards the nuclear periphery, which contrasts with the significant transcriptional up-regulation observed in Fig 5.5 C, whereby the transcript level has increased to 4.8 fold. Interestingly, the drop in transcript level observed at the 5 hr stage in Fig. 5.5 A and B of 1.4 and 0.8 fold respectively, results in the shift of the actin gene towards the interior of the nucleus. At 24 hr, the actin has an intermediate position with a slight bias towards the nuclear periphery (Fig 5.5 E); this movement is concomitant with an increase in transcript level to 3.0 and 1.7 in Fig 5.6 A and B respectively.

5.4 Discussion

The research field of host-parasite interactions with regards to *B. glabrata* and *S. mansoni* is continually growing and is often led through studies into changes in gene expression in *B. glabrata* upon *S. mansoni* infection. Often the pertinent genes in question play a role in the snail resistance or susceptibility to the parasite infection. Hence, studying the genomic changes in *B. glabrata* via nuclear organisation provides the field with a new avenue of investigation of host-parasite interaction. The data provided here perhaps implicates the importance of future research along the genome organisation path. Indeed, the observation that non-randomly positioned gene loci in interphase nucleus alter position upon parasitic infection concomitantly with changes in gene expression are very important. The genes ferritin and actin were chosen originally for this study, due to the proven reliability of their genetic mapping i.e. (1) both genes mapped onto homologous, diploid metaphase chromosomes of the Bge cells, with clear signals on two chromatids (2) using FISH probes, two gene signals were observed consistently in the interphase nucleus of the Bge cells. It should also be noted that these probes were derived from a BAC library created from the *B. glabrata* snail. The genes were also considered in relation to the effects of parasite infection. It has been postulated by Lockyer et al (2007) that ferritin may function in regulating the reactive oxygen species produced by snails during the destruction of *S. mansoni* (Lockyer et al., 2007). In the same study the transcript levels were noted to be elevated in resistant snail in comparison to susceptible snails. As a control, the actin gene was chosen since there has been no documented studies linking actin expression to parasitic infection in *B. glabrata*.

The ferritin and actin gene probes from the *B. glabrata* BAC library were hybridized to the interphase nuclei from the Bge cells which had been exposed to *S. mansoni* miracidia for different durations of time. Fig 5.2 and 5.4 display the histograms depicting the radial

distribution of the genes in the Bge cell nuclei. The ferritin gene is observed in Fig 5.2 A to alter its peripheral position pre exposure to the *S. mansoni* miracidia and adopt an internal position 0.5 hr post exposure (Fig 5.2 B). The ferritin gene remains positioned towards the interior of the interphase nucleus throughout the post exposure phase (2, 5 and 24 hr). Such a pronounced and consistent (with respect to the ferritin gene remaining in an internal position throughout the post exposure stage) change in gene position may indicate that the *S. mansoni* can influence re-organisation the genome of the Bge cells. Indeed, the actin gene also shows movement upon parasitic infection; however the pattern of gene distribution was not as consistent as that of ferritin. The actin gene shifted from a distribution towards the interior, to a biomodal distribution at 0.5 hr, followed by a shift towards the periphery at 2 hr and a movement back to the interior, before shifting back towards the periphery. As described earlier, there is a considerable amount of published data correlating changes/alterations in nuclear organisation with transcriptional activity. Are the aforementioned correlations reflected in this study?

The real-time Q-RT-PCR was performed twice by collaborators at the BRI laboratory (Rockville, USA). The ferritin transcript is observed in to be significantly up regulated at 0.25 hr post exposure in Fig 5.3 A and B, which shows that the influence of the parasite on the Bge cell genome occurs before the aforementioned repositioning of the ferritin at 0.5 hr. However, in Fig 5.3 B at 0.5 hr, the expression of ferritin remains at almost basal level at 0.9 fold. Using the hypothesis that movement to the nuclear interior reflects transcriptional up-regulation; then the adopted post exposure internal position of ferritin gene at 0.5 hr is at odds with the respective transcript level. Indeed, at 2 hr post exposure (Fig 5.3 B) the ferritin gene, in an internal position, has a transcript level of 0.8 fold, which is again close to the basal level of 1 (pre exposure to miracidia). However, the subsequent 5 and 24 hr (Fig 5.3 A and B) both depicted an up-regulation in transcriptional activity

(significantly so in Fig 5.3 A). In fact, the ferritin gene moves to a more internal position from 5 to 24 hr and the transcript level increase concurrently. The actin gene as with the ferritin gene, is transcriptional up-regulated 0.25 hr post exposure (Fig 5.6 A and B). At 0.5 hr post exposure (Fig 5.6 B) the actin transcript level falls to 0.8 fold. At this stage the actin gene is observed to be distributed bimodally with slight bias towards the interior. The biomodal distribution may indicate the sample analysed was from two Bge cell populations or from two genes (one transcriptionally activated whilst other is transcriptionally silent); maybe the future deployment of RNA FISH to visualise the transcripts of the different alleles may go some way to an answering this question. Another possibility is the co-culturing of the Bge cells with miracidia by the BRI laboratory resulted in the miracidia altering the actin gene position of only some and not all Bge cell nuclei. At 2 hr post exposure the actin transcript level increases by 4.8 fold (Fig 5.6 B), at this stage the actin gene moves to a more peripheral position. The actin transcript level remains close to basal level for the 5 hr stage whilst the gene is in an internal position. At 24 hr post exposure the transcript level increases as the actin gene is observed to adopt an intermediate position with a slight bias towards the periphery.

The results show that the *S. mansoni* parasite may alter the genome of *B. glabrata* in terms of the organisation of ferritin and actin genes in the interphase nuclei of the Bge cells and their expression. As mentioned previously, the nuclear periphery and interior are not exclusive regions of transcription suppression and transcriptional up-regulation. As Bickmore and colleagues have shown, some genes which are repositioned to the nuclear periphery are still transcriptionally active (Finlan et al., 2008). In yeast, transcriptional active genes are found around the nuclear pore (Brown and Silver, 2007). Another caveat that should be heeded, is the fact that most of the research into gene positioning and transcriptional modulation is in mammalian organisms. Can the data from these studies be

extrapolated to a molluscan organism? Perhaps the changes in gene position here merely reflect a different type of re-organisation which cannot be correlated with those observed in mammalian nuclei. As mentioned previously, publish studies by the laboratory of Peter Fraser (Osborne et al., 2004, Osborne et al., 2007) have shown that the position of genes in the interphase nucleus may relate to the location of different transcription factories; i.e. genes may relocate to active transcription factories upon induction (Osborne et al., 2004, Osborne et al., 2007). Perhaps this is what is happening to the ferritin and actin genes in the interphase nucleus during the tr**a**nscriptional up-regulation? More importantly, what role (if any) does actin play in parasitic infection in *B. glabrata,* considering it alters its nuclear position and gene expression in the Bge cell nuclei upon exposure to *S. mansoni*?

Further research into the nuclear gene positions post infection to *S. mansoni* should focus at looking into the position of other genes such as *SOD 1* and genes from the FREP gene family. The *SOD1* gene codes for a transcript super oxide dismutase which facilitates the production of ROS H_2O_2 from O_2^- which plays a role in the destruction of *S. mansoni* by haemocytes upon parasitic infection. The work by the Bayne laboratory suggests that the *SOD 1* gene may be a crucial factor in resistance and susceptibility of the snail to the parasite. Considering the aneuploidy observed in chapter 2, one might suggest that the Bge cell line is not a good model for reflecting genomic function in *B. glabrata*. Yet the Bge cell line is able maintain and propagate *S. mansoni* from mother sporocyst to daughter sporocyst, it is also able to surround and encapsulate the parasite much in same way as the haemocytes and the Bge cells possess a lysosomal content similar to that of the haemocytes (Coustau et al., 2003).

Chapter 6:

B. glabrata chromatin organisation: An *ex vivo* analysis of host parasite interactions

6. *B. glabrata* chromatin organisation: An *ex vivo* analysis of host parasite interactions

6.1 Introduction

6.1.1 Histone modifications

The amino acid residue termini of histones (namely H3 and H4) are the subject of covalent post-translational modifications (Strahl and Allis, 2000, Sarmento et al., 2004). Such modifications can entail methylation, acetylation, ubiquitination, phosphorylation, sumoylation, citrullination and ADP-ribosylation (Strahl and Allis, 2000). These modifications function in regulating gene expression via influencing the interaction between histones and DNA through altering the hydrophobicity of the histone tail (Strahl and Allis, 2000, Jenuwein and Allis, 2001). Changes in the association between histones and DNA are postulated to transitorily alter the accessibility of transcriptional factors such as activators and inhibitors thereby increasing and decreasing the transcription of genes (Boggs et al., 2002).

The most widely researched post-translational modifications are acetylation and methylation of the lysine residue. Acetylation is catalysed by the enzymes histone acetyltransferases (HAT) and is regularly associated with actively transcribed chromatin regions, whereas histone deacetylation is mediated by histone deacetylases (HDAC) and is related to reduced transcription and condensed chromatin configurations (Skalnikova et al., 2007). Indeed, hypoacetylated chromatin is often found around the periphery of the nucleus concomitantly with high concentrations of HDAC (Sadoni et al., 1999). Methylation of lysine residues by histone methyltransferases (HMT) often correlates with heterochromatic formation (Rice et al., 2003, Skalnikova et al., 2007). The type of histone

and the residue under modification also determines chromatin configuration (Shi and Dawe, 2006). The lysine residues on histones 3 such as 9, 14, 18 and 23 are sites for acetylation and methylation (Strahl and Allis, 2000).

6.1.2 The epigenetic imprint of methylation

Of particular interest to researchers is the methylation of the lysine 9 residue of Histone 3 (H3MeK9) which *in vivo* can occur in mono (Me), di (Me_2) and trimethyl (Me_3) states and has been documented to be associated with the formation of heterochromatin and gene repression (Peters et al., 2002, Boggs et al., 2002, Strahl and Allis, 2000). A notable example of this modification is the previously mentioned inactivation of the X chromosome in female mammals, which has been shown to be enriched with H3MeK9 and is thought to be necessary for the dosage compensation of X-linked genes (Boggs et al., 2002, Peters et al., 2002). H3K9 methylation also has an influence in immunological developmental pathways, such as the inhibition of endogenous inmmunoglobin heavy chain rearrangement (V_H to DJ_H) which prevents murine B cells progenitors from becoming B cells (Johnson et al., 2004). Indeed, Johnson et al (2004) demonstrated that the removal of H3K9 methylation is concurrent with B cell commitment. This type of lysine methylation has also been correlated with different forms of chromatin (Johnson et al., 2004). In mammals, mono and dimethyl modifications of K9 have been found located in specific regions of silent chromatin in euchromatin, whereas trimethylation of K9 localised to pericentric constitutive heterochromatic regions (Rice et al., 2003). Interestingly, the role of H3K9 methylation is not exclusively associated with gene suppression, in leukaemia and medulloblastoma cancer cells, the $H3Me_3K9$ was found to be associated with active genes (Wiencke et al., 2008).

The tri and di methylation of the lysine residue 4 on histone 3 has been shown to be associated with regions in eukaryotic genomes of active transcription (euchromatin) (Santos-Rosa et al., 2002). H3Me_3K4 functions in regulating development in *Drosophila* (Christensen et al., 2007). Christensen et al (2007) reported the correlation between the increase of H3Me_3K4 with an increase in the expression of *Hox* genes during embryonic stem cell development (Christensen et al., 2007). The methylation of H3K4 plays a crucial role in prefrontal dysfunction in schizophrenia (Huang et al., 2007). Within the human prefrontal cortex the methylation of H3K4 at *GAD* 1 (encodes an enzyme for GABA synthesis) and GABAergic gene promoters is progressive from childhood and throughout adulthood (Huang et al., 2007). Huang et al (2007) also noted a decrease in H3Me_3K4 and *GAD* 1 expression in schizophrenics' (Huang et al., 2007). Indeed, the role of histone post-translational modifications in schizophrenia extends to H3Me_2K9, which is demonstrably elevated in schizophrenic patients; Gavin et al (2009) postulated that schizophrenia is associated with repressed chromatin formations (Gavin et al., 2009).

Modifications to H4, in particular H4Me_3K20, are commonly associated with heterochromatic formation (Kourmouli et al., 2004, Fraga et al., 2005). The importance of H4Me_3K20 in heterochromatic formation and gene repression has been exhibited by Fraga et al (2005), who noted a loss of H4Me_3K20 in cancer cell line (leukemic in origin) and human primary lymphomas (Fraga et al., 2005).

6.1.3 Nuclear organisation and chromatin modifications

The distribution of particular histone protein modifications in the interphase nucleus can be very distinct, with the modifications forming organised and sometimes compartmentalized patterns of distribution (Kourmouli et al., 2004, Fraga et al., 2005, Bartova et al., 2005, Payne and Braun, 2006). Such organisation has been documented in mammalian nuclei.

Zinner et al (2006) presented a study of the role of histone protein modification in nuclear organisation whereby $H3Me_3K4$, H4MeK20, $H4Me_3K20$, H3MeK9 and $H3Me_3K27$ were investigated. Of particular interest were the $H3Me_3K4$ and $H4Me_3K20$ staining patterns. The $H3Me_3K4$ pattern was observed as a network of intensely stained chromatin distributed ubiquitously around the nucleus (Zinner et al., 2006). A paucity of staining at the outermost periphery of the nucleus was also discerned. $H4Me_3K20$ antibody staining was demonstrated to stain regions of dense heterochromatin (Zinner et al., 2006). Kourmouli et al (2004) utilised mouse spermatogonia cells to investigate the distribution of $H4Me_3K20$ modified chromatin, which was distributed as large blocks of stained foci spread uniformly around the nucleus (Kourmouli et al., 2004). Indeed, this pattern has been documented by Fraga et al (2005) and Schotta et al (2004) with mouse embryonic stem cell nuclei and also again by Payne and Braun (2006) with mouse spermatogonia. In addition to the aforesaid pattern of $H4Me_3K20$, Payne and Braun (2006) also discerned a perinuclear ring-like formation of heterochromatin in some nuclei. The distribution of $H3Me_2K9$ in mammalian nuclei, has been shown to stain as discrete punctate foci uniformly distributed around the nucleus (Bartova et al., 2005, Payne and Braun, 2006).

6.1.4 The spatial organisation of modified histone chromatin within the interphase nuclei of *B. glabrata*

The organisation of chromatin in the interphase nucleus plays an important role in nuclear processes and is strongly correlated with the expression of genomic regions. The research presented in this chapter will focus on the spatial organisation of modified histone chromatin within the *B. glabrata* interphase nucleus *in vitro* and *ex vivo*. The *ex vivo* study entails the investigation of modified chromatin in different snail types of particular interest to the host-parasite relationship of *B. glabrata* and *S. mansoni*. These snails are the adult

NMRI susceptible snails, adult NMRI susceptible snails exposed to miracidia, adult BS90 resistant snails and juvenile NMRI susceptible snails. Histone modifications of genomic regions can alter with development and change the expression of certain genes (Johnson et al., 2004). The parasite resistance and susceptibility genetics differ between juvenile and adult snails; in adult snails resistance follows mendelian genetics (resistance is a dominant trait) as oppose to juvenile snails which is multi locus. An article by Richards (1984) has shown that susceptibility can alter with snail maturity in certain snail types (Richards and Merritt, 1972, Richards, 1984). Indeed Niemann and Lewis (1990) have shown that juvenile snails are more susceptible to infection than adult snails (Niemann and Lewis, 1990).

6. 2 Materials and Methods

6.2.1 Snail husbandry

The snails used in these experiments were derived from collaborators at the Biomedical Research Institute (BRI) in the USA. The *B. glabrata* snails used in this study originated from two stocks of different susceptibility types; the Brazilian resistant isolate BS90, (Paraense and Correa, 1963) and the susceptible lab derived NMRI (Lewis et al., 1986). The snails were grown in both labs and in the same manner however, the adult NMRI snails exposed to miracidia were grown solely at the BRI. The adult and juvenile snail stocks BS90 and NMRI were grown in separate tanks (12,000 cm^3) containing water of a low chlorine content (the water was obtained after being passed through a charcoal filter). The snails grow in higher numbers at a temperature of 27^oC however, although this temperature is the equivalent to that of their natural habitat, through experience there was generally a higher level of mortality. Hence, the snails were grown at 25^oC (this temperature is maintained using Visitherm aquatic thermostats). The *B. glabrata* snails

were kept on a staple diet of organic Romaine lettuce and Tetramin fish flakes (Spectrum brands, Inc, Germany). Occasionally the infant snail diet was supplemented with calcium from cuttlefish (an additional source mineral required for shell development) and Cyanobactrium *nostoc*, which is grown over autoclaved mud.

6.2.2 Parasite exposure

The unexposed adult BS90 and NMRI snails (6-10 mm in diameter) and the unexposed juvenile NMRI snails (up to 4 mm in diameter) were used in this experiment and grown at Brunel University.

Adult NMRI snails were exposed to 25 *S. mansoni* (NMRI strain) miracidia for 6 hr. The snails were subsequently fixed (as described in 6.2.3) and despatched to the Laboratory of Nuclear and Genomic health at Brunel University.

6.2.3 Snail histology and tissue preparation

The unexposed snails prepared at Brunel University were carefully removed from their shells and washed thrice in 1 X PBS, before being incubated in a solution of 10 % neutral buffered formalin (v/v) for 24 hrs. Unexposed and exposed snails from the BRI laboratory were fixed in the same way and sent to our lab enclosed in 30% glycerol (v/v). Upon arrival, the snails were incubated in 70% ethanol for 24 hr before processing. Before processing, the head-foot of large adult snails (6-10 mm in diameter) was separated from the body. Whole snail tissue was used for the juvenile snails (upto 4 mm in diameter). Snails from both labs were processed overnight with a tissue processor (Leica Microsystems, Germany) and then subsequently embedded with paraffin wax. The paraffin embedded tissue was cooled on a 4^{o}C block overnight, before being sectioned with a microtome at a thickness of 5µm. The tissue sections were mounted onto Super frost Plus

adhesion microscope slides (Menzel-Gläser, Germany). The slides were kept at 4^{o}C until antibody staining.

6.2.4 Deparafination and rehydration

This protocol was derived and modified from Abcam's Immunohistochemistry protocol (www.abcam.com/technical).

The deparafination involved a series of washes in the solvents xylene and ethanol. The slides were allowed to reach room temperature, before being washed twice in for 3 min in xylene. This was followed by a wash in 1:1 xylene and ethanol (v/v) for 3 min. Subsequently, the slides were washed twice for 3 min in 100% ethanol and once in 95%, 75%, and 50% ethanol (v/v) for 3 mins. The slide were rinsed with running cold water and finally rehydrated by incubating them in cold water.

6.2.5 Antigen retrieval of snail tissue

The method described here is routinely used to break methylene bridges formed during the fixation in 10% neutral buffered formalin (NBF) and expose the antigenic site to the antibody. I utilised the heat-mediated antigen retrieval method as opposed to enzymatic retrieval in order to conserve the morphology of the snail tissue. The heat mediated protocol was derived and modified from Abcam's Immunohistochemistry protocol (www.abcam.com/technical).

A solution of Tris-EDTA buffer (10mM Tris Base, 1mM EDTA solution, 0.05% Tween 20, pH 9.0) was prepared in a 500 ml vessel. The vessel was placed in a pressure cooker and heated until boiled with the lid slightly ajar; the slides were subsequently transferred to the vessel containing the buffer and the lid secured. The pressure cooker was heated until it reached full pressure, from which point a duration of 3 min was allowed before switching

the cooker off. The slides were allowed to cool in the buffer before being transferred to 1 X Tris buffered saline (TBS).

6.2.6 Histone antibody staining of snail tissue

The slides were washed twice for 5 min in TBS and 0.025% Triton X-100 (v/v) with gentle agitation. The tissue sections were subsequently blocked in 10% NCS with 1% BSA in TBS for 2 hr at room temperature.

The slides were then stained with anti-histone H4, trimethyl modification to the lysine 20 residue, rabbit polyclonal antibody (anti-H4Me_3K20, Abcam, UK) and anti-histone H3, dimethyl modification to the lysine 9 reisdue, mouse monoclonal antibody (H3Me_2K9, Abcam, UK). The antibodies were prepared as a 1/300 dilution with TBS and 1% BSA (v/v). The antibodies were applied as 20 µl aliquots onto the sections. The slides were incubated with the antibody overnight at 4^oC in a humidified chamber.

6.2.7 Washing

The primary antibody was washed from the slide twice for 5 min in 1X TBS with 0.025% Triton X with gentle agitation. The secondary antibodies of porcine anti-rabbit conjugated with cyanine 3 (Jackson Laboratory) and donkey anti-mouse conjugated with FITC were used for the H4Me_3K20 and H3Me_2K9 primary antibodies respectively. They were prepared as 1/80 dilutions with 1% BSA in TBS (w/v) and added to the sections as 20 µl aliquots. The slides were incubated in the dark with the secondary antibodies for 1 hr at room temperature. Finally the slides were washed thrice for 5 min in TBS and mounted with Vectorshield anti-fade mountant containing DAPI (Vectorlabs) before subsequently mounting the sections with 13 mm diameter circular slides coverslips.

6.2.8 Histone antibody staining of the Bge cells

Bge cells from isolate 1 were stained with histone antibodies $H3Me_2K9$, $H3Me_3K4$, and $H4Me_3K20$ (Abcam, UK). The Bge cells were grown and prepared for histone antibody staining using the method described in chapter 4. Briefly, the Bge cells were grown on 13 mm diameter coverslips and fixed at a confluence of 70% using ice cold 1:1 acetone and methanol (v/v) for 4 min. Subsequently, the fixative was removed and the coverslips washed thrice in 1 X PBS. The antibodies were prepared diluted 1:300 in 1% new born calf serum (NCS) in 1 % PBS (v/v) and incubated with the fixed Bge cells for 1 hour at room temperature. The coverslips were subsequently washed thrice with 1 X PBS and the Bge cells stained with the secondary antibodies of porcine anti-rabbit conjugated with fluorescein isothiocyanate (FITC) (Jackson Laboratory) for anti-$H4Me_3K20$ and anti-$H3Me_3K4$ and donkey anti-mouse conjugated with FITC (Jackson Laboratory) were used for anti-$H3Me_2K9$. These were prepared as a 1/80 dilution with 1% NCS in 1 X PBS. The Bge cells on the coverslips were incubated with the antibodies for 1 hour at room temperature. The antibody was removed by washing the coverslips thrice in 1 X PBS before a brief rinse in ddH_2O. The excess water was drained from the coverslips before counterstaining and mounting with Vectorshield anti-fade mountant containing DAPI (Vectorlabs) and subsequently mounting the coverslips onto 22 X 50 mm slides.

6.2.9 Control experiment

The antibodies for modifications $H3Me_2K9$, $H4Me_3K20$ and $H3Me_3K4$ were of the IgG isotype. Consequently, the control experiment utilised two primary antibodies of the IgG isotype on the *B. glabrata* head-foot tissue. The antibodies were anti-human Lamin A goat polyclonal (Santa Cruz Biotechnology) and anti-human Emerin goat polyclonal (Santa Cruz Biotechnology). In addition to the primary antibody controls, another control

experiment was performed using solely the secondary antibody (no primary antibody). The control experiments were conducted using the methods stipulated in section 6.26- 6.28.

6.2.10 Image capture and analysis

The images of nuclei from the Bge cells and *B. glabrata* tissue stained with $H3Me_2K9$, $H3Me_3K4$ and $H4Me_3K20$ antibodies were captured using an Olympus UPlan FLN 100X oil immersion lens (Olympus) on an Olympus BX41 fluorescence microscope and a Model viewpoint GS gray scale digital camera (Digital Scientific). These images were pseudo-coloured and merged using Digital Scientific software, Smart capture 3.0.0 (Digital Scientific Ltd).

For the analysis of the frequency distribution of the histone modification patterns, counts of up to 1000 positively modified nuclei (for $H3Me_2K9$ and $H4Me_3K20$) were performed on the head-foot tissue from adult NMRI susceptible, adult NMRI susceptible exposed to miracidia, adult BS90 resistant and juvenile NMRI susceptible snails (three snails for each snail-type were analysed). In order to determine the significant difference ($P < 0.05$) in the frequency of patterns of $H3Me_2K9$ and $H4Me_3K20$ in *B. glabrata* snail types, the P- value was calculated by comparing the frequencies from the adult NMRI susceptible snails with that of the other snail types (adult NMRI susceptible exposed to miracidia, adult BS90 resistant and juvenile susceptible NMRI *B. glabrata* snails) using unpaired, unequal variance, two tailed Students t-test.

The ImageJ (NIH) program was utilised for quantitative estimation of the intensity of the $H3Me_2K9$ and $H4Me_3K20$ antibody fluorescence with the head-foot nuclei from *B. glabrata*. The images of the nuclei were captured using a fluorescence microscope set to a constant exposure of 0.2 sec. The program determined the mean gray values (0 = black to

255 = white) from the *B. glabrata* nuclei. The mean gray values are defined as the sum of the gray values of all the pixels in the image of nucleus divided by the number of pixels. The fluorescence intensity was determined from the gray values analysed from three different snails of adult NMRI susceptible, adult NMRI susceptible exposed to miracidia, adult BS90 resistant, and juvenile NMRI susceptible *B. glabrata* snails. 200 nuclei were analysed from each snail and the gray values averaged.

6.3 RESULTS

6.3.1 Control antibody experiment

In order to assess the specificity of IgG isotype histone antibodies, a control experiment was conducted using IgG type antibodies that react with nuclear antigens in human cells. Fig 6.1 displays representative images from the staining of the *B. glabrata* head-foot tissue using primary antibodies goat anti-human Lamin A (Fig 6.1 A) and goat anti-human Emerin (Fig 6.1B). The nuclei in all of the regions of the *B. glabrata* head –foot tissue were negative for antibody binding. As observed in Fig 6.1 (a representative image of the thousands of negative nuclei), the DAPI stained nuclei (blue) displayed the absence of non-specific antibody binding. Background staining (green) was observed in some of the tissue surrounding the nuclei. In addition to using a control primary IgG antibody, the non-specific binding of the secondary antibody was also analysed. Fig 6.2 displays a representative image of *B. glabrata* head-foot tissue stained with donkey anti-mouse antibody conjugated to FITC (green). The nuclei in all the regions of the *B. glabrata* head-foot tissue were negative for secondary antibody binding. The secondary antibody did not bind to the nuclei (blue), however minimal background staining (green) was observed in the tissue surrounding the nuclei. The secondary antibody used in this experiment was the

same as the one subsequently used to stain the histone antibodies. This means that the subsequent staining patterns observed with the histone antibodies are not due to any non-specific binding and are real.

Figure 6.1: Other IgG primary antibody staining on the head-foot tissue of *B. glabrata*

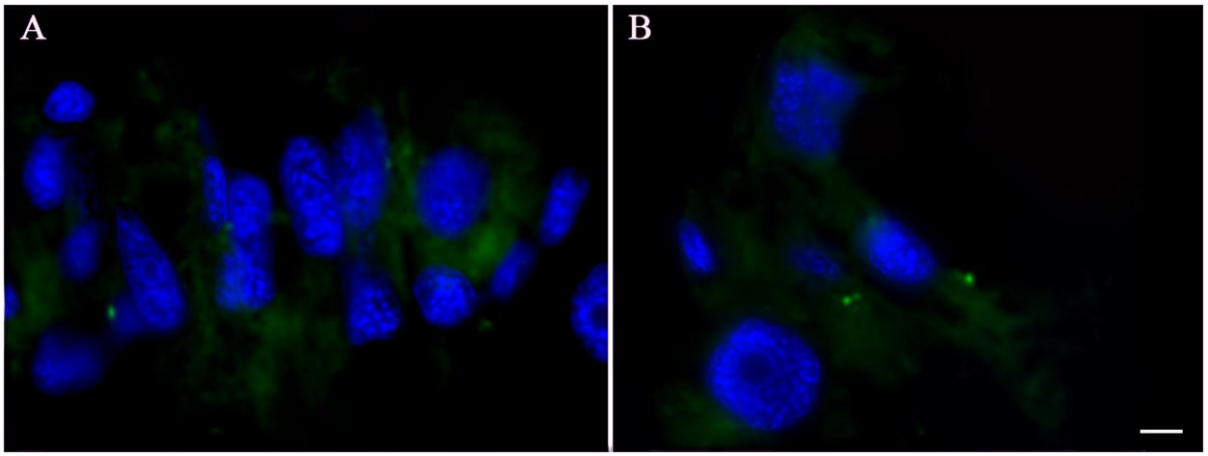

Paraffin tissue sections (with a thickness of 5 µm) from the head-foot of *B. glabrata* were stained with a primaryanti human Lamin A goat polyclonal antibody (Image A) and a primary anti-human Emerin goat polyclonal (Image B). A secondary porcine anti-goat antibody conjugated with FITC (green) was used and the nuclei were counterstained with DAPI (blue). Bar, 5 µm.

Figure 6.2: Secondary antibody only staining on the head-foot tissue of *B. glabrata*

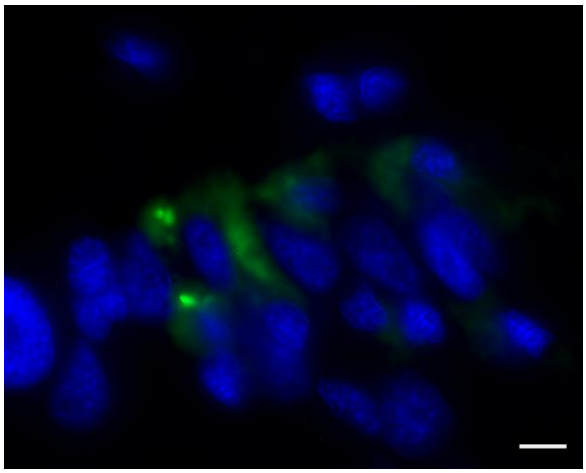

Paraffin tissue sections (with a thickness of 5 µm) from the head-foot of *B. glabrata* were stained with a donkey anti-mouse antibody conjugated with FITC (green). The nuclei were counterstained with DAPI (blue). Bar, 5 µm.

6.3.2 Histone lysine methylation patterns in the nuclei of the Bge cells

The Bge cells from isolate 1 were stained with histone post-translational lysine methylation modification antibodies; anti-H3Me$_2$K9, anti-H4Me$_3$K20 and anti-H3Me$_3$K4. The H3Me$_2$K9 antibody was raised in mouse as a monoclonal antibody, the H4Me$_3$K20 and H3Me$_3$K4 antibodies were raised in rabbits as polyclonal antibodies. These antibodies have been shown to stain specific subsets of chromatin in organisms such as *Arabidopis,* mice and humans (Adema et al., 2006, Young et al., 2006, Lee et al., 2007, Zhu et al., 2008, Lupien et al., 2008). Fig 6.3 displays representative images from the staining of the Bge cells with the aforesaid histone modification antibodies. The modifications are shown as green foci, reticulated throughout the nucleus. Fig 6.3A shows the H3Me$_2$K9 modification in the Bge cell nucleus, the H3Me$_2$K9 stained chromatin is observed as punctate foci spread uniformly around the nucleus. The H3Me$_2$H9 foci are similar in size, with some foci brighter than others; there is also some intermingling between different foci.

Figure 6.3: Representative images of post-translational modifications to histone proteins in the interphase nuclei of the Bge cells.

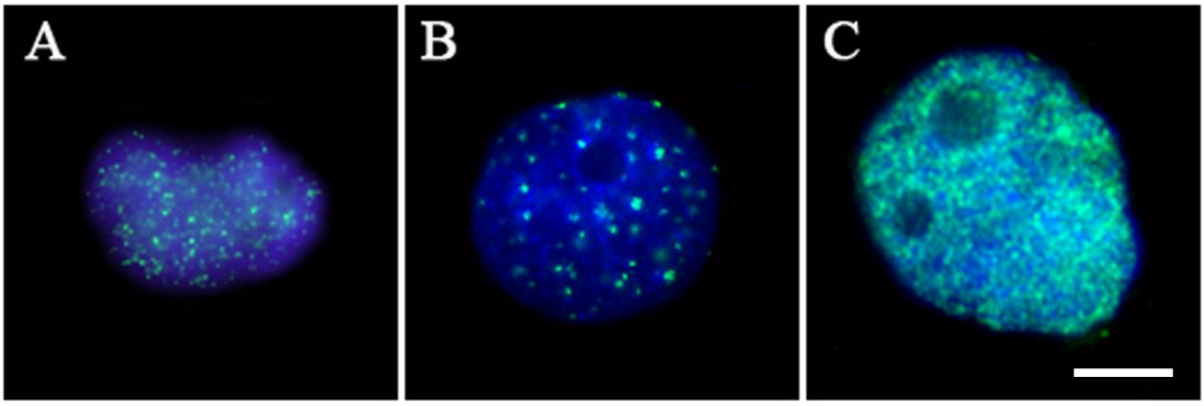

The nuclei from Bge cell isolate (1) were fixed with 1:1 methanol and acetone. Three primary histone antibodies were used (A) $H3Me_2K9$, mouse monoclonal (B) $H4Me_3K20$, rabbit polyclonal and (C) $H3Me_3K4$, rabbit polyclonal. The modifications were identified (as green) using secondary antibodies of porcine anti-rabbit conjugated with FITC (Jackson Laboratory) for $H4Me_3K20$ and $H3Me_3K4$; donkey anti-mouse conjugated with FITC was used for $H3Me_2K9$. The nuclei were counterstained with DAPI (blue). Bar, 5 µm.

The $H4Me_3K20$ modification in Fig 6.3 B exhibits larger and more discretely stained foci, there is also a slight variation in size and brightness of the $H4Me_3K20$ foci as well as an absence of staining in the nucleolus. Fig 6.3 C shows the staining pattern of the $H3Me_3K4$ modification which displays an intensely stained ubiquitously distributed foci except for the nucleoli. The anti-$H3Me_3K4$ staining is very dense and there is a large amount of intermingling and as such it is difficult in some areas to discern the individual foci. The distribution of the lysine methylation modifications in the Bge cell nuclei are indicative of unique chromatin organisation characteristics. The aforementioned heterochromatic $H3Me_2K9$ and $H4Me_3K20$ modifications (as represented respectively in Fig 6.3 A and B) within the Bge cell nuclei, are regions of silent repressed chromatin that are distributed universally around the nucleus. The large $H4Me_3K20$ modified foci (Fig 6.3 B) which is distributed throughout the nucleus spread in Fig 6.3 B may represent high level of chromatin modification at the centromere and juxtaposed centromeric positions, a genomic region typified by large amounts of heterochromatin. The smaller, discrete foci in Fig 6.3 A and B, perhaps shows the modification of regions distal to the centromere. In contrast, the $H3Me_3K4$ modification (Fig 6.3 C) for actively transcribed genes or those regions primed for transcription, demonstrates that the global distribution of euchromatin in the nuclei of the Bge cells. Indeed, not only are these regions spread around the nucleus but they are found in close proximity to one another.

6.3.3 Histone 3 dimethylation to lysine 9 modification patterns in the head-foot nuclei of the *B .glabrata*

The histone lysine modifications antibodies $H3Me_2K9$ was used to stain the head-foot tissue sections (5 µm in depth) from the adult NMRI susceptible, adult NMRI susceptible exposed to miracidia, adult BS90 resistant and juvenile NMRI susceptible *B. glabrata* snails. As the primary entry for miracidial infection, the head-foot provides an apt target for analysis of potential changes in genome organization upon schistosome exposure. The $H3Me_2K9$ antibody used in this experiment is the same used in section 6.3.2; having analysed a number of $H3Me_2K9$ modified nuclei, Fig 6.4 displays a selection of representative images of different $H3Me_2K9$ modification patterns observed in the *B. glabrata* nuclei from the aforementioned snail types. The distribution of $H3Me_2K9$ modification chromatin in pattern 1 (as observed in Fig 6.4 A) is not dissimilar from that documented in the Bge cells (Fig 6.3 A), the $H3Me_2K9$ modification (shown in green) is observed as punctate foci distributed throughout the nucleus. When compared to the level of $H3Me_2K9$ modification observed in pattern 2 (representative image shown in Fig 6.4 B), pattern 1 (Fig 6.4 A) is relatively sparsely modified. Indeed, the representative nucleus in Fig 6.4 B is indicative of a pattern observed whereby the nuclei were heavily modified, with the occurrence of both large and small $H3Me_2K9$ foci distributed ubiquitously around the nucleus. In contrast, the nuclei with pattern 3 (Fig 6.4 C) display the third pattern of $H3Me_2K9$ chromatin distribution observed in *B. glabrata*, whereby there is a discernible bias of large globular shaped $H3Me_2K9$ foci around the nucleolus. As well as an accumulation around the nucleolus, the large foci is distributed around nucleus is more compartmentalized than that observed in pattern 1 and 2 (Fig 6.4 A and B). These large foci may represent modified silent heterochromatic regions of the genome accumulating at the nucleolus. The fourth pattern (as represented by Fig 6.4 D) is similar to the $H3Me_2K9$

distribution observed in the nuclei with pattern 3 (Fig 6.4 C), inasmuch as there is a bias of modified foci around the nucleolus, however the patterns 3 and 4 (Fig 6.4 C and D) differ in foci size and compartmentalization whereby the pattern 4 has small and large foci which are less compartmentalised than that seen in pattern 3. There is also a slight peripheral bias of $H3Me_2K9$ modified chromatin.

Figure 6.4: Representative images of post-translational histone modification $H3Me_2K9$ distribution patterns in nuclei from the head-foot of *B. glabrata.*

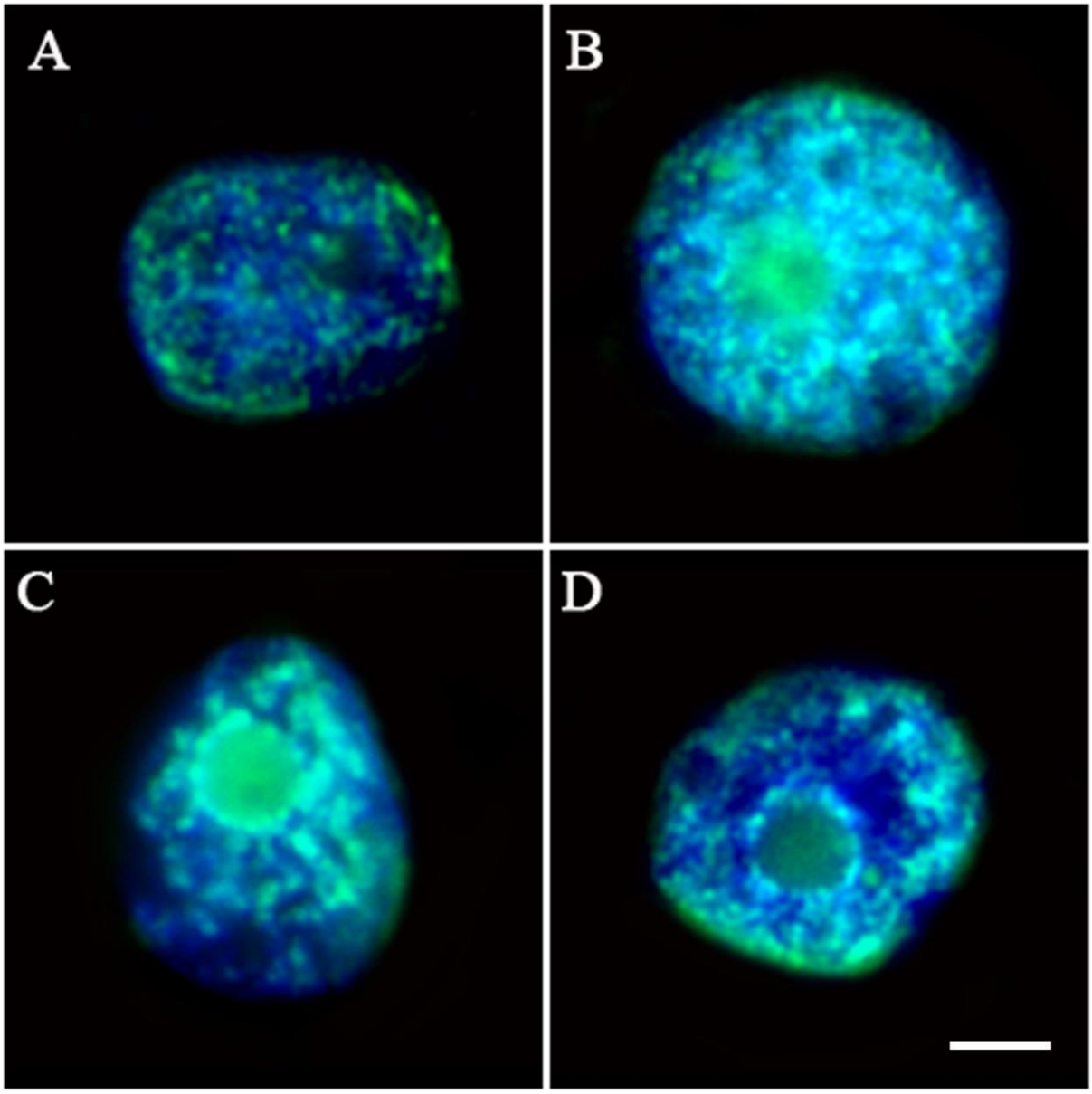

Paraffin tissue sections (with a thickness of 5 µm) from the head-foot of *B. glabrata* were stained with a primary $H3Me_2K9$ mouse monoclonal antibody and subsequently with a secondary donkey anti-mouse antibody conjugated with FITC. The $H3Me_2K9$ modifications were observed as green and the nuclei were counterstained with DAPI (blue). Images of different distributions of $H3Me_2K9$ in the nuclei of *B .glabrata* are displayed from A-D. Bar, 5 µm.

6.3.4 The frequency distribution of different $H3Me_2K9$ patterns in the head-foot nuclei of *B. glabrata* snail types

As shown in section 6.3.3, the spatial organisation of $H3Me_2K9$ modified chromatin can be observed as different nuclear patterns. Such distinct patterns indicate global genomic differences amongst the *B. glabrata* head-foot nuclei. In order to assess the frequency of these patterns amongst the different *B. glabrata* snail types, counts of up to 1000 positively modified nuclei were performed on the head-foot tissue from adult NMRI susceptible, adult NMRI susceptible exposed to miracidia, adult BS90 resistant and juvenile NMRI susceptible snails (three snails for each snail-type were analysed). The patterns described in section 6.3.3 (representative images of the patterns observed in Fig 6.4), were designated as pattern 1 (Fig 6.4 A), pattern 2 (Fig 6.4 B), pattern 3 (Fig 6.4 C) and Fig 6.4 D as pattern 4. Fig 6.5 A-C, displays the percentage of $H3Me_2K9$ modification patterns in three adult NMRI susceptible snails. Fig 6.5 A and B show the absence of pattern 1 in snails 1 and 2. In Fig 6.5 A, pattern 2 is the most frequent in snail 1, but is exceeded by pattern 4 in snail 2 (Fig 6.5 B). Pattern 1 is present in snail 3, (Fig 6.5) and is exceed by pattern 2, 3 and 4. Fig 6.5 D displays the mean percentage of the $H3Me_2K9$ modification patterns from the three snails. The standard error of the mean bars are small, showing that the variation in the percentage of the patterns between the three snails is not too great. Pattern 3 is the most frequent amongst the modified nuclei from adult NMRI susceptible snails and this is followed in descending order by patterns 4, 2 and 1.

Figure 6.5: The percentage of H3Me$_2$K9 modification patterns in the head-foot nuclei of adult NMRI susceptible *B. glabrata* snails

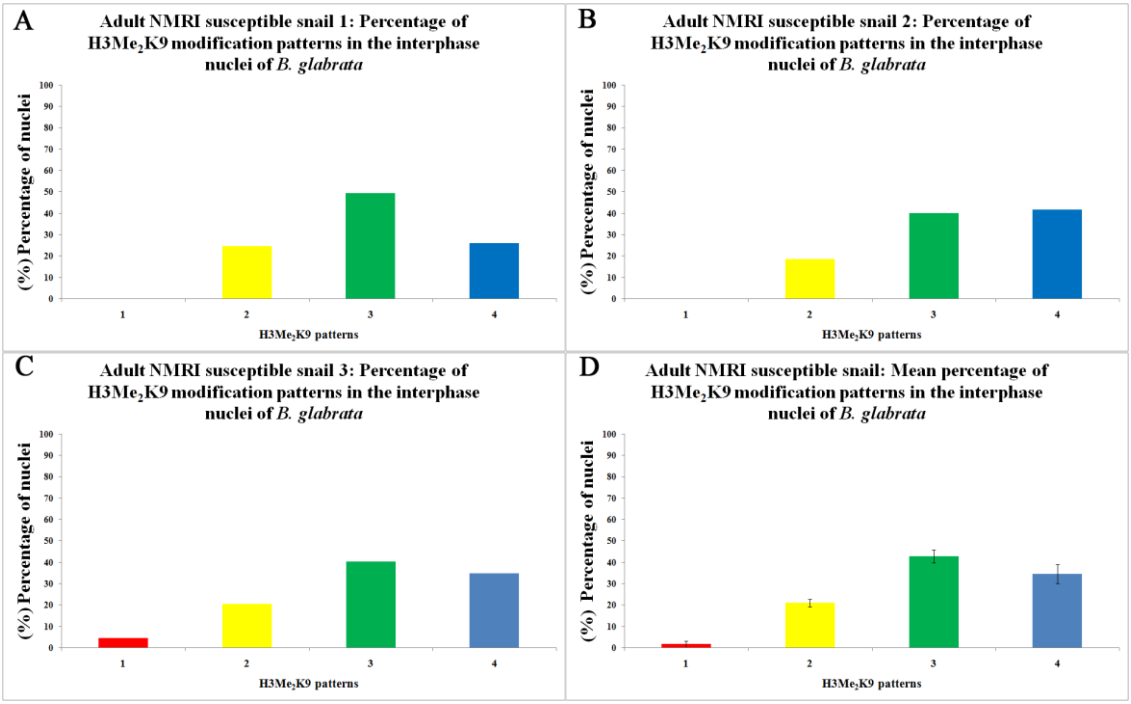

The H3Me$_2$K9 modification patterns were observed in the head-foot of 3 adult NMRI susceptible *B. glabrata* snails. 1000 positive nuclei were counted and percentage of each pattern documented in A (snail 1), B (snail 2) and C (snail 3). The mean distribution of H3Me$_2$K9 patterns is displayed in D, with the standard error of the mean bars (SEMs). Pattern (1) in red Pattern (2) in yellow Pattern (3) in green Pattern (4) in blue.

The distribution of the H3Me$_2$K9 patterns amongst the head-foot nuclei from the adult NMRI susceptible snails exposed to miracidia varies also between the snails. Fig 6.6 A shows the frequency distribution of H3Me$_2$K9 patterns in snail 1; pattern 3 is the most frequent, followed by pattern 2 and to a lesser extent pattern 4. Pattern 1, as exhibited previously in Fig 6.5, is present in the lowest amounts, indeed it is absent in snail 2 and 3. Pattern 2 was found to be the most frequent in snail 2, whereas as with snail 1, pattern 3 was prominently present in snail 3. The mean distribution displayed in Fig 6.6 D, shows that pattern 3 was the most frequently present amongst the head-foot nuclei from *B.*

glabrata adult NMRI snails exposed to miracidia. This pattern is followed by pattern 4 and 2; pattern 1 is found very infrequently in these snails.

Figure 6.6: The percentage of $H3Me_2K9$ modification patterns in the head-foot nuclei of adult NMRI susceptible *B. glabrata* snails exposed to miracidia.

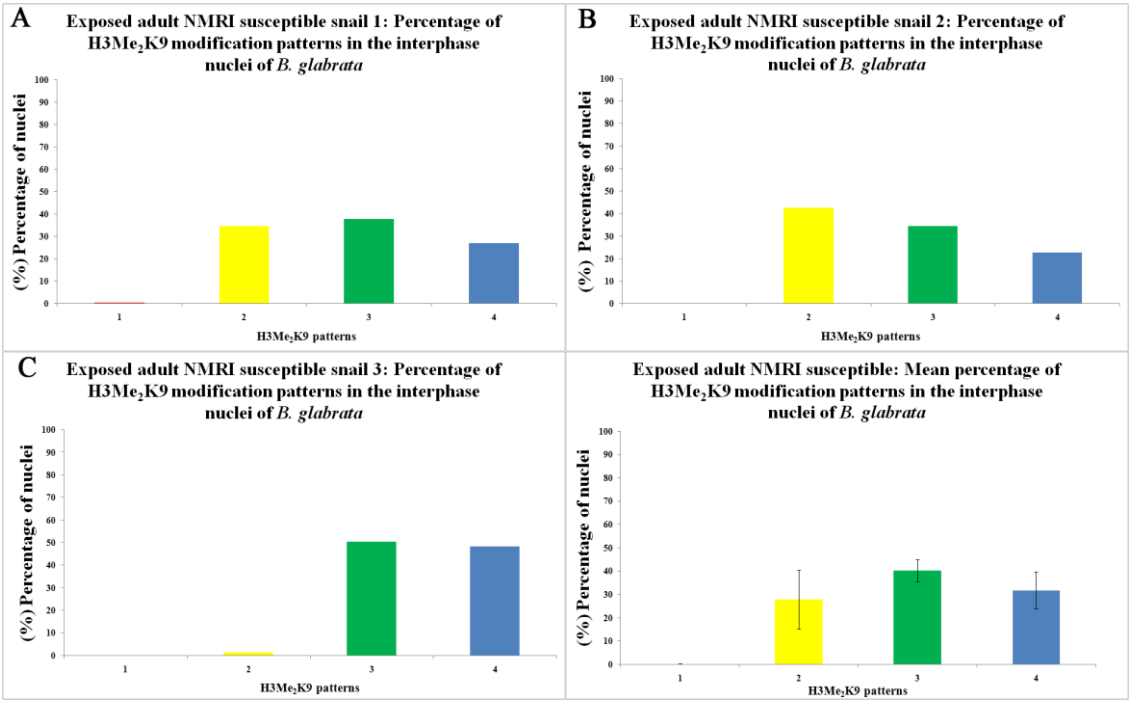

The $H3Me_2K9$ modification patterns were observed in the head-foot of 3 adult NMRI susceptible *B. glabrata* snails exposed to miracidia. 1000 positive nuclei were counted and percentage of each pattern documented in A (snail 1), B (snail 2) and C (snail 3). The mean distribution of $H3Me_2K9$ patterns is displayed in D, with the standard error of the mean bars (SEMs). An unpaired, unequal variance, two tailed student t-test was performed against unexposed adult NMRI snails (observed in Fig 6.5) using $P < 0.05$ %. No statistical difference was observed between the unexposed and exposed adult NMRI snails. Pattern (1) in red Pattern (2) in yellow Pattern (3) in green Pattern (4) in blue.

Amongst the adult BS90 resistant *B. glabrata* snails pattern 3 is the most prevalent, as shown in Fig 6.7. It is found in the highest quantities in all three snails in almost twice the amount of patterns 2 and 4. Pattern 1 is present at the lowest frequency in snails 1 and 2 (Fig 6.7 A and B respectively) however it is absent from snail 3. The mean distribution of

the $H3Me_2K9$ is displayed in Fig 6.7 D, and shows pattern 3 as the prominent, followed in descending order by patterns 4, 2 and 1.

Figure 6.7: The percentage of $H3Me_2K9$ modification patterns in the head-foot nuclei of adult BS90 resistant *B. glabrata* snails

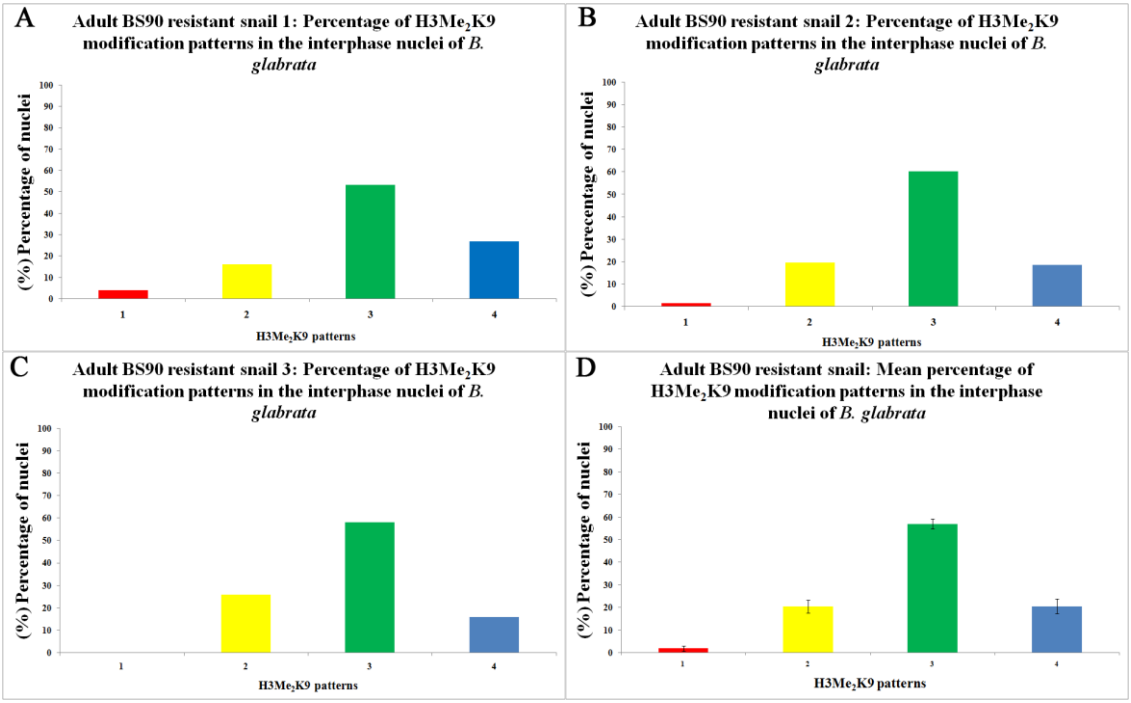

The $H3Me_2K9$ modification patterns were observed in the head-foot of 3 adult BS90 resistant *B. glabrata* snails. 1000 positive nuclei were counted and percentage of each pattern documented in A (snail 1), B (snail 2) and C (snail 3). The mean distribution of $H3Me_2K9$ patterns is displayed in D, with the standard error of the mean bars (SEMs). An unpaired, unequal variance, two tailed A student t-test was performed against adult NMRI snails (observed in Fig 6.5) using $P < 0.05$ %. However, no statistical difference was observed between the adult NMRI snails and the adult BS90 snails. Pattern (1) in red Pattern (2) in yellow Pattern (3) in green Pattern (4) in blue.

Figure 6.8: The percentage of H3Me$_2$K9 modification patterns in the head-foot nuclei of juvenile NMRI susceptible *B. glabrata* snails.

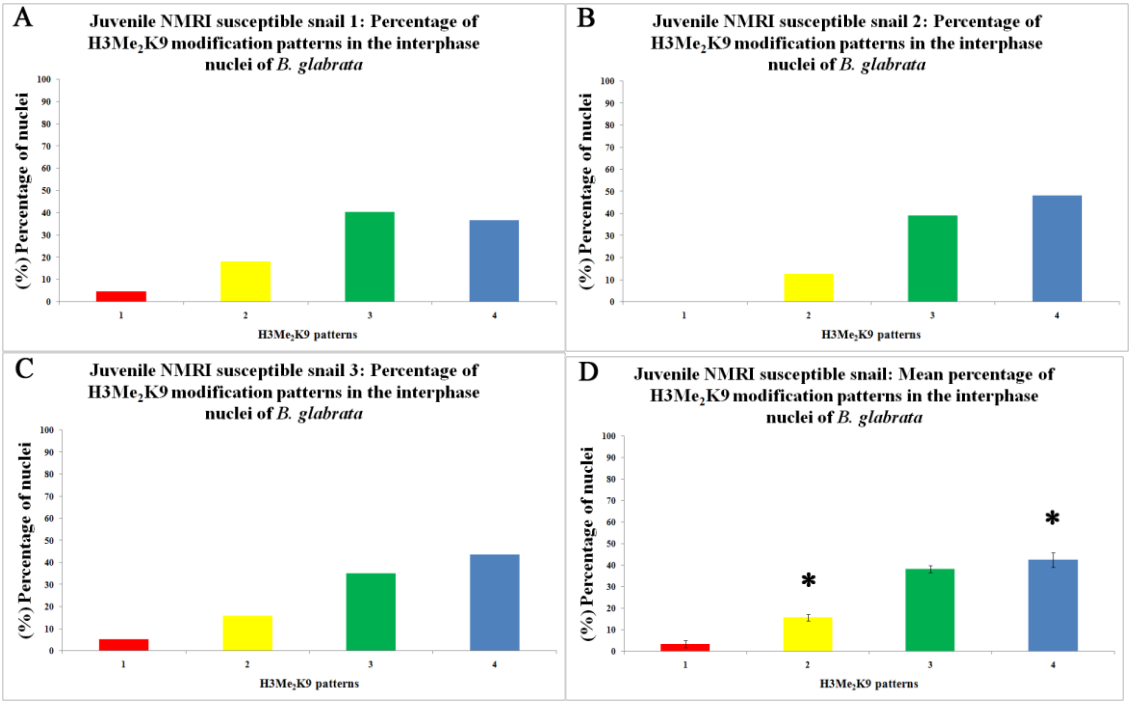

The H3Me$_2$K9 modification patterns were observed in the head-foot of 3 juvenile NMRI *B. glabrata* snails. 1000 positive nuclei were counted and percentage of each pattern documented in A (snail 1), B (snail 2) and C (snail 3). The mean distribution of H3Me$_2$K9 patterns is displayed in D, with the standard error of the mean bars (SEMs) and stars to represent data that is significantly different (at the top of the bars) from adult NMRI snails (Fig 6.5). These results were assessed at $P < 0.05$ % using unpaired, unequal variance, two tailed Student t-test. Pattern (1) in red Pattern (2) in yellow Pattern (3) in green Pattern (4) in blue.

The data attained from the distribution of H3Me$_2$K9 modification patterns in juvenile NMRI susceptible snails was intriguing. Fig 6.8 shows that patterns 3 and 4 were found in similar quantities in all three snails followed by pattern 2. As with the previously mentioned snail types, pattern 1 was the most infrequent. The mean distribution of H3Me$_2$K9 modification patterns in the head-foot nuclei of juvenile NMRI susceptible snails shows the prevalence of pattern 4 followed in descending order by 3, 2 and 1. Moreover, pattern 4 was found to be significantly more prevalent ($P < 0.05$) in juveniles

than in adult NMRI susceptible snails. Indeed, pattern 2 was found to be significantly less prevalent in juvenile NMRI susceptible snails than in adults.

Table 6.1: Showing the percentage (%) of $H3Me_2K9$ positive nuclei observed in head-foot nuclei of *B. glabrata*

***B. glabrata* snail**	**Snail 1**	**Snail 2**	**Snail 3**	**Mean**
Adult NMRI susceptible	35.1	44.6	38.1	39.5
Adult NMRI susceptible Ex	47.8	68.7	76.6	62.4
Adult BS90 resistant	59.8	34.0	69.2	62.3
Juvenile NMRI susceptible	31.7	10.31	48.8	33.8

Table 6.1 displays the percentage of $H3Me_2K9$ positively stained nuclei from the head-foot of *B. glabrata*. The adult NMRI susceptible exposed to miracidia and adult BS90 snails have the highest mean percentage of modified nuclei in the head-foot at 62.4 and 62.3% respectively. These results are very much higher than that observed in the adult and juvenile NMRI susceptible snails which had a respective 39.5 and 33.8% mean percentage of positive nuclei. The variation in the amount of positive nuclei amongst the snail types is quite marked in the juvenile snails whereby snail 3 exhibited 48.8 % positively stained nuclei and the nuclei of snail 2 were demonstrably less positive at 10.31% , which is almost quarter that of snail 3. Indeed, Table 6.1 shows that the other snail types displayed similar variations, most notable in the adult BS90 resistant snails, where snail 3 has 35.2% more positive nuclei than snail 2.

6.3.5 Histone 4 trimethylation to lysine 20 modification patterns in the head-foot nuclei of *B .glabrata*

The $H4Me_3K20$ modification antibody was also used to stain the nuclei from the head-foot of *B .glabrata*. Paraffin tissue sections (5 µm in depth) were prepared from the adult NMRI susceptible, adult NMRI susceptible exposed to miracidia, adult BS90 resistant and juvenile NMRI susceptible *B. glabrata* snails. The $H4Me_3K20$ antibody used upon the *B. glabrata* snails was the same used for the Bge cells. Fig 6.9 displays a selection of images representative of the patterns of $H4Me_3K20$ distribution documented in the nuclei of *B .glabrata*, the $H4Me_3K20$ modified chromatin is observed as red. Fig 6.9 A displays a nucleus where the $H4Me_3K20$ chromatin are organised into large compartmentalised foci distributed internally in the nucleus as well as forming a ring around the periphery of the nucleus. Indeed, the nucleus is heavily modified with $H4Me_3K20$ to the extent whereby the foci are in very close proximity with one another. The second pattern show in Fig 6.9 B shows a biased distribution of $H4Me_3K20$ internally in the nucleus. The nuclei that were observed with this spatial organisation of $H4Me_3K20$ chromatin also had large compartmentalised foci. The aforementioned patterns shown in Fig 6.9 A and B contrast with that displayed in Fig 6.9 C in that there is a stark difference in $H4Me_3K20$ foci size, which was considerably smaller and more punctate in the third pattern (Fig 6.9 C). As well as smaller foci, the distribution is more ubiquitous, with the absence of regionally bias in the nucleus. From the $H4Me_3K20$ patterns observed in *B. glabrata*, the distribution of modified chromatin in Fig 6.9 C is the most similar to that observed in the Bge cells, although the pattern in Fig 6.9 C displays smaller $H4Me_3K20$ foci.

Figure 6.9: Representative images of post-translational histone modification $H4Me_3K20$ distribution patterns in nuclei from the head-foot of *B. glabrata*

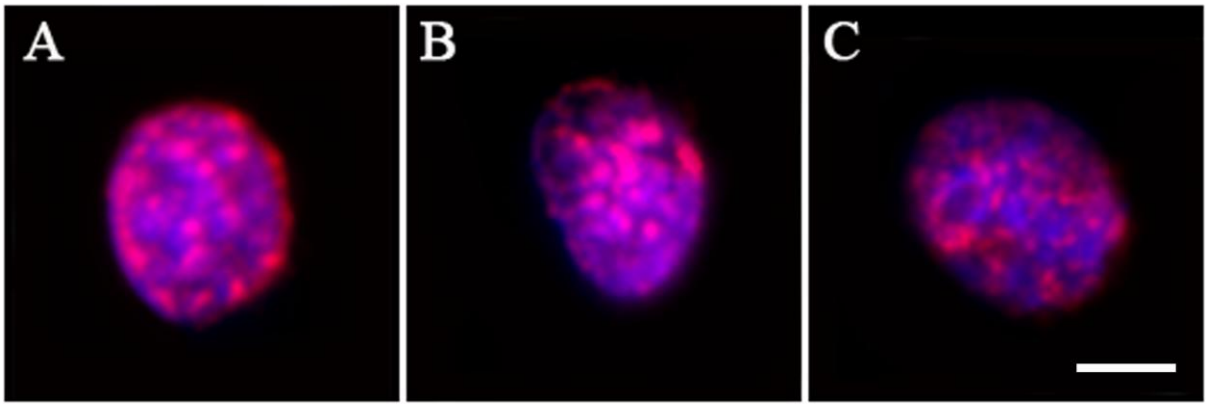

Paraffin tissue sections (with a depth of 5 µm) from the head-foot of *B. glabrata* were stained with a primary $H4Me_3K20$ rabbit polyclonal antibody and subsequently with a secondary porcine anti-rabbit antibody conjugated with cyanine 3. The $H4Me_3K20$ modifications were observed as red and the nuclei were counterstained with DAPI (blue). Images of different distributions of $H4Me_3K20$ in the interphase nuclei of *B .glabrata* are displayed from A-C. Bar, 5 µm.

6.3.6 The frequency distribution of different $H4Me_3K20$ patterns in the head-foot nuclei of *B. glabrata* snail types

As shown in section 6.3.5, nuclear distribution of $H4Me_3K20$ modified chromatin can vary amongst the *B. glabrata* head-foot nuclei. The frequency of $H4Me_3K20$ modified chromatin nuclear patterns was also assessed in the four snail types; adult NMRI susceptible, adult NMRI susceptible exposed to miracidia, adult BS90 resistant and juvenile NMRI susceptible. The patterns documented in Fig 6.9 were designated as Fig 6.9 A: pattern 1, Fig 6.9 B: pattern 2 and Fig 6.9 C: pattern 3. The frequency distribution of these patterns was assessed as described in section 6.3.4. Fig 6.10 displays the graph distribution of $H4Me_3K20$ patterns in adult NMRI susceptible *B. glabrata* snails. Fig 6.10 A and B show the frequency of the patterns in snails 1 and 2 respectively. The fraction of the patterns was very similar in these snails with pattern 3 the most prominent followed by

2 and 1. Snail 3 in Fig 6.10 C, exhibited a different distribution of H4Me$_3$K20 patterns, with pattern 2 present in the highest levels, almost double that of patterns 3 and 1. Fig 6.10 D shows the mean distribution of H4Me$_3$K20 patterns of which, 2 and 3 are present in equal amounts and pattern 1 to a lesser extent.

Figure 6.10: The percentage of H4Me$_3$K20 modification patterns in the head-foot nuclei of adult NMRI susceptible *B. glabrata* snails

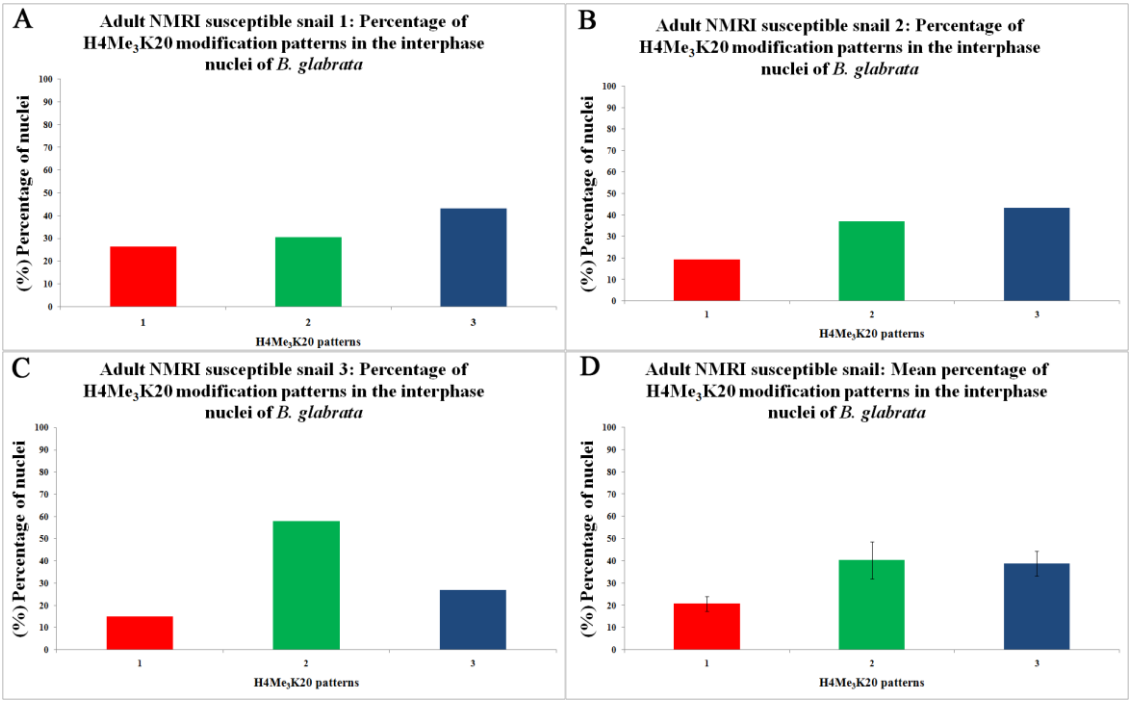

The H4Me$_3$K20 modification patterns were observed in the head-foot of 3 adult NMRI susceptible *B. glabrata* snails. 1000 positive nuclei were counted and percentage of each pattern documented in A (snail 1), B (snail 2) and C (snail 3). The mean distribution of H4Me$_3$K20 patterns is displayed in D. Pattern 1 is in red, Pattern 2 in green, Pattern 3 in blue.

The frequency distribution of the H4Me$_3$K20 patterns in adult NMRI susceptible snails exposed to miracidia is displayed in Fig 6.11. Pattern 2 is the most prominent in snails 1, 2 and 3. Patterns 1 and 3 are present in similar quantity; and as reflected in Fig 6.11 D, the mean frequency distribution of the H4Me$_3$K20 patterns shows that pattern 2 is the most frequent followed by patterns 1 and 3 in similar quantities.

Figure 6.11 The percentage of H4Me$_3$K20 modification patterns in the head-foot nuclei of adult NMRI susceptible *B. glabrata* snails exposed to miracidia

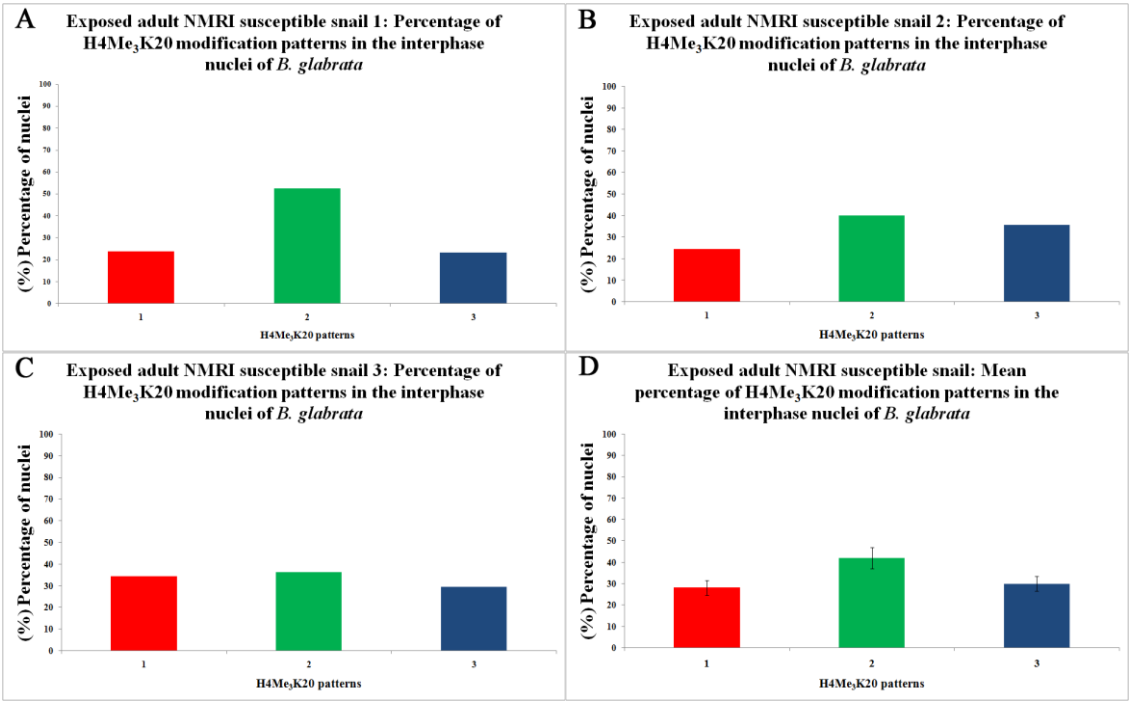

The H4Me$_3$K20 modification patterns were observed in the head-foot of 3 adult NMRI susceptible *B. glabrata* snails exposed to miracidia. 1000 positive nuclei were counted and percentage of each pattern documented in A (snail 1), B (snail 2) and C (snail 3). The mean distribution of H4Me$_3$K20 patterns is displayed in (D). An unpaired, unequal variance, two tailed A student t-test was performed against adult NMRI snails (observed in Fig 6.10) using $P < 0.05$ %. No statistical difference was observed between the unexposed and the exposed adult NMRI snails. Pattern 1 is in red, Pattern 2 in green, Pattern 3 in blue.

Fig 6.12 shows that the adult BS90 resistant *B .glabrata* snails displayed similar frequency distributions of H4Me$_3$K20 nuclear patterns as observed in adult NMRI susceptible snails (Fig 6.10). The mean frequency distribution of the patterns is exhibited in Fig 6.12 D, patterns 2 and 3 are observed in similar amounts followed by pattern 1.

Figure 6.12: The percentage of H4Me$_3$K20 modification patterns in the head-foot nuclei of adult BS90 resistant *B. glabrata* snails.

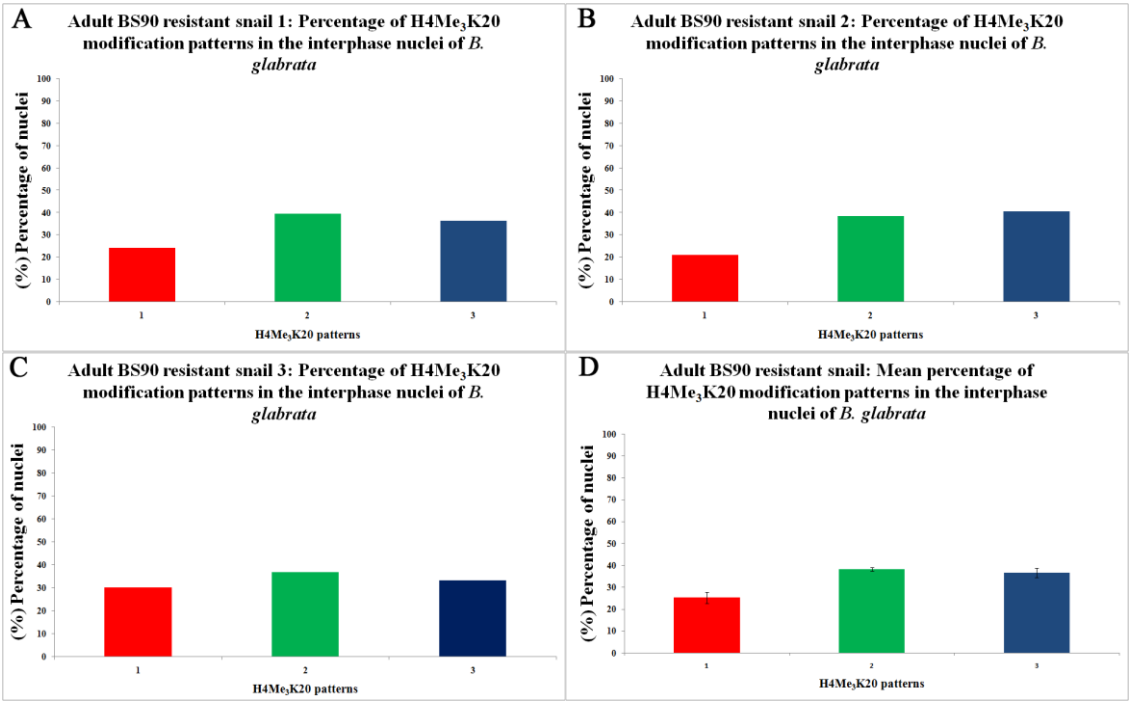

The H4Me$_3$K20 modification patterns were observed in the head-foot of 3 adult BS90 resistant *B. glabrata* snails. 1000 positive nuclei were counted and percentage of each pattern documented in A (snail 1), B (snail 2) and C (snail 3). The mean distribution of H4Me$_3$K20 patterns is displayed in (D). An unpaired, unequal variance, two tailed A student t-test was performed against adult NMRI snails (observed in Fig 6.10) using $P < 0.05$ %. No statistical difference was observed between the adult NMRI snails and the adult BS90 snails. Pattern 1 is in red, Pattern 2 in green, Pattern 3 in blue.

The results from the juvenile NMRI susceptible snail H4Me$_3$K20 pattern frequency distribution are shown in Fig 6.13. Fig 6.13 A shows that pattern 3 was the most abundant in snail 1 and was present in almost double the quantity of pattern 1 and 2. This contrasts with snail 2 (Fig 6.13 B) whereby pattern 1 was the most prominent followed by 3 and 2. Snail 3 (Fig 6.13 C) has a frequency distribution whereby pattern 1 and 3 were observed in similar quantities, followed by pattern 2. The mean distribution of the H4Me$_3$K20 patterns

is shown in Fig 6.13 D and displays the pattern 1 and 3 at similar frequencies followed by pattern 2.

Figure 6.13: The percentage of $H4Me_3K20$ modification patterns in the head-foot nuclei of juvenile *B. glabrata* snails.

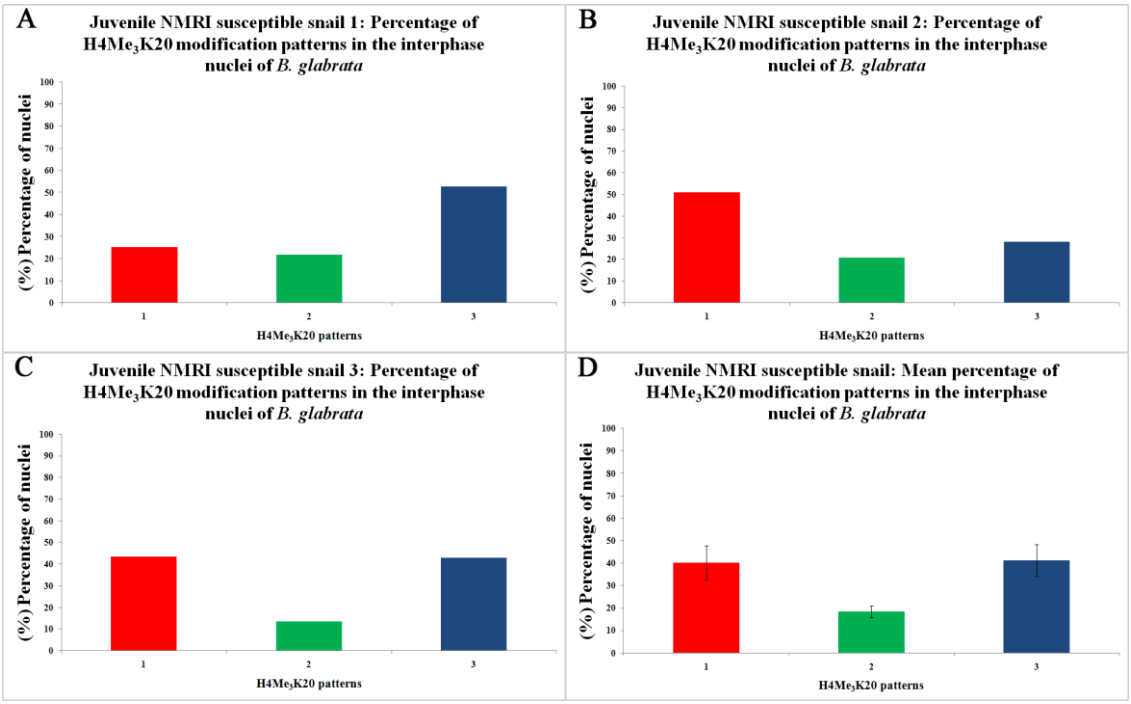

The $H4Me_3K20$ modification patterns were observed in the head-foot of 3 adult BS90 resistant *B. glabrata* snails. 1000 positive nuclei were counted and percentage of each pattern documented in A (snail 1), B (snail 2) and C (snail 3). The mean distribution of $H4Me_3K20$ patterns is displayed in (D). An unpaired, unequal variance, two tailed A student t-test was performed against adult NMRI snails (observed in Fig 6.10) using $P < 0.05$ %. No statistical difference was observed between the juvenile and the adult NMRI snails. Pattern 1 is in red, Pattern 2 in green, Pattern 3 in blue.

Table 6.2: Showing the percentage (%) of $H4Me_3K20$ positive nuclei observed in head-foot nuclei of *B. glabrata*

***B. glabrata* snail**	**Snail 1**	**Snail 2**	**Snail 3**	**Mean**
Adult NMRI susceptible	24.2	41.7	46.2	36.6
Adult NMRI susceptible Ex	51.1	69.2	57.1	58.2
Adult BS90 resistant	48.8	30.8	42.8	40.8
Juvenile NMRI susceptible	30.1	49.1	23.4	36.2

In addition to analysing the frequency distribution of the $H4Me_3K20$ patterns observed in the *B. glabrata* snail types, the percentage of positively stained head-foot nuclei was also analysed. Table 6.2 displays the results from this analysis. The adult NMRI susceptible snails exposed to miracidia show the highest mean percentage of positively stained nuclei at 58.2%, which is followed by the adult BS90 resistant at 40.8% and the unexposed adult and juvenile NMRI susceptible at 36.6% and 36.2% respectively. The variation between the adult NMRI susceptible snails is quite pronounced, wherein the amount of positive nuclei in snail 1 is almost half that of snails 2 and 3. Amongst the juvenile snails, snail 2 at 49.1 % is considerably more positive than snail 3 at 23.4%.

6.3.6 Quantitative estimation of $H3Me_2K9$ and $H4Me_3K20$ antibody binding with the head-foot nuclei from *B. glabrata*

Images of the head-foot tissue sections for adult NMRI susceptible, adult NMRI susceptible exposed to miracidia, adult BS90 resistant and juvenile NMRI susceptible snails stained with the $H3Me_2K9$ and $H4Me_3K20$ antibodies are shown in Fig 6.14-6.15. The immunofluorescent staining for the aforementioned modifications was captured using

a fluorescence microscope at a constant exposure time of 0.2 sec. Hence, this provides a quantitative estimation of the antibodies binding within the interphase nuclei. Fig 6.14 A-D and Fig 6.15 A-D, displays a selection of images captured for $H3Me_2K9$ and $H4Me_3K20$ staining respectively.

Figure 6.14: Representative images of post-translational histone modification $H3Me_2K9$ in nuclei from the head-foot of NMRI susceptible *B. glabrata*.

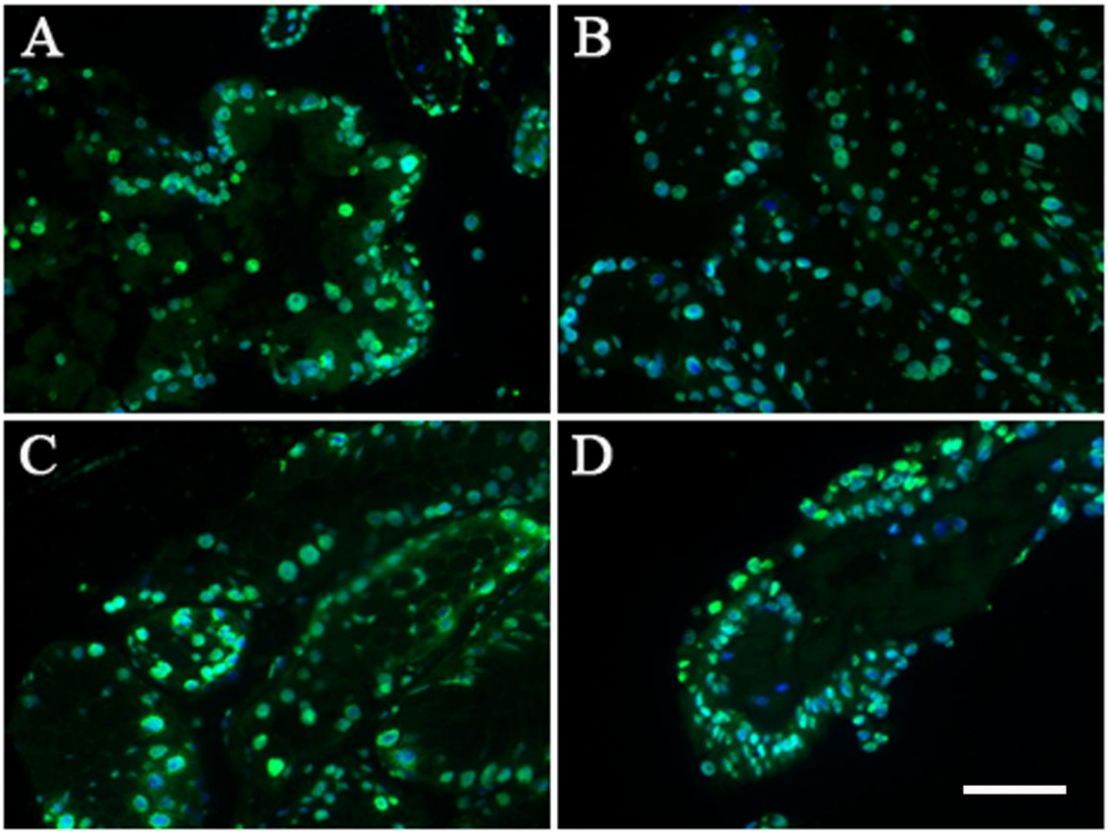

Paraffin tissue sections (with a thickness of 5 µm) from the head-foot of *B. glabrata* were stained with a primary $H3Me_2K9$ mouse monoclonal antibody and subsequently with a secondary donkey anti-mouse antibody conjugated with FITC. The $H3Me_2K9$ modifications were observed as green and the nuclei were counterstained with DAPI (blue). The images displayed are of nuclei from (A) adult NMRI susceptible *B .glabrata*, (B) adult NMRI susceptible *B. glabrata* exposed to miracidia, (C) adult BS90 resistant *B. glabrata* and (D) Juvenile NMRI susceptible *B. glabrata*. The images were captured with a fluorescence microscope, at an exposure time of 0.2 seconds. Bar, 25 µm.

Fig. 6.14 and Fig 6.15 show the variation in the fluorescent intensity of the stained head-foot nuclei within the cell population. As shown in Fig 6.14 C, the staining of $H3Me_2K9$ antibody in the head-foot tissue from adult BS90 resistant snails exhibit intense staining (in green, nuclei were counterstained with DAPI, blue) of nuclei in some regions. The selected image of the juvenile NMRI susceptible $H3Me_2K9$ stained tissue shows bright green stained regions of nuclei as well as regions of nuclei where the green fluorescence of $H3Me_2K9$ antibody binding is absent. Indeed a similar type of staining is observed in Fig 6.15 B, where the $H4Me_3K20$ staining (red) of adult NMRI susceptible snails exposed to miracidia is prominent in some nuclei and absent in others.

Figure 6.15: Representative images of post-translational histone modification $H4Me_3K20$ in nuclei from the head-foot of NMRI susceptible *B. glabrata*.

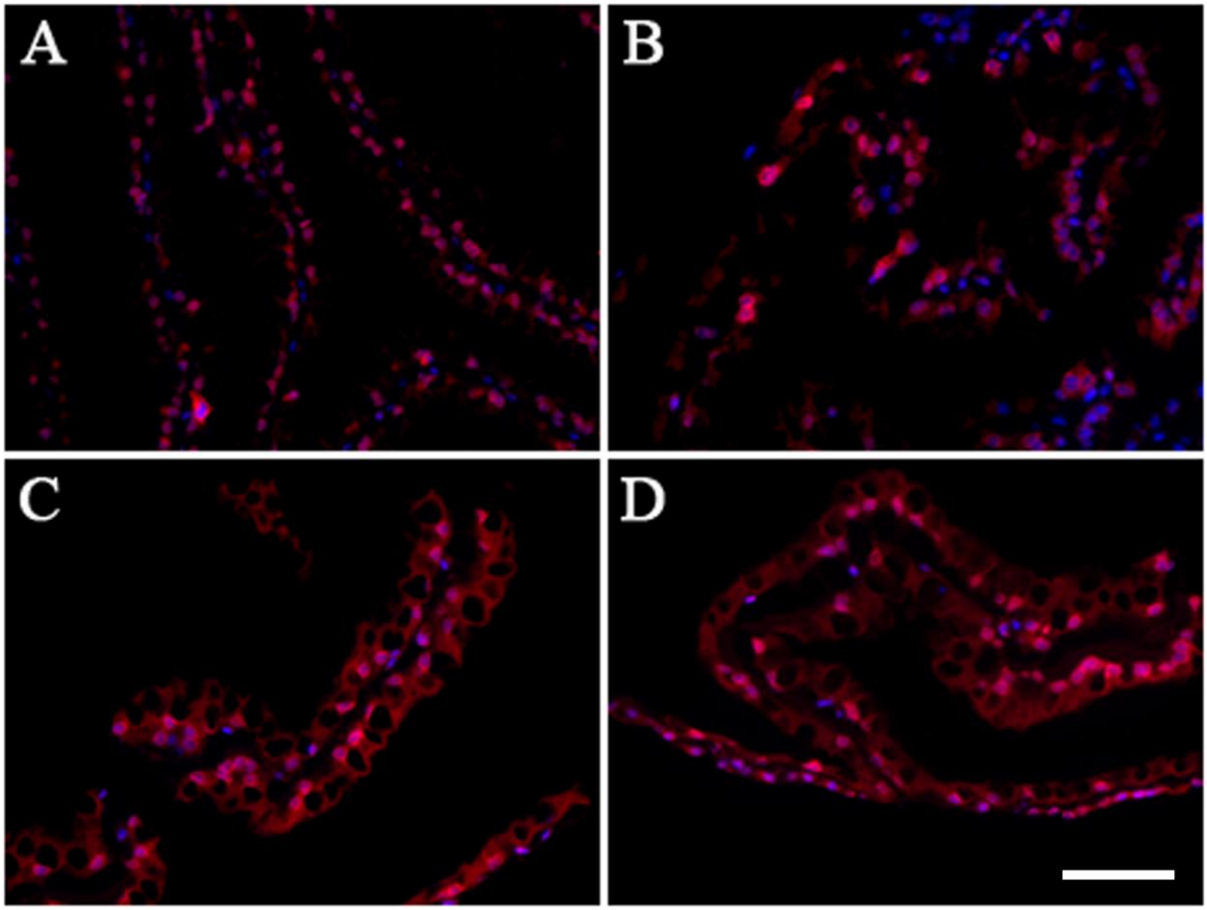

Paraffin tissue sections (with a thickness of 5 µm) from the head-foot of *B. glabrata* were stained with a primary $H4Me_3K20$ mouse monoclonal antibody and subsequently with a secondary porcine anti-rabbit antibody conjugated with cyanine 3. The $H4Me_3K20$ modifications were observed as red and the nuclei were counterstained with DAPI (blue). The images displayed are of nuclei from (A) adult NMRI susceptible *B .glabrata*, (B) adult NMRI susceptible *B. glabrata* exposed to miracidia, (C) adult BS90 resistant *B. glabrata* and (D) juvenile NMRI susceptible *B. glabrata*. The images were captured with a fluorescence microscope, at an exposure time of 0.2 seconds. Bar, 25 µm.

The histograms presented in Fig 6.16-6.20 display the results from the intensity of the antibodies in the head-foot tissue of *B. glabrata.* The aforesaid four snail types were analysed, three snails per snail type. For each snail, 200 nuclei were used to calculate the mean gray values (as described in section 6.2). The intensity of the antibodies is dependent on the amount of modified histone proteins present in the interphase nuclei. As a consequence, the size of the nuclei and the amount of DNA present (interphase cells in S and G2 phase of the cell cycle will have more chromatin) will have an influence on the amount of antibody binding and the subsequent fluorescent intensity. Hence, the signal intensity of the histone antibodies was normalised by both nuclear area and DAPI signal intensity.

Fig 6.16 and 6.17 shows the results attained from the analysis of fluorescence intensity of the $H3Me_2K9$ antibody respectively normalised by nuclear area and DAPI signal intensity. Fig 6.16 and 6.17 show that there is variation in the fluorescence intensity amongst the three snails of the four snail types. The most pronounced variations is observed in Fig 6.16 B, whereby the intensity signal from the adult NMRI susceptible exposed to miracidia snail 3 is almost three times the amount of snail 1. Indeed a similar variation was observed in the juvenile NMRI susceptible snails (Fig 6.16 D) in which snail 1 has double the fluorescence

intensity of snail 3. In contrast, the variation in fluorescence intensity as normalised by DAPI intensity (Fig 6.17) exhibited a less pronounced variation between the snails.

Fig 6.18 shows the mean fluorescence intensity of the $H3Me_2K9$ antibody from the three snails of the four different snail types. Fig 6.18 A and B show the mean fluorescence intensity as respectively normalised by nuclear area and DAPI intensity. Interestingly, both histograms show the same trend whereby, the juvenile NMRI susceptible snails have the highest signal intensity, followed by the adult BS90 resistant, adult NMRI susceptible and lastly by exposed adult NMRI susceptible.

Figure 6.16: Graphs displaying the fluorescent signal intensity from *B. glabrata* head-foot nuclei stained with the $H3Me_2K9$ antibody as normalised by nuclear area

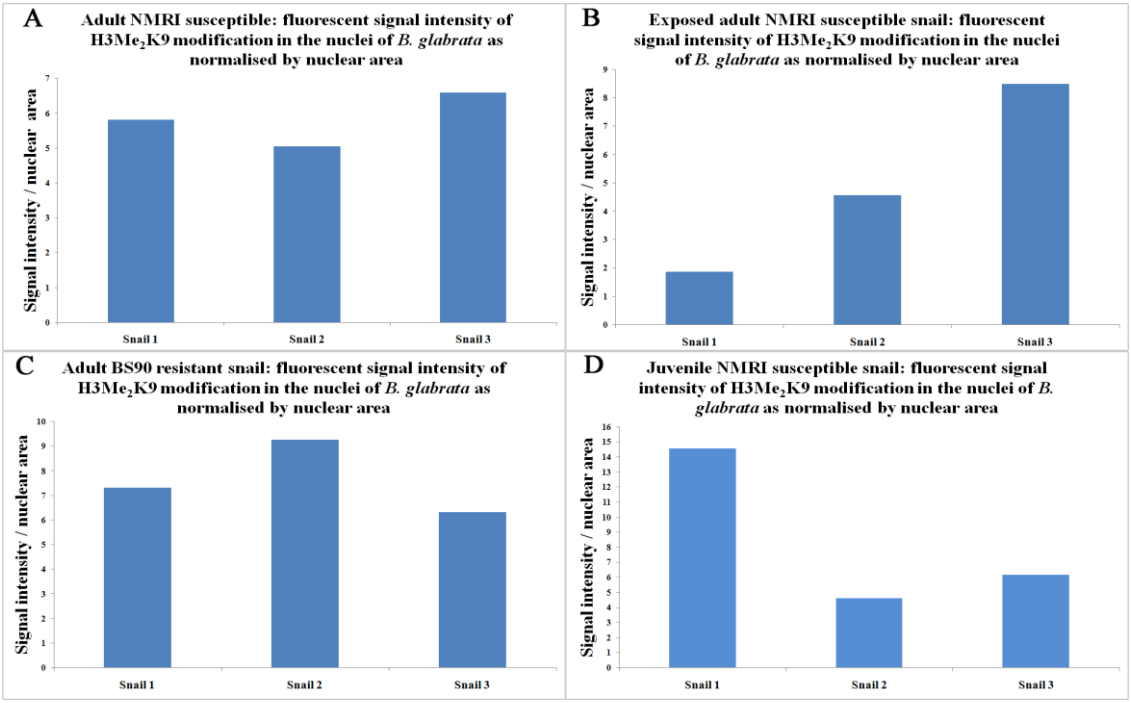

Figure 6.17: Graphs displaying the fluorescent signal intensity from *B. glabrata* head-foot nuclei stained with the H3Me$_2$K9 antibody as normalised by DAPI intensity

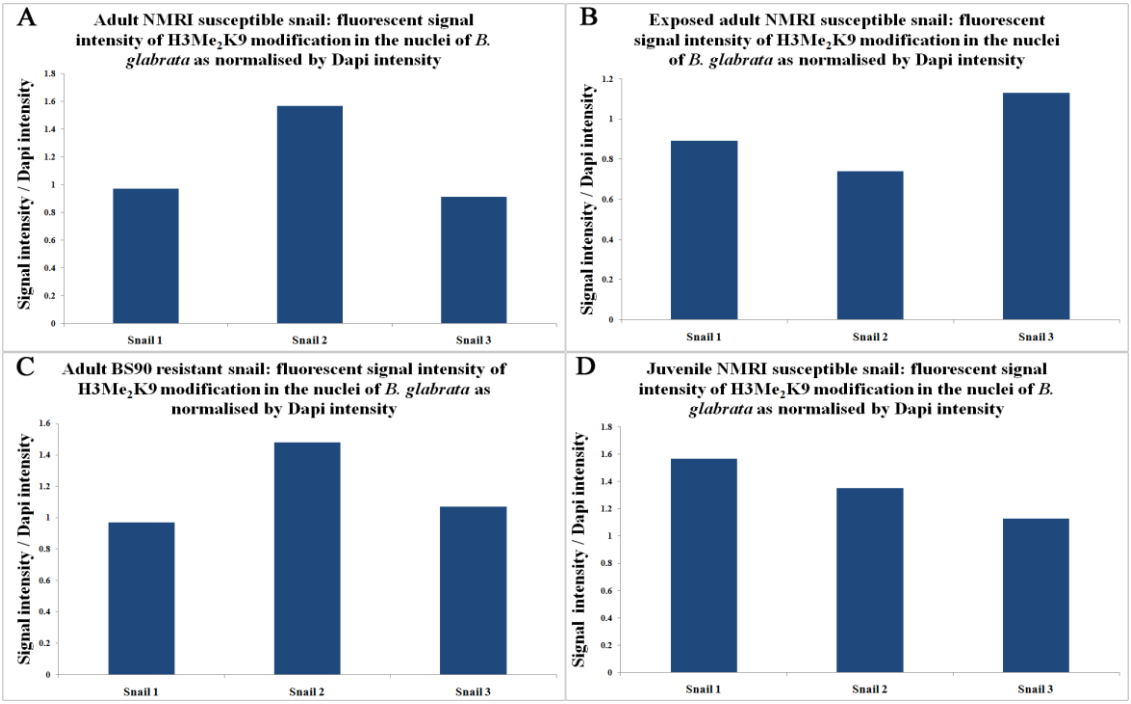

Figure 6.18: Graphs displaying the mean fluorescent signal intensity from *B. glabrata* head-foot nuclei stained with the H3Me$_2$K9 antibody as normalised by nuclear area and DAPI intensity.

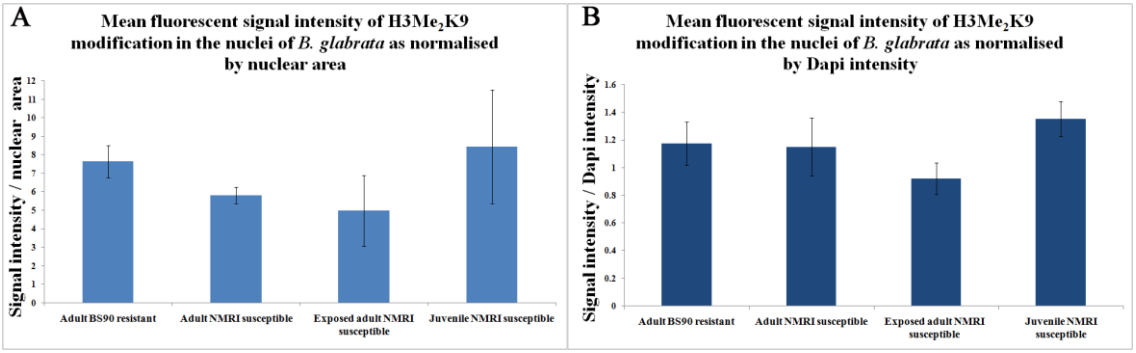

The fluorescence intensity results for the $H4Me_3K20$ antibody are displayed in Fig 6.19 and 6.20 (normalised by nuclear area and DAPI intensity respectively). Fig 6.19 A shows the distribution of the adult NMRI susceptible snails, the three snails have a similar intensity. However, Fig 6.19 B, C and D (respectively for adult NMRI susceptible exposed to miracidia, adult BS90 resistant and juvenile NMRI susceptible snails) display more variation amongst the snails; as noted in Fig 6.19 B, snail 2 has a fluorescence intensity which is approximately four times larger than snail 3. The $H4Me_3K20$ fluorescence intensity results as normalised by DAPI intensity (Fig 6.20), show variations in $H4Me_3K20$ intensity between the snails, most noticeably within the adult NMRI susceptible snails exposed to miracidia (Fig 6.20 B) whereby the fluorescence intensity from snail 2 is almost four times that of snail 3.

As observed with the mean fluorescence intensity results from the $H3Me_2K9$ (Fig 6.18), a similar trend is seen between the $H4Me_3K20$ results normalised by nuclear area and DAPI intensity (Fig 6.21). As displayed in Fig 6.21 A and B, the juvenile NMRI susceptible snails have the highest mean fluorescence intensity, followed by adult NMRI susceptible and adult BS90 resistant snails at similar intensities and lastly by the adult NMRI snails exposed to miracidia.

Figure 6.19: Graphs displaying the fluorescent signal intensity from *B. glabrata* head-foot nuclei stained with the H4Me$_3$K20 antibody as normalised by nuclear area

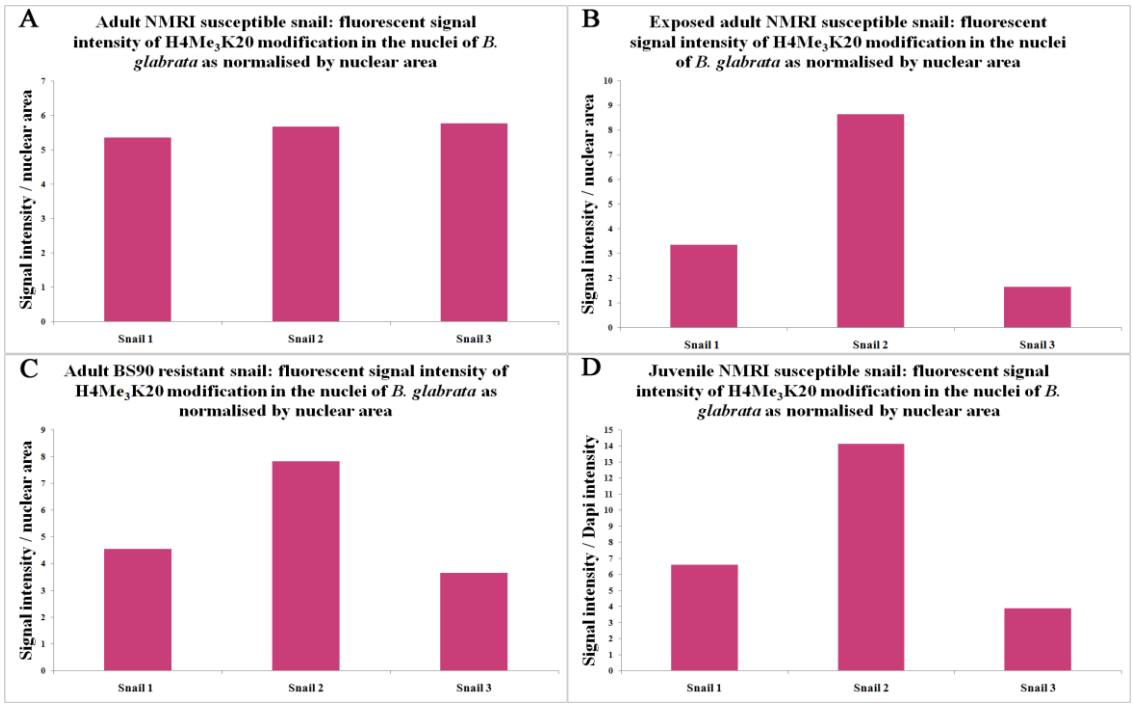

Figure 6.20: Graphs displaying the fluorescent signal intensity from *B. glabrata* head-foot nuclei stained with the H4Me$_3$K20 antibody as normalised by DAPI intensity

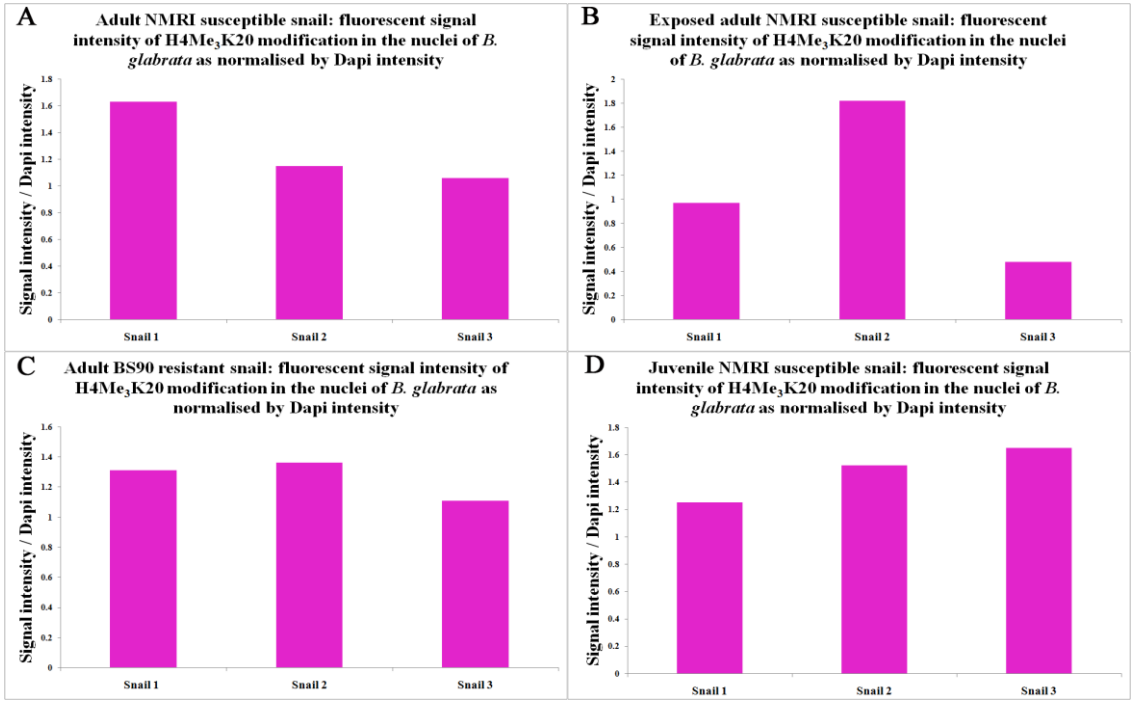

Figure 6.21: Graphs displaying the mean fluorescent signal intensity from *B. glabrata* head-foot nuclei stained with the H4Me$_3$K20 antibody as normalised by nuclear area and DAPI intensity

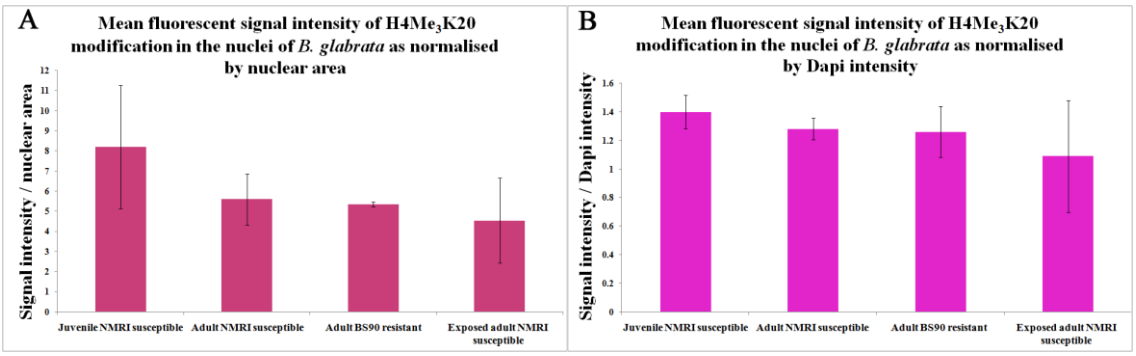

6.4 Discussion

Research into chromatin organisation in the eukaryotic interphase nucleus of *B. glabrata* to date is limited to this present study. Yet, despite the lack of a prelude of published experiments pertaining to nuclear chromatin organisation in this mollusc, the data yielded from this investigation is very exciting and provides a platform for future researchers aiming to pursue this topic further.

Using both the Bge cells and *B. glabrata* it was possible to analyse the spatial nuclear organisation of the modified methylated chromatin using the histone antibodies of H3Me$_2$K9, H3Me$_3$K4, and H4Me$_3$K20. These experiments were designed to examine *B. glabrata in vitro* and *ex vivo*. The Bge cells provided the *in vitro* source for experimenting on *B. glabrata*, the cells were grown on coverslips (as described in section 6.2), fixed, and stained with H3Me$_2$K9, H3Me$_3$K4 and H4Me$_3$K20 antibodies. The interphase nuclei of the Bge cells displayed unique patterns of modified chromatin distribution specific to the particular type of lysine methylation. The histone antibodies associated with heterochromatic formation, H3Me$_2$K9 and H4Me$_3$K20, exhibited different spatial

organisations in the Bge cell nuclei. The $H3Me_2K9$ modified chromatin was observed as a relatively small punctate foci, spread uniformly around the nucleus. In contrast, the chromatin of $H4Me_3K20$ was larger, with more variation in foci size. The use of $H3Me_3K4$ antibody, a marker of active gene expression and for regions of the genome poised for transcription provided further differences in modified chromatin nuclear organisation. The Bge cell nuclei stained with $H3Me_3K4$ exhibited an intense presence of this modification, manifesting as small, punctate foci spread around nucleus, negating the nucleolus and some parts of the outermost periphery. These modifications have been documented to be linked with both heterochromatic ($H3Me_2K9$ and $H4Me_3K20$, associated with silent/ transcriptionally repressed chromatin) and euchromatin ($H3Me_3K4$, associated open/transcriptionally active chromatin).

The *ex vivo* analysis of *B. glabrata* using $H3Me_2K9$ and $H4Me_3K20$ presented more than one nuclear modification pattern for the aforementioned histone antibodies. Indeed, the analysis of four different sample types of snails (adult NMRI susceptible, adult NMRI susceptible exposed to miracidia, adult resistant BS90 and juvenile susceptible NMRI) produced four different patterns amongst the nuclei stained with $H3Me_2K9$ and three patterns amongst the nuclei stained with $H4Me_3K20$. The $H3Me_2K9$ modified chromatin distribution varied in foci size and spatial organisation within the nucleus. The first pattern observed in Fig 6.4 A is very similar to that shown in the Bge cell nuclei, displaying small punctate foci, pattern 2 (Fig 6.4 B) was typified by large and small foci. A regional bias of the $H3Me_2K9$ modified foci was observed in Fig 6.4 C (pattern 3) and Fig 6.4 D (pattern 4), whereby the $H3Me_2K9$ exhibited an ostensible bias towards the nucleoli within the nucleus. These patterns differed in the compartmentalisation of the modified foci, inasmuch as pattern 3 displayed higher compartmentalisation of foci. With regards to the $H4Me_3K20$ patterns, Fig 6.9 A displays pattern 1, with large modified chromatin forming

compartmentalised ringing of the nuclear periphery as well as dispersed foci throughout the nucleus, pattern 2 (Fig 6.9 B) was observed in the *B. glabrata* nuclei as having similarly sized foci, but with a distribution more ubiquitous and slightly to the interior of the nucleus. The nuclei exhibiting the third pattern (Fig 6.9 C) were observed with small punctate foci distributed uniformly around the nucleus.

The $H3Me_2K9$ and $H4Me_3K20$ patterns were observed at different frequencies levels in all the aforementioned *B. glabrata* snail types. As documented by other published researchers, these modifications are associated with the transcriptional repression of genes (Boggs et al., 2002, Skalnikova et al., 2007). One may hypothesise that these differences in patterns could be indicative of differences in histone post-translational methylation levels in different regions of the *B. glabrata* genome. Indeed, as documented in other eukaryotic organism, heterochromatin formation is often prevalent in the peripheral regions of the nucleus, consequently, the ring-like formation of $H4Me_3K20$ foci at the periphery of *B. glabtrata* nuclei may present evidence for such structural formations (Fig 6.9 A). Indeed, this perinuclear formation of chromatin has been documented by Payne and Braun (2006) and was correlated with the expression of the transcriptional repressor Plzf (promyelocytic leukemia zinc-finger) in mouse spermatogonia (Payne and Braun, 2006). The loss of Plzf, resulted in the $H4Me_3K20$ chromatin occupying a more punctate, uniform nuclear distribution (Payne and Braun, 2006). The presence of the $H3Me_2K9$ and $H4Me_3K20$ modified chromatin patterns in all the snail types hints that these patterns exist normally and are perhaps a function of the cell cycle or a cell type specific form of chromatin organisation relating to specific expression of regions of the *B. glabrata* genome.

The statistically significant frequency distribution level differences in patterns 2 and 4 in juvenile NMRI susceptible snails may indicate developmental changes to the *B. glabrata*

NMRI genome. Indeed, it's intriguing that the juveniles are also the snail type with the highest fluorescence intensity for both the histone modification antibodies.

Pattern 2 was shown to be significantly lower in juvenile snails and pattern 4 significantly higher in comparison to the adult equivalents. The results from these changes in $H3Me_2K9$ modified chromatin nuclear organisation could imply that different regions of the *B. glabrata* genome are repressed at different stages of development; as observed in mice with regards to B cell development (Johnson et al., 2004). Whether this remodelling of chromatin architecture has a global influence on genomic expression requires further investigation. Perhaps a future experiment could encompass the chromatin immunoprecipitation (ChIP) (from samples of juvenile and adult NMRI susceptible snails as well as the BS90 resistant snails) with antibodies for $H3Me_2K9$. This could be followed by the analysis of associations of $H3Me_2K9$ with promoters of genes correlated with resistance and susceptibility in *B. glabrata* i.e. *SOD1* and *FREP 2* (Goodall et al., 2006, Hertel et al., 2005).

Evidence for changes to methylated chromatin with age has been reported in mammalian tissue (Sarg et al., 2002). An article by Sarg et al (2002) investigated histone methylation patterns of $H4Me_3K20$ in rat kidneys and liver; an increase in $H4Me_3K20$ with age was noted. The increase was observed in 30-450 day old rats. The most pronounced increase was in rat liver, $H4Me_3K20$ was 150% higher in old rats compared to young rats. Such a dramatic increase hints at a considerable amount chromatin remodelling with age.

Although this study has produced alot of interesting data such as the identification of organised modified chromatin in the nucleus of *B. glabrata* and the Bge cells and statistical differences in the frequency of $H3Me_2K9$ patterns between the adult and juvenile NMRI *B. glabrata* snails; an objective critique of this study would highlight the sample size of snails used. Perhaps a sample size of more than three snails per snail type would have yielded

further statistically significant results. Additionally, it would be interesting for those wishing to pursue this avenue of research to intercalate juvenile NMRI susceptible snails exposed to miracidia into this study.

The deployment of a larger panel of histone modification antibodies marking both euchromatic and heterochromatic formations in the nucleus may well be the next step in the analysis of nuclear chromatin formation in *B. glabrata*. Indeed, as well as more antibodies, a clear definition of cell types present in *B. glabrata* head-foot tissue as well as the ability to differentiate between them would increase the scope of analysis. Perhaps a subsequent study in relation to the schistosome parasite's ability to alter the genome of *B. glabrata* could focus solely on chromatin organisation within the nuclei of the haemocytes? Indeed, this experiment could potentially be extended to other parts of *B. glabrata*.

As shown previously in chapter 5, upon parasite exposure, there is marked change in genome organisation with respect to the spatial position of gene loci in the interphase nucleus of the Bge cells and their transcriptional profile. The possibility for further analysis could entail the staining of the Bge cell nuclei with histone modification antibodies post exposure to miracidia. The staining of the Bge cell nuclei with these antibodies could be combined with the hybridization specific gene loci using FISH. This would allow for a new prospective for analysis e.g. investigating the structural changes to chromatin around the gene loci region upon parasite exposure. Indeed, using the FISH methodology established in chapter 3 and 4 (Odoemelam et al., 2009), this investigation could be extended to using FISH and histone antibodies on *B. glabrata* tissue.

The potential role of post-translational modifications to histone proteins and modulations in gene expression upon parasitic invasion of *B. glabrata* could also be investigated by focusing on the role of histone acetyltransferases (HAT, such Suv39H1, necessary for

H3K9 methylation) and histone deacetyltransferases (HDAC, LSD1, catalyses the demethylation of H3K4) (Bartova et al., 2005, Shi and Dawe, 2006). These enzymes catalyse the acetylation (HAT) and deacetylation (HDAC) of histone proteins (Strasak et al., 2009). It is possible to effectively inhibit the activity of HDACs using inhibitors (HDACi) such as sodium butyrate and trichostatin A (Strasak et al., 2009, Bartova et al., 2005). Indeed, this has been shown to promote the decondensation of chromatin, alter the distribution of acetylated and methylated chromatin foci within the nucleus and increase the levels $H3Me_2K9$ (Strasak et al., 2009). In addition, HDACi have been shown to function in the global remodelling of chromatin architecture (Gilchrist et al., 2004, Taddei et al., 2001, Taddei et al., 2005, Bartova et al., 2005).

Chapter 7:
Discussion

7. Discussion

The waterborne mollusc *Biomphalaria glabrata* is the intermediate host for the parasite *Schistosoma mansoni*, which is responsible for the disease schistosomiasis (also known as Bilharzia). This disease affects over 200 million people every year and as a consequence is the subject of intense research by many laboratories (Miller et al., 2001). Research into halting the transmission from intermediate host to humans has focused on the snail's ability to fight parasitic invasion via immunological and molecular means (Raghavan et al., 2003, Goodall et al., 2006, Hahn et al., 2001, Leonard et al., 2001, Jiang et al., 2006). Indeed, the genetic basis of parasite susceptibility in *B. glabrata* has guided the research into snail strains which are resistant (BS90) and susceptible (NMRI) to *S. mansoni* (Knight et al., 2009). The up/down modulation of *B. glabrata* genes upon parasitic infection has been reported in many published articles (Knight et al., 2009, Hertel et al., 2005, Jiang et al., 2006, Coustau et al., 2003). Consequently, candidate markers of genetic resistance have been put forward; of notable interest are the genes *SOD1*, for super oxide dismutase (Goodall et al., 2006), *FREP*, fibrinogen related protein (Hertel et al., 2005, Jiang et al., 2006) and *BgPrx4*, peroxiredoxin (Knight et al., 2009). Yet, the complete elucidation of this host-parasite interactions remains elusive. An obviate of many researchers studying the interactions between *B. glabrata* and *S. mansoni* is the paucity of knowledge pertaining to the genome of *B. glabrata* in comparison to other well studied organisms such as humans and mice. The genome of *B. glabrata* is currently being sequenced by Genome Sequencing Center (GSC, Washington University in St. Louis, USA) (reviewed by Raghavan and Knight, 2006). The fully sequenced genome of *B. glabrata* will aid the research into host-parasite interaction; in addition the continued study of it's genome on a biochemical, chromosomal and genomic will aid the effort towards curtailing the spread of schistosomiasis.

The intention of the research presented in PhD thesis, was to provide a better understanding of the *B. glabrata's* host parasite interactions with *S. mansoni* through analysis of the snails' genome at the chromosomal and nuclear level.

The utilisation of the Bge cells provided an *in vitro* model for the study *B. glabrata* in this thesis (Hansen, 1976). Indeed, this cell line is an important tool for community of researchers studying schistosomiasis. It is the only molluscan cell line in existence and is used by many laboratories to maintain the *S. mansoni* parasite. In addition, the cell line is used to investigate genomic change the Bge genome upon incubation with the parasite. Until this study, analysis of the Bge chromosomes was rooted in publication from Bayne et al (1979) which discerned a chromosomal number of 2n: 36 (Bayne et al., 1979). This was congruent with Raghunathan (1976) and Goldman et al (1984) assessment of the chromosomal complement from *B. glabrata* (Raghunathan et al., 1976, Goldman et al., 1984). An investigation upon two Bge cell line isolates cultured in separate labs uncovered extensive aneuploidy. Bge cell line isolates 1 and 2 contained a mean complement of 63 and 67 chromosomes respectively (chapter 2), which is a marked departure from the 36 chromosome complement of the snail *in vivo* (Odoemelam et al., 2009). Karyotypes produced from these isolates showed that rather than being a simple case polyploidy (which would have a theoretical chromosome number of 54) the aneuploidy was uneven and most prominent in the relatively medium sized chromosomes. These results are a cautionary finding for those wishing to extrapolate *in vitro* results to those *in vivo.* Indeed, the characterisation of genes is necessary before beginning expression studies utilising the Bge cells. The characterisation of *B. glabrata* genes in the Bge cell line was documented in chapters 3, 4 and 5.

The availability of a physical map for *B. glabrata* would be a valuable asset to the field. The mapping of the repetitive retrotransposon gene showed the Bge cells can be used to

begin such types of mapping (Knight et al., 2007). Before this study, there existed no comprehensive technique to map single copy genes onto chromosomes from the Bge cells; unlike organisms such as human, mice, pigs, dogs and chickens, in which the protocols are abundant and the genes from these organisms are routinely mapped. As such, to effectively map single copy genes onto the chromosomes of the Bge cells, a thorough development of a FISH protocol for the Bge cells was required. Indeed, such a protocol had to take into consideration a number of variables which can alter the hybridization of genes onto homologous genetic regions. One such variable was the denaturation of the metaphase chromosomes, a necessary step in FISH. By analysing the morphology of the Bge cell chromosomes heat-denatured at different lengths of time, it was possible to select the duration of 1.5 minutes as the most suitable denaturation time. In addition to assessing the denaturation time, it was also imperative that the repetitive sequences of the Bge cell genome were suppressed in order to properly identify the unique hybridized single copy gene signals. In human FISH protocols, this suppression is achieved via the deployment of human C_0t-1 DNA together with the gene probe. In its' absence, the utilisation of sonicated genomic Bge cell DNA was used as a suppressive reagent. The analysis of the hybridized signal with different amounts of DNA resulted in 40 µg as an effective amount to suppress the repetitive sequences. Consequently, with the aid of the aforementioned specificities for the Bge cell chromosomes and the Bge cell karyotype from chapter 2, the mapping of four single copy *B. glabrata* genes (*BgPrx*$_4$, actin, ferritin and *piwi*) was achieved. Interestingly, despite its' inherent aneuploidy, the Bge cell chromosomes of the aforesaid genes were diploid in nature. Hence, this protocol provides a valuable tool for the future construction of a physical map from ex *vivo* chromosomes.

The eukaryotic interphase nucleus is highly organised and chromosomes occupy compartmentalised territories (Cremer et al., 2006). In mammalian interphase nuclei, these

chromosome territories are spatial organised in a non-random manner. The presence of such territories has been documented in several organisms such as humans (Boyle et al., 2001, Cremer et al., 1988), old world monkeys'(Neusser et al., 2007), pigs (Foster et al., 2005, Szczerbal et al., 2009), chicken (Habermann et al., 2001), mouse (Mayer et al., 2005), *Drosophila* (Hochstrasser and Sedat, 1987), parasites such as *Trypansoma brucei* (Ogbadoyi et al., 2000), *hydra* (Alexandrova et al., 2003), yeast (Bystricky et al., 2005) and plants (Lysak et al., 2001). The spatial organisation of these territories and gene loci in the interphase nucleus is thought to have regulatory functions in terms of gene expression. Yet the question still remains of whether the nuclear organisation has a causative role in genomic expression or if it is just a consequence of modulations in transcriptional activity?

Chapter 4 provides the first ever description of interphase chromosome territories in the *B. glabrata* using the Bge cells as an *in vitro* model. The genome of the Bge cells was pulse labelled with the thymidine analog BrdU and the cells allowed to divide so that the individually labelled chromosomes could be identified in the interphase nucleus using a secondary antibody. The chromosome territories of the Bge cells differed in size and were shown to be distributed radially around the nucleus (as opposed to the Rabl distribution observed in *Drosophila* (Hochstrasser and Sedat, 1987) and plants (Lysak et al., 2001). Analysis of the radial position of these territories found a correlation between territory size and spatial position. The large territories occupied an intermediate position in the interphase nucleus and the small chromosomes were positioned towards the interior. Indeed, the organised manner of the Bge cell genome extended to the gene loci, whereby examination of four mapped genes (via FISH) onto the Bge cell interphase nuclei showed that they occupied specific positions. The genes actin, *BgPrx4* and *piwi* were located towards the interior. In contrast, the ferritin gene was position at the periphery of the nucleus. With the knowledge that the interphase nucleus of *B. glabrata* is organised akin in

manner to that of mammalian nuclei, future researchers may utilise the assays developed in chapter 4 for further investigations into genome organisation in *B. glabrata* or perhaps other molluscan organisms. In terms of the host-parasite relationship, the results from chapter 5 are intriguing. Following the identification of spatially organised chromosome territories and gene loci, the analysis of the Bge cell genome proceeded in investigating the effects of the *S. mansoni* parasite on the cells. The Bge cells were grown and cultured with miracidia for different lengths of time up to 24 hr, before cellular fixation. The *B. glabrata* genes actin and ferritin were hybridized onto the Bge cell interphase nuclei from the different exposure times and radially positioned. Both genes were shown to alter position upon parasite exposure; the ferritin gene altered from a peripheral position to a more internal position and the actin gene altering position with the histograms displaying a bimodal distribution. In addition to changes in gene loci position, expression studies on the Bge cells at the different post exposure time points showed modulation in the gene expression, which at some time points were congruent with published theories regarding genomic locations and gene expression. Indeed, it is possible that the *S. mansoni* parasite is able to induce global changes in the genome of *B. glabrata,* as shown by the movement of genes post exposure. The possibility that such changes are the result of transcriptional up regulation/ down regulation or actually contribute to changes in transcription are very exciting. Future work into gene loci positioning in *B. glabrata* could employ the use of the lac O/ lac I interaction, as demonstrated by Bickmore and colleagues (Finlan et al., 2008). This method has been used to tether genetic sequences to the nuclear periphery in human cells and resulted in a transcriptional down-regulation of those genes which were tethered (Finlan et al., 2008). If such results could be replicated *in vitro* in the Bge cells or *in vivo* in *B. glabrata,* it would open a door to a vast amount of pertinent experiments i.e.

investigating whether altering the nuclear location of gene loci relevant to resistance/ susceptibility alters gene expression or indeed resistance/ susceptibility to the parasite.

The analysis of chromatin organisation in *B. glabrata* produced interesting results. This study (chapter 6) focused on analysing the nuclear distribution of modified histones in the interphase nucleus of *B. glabrata in vitro* and *ex vivo*. The utilisation $H3Me_2K9$, $H3me_3K4$ and H4Me3K20 on the Bge cells, showed that different type of heterochromatin and euchromatin are organised in a unique manner in the *B. glabrata* genome. An examination of the interphase nuclei from the head-foot of *B. glabrata* revealed more than one pattern for $H3Me_2K9$ and $H4Me_3K20$. Four patterns were discerned for the $H3Me_2K9$ modification and three patterns for the $H4Me_3K20$ modification. The frequency of these patterns varied amongst the snails and between different snail types and was statistically different between adult NMRI susceptible snails and it's juvenile counterpart with regards to the $H3Me_2K9$ patterns (chapter 6). Indeed, the statistical significant difference in patterns 2 and 4 between the adult and the juvenile NMRI snails may indicate global developmental differences in chromatin organisation. Whether or not these differences are relevant to resistance and susceptibility remains to be answered. However it should be noted that there have been published articles commenting on the differences in infectivity of juvenile snails to their adult counter parts (adults being more refractory to infection) (Niemann and Lewis, 1990, Richards and Merritt, 1972, Richards, 1984). A quantitative estimation of the antibody binding via fluorescence intensity placed juveniles as the highest.

In summary, analysis of the genome of *B. glabrata in vitro* and *ex vivo* has demonstrated a complexity akin to that of mammalian genomes. The successfully karyotyping of the Bge cell chromosomes and the mapping of single copy genes onto metaphase chromosomes, revealed the presence of inherent aneuploidy which should be taken in account when

conducting future research using the Bge cell line; yet the four genes mapped onto two homologous chromosomes, which lends credence to the Bge cells as a still reliable source for *in vitro B. glabrata* research. Indeed, the identification of interphase chromosome territories, positioned in a non-random manner as well as the gene loci presents the *B. glabrata* genome as highly organised. *B. glabrata*'s interactions with the *S. mansoni* parasite resulted in global changes to gene loci position in the interphase nucleus and changes to gene expression. These results are very exciting and open the door to the initiation of further experiments in this field of research. The identification of unique histone modification chromatin patterns and variations amongst different snails, statistically significant in juveniles NMRI susceptible snails' type perhaps indicates that chromatin structure plays a crucial role in nuclear processes.

It is hoped that this research will not only aid those working in the field of Schistosomiasis but also those wishing to utilise the assays established for *B. glabrata* on other molluscan organisms; indeed this study has shown that *B. glabrata* is an apt candidate for a model molluscan organism.

References

(WHO), W. H. O. (1997) *Fresh water snails, Vector Control - Methods for Use by Individuals and Communities: Chapter 8*

ADEMA, C. M., ARGUELLO, D. F., 2ND, STRICKER, S. A. & LOKER, E. S. (1994a) A time-lapse study of interactions between Echinostoma paraensei intramolluscan larval stages and adherent hemocytes from Biomphalaria glabrata and Helix aspersa. *J Parasitol,* 80**,** 719-27.

ADEMA, C. M., KNIGHT, M., LEWIS, F. & LOKER, E. S. (2002) Request for making a BAC library from *Biomphalaria glabrata* (gastropod mollusc), the prominent snail species contributing to transmission of human schistosomiasis. *Members of the Biomphalaria glabrata genome initiative*.

ADEMA, C. M., LUO, M. Z., HANELT, B., HERTEL, L. A., MARSHALL, J. J., ZHANG, S. M., DEJONG, R. J., KIM, H. R., KUDRNA, D., WING, R. A., SODERLUND, C., KNIGHT, M., LEWIS, F. A., CALDEIRA, R. L., JANNOTTI-PASSOS, L. K., CARVALHO ODOS, S. & LOKER, E. S. (2006) A bacterial artificial chromosome library for Biomphalaria glabrata, intermediate snail host of Schistosoma mansoni. *Mem Inst Oswaldo Cruz,* 101 Suppl 1**,** 167-77.

ADEMA, C. M., VAN DEUTEKOM-MULDER, E. C., VAN DER KNAAP, W. P. & SMINIA, T. (1994b) Schistosomicidal activities of Lymnaea stagnalis haemocytes: the role of oxygen radicals. *Parasitology,* 109 (Pt 4)**,** 479-85.

ALEXANDROVA, O., SOLOVEI, I., CREMER, T. & DAVID, C. N. (2003) Replication labeling patterns and chromosome territories typical of mammalian nuclei are conserved in the early metazoan Hydra. *Chromosoma,* 112**,** 190-200.

ANDRADE, Z. A. (2009) Schistosomiasis and liver fibrosis. *Parasite Immunol,* 31**,** 656-63.

ANDRULIS, E. D., NEIMAN, A. M., ZAPPULLA, D. C. & STERNGLANZ, R. (1998) Perinuclear localization of chromatin facilitates transcriptional silencing. *Nature,* 394**,** 592-5.

BALLABIO, E., CANTARELLA, C. D., FEDERICO, C., DI MARE, P., HALL, G., HARBOTT, J., HUGHES, J., SACCONE, S. & TOSI, S. (2009) Ectopic expression of the HLXB9 gene is associated with an altered nuclear position in t(7;12) leukaemias. *Leukemia,* 23**,** 1179-82.

BARRACCO, M. A., STEIL, A. A. & GARGIONI, R. (1993) Morphological characterization of the hemocytes of the pulmonate snail Biomphalaria tenagophila. *Mem Inst Oswaldo Cruz,* 88**,** 73-83.

BARTOVA, E., PACHERNIK, J., HARNICAROVA, A., KOVARIK, A., KOVARIKOVA, M., HOFMANOVA, J., SKALNIKOVA, M., KOZUBEK, M. & KOZUBEK, S. (2005) Nuclear levels and patterns of histone H3 modification and HP1 proteins after inhibition of histone deacetylases. *J Cell Sci,* 118**,** 5035-46.

BAXTER, J., SAUER, S., PETERS, A., JOHN, R., WILLIAMS, R., CAPARROS, M. L., ARNEY, K., OTTE, A., JENUWEIN, T., MERKENSCHLAGER, M. & FISHER, A. G. (2004) Histone hypomethylation is an indicator of epigenetic plasticity in quiescent lymphocytes. *Embo J,* 23**,** 4462-72.

BAYNE, C. J. (1976) Culture of molluscan organs: A review. *Academic Press, New York, San Francisco, London***,** 61-74.

BAYNE, C. J., HAHN, U. K. & BENDER, R. C. (2001) Mechanisms of molluscan host resistance and of parasite strategies for survival. *Parasitology,* 123**,** 158-167.

BAYNE, C. J., OWCZARZAK, A. & ALLEN, J. R. (1978) Molluscan (Biomphalaria) cell line: Serology, karyotype, behavioural and enzyme electrophoretic characterization. *Journal of invertebrate pathology.,* 32**,** 35-39.

BENDER, R. C., GOODALL, C. P., BLOUIN, M. S. & BAYNE, C. J. (2007) Variation in expression of Biomphalaria glabrata SOD1: a potential controlling factor in susceptibility/resistance to Schistosoma mansoni. *Dev Comp Immunol,* 31**,** 874-8.

BENEX, J. (1961) [Survival of explants of Planorbidae (Australorbis glabratus) in a synthetic, antiseptic and nutritive medium.]. *C R Hebd Seances Acad Sci,* 253**,** 734-6.

BENEX, J. (1965) [Attempts at Infestation, by Schistosoma Mansoni Miracidia, of Planorbid Tentacles Maintained in Organ-Type Culture in Renewed Liquid Medium.]. *C R Hebd Seances Acad Sci,* 260**,** 4080-2.

BERGQUIST, R., AL-SHERBINY, M., BARAKAT, R. & OLDS, R. (2002) Blueprint for schistosomiasis vaccine development. *Acta Trop,* 82**,** 183-92.

BERRIMAN, M., HAAS, B. J., LOVERDE, P. T., WILSON, R. A., DILLON, G. P., CERQUEIRA, G. C., MASHIYAMA, S. T., AL-LAZIKANI, B., ANDRADE, L. F., ASHTON, P. D., ASLETT, M. A., BARTHOLOMEU, D. C., BLANDIN, G., CAFFREY, C. R., COGHLAN, A., COULSON, R., DAY, T. A., DELCHER, A., DEMARCO, R., DJIKENG, A., EYRE, T., GAMBLE, J. A., GHEDIN, E., GU, Y.,

HERTZ-FOWLER, C., HIRAI, H., HIRAI, Y., HOUSTON, R., IVENS, A., JOHNSTON, D. A., LACERDA, D., MACEDO, C. D., MCVEIGH, P., NING, Z., OLIVEIRA, G., OVERINGTON, J. P., PARKHILL, J., PERTEA, M., PIERCE, R. J., PROTASIO, A. V., QUAIL, M. A., RAJANDREAM, M. A., ROGERS, J., SAJID, M., SALZBERG, S. L., STANKE, M., TIVEY, A. R., WHITE, O., WILLIAMS, D. L., WORTMAN, J., WU, W., ZAMANIAN, M., ZERLOTINI, A., FRASER-LIGGETT, C. M., BARRELL, B. G. & EL-SAYED, N. M. (2009) The genome of the blood fluke Schistosoma mansoni. *Nature,* 460**,** 352-8.

BLANCHARD, T. J. (2004) Schistosomiasis. *Travel Med Infect Dis,* 2**,** 5-11.

BOGGS, B. A., CHEUNG, P., HEARD, E., SPECTOR, D. L., CHINAULT, A. C. & ALLIS, C. D. (2002) Differentially methylated forms of histone H3 show unique association patterns with inactive human X chromosomes. *Nat Genet,* 30**,** 73-6.

BOLZER, A., KRETH, G., SOLOVEI, I., KOEHLER, D., SARACOGLU, K., FAUTH, C., MULLER, S., EILS, R., CREMER, C., SPEICHER, M. R. & CREMER, T. (2005) Three-dimensional maps of all chromosomes in human male fibroblast nuclei and prometaphase rosettes. *PLoS Biol,* 3**,** e157.

BOORMANS, E. M., BIRNIE, E., BILARDO, C. M., OEPKES, D., BONSEL, G. J. & VAN LITH, J. M. (2009) Karyotyping or rapid aneuploidy detection in prenatal diagnosis? The different views of users and providers of prenatal care. *Bjog,* 116**,** 1396-9.

BOUILLY, K., BONNARD, M., GAGNAIRE, B., RENAULT, T. & LAPEGUE, S. (2007) Impact of diuron on aneuploidy and hemocyte parameters in Pacific oyster, Crassostrea gigas. *Arch Environ Contam Toxicol,* 52**,** 58-63.

BOUILLY, K., GAGNAIRE, B., BONNARD, M., THOMAS-GUYON, H., RENAULT, T., MIRAMAND, P. & LAPEGUE, S. (2006) Effects of cadmium on aneuploidy and hemocyte parameters in the Pacific oyster, Crassostrea gigas. *Aquat Toxicol,* 78**,** 149-56.

BOYLE, S., GILCHRIST, S., BRIDGER, J. M., MAHY, N. L., ELLIS, J. A. & BICKMORE, W. A. (2001) The spatial organization of human chromosomes within the nuclei of normal and emerin-mutant cells. *Hum Mol Genet,* 10**,** 211-9.

BRANCO, M. R. & POMBO, A. (2006) Intermingling of chromosome territories in interphase suggests role in translocations and transcription-dependent associations. *PLoS Biol,* 4**,** e138.

BRIDGER, J. M. & BICKMORE, W. A. (1998) Putting the genome on the map. *Trends Genet,* 14**,** 403-9.

BRIDGER, J. M., BOYLE, S., KILL, I. R. & BICKMORE, W. A. (2000) Re-modelling of nuclear architecture in quiescent and senescent human fibroblasts. *Curr Biol,* 10**,** 149-52.

BRIDGER, J. M., KILL, I. R. & LICHTER, P. (1998) Association of pKi-67 with satellite DNA of the human genome in early G1 cells. *Chromosome Res,* 6**,** 13-24.

BROWN, C. R. & SILVER, P. A. (2007) Transcriptional regulation at the nuclear pore complex. *Curr Opin Genet Dev,* 17**,** 100-6.

BROWN, D. S., CURTIS, B. A. & ROLLINSON, D. (1996) The freshwater snail *Bulinus tropicus* (Planorbidae) in Namibia characterised according to chromosome number, enzymes and morphology. *Hydrologia,* 317**,** 125-139.

BRUMPT, E. (1941) Observation biologiques diverges concenant planorbis (Australorbis Tralorbis) glabratus, hote intermediare de Schistosoma mansoni. . *Am parasitol humaine et comparee, ,* 18**,** 9-45.

BRUSCA, B. A. (2005) *The molluscan phylum,* The University of Washington.

BURCH, J. B. (1960a) Chromosome morphology of aquatic pulmonate snails (Mollusca, Gastropoda). *Trans Amr Microsc Soc,* 79**,** 451-461.

BURCH, J. B. (1960b) Chromosome numbers of schistosome vector snails. *Z Tropenmed Parasitol,* 11**,** 449-52.

BURCH, J. B. (1967) Chromosomes of intermediate hosts of human bilharziasis. *Malacologia,* 5**,** 127-135.

BYSTRICKY, K., LAROCHE, T., VAN HOUWE, G., BLASZCZYK, M. & GASSER, S. M. (2005) Chromosome looping in yeast: telomere pairing and coordinated movement reflect anchoring efficiency and territorial organization. *J Cell Biol,* 168**,** 375-87.

CANTERO, G., PASTOR, N., MATEOS, S., CAMPANELLA, C. & CORTES, F. (2006) Cisplatin-induced endoreduplication in CHO cells: DNA damage and inhibition of topoisomerase II. *Mutat Res,* 599**,** 160-6.

CHEEVER, A. W., LENZI, J. A., LENZI, H. L. & ANDRADE, Z. A. (2002) Experimental models of Schistosoma mansoni infection. *Mem Inst Oswaldo Cruz,* 97**,** 917-40.

CHEN, S. N. & WANG, C. S. (1999) Establishment of cell lines derived from oyster, Crassostrea gigas Thunberg and hard clam, Meretrix lusoria Roding. *Methods Cell Sci,* 21**,** 183-92.

CHRISTENSEN, J., AGGER, K., CLOOS, P. A., PASINI, D., ROSE, S., SENNELS, L., RAPPSILBER, J., HANSEN, K. H., SALCINI, A. E. & HELIN, K. (2007) RBP2 belongs to a family of demethylases, specific for tri-and dimethylated lysine 4 on histone 3. *Cell,* 128**,** 1063-76.

COLOMBA, M. S., VITTURI, R., CASTRIOTA, L., BERTONI, R. & LIBERTINI, A. (2002) FISH mapping of 18S-28S and 5S ribosomal DNA, (GATA)n and (TTAGGG)n telomeric repeats in the periwinkle Melarhaphe neritoides (Prosobranchia, Gastropoda, Caenogastropoda). *Heredity,* 88**,** 381-4.

COUSTAU, C., ATAEV, G., JOURDANE, J. & YOSHINO, T. P. (1997) Schistosoma japonicum: in vitro cultivation of miracidium to daughter sporocyst using a Biomphalaria glabrata embryonic cell line. *Exp Parasitol,* 87**,** 77-87.

COUSTAU, C., MITTA, G., DISSOUS, C., GUILLOU, F., GALINIER, R., ALLIENNE, J. F. & MODAT, S. (2003) Schistosoma mansoni and Echinostoma caproni excretory-secretory products differentially affect gene expression in Biomphalaria glabrata embryonic cells. *Parasitology,* 127**,** 533-42.

COUSTAU, C. & YOSHINO, T. P. (2000) Flukes without snails: advances in the in vitro cultivation of intramolluscan stages of trematodes. *Exp Parasitol,* 94**,** 62-6.

COWAN, C. R., CARLTON, P. M. & CANDE, W. Z. (2001) The polar arrangement of telomeres in interphase and meiosis. Rabl organization and the bouquet. *Plant Physiol,* 125**,** 532-8.

CREMER, M., KUPPER, K., WAGLER, B., WIZELMAN, L., VON HASE, J., WEILAND, Y., KREJA, L., DIEBOLD, J., SPEICHER, M. R. & CREMER, T. (2003) Inheritance of gene density-related higher order chromatin arrangements in normal and tumor cell nuclei. *J Cell Biol,* 162**,** 809-20.

CREMER, M., VON HASE, J., VOLM, T., BRERO, A., KRETH, G., WALTER, J., FISCHER, C., SOLOVEI, I., CREMER, C. & CREMER, T. (2001) Non-random radial higher-order chromatin arrangements in nuclei of diploid human cells. *Chromosome Res,* 9**,** 541-67.

CREMER, T., CREMER, M., DIETZEL, S., MULLER, S., SOLOVEI, I. & FAKAN, S. (2006) Chromosome territories--a functional nuclear landscape. *Curr Opin Cell Biol,* 18**,** 307-16.

CREMER, T., LICHTER, P., BORDEN, J., WARD, D. C. & MANUELIDIS, L. (1988) Detection of chromosome aberrations in metaphase and interphase tumor cells by

in situ hybridization using chromosome-specific library probes. *Hum Genet,* 80**,** 235-46.

CROFT, J. A., BRIDGER, J. M., BOYLE, S., PERRY, P., TEAGUE, P. & BICKMORE, W. A. (1999) Differences in the localization and morphology of chromosomes in the human nucleus. *J Cell Biol,* 145**,** 1119-31.

DEMARCO, R. & VERJOVSKI-ALMEIDA, S. (2009) Schistosomes--proteomics studies for potential novel vaccines and drug targets. *Drug Discov Today,* 14**,** 472-8.

DOENHOFF, M. J., KUSEL, J. R., COLES, G. C. & CIOLI, D. (2002) Resistance of Schistosoma mansoni to praziquantel: is there a problem? *Trans R Soc Trop Med Hyg,* 96**,** 465-9.

DONG, F. & JIANG, J. (1998) Non-Rabl patterns of centromere and telomere distribution in the interphase nuclei of plant cells. *Chromosome Res,* 6**,** 551-8.

EBRAHIMI, H. & DONALDSON, A. D. (2008) Release of yeast telomeres from the nuclear periphery is triggered by replication and maintained by suppression of Ku-mediated anchoring. *Genes Dev,* 22**,** 3363-74.

FEDERICO, C., SCAVO, C., CANTARELLA, C. D., MOTTA, S., SACCONE, S. & BERNARDI, G. (2006) Gene-rich and gene-poor chromosomal regions have different locations in the interphase nuclei of cold-blooded vertebrates. *Chromosoma,* 115**,** 123-8.

FERREIRA, J., PAOLELLA, G., RAMOS, C. & LAMOND, A. I. (1997) Spatial organization of large-scale chromatin domains in the nucleus: a magnified view of single chromosome territories. *J Cell Biol,* 139**,** 1597-610.

FINLAN, L. E., SPROUL, D., THOMSON, I., BOYLE, S., KERR, E., PERRY, P., YLSTRA, B., CHUBB, J. R. & BICKMORE, W. A. (2008) Recruitment to the nuclear periphery can alter expression of genes in human cells. *PLoS Genet,* 4**,** e1000039.

FITZPATRICK, J. M., HIRAI, Y., HIRAI, H. & HOFFMANN, K. F. (2007) Schistosome egg production is dependent upon the activities of two developmentally regulated tyrosinases. *Faseb J,* 21**,** 823-35.

FITZPATRICK, J. M. & HOFFMANN, K. F. (2006) Dioecious Schistosoma mansoni express divergent gene repertoires regulated by pairing. *Int J Parasitol,* 36**,** 1081-9.

FITZPATRICK, J. M., PROTASIO, A. V., MCARDLE, A. J., WILLIAMS, G. A., JOHNSTON, D. A. & HOFFMANN, K. F. (2008) Use of Genomic DNA as an Indirect Reference for Identifying Gender-Associated Transcripts in

Morphologically Identical, but Chromosomally Distinct, Schistosoma mansoni Cercariae. *PLoS Negl Trop Dis,* 2**,** e323.

FOSTER, H. A., ABEYDEERA, L. R., GRIFFIN, D. K. & BRIDGER, J. M. (2005) Non-random chromosome positioning in mammalian sperm nuclei, with migration of the sex chromosomes during late spermatogenesis. *J Cell Sci,* 118**,** 1811-20.

FOSTER, H. A. & BRIDGER, J. M. (2005) The genome and the nucleus: a marriage made by evolution. Genome organisation and nuclear architecture. *Chromosoma,* 114**,** 212-29.

FRAGA, M. F., BALLESTAR, E., VILLAR-GAREA, A., BOIX-CHORNET, M., ESPADA, J., SCHOTTA, G., BONALDI, T., HAYDON, C., ROPERO, S., PETRIE, K., IYER, N. G., PEREZ-ROSADO, A., CALVO, E., LOPEZ, J. A., CANO, A., CALASANZ, M. J., COLOMER, D., PIRIS, M. A., AHN, N., IMHOF, A., CALDAS, C., JENUWEIN, T. & ESTELLER, M. (2005) Loss of acetylation at Lys16 and trimethylation at Lys20 of histone H4 is a common hallmark of human cancer. *Nat Genet,* 37**,** 391-400.

FRIEDMAN, J. F., KANZARIA, H. K. & MCGARVEY, S. T. (2005) Human schistosomiasis and anemia: the relationship and potential mechanisms. *Trends Parasitol,* 21**,** 386-92.

FUKS, F. (2005) DNA methylation and histone modifications: teaming up to silence genes. *Curr Opin Genet Dev,* 15**,** 490-5.

GANEM, N. J., STORCHOVA, Z. & PELLMAN, D. (2007) Tetraploidy, aneuploidy and cancer. *Curr Opin Genet Dev,* 17**,** 157-62.

GAVIN, D. P., ROSEN, C., CHASE, K., GRAYSON, D. R., TUN, N. & SHARMA, R. P. (2009) Dimethylated lysine 9 of histone 3 is elevated in schizophrenia and exhibits a divergent response to histone deacetylase inhibitors in lymphocyte cultures. *J Psychiatry Neurosci,* 34**,** 232-7.

GHOSH, S. & GHOSH, I. (1975) Variation of stemline karyotype in a HeLa cell line. *Z Krebsforsch Klin Onkol Cancer Res Clin Oncol,* 84**,** 129-33.

GILCHRIST, S., GILBERT, N., PERRY, P. & BICKMORE, W. A. (2004) Nuclear organization of centromeric domains is not perturbed by inhibition of histone deacetylases. *Chromosome Res,* 12**,** 505-16.

GOLDMAN, M. A. & LOVERDE, P. T. (1983) Hybrid origin of polyploidy in freshwater snails of the genus Bulinus (Mollusca:Planorbidae). . *Evolution,* 37**,** 592-600.

GOLDMAN, M. A., LOVERDE, P. T. & CHRISMAN, C. L. (1980) Comparative karyology of the freshwater snails Bulinus tropicus and B. natalensis. *Can J Genet Cytol,* 22**,** 361-7.

GOLDMAN, M. A., LOVERDE, P. T., CHRISMAN, C. L. & FRANKLIN, D. A. (1984) Chromosomal evolution in planorbid snails of the genera bulinus and biomphalaria. *Malacologia,* 25**,** 427-446.

GOLDMAN, M. A., LOVERDE, P. T., CHRISMAN, C. L., FRANKLIN, D. A., MATTHEWS, F., PITCHFORD, R. J. & RICHARDS, C. S. (1983) Nucleolar organizer regions in Biomphalaria and Bulinus snails. *Experimentia,* 39**,** 911-913.

GOODALL, C. P., BENDER, R. C., BROOKS, J. K. & BAYNE, C. J. (2006) Biomphalaria glabrata cytosolic copper/zinc superoxide dismutase (SOD1) gene: association of SOD1 alleles with resistance/susceptibility to Schistosoma mansoni. *Mol Biochem Parasitol,* 147**,** 207-10.

GREGORY, T. R. (2003) Genome size estimates for two important freshwater molluscs, the zebra mussel (Dreissena polymorpha) and the schistosomiasis vector snail (Biomphalaria glabrata). *Genome,* 46**,** 841-4.

GRYSEELS, B., POLMAN, K., CLERINX, J. & KESTENS, L. (2006) Human schistosomiasis. *Lancet,* 368**,** 1106-18.

HABERMANN, F. A., CREMER, M., WALTER, J., KRETH, G., VON HASE, J., BAUER, K., WIENBERG, J., CREMER, C., CREMER, T. & SOLOVEI, I. (2001) Arrangements of macro- and microchromosomes in chicken cells. *Chromosome Res,* 9**,** 569-84.

HAGOS, E. G., GHALEB, A. M., DALTON, W. B., BIALKOWSKA, A. B. & YANG, V. W. (2009) Mouse embryonic fibroblasts null for the Kruppel-like factor 4 gene are genetically unstable. *Oncogene,* 28**,** 1197-205.

HAHN, U. K., BENDER, R. C. & BAYNE, C. J. (2001a) Involvement of nitric oxide in killing of Schistosoma mansoni sporocysts by hemocytes from resistant Biomphalaria glabrata. *J Parasitol,* 87**,** 778-85.

HAHN, U. K., BENDER, R. C. & BAYNE, C. J. (2001b) Killing of Schistosoma mansoni sporocysts by hemocytes from resistant Biomphalaria glabrata: role of reactive oxygen species. *J Parasitol,* 87**,** 292-9.

HAMTA, A., ADAMOVIC, T., SAMUELSON, E., HELOU, K., BEHBOUDI, A. & LEVAN, G. (2006) Chromosome ideograms of the laboratory rat (Rattus norvegicus) based on high-resolution banding, and anchoring of the cytogenetic

map to the DNA sequence by FISH in sample chromosomes. *Cytogenet Genome Res,* 115**,** 158-68.

HANSEN, E. L. (1976) A cell line from embryos of Biomphalaria glabrata (Pulmonata): Establishment and characteristics. *In Invertebrate Tissue Culture: Research Applications***,** 77-97.

HERTEL, L. A., ADEMA, C. M. & LOKER, E. S. (2005) Differential expression of FREP genes in two strains of Biomphalaria glabrata following exposure to the digenetic trematodes Schistosoma mansoni and Echinostoma paraensei. *Dev Comp Immunol,* 29**,** 295-303.

HEYNEMAN, D. (1976) Snail tissue culture: Current development and applications in parasitology, an introductory statementIn: Invertebrate tissue culture. *New York: Academic Press* 57–60.

HIRAYAMA, K. (2004) Immunogenetic analysis of post-schistosomal liver fibrosis. *Parasitol Int,* 53**,** 193-6.

HOCHSTRASSER, M. & SEDAT, J. W. (1987) Three-dimensional organization of Drosophila melanogaster interphase nuclei. II. Chromosome spatial organization and gene regulation. *J Cell Biol,* 104**,** 1471-83.

HUANG, H. S., MATEVOSSIAN, A., WHITTLE, C., KIM, S. Y., SCHUMACHER, A., BAKER, S. P. & AKBARIAN, S. (2007) Prefrontal dysfunction in schizophrenia involves mixed-lineage leukemia 1-regulated histone methylation at GABAergic gene promoters. *J Neurosci,* 27**,** 11254-62.

HUMPHRIES, J. E. & YOSHINO, T. P. (2003) Cellular receptors and signal transduction in molluscan haemocytes: connections with the innate immune system of invertebrates. *Integrative and comparative biology,* 43**,** 305-312.

HUMPHRIES, J. E. & YOSHINO, T. P. (2006) Schistosoma mansoni excretory-secretory products stimulate a p38 signalling pathway in Biomphalaria glabrata embryonic cells. *Int J Parasitol,* 36**,** 37-46.

IANNUZZI, L., DI MEO, G. P., PERUCATTI, A. & FERRARA, L. (1990) The high resolution G- and R-banding pattern in chromosomes of river buffalo (Bubalus bubalis L.). *Hereditas,* 112**,** 209-15.

ISNARD, A. & CHEVILLARD, C. (2008) Recent advances in the characterization of genetic factors involved in human susceptibility to infection by schistosomiasis. *Curr Genomics,* 9**,** 290-300.

ITTIPRASERT, W., NENE, R., MILLER, A., RAGHAVAN, N., LEWIS, F., HODGSON, J. & KNIGHT, M. (2009) Schistosoma mansoni infection of juvenile Biomphalaria glabrata induces a differential stress response between resistant and susceptible snails. *Exp Parasitol,* 123**,** 203-11.

IVANCHENKO, M. G., LERNER, J. P., MCCORMICK, R. S., TOUMADJE, A., ALLEN, B., FISCHER, K., HEDSTROM, O., HELMRICH, A., BARNES, D. W. & BAYNE, C. J. (1999) Continuous in vitro propagation and differentiation of cultures of the intramolluscan stages of the human parasite Schistosoma mansoni. *Proc Natl Acad Sci U S A,* 96**,** 4965-70.

JENUWEIN, T. & ALLIS, C. D. (2001) Translating the histone code. *Science,* 293**,** 1074-80.

JEZIORSKI, M. C. & GREENBERG, R. M. (2006) Voltage-gated calcium channel subunits from platyhelminths: potential role in praziquantel action. *Int J Parasitol,* 36**,** 625-32.

JIANG, Y., LOKER, E. S. & ZHANG, S. M. (2006) In vivo and in vitro knockdown of FREP2 gene expression in the snail Biomphalaria glabrata using RNA interference. *Dev Comp Immunol,* 30**,** 855-66.

JOHNSON, K., PFLUGH, D. L., YU, D., HESSLEIN, D. G., LIN, K. I., BOTHWELL, A. L., THOMAS-TIKHONENKO, A., SCHATZ, D. G. & CALAME, K. (2004) B cell-specific loss of histone 3 lysine 9 methylation in the V(H) locus depends on Pax5. *Nat Immunol,* 5**,** 853-61.

KALMAROVA, M., SMIRNOV, E., KOVACIK, L., POPOV, A. & RASKA, I. (2008) Positioning of the NOR-bearing chromosomes in relation to nucleoli in daughter cells after mitosis. *Physiol Res,* 57**,** 421-5.

KALMAROVA, M., SMIRNOV, E., MASATA, M., KOBERNA, K., LIGASOVA, A., POPOV, A. & RASKA, I. (2007) Positioning of NORs and NOR-bearing chromosomes in relation to nucleoli. *J Struct Biol,* 160**,** 49-56.

KAPLAN, M. H., WHITFIELD, J. R., BOROS, D. L. & GRUSBY, M. J. (1998) Th2 cells are required for the Schistosoma mansoni egg-induced granulomatous response. *J Immunol,* 160**,** 1850-6.

KILL, I. R., BRIDGER, J. M., CAMPBELL, K. H., MALDONADO-CODINA, G. & HUTCHISON, C. J. (1991) The timing of the formation and usage of replicase clusters in S-phase nuclei of human diploid fibroblasts. *J Cell Sci,* 100 (Pt 4)**,** 869-76.

KNIGHT, M., ADEMA, C. M., RAGHAVAN, N., LOKER, E. S., LEWIS, F. & TETTELIN, H. (2002) Obtaining the genome sequence of the mollusc Biomphalaria glabrata: a major intermediate host for the parasite causing human schistosomiasis. *Biomedical research institute (BRI)*.

KNIGHT, M., BRIDGER, J., ITTIPRASERT, W., ODOEMELAM, E., MASABANDA, J. S., MILLER, A. & RAGHAVAN, N. (2007) *Endogenous retrotransposon sequences of the Schistosoma mansoni intermediate snail host, Biomphalaria glabrata.*, Landes bioscience.

KNIGHT, M., ONGELE, E. & LEWIS, F. A. (2000) Molecular studies of Biomphalaria glabrata, an intermediate host of Schistosoma mansoni. *Int J Parasitol,* 30**,** 535-41.

KNIGHT, M., RAGHAVAN, N., GOODALL, C., COUSIN, C., ITTIPRASERT, W., SAYED, A., MILLER, A., WILLIAMS, D. L. & BAYNE, C. J. (2009) Biomphalaria glabrata peroxiredoxin: effect of schistosoma mansoni infection on differential gene regulation. *Mol Biochem Parasitol,* 167**,** 20-31.

KNUDSEN, G. M., MEDZIHRADSZKY, K. F., LIM, K. C., HANSELL, E. & MCKERROW, J. H. (2005) Proteomic analysis of Schistosoma mansoni cercarial secretions. *Mol Cell Proteomics,* 4**,** 1862-75.

KONDO, Y., SHEN, L., AHMED, S., BOUMBER, Y., SEKIDO, Y., HADDAD, B. R. & ISSA, J. P. (2008) Downregulation of histone H3 lysine 9 methyltransferase G9a induces centrosome disruption and chromosome instability in cancer cells. *PLoS One,* 3**,** e2037.

KOPS, G. J., WEAVER, B. A. & CLEVELAND, D. W. (2005) On the road to cancer: aneuploidy and the mitotic checkpoint. *Nat Rev Cancer,* 5**,** 773-85.

KOURMOULI, N., JEPPESEN, P., MAHADEVHAIAH, S., BURGOYNE, P., WU, R., GILBERT, D. M., BONGIORNI, S., PRANTERA, G., FANTI, L., PIMPINELLI, S., SHI, W., FUNDELE, R. & SINGH, P. B. (2004) Heterochromatin and tri-methylated lysine 20 of histone H4 in animals. *J Cell Sci,* 117**,** 2491-501.

KUKEKOVA, A. V., VOROBIEVA, N. V., BEKLEMISHEVA, V. R., JOHNSON, J. L., TEMNYKH, S. V., YUDKIN, D. V., TRUT, L. N., ANDRE, C., GALIBERT, F., AGUIRRE, G. D., ACLAND, G. M. & GRAPHODATSKY, A. S. (2009) Chromosomal mapping of canine-derived BAC clones to the red fox and American mink genomes. *J Hered,* 100 Suppl 1**,** S42-53.

KUMARAN, R. I., THAKAR, R. & SPECTOR, D. L. (2008) Chromatin dynamics and gene positioning. *Cell,* 132**,** 929-34.

LACHNER, M. & JENUWEIN, T. (2002) The many faces of histone lysine methylation. *Curr Opin Cell Biol,* 14**,** 286-98.

LAURSEN, J. R., DI LIU, H., WU, X. J. & YOSHINO, T. P. (1997) Heat-shock response in a molluscan cell line: characterization of the response and cloning of an inducible HSP70 cDNA. *J Invertebr Pathol,* 70**,** 226-33.

LAURSEN, J. R. & YOSHINO, T. P. (1999) Biomphalaria glabrata embryonic (Bge) cell line supports in vitro miracidial transformation and early larval development of the deer liver fluke, Fascioloides magna. *Parasitology,* 118 (Pt 2)**,** 187-94.

LEONARD, P. M., ADEMA, C. M., ZHANG, S. M. & LOKER, E. S. (2001) Structure of two FREP genes that combine IgSF and fibrinogen domains, with comments on diversity of the FREP gene family in the snail Biomphalaria glabrata. *Gene,* 269**,** 155-65.

LEVAN, A., FREDGA, K. & SANDBERG, A. A. (1964) Nomenclature for centromeric position on chromosomes. . *Hereditas,* 52**,** 201-220.

LEWIS, F. A., PATTERSON, C. N., KNIGHT, M. & RICHARDS, C. S. (2001) The relationship between Schistosoma mansoni and Biomphalaria glabrata: genetic and molecular approaches. *Parasitology,* 123 Suppl**,** S169-79.

LEWIS, F. A., STIREWALT, M. A., SOUZA, C. P. & GAZZINELLI, G. (1986) Large-scale laboratory maintenance of Schistosoma mansoni, with observations on three schistosome/snail host combinations. *J Parasitol,* 72**,** 813-29.

LICHTER, P., CREMER, T., BORDEN, J., MANUELIDIS, L. & WARD, D. C. (1988) Delineation of individual human chromosomes in metaphase and interphase cells by in situ suppression hybridization using recombinant DNA libraries. *Hum Genet,* 80**,** 224-34.

LOCKYER, A. E., SPINKS, J., NOBLE, L. R., ROLLINSON, D. & JONES, C. S. (2007) Identification of genes involved in interactions between Biomphalaria glabrata and Schistosoma mansoni by suppression subtractive hybridization. *Mol Biochem Parasitol,* 151**,** 18-27.

LOKER, E. S. & BAYNE, C. J. (2001) Molecular studies of the molluscan response to digenean infection. *Adv Exp Med Biol,* 484**,** 209-22.

LOVERDE, P. T., HIRAI, H., MERRICK, J. M., LEE, N. H. & EL-SAYED, N. (2004) Schistosoma mansoni genome project: an update. *Parasitol Int,* 53**,** 183-92.

LYSAK, M. A., FRANSZ, P. F., ALI, H. B. & SCHUBERT, I. (2001) Chromosome painting in Arabidopsis thaliana. *Plant J,* 28**,** 689-97.

MAHY, N. L., PERRY, P. E. & BICKMORE, W. A. (2002) Gene density and transcription influence the localization of chromatin outside of chromosome territories detectable by FISH. *J Cell Biol,* 159**,** 753-63.

MARIN, F., LUQUET, G., MARIE, B. & MEDAKOVIC, D. (2008) Molluscan shell proteins: primary structure, origin, and evolution. *Curr Top Dev Biol,* 80**,** 209-76.

MASABANDA, J. S., BURT, D. W., O'BRIEN, P. C., VIGNAL, A., FILLON, V., WALSH, P. S., COX, H., TEMPEST, H. G., SMITH, J., HABERMANN, F., SCHMID, M., MATSUDA, Y., FERGUSON-SMITH, M. A., CROOIJMANS, R. P., GROENEN, M. A. & GRIFFIN, D. K. (2004) Molecular cytogenetic definition of the chicken genome: the first complete avian karyotype. *Genetics,* 166**,** 1367-73.

MAYER, R., BRERO, A., VON HASE, J., SCHROEDER, T., CREMER, T. & DIETZEL, S. (2005) Common themes and cell type specific variations of higher order chromatin arrangements in the mouse. *BMC Cell Biol,* 6**,** 44.

MEABURN, K. J., CABUY, E., BONNE, G., LEVY, N., MORRIS, G. E., NOVELLI, G., KILL, I. R. & BRIDGER, J. M. (2007) Primary laminopathy fibroblasts display altered genome organization and apoptosis. *Aging Cell,* 6**,** 139-53.

MEABURN, K. J. & MISTELI, T. (2007) Cell biology: chromosome territories. *Nature,* 445**,** 379-781.

MEABURN, K. J. & MISTELI, T. (2008) Locus-specific and activity-independent gene repositioning during early tumorigenesis. *J Cell Biol,* 180**,** 39-50.

MEABURN, K. J., NEWBOLD, R. F. & BRIDGER, J. M. (2008) Positioning of human chromosomes in murine cell hybrids according to synteny. *Chromosoma,* 117**,** 579-91.

MELO, F. L., GOMES, A. L., BARBOSA, C. S., WERKHAUSER, R. P. & ABATH, F. G. (2006) Development of molecular approaches for the identification of transmission sites of schistosomiasis. *Trans R Soc Trop Med Hyg,* 100**,** 1049-55.

MERMOUD, J. E., POPOVA, B., PETERS, A. H., JENUWEIN, T. & BROCKDORFF, N. (2002) Histone H3 lysine 9 methylation occurs rapidly at the onset of random X chromosome inactivation. *Curr Biol,* 12**,** 247-51.

MILLER, A. N., OFORI, K., LEWIS, F. & KNIGHT, M. (1996) Schistosoma mansoni: use of a subtractive cloning strategy to search for RFLPs in parasite-resistant Biomphalaria glabrata. *Exp Parasitol,* 84**,** 420-8.

MILLER, A. N., RAGHAVAN, N., FITZGERALD, P. C., LEWIS, F. A. & KNIGHT, M. (2001) Differential gene expression in haemocytes of the snail Biomphalaria glabrata: effects of Schistosoma mansoni infection. *Int J Parasitol,* 31**,** 687-96.

MINCHELLA, D. J. & LOVERDE, P. T. (1983) Laboratory comparison of the relative success of Biomphalaria glabrata stocks which are susceptible and insusceptible to infection with Schistosoma mansoni. *Parasitology,* 86 (Pt 2)**,** 335-44.

MURTHY, S. K., MALHOTRA, A. K., JACOB, P. S., NAVEED, S., AL-ROWAISHED, E. E., MANI, S., PADARIYAKAM, S., PRAMATHAN, R., NATH, R., AL-ALI, M. T. & AL-GAZALI, L. (2008) Analphoid supernumerary marker chromosome characterized by aCGH and FISH as inv dup(3)(q25.33qter) de novo in a child with dysmorphic features and streaky pigmentation: case report. *Mol Cytogenet,* 1**,** 19.

NEUSSER, M., SCHUBEL, V., KOCH, A., CREMER, T. & MULLER, S. (2007) Evolutionarily conserved, cell type and species-specific higher order chromatin arrangements in interphase nuclei of primates. *Chromosoma,* 116**,** 307-20.

NEWTON, W. L. (1953) The inheritance of susceptibility to infection with schistosoma mansoni in *Australorbis glabratus*. *Experimental parasitology,* 2**,** 242-257.

NEWTON, W. L. (1954) Albinism in *Australorbis glabratus*. *Proceeding of the Helminthological Society of Washington,* 21**,** 72-74.

NEWTON, W. L. (1955) The establishment of a strain of Australorbis glabratus which combines albinism and high susceptibility to infection with Schistosoma mansoni. *J Parasitol,* 41**,** 526-8.

NIEMANN, G. M. & LEWIS, F. A. (1990) Schistosoma mansoni: influence of Biomphalaria glabrata size on susceptibility to infection and resultant cercarial production. *Exp Parasitol,* 70**,** 286-92.

O'KEEFE, R. T., HENDERSON, S. C. & SPECTOR, D. L. (1992) Dynamic organization of DNA replication in mammalian cell nuclei: spatially and temporally defined replication of chromosome-specific alpha-satellite DNA sequences. *J Cell Biol,* 116**,** 1095-110.

ODOEMELAM, E., RAGHAVAN, N., MILLER, A., BRIDGER, J. M. & KNIGHT, M. (2009) Revised karyotyping and gene mapping of the Biomphalaria glabrata embryonic (Bge) cell line. *Int J Parasitol,* 39**,** 675-81.

OGBADOYI, E., ERSFELD, K., ROBINSON, D., SHERWIN, T. & GULL, K. (2000) Architecture of the Trypanosoma brucei nucleus during interphase and mitosis. *Chromosoma,* 108**,** 501-13.

OGLE, B. M., CASCALHO, M. & PLATT, J. L. (2005) Biological implications of cell fusion. *Nat Rev Mol Cell Biol,* 6**,** 567-75.

OSBORNE, C. S., CHAKALOVA, L., BROWN, K. E., CARTER, D., HORTON, A., DEBRAND, E., GOYENECHEA, B., MITCHELL, J. A., LOPES, S., REIK, W. & FRASER, P. (2004) Active genes dynamically colocalize to shared sites of ongoing transcription. *Nat Genet,* 36**,** 1065-71.

OSBORNE, C. S., CHAKALOVA, L., MITCHELL, J. A., HORTON, A., WOOD, A. L., BOLLAND, D. J., CORCORAN, A. E. & FRASER, P. (2007) Myc dynamically and preferentially relocates to a transcription factory occupied by Igh. *PLoS Biol,* 5**,** e192.

PARADA, L. & MISTELI, T. (2002) Chromosome positioning in the interphase nucleus. *Trends Cell Biol,* 12**,** 425-32.

PARADA, L. A., SOTIRIOU, S. & MISTELI, T. (2004) Spatial genome organization. *Exp Cell Res,* 296**,** 64-70.

PASSAMANECK, Y. J., SCHANDER, C. & HALANYCH, K. M. (2004) Investigation of molluscan phylogeny using large-subunit and small-subunit nuclear rRNA sequences. *Mol Phylogenet Evol,* 32**,** 25-38.

PAYNE, C. & BRAUN, R. E. (2006) Histone lysine trimethylation exhibits a distinct perinuclear distribution in Plzf-expressing spermatogonia. *Dev Biol,* 293**,** 461-72.

PEARCE, E. J. & MACDONALD, A. S. (2002) The immunobiology of schistosomiasis. *Nat Rev Immunol,* 2**,** 499-511.

PEARCE, E. J. (2003) Progress towards a vaccine for schistosomiasis. *Acta Trop,* 86**,** 309-13.

PEARCE, E. J., C, M. K., SUN, J., J, J. T., MCKEE, A. S. & CERVI, L. (2004) Th2 response polarization during infection with the helminth parasite Schistosoma mansoni. *Immunol Rev,* 201**,** 117-26.

PERRY, P., SAUER, S., BILLON, N., RICHARDSON, W. D., SPIVAKOV, M., WARNES, G., LIVESEY, F. J., MERKENSCHLAGER, M., FISHER, A. G. & AZUARA, V. (2004) A dynamic switch in the replication timing of key regulator genes in embryonic stem cells upon neural induction. *Cell Cycle,* 3**,** 1645-50.

PETERS, A. H., MERMOUD, J. E., O'CARROLL, D., PAGANI, M., SCHWEIZER, D., BROCKDORFF, N. & JENUWEIN, T. (2002) Histone H3 lysine 9 methylation is an epigenetic imprint of facultative heterochromatin. *Nat Genet,* 30**,** 77-80.

POMBO, A. & BRANCO, M. R. (2007) Functional organisation of the genome during interphase. *Curr Opin Genet Dev,* 17**,** 451-5.

RABL, K. (1885) Uber Zelltheilung. *Gegenbaurs Morphol Jahrb,* 10**,** 214-330.

RAGHAVAN, N. & KNIGHT, M. (2006) The snail (Biomphalaria glabrata) genome project. *Trends Parasitol,* 22**,** 148-51.

RAGHAVAN, N., MILLER, A. N., GARDNER, M., FITZGERALD, P. C., KERLAVAGE, A. R., JOHNSTON, D. A., LEWIS, F. A. & KNIGHT, M. (2003) Comparative gene analysis of Biomphalaria glabrata hemocytes pre- and post-exposure to miracidia of Schistosoma mansoni. *Mol Biochem Parasitol,* 126**,** 181-91.

RAGHAVAN, N., TETTELIN, H., MILLER, A., HOSTETLER, J., TALLON, L. & KNIGHT, M. (2007) Nimbus (BgI): an active non-LTR retrotransposon of the Schistosoma mansoni snail host Biomphalaria glabrata. *Int J Parasitol,* 37**,** 1307-18.

RAGHUNATHAN, L. (1976) The karyotype of Biomphalaria glabrata, the snail vector of Schistosoma mansoni. *Malacologia,* 15**,** 447-50.

RAGOCZY, T., TELLING, A., SAWADO, T., GROUDINE, M. & KOSAK, S. T. (2003) A genetic analysis of chromosome territory looping: diverse roles for distal regulatory elements. *Chromosome Res,* 11**,** 513-25.

RAO, C. V., YAMADA, H. Y., YAO, Y. & DAI, W. (2009) Enhanced genomic instabilities caused by deregulated microtubule dynamics and chromosome segregation: a perspective from genetic studies in mice. *Carcinogenesis,* 30**,** 1469-74.

REDDY, K. L., ZULLO, J. M., BERTOLINO, E. & SINGH, H. (2008) Transcriptional repression mediated by repositioning of genes to the nuclear lamina. *Nature,* 452**,** 243-7.

REGHA, K., SLOANE, M. A., HUANG, R., PAULER, F. M., WARCZOK, K. E., MELIKANT, B., RADOLF, M., MARTENS, J. H., SCHOTTA, G., JENUWEIN, T. & BARLOW, D. P. (2007) Active and repressive chromatin are interspersed without spreading in an imprinted gene cluster in the mammalian genome. *Mol Cell,* 27**,** 353-66.

RENS, W., GRUTZNER, F., O'BRIEN P, C., FAIRCLOUGH, H., GRAVES, J. A. & FERGUSON-SMITH, M. A. (2004) Resolution and evolution of the duck-billed

platypus karyotype with an X1Y1X2Y2X3Y3X4Y4X5Y5 male sex chromosome constitution. *Proc Natl Acad Sci U S A,* 101**,** 16257-61.

RENS, W., O'BRIEN, P. C., GRAVES, J. A. & FERGUSON-SMITH, M. A. (2003) Localization of chromosome regions in potoroo nuclei (Potorous tridactylus Marsupialia: Potoroinae). *Chromosoma,* 112**,** 66-76.

RENS, W., O'BRIEN, P. C., GRUTZNER, F., CLARKE, O., GRAPHODATSKAYA, D., TSEND-AYUSH, E., TRIFONOV, V. A., SKELTON, H., WALLIS, M. C., JOHNSTON, S., VEYRUNES, F., GRAVES, J. A. & FERGUSON-SMITH, M. A. (2007) The multiple sex chromosomes of platypus and echidna are not completely identical and several share homology with the avian Z. *Genome Biol,* 8**,** R243.

RICE, J. C., BRIGGS, S. D., UEBERHEIDE, B., BARBER, C. M., SHABANOWITZ, J., HUNT, D. F., SHINKAI, Y. & ALLIS, C. D. (2003) Histone methyltransferases direct different degrees of methylation to define distinct chromatin domains. *Mol Cell,* 12**,** 1591-8.

RICHARDS, C. S. (1975) Variation in size of Biomphalaria glabrata at maturity. *The veliger,* 17**,** 393-395.

RICHARDS, C. S. (1980) Genetic studies on Amebocytic accumulation in *Biomphalaria glabrata*. *Journal of invertebrate pathology.,* 35.

RICHARDS, C. S. (1984) Influence of snail age on genetic variations in susceptibility of *Biomphalaria glabrata* for infection with *schistosoma mansoni.* . *Malacologia,* 25**,** 493-502.

RICHARDS, C. S. (1985) A new pigmentation mutant in *Biomphalaria glabrata*. *Malacologia,* 26**,** 145-151.

RICHARDS, C. S. & MERRITT, J. W., JR. (1972) Genetic factors in the susceptibility of juvenile Biomphalaria glabrata to Schistosoma mansoni infection. *Am J Trop Med Hyg,* 21**,** 425-34.

ROBERTS, L. S. & JANOVY, J. (2000) Foundations of parasitology. *McGraw-Hill Science, 6th ed.* .

ROESSLER, S., GYORY, I., IMHOF, S., SPIVAKOV, M., WILLIAMS, R. R., BUSSLINGER, M., FISHER, A. G. & GROSSCHEDL, R. (2007) Distinct promoters mediate the regulation of Ebf1 gene expression by interleukin-7 and Pax5. *Mol Cell Biol,* 27**,** 579-94.

ROONEY, D. E. (2001) Human cytogenetics constitutional analysis, 3rd ed. *Oxford University press.*

ROSS, A. G., VICKERS, D., OLDS, G. R., SHAH, S. M. & MCMANUS, D. P. (2007) Katayama syndrome. *Lancet Infect Dis,* 7**,** 218-24.

RUNNEGAR, B. & POJETA, J., JR. (1974) Molluscan Phylogeny: The Paleontological Viewpoint. *Science,* 186**,** 311-317.

SADONI, N., LANGER, S., FAUTH, C., BERNARDI, G., CREMER, T., TURNER, B. M. & ZINK, D. (1999) Nuclear organization of mammalian genomes. Polar chromosome territories build up functionally distinct higher order compartments. *J Cell Biol,* 146**,** 1211-26.

SAMBROOK, J. & RUSSEL, P. (2001) *Molecular cloning: A laboratory manual,* CSHL press.

SANO, Y., AKIMARU, H., OKAMURA, T., NAGAO, T., OKADA, M. & ISHII, S. (2005) Drosophila activating transcription factor-2 is involved in stress response via activation by p38, but not c-Jun NH(2)-terminal kinase. *Mol Biol Cell,* 16**,** 2934-46.

SANTOS-ROSA, H., SCHNEIDER, R., BANNISTER, A. J., SHERRIFF, J., BERNSTEIN, B. E., EMRE, N. C., SCHREIBER, S. L., MELLOR, J. & KOUZARIDES, T. (2002) Active genes are tri-methylated at K4 of histone H3. *Nature,* 419**,** 407-11.

SANTOS, A. P. & SHAW, P. (2004) Interphase chromosomes and the Rabl configuration: does genome size matter? *J Microsc,* 214**,** 201-6.

SARG, B., KOUTZAMANI, E., HELLIGER, W., RUNDQUIST, I. & LINDNER, H. H. (2002) Postsynthetic trimethylation of histone H4 at lysine 20 in mammalian tissues is associated with aging. *J Biol Chem,* 277**,** 39195-201.

SARMENTO, O. F., DIGILIO, L. C., WANG, Y., PERLIN, J., HERR, J. C., ALLIS, C. D. & COONROD, S. A. (2004) Dynamic alterations of specific histone modifications during early murine development. *J Cell Sci,* 117**,** 4449-59.

SAVIOLI, L., ALBONICO, M., ENGELS, D. & MONTRESOR, A. (2004) Progress in the prevention and control of schistosomiasis and soil-transmitted helminthiasis. *Parasitol Int,* 53**,** 103-13.

SCHOTTA, G., LACHNER, M., SARMA, K., EBERT, A., SENGUPTA, R., REUTER, G., REINBERG, D. & JENUWEIN, T. (2004) A silencing pathway to induce H3-K9 and H4-K20 trimethylation at constitutive heterochromatin. *Genes Dev,* 18**,** 1251-62.

SHI, J. & DAWE, R. K. (2006) Partitioning of the maize epigenome by the number of methyl groups on histone H3 lysines 9 and 27. *Genetics,* 173**,** 1571-83.

SHIZUYA, H., BIRREN, B., KIM, U. J., MANCINO, V., SLEPAK, T., TACHIIRI, Y. & SIMON, M. (1992) Cloning and stable maintenance of 300-kilobase-pair fragments of human DNA in Escherichia coli using an F-factor-based vector. *Proc Natl Acad Sci U S A,* 89**,** 8794-7.

SKALNIKOVA, M., BARTOVA, E., ULMAN, V., MATULA, P., SVOBODA, D., HARNICAROVA, A., KOZUBEK, M. & KOZUBEK, S. (2007) Distinct patterns of histone methylation and acetylation in human interphase nuclei. *Physiol Res,* 56**,** 797-806.

SKINNER, B. M., ROBERTSON, L. B., TEMPEST, H. G., LANGLEY, E. J., IOANNOU, D., FOWLER, K. E., CROOIJMANS, R. P., HALL, A. D., GRIFFIN, D. K. & VOLKER, M. (2009) Comparative genomics in chicken and Pekin duck using FISH mapping and microarray analysis. *BMC Genomics,* 10**,** 357.

SOLLER, J. T., BEUING, C., ESCOBAR, H. M., WINKLER, S., REIMANN-BERG, N., DRIESCHNER, N., DOLF, G., SCHELLING, C., NOLTE, I. & BULLERDIEK, J. (2008) Chromosomal assignment of canine THADA gene to CFA 10q25. *Mol Cytogenet,* 1**,** 11.

SOPPE, W. J., JASENCAKOVA, Z., HOUBEN, A., KAKUTANI, T., MEISTER, A., HUANG, M. S., JACOBSEN, S. E., SCHUBERT, I. & FRANSZ, P. F. (2002) DNA methylation controls histone H3 lysine 9 methylation and heterochromatin assembly in Arabidopsis. *Embo J,* 21**,** 6549-59.

SOUTOGLOU, E. & MISTELI, T. (2008) On the contribution of spatial genome organization to cancerous chromosome translocations. *J Natl Cancer Inst Monogr***,** 16-9.

STEINMANN, P., KEISER, J., BOS, R., TANNER, M. & UTZINGER, J. (2006) Schistosomiasis and water resources development: systematic review, meta-analysis, and estimates of people at risk. *Lancet Infect Dis,* 6**,** 411-25.

STRAHL, B. D. & ALLIS, C. D. (2000) The language of covalent histone modifications. *Nature,* 403**,** 41-5.

STRASAK, L., BARTOVA, E., HARNICAROVA, A., GALIOVA, G., KREJCI, J. & KOZUBEK, S. (2009) H3K9 acetylation and radial chromatin positioning. *J Cell Physiol,* 220**,** 91-101.

SUN, H. B., SHEN, J. & YOKOTA, H. (2000) Size-dependent positioning of human chromosomes in interphase nuclei. *Biophys J,* 79**,** 184-90.

SZCZERBAL, I., FOSTER, H. A. & BRIDGER, J. M. (2009) The spatial repositioning of adipogenesis genes is correlated with their expression status in a porcine mesenchymal stem cell adipogenesis model system. *Chromosoma*.

SZCZERBAL, I. & MICHALAK, E. (2003) FISH-localization of the nucleolar organizer region on the feline E1p12 chromosome. *Anim Genet,* 34**,** 386-7.

TADDEI, A., MAISON, C., ROCHE, D. & ALMOUZNI, G. (2001) Reversible disruption of pericentric heterochromatin and centromere function by inhibiting deacetylases. *Nat Cell Biol,* 3**,** 114-20.

TADDEI, A., ROCHE, D., BICKMORE, W. A. & ALMOUZNI, G. (2005) The effects of histone deacetylase inhibitors on heterochromatin: implications for anticancer therapy? *EMBO Rep,* 6**,** 520-4.

TAGUCHI, T., HIRAI, Y., LOVERDE, P. T., TOMINAGA, A. & HIRAI, H. (2007) DNA probes for identifying chromosomes 5, 6, and 7 of Schistosoma mansoni. *J Parasitol,* 93**,** 724-6.

TAKEUCHI, M., TAKEUCHI, K., OZAWA, Y., KOHARA, A. & MIZUSAWA, H. (2009) Aneuploidy in immortalized human mesenchymal stem cells with non-random loss of chromosome 13 in culture. *In Vitro Cell Dev Biol Anim,* 45**,** 290-9.

TANABE, H., MULLER, S., NEUSSER, M., VON HASE, J., CALCAGNO, E., CREMER, M., SOLOVEI, I., CREMER, C. & CREMER, T. (2002) Evolutionary conservation of chromosome territory arrangements in cell nuclei from higher primates. *Proc Natl Acad Sci U S A,* 99**,** 4424-9.

TELENIUS, H., CARTER, N. P., BEBB, C. E., NORDENSKJOLD, M., PONDER, B. A. & TUNNACLIFFE, A. (1992) Degenerate oligonucleotide-primed PCR: general amplification of target DNA by a single degenerate primer. *Genomics,* 13**,** 718-25.

THIRIOT-QUIEVREUX, C. (2003) Advances in chromosomal studies of gastropod molluscs. *Journal of molluscan studies,* 69**,** 187-201.

THOMPSON, M., HAEUSLER, R. A., GOOD, P. D. & ENGELKE, D. R. (2003) Nucleolar clustering of dispersed tRNA genes. *Science,* 302**,** 1399-401.

TRASK, B. J. (1991) Fluorescence in situ hybridization: applications in cytogenetics and gene mapping. *Trends Genet,* 7**,** 149-54.

TRIMBORN, M., BELL, S. M., FELIX, C., RASHID, Y., JAFRI, H., GRIFFITHS, P. D., NEUMANN, L. M., KREBS, A., REIS, A., SPERLING, K., NEITZEL, H. &

JACKSON, A. P. (2004) Mutations in microcephalin cause aberrant regulation of chromosome condensation. *Am J Hum Genet,* 75**,** 261-6.

TUTT, A., GABRIEL, A., BERTWISTLE, D., CONNOR, F., PATERSON, H., PEACOCK, J., ROSS, G. & ASHWORTH, A. (1999) Absence of Brca2 causes genome instability by chromosome breakage and loss associated with centrosome amplification. *Curr Biol,* 9**,** 1107-10.

UTZINGER, J., BERGQUIST, R., SHU-HUA, X., SINGER, B. H. & TANNER, M. (2003) Sustainable schistosomiasis control--the way forward. *Lancet,* 362**,** 1932-4.

VALENTIM, C. L., GOMES, M. S., JEREMIAS, W. J., CUNHA, J. C., OLIVEIRA, G. C., BOTELHO, A. C., PIMENTA, P. F., JANOTTI-PASSOS, L. K., GUERRA-SA, R. & BABA, E. H. (2008) Physical localization of the retrotransposons Boudicca and Perere 03 in Schistosoma mansoni. *J Parasitol,* 94**,** 993-5.

VANAGAITE, L., DAVIDOV, B., FRIEDMAN, J., YESHAYA, Y., MAGAL, N., DRASINOVER, V. & SHOHAT, M. (2006) Amniotic trisomy 11 mosaicism--is it a benign finding? *Prenatal diagnosis,* 26.

VENTER, J. C., ADAMS, M. D., MYERS, E. W., LI, P. W., MURAL, R. J., SUTTON, G. G., SMITH, H. O., YANDELL, M., EVANS, C. A., HOLT, R. A., GOCAYNE, J. D., AMANATIDES, P., BALLEW, R. M., HUSON, D. H., WORTMAN, J. R., ZHANG, Q., KODIRA, C. D., ZHENG, X. H., CHEN, L., SKUPSKI, M., SUBRAMANIAN, G., THOMAS, P. D., ZHANG, J., GABOR MIKLOS, G. L., NELSON, C., BRODER, S., CLARK, A. G., NADEAU, J., MCKUSICK, V. A., ZINDER, N., LEVINE, A. J., ROBERTS, R. J., SIMON, M., SLAYMAN, C., HUNKAPILLER, M., BOLANOS, R., DELCHER, A., DEW, I., FASULO, D., FLANIGAN, M., FLOREA, L., HALPERN, A., HANNENHALLI, S., KRAVITZ, S., LEVY, S., MOBARRY, C., REINERT, K., REMINGTON, K., ABU-THREIDEH, J., BEASLEY, E., BIDDICK, K., BONAZZI, V., BRANDON, R., CARGILL, M., CHANDRAMOULISWARAN, I., CHARLAB, R., CHATURVEDI, K., DENG, Z., DI FRANCESCO, V., DUNN, P., EILBECK, K., EVANGELISTA, C., GABRIELIAN, A. E., GAN, W., GE, W., GONG, F., GU, Z., GUAN, P., HEIMAN, T. J., HIGGINS, M. E., JI, R. R., KE, Z., KETCHUM, K. A., LAI, Z., LEI, Y., LI, Z., LI, J., LIANG, Y., LIN, X., LU, F., MERKULOV, G. V., MILSHINA, N., MOORE, H. M., NAIK, A. K., NARAYAN, V. A., NEELAM, B., NUSSKERN, D., RUSCH, D. B., SALZBERG, S., SHAO, W., SHUE, B., SUN, J., WANG, Z., WANG, A., WANG, X., WANG, J., WEI, M., WIDES, R.,

XIAO, C., YAN, C., et al. (2001) The sequence of the human genome. *Science,* 291**,** 1304-51.

VITTURI, R., LIBERTINI, A., SINEO, L., SPARACIO, I., LANNINO, A., GREGORINI, A. & COLOMBA, M. (2005) Cytogenetics of the land snails Cantareus aspersus and C. mazzullii (Mollusca: Gastropoda: Pulmonata). *Micron,* 36**,** 351-7.

VOLPI, E. V., CHEVRET, E., JONES, T., VATCHEVA, R., WILLIAMSON, J., BECK, S., CAMPBELL, R. D., GOLDSWORTHY, M., POWIS, S. H., RAGOUSSIS, J., TROWSDALE, J. & SHEER, D. (2000) Large-scale chromatin organization of the major histocompatibility complex and other regions of human chromosome 6 and its response to interferon in interphase nuclei. *J Cell Sci,* 113 (Pt 9)**,** 1565-76.

WANG, L., UTZINGER, J. & ZHOU, X. N. (2008) Schistosomiasis control: experiences and lessons from China. *Lancet,* 372**,** 1793-5.

WEAVER, Z., MONTAGNA, C., XU, X., HOWARD, T., GADINA, M., BRODIE, S. G., DENG, C. X. & RIED, T. (2002) Mammary tumors in mice conditionally mutant for Brca1 exhibit gross genomic instability and centrosome amplification yet display a recurring distribution of genomic imbalances that is similar to human breast cancer. *Oncogene,* 21**,** 5097-107.

WEN, B., WU, H., SHINKAI, Y., IRIZARRY, R. A. & FEINBERG, A. P. (2009) Large histone H3 lysine 9 dimethylated chromatin blocks distinguish differentiated from embryonic stem cells. *Nat Genet,* 41**,** 246-50.

WIENCKE, J. K., ZHENG, S., MORRISON, Z. & YEH, R. F. (2008) Differentially expressed genes are marked by histone 3 lysine 9 trimethylation in human cancer cells. *Oncogene,* 27**,** 2412-21.

WILLIAMS, R. R., AZUARA, V., PERRY, P., SAUER, S., DVORKINA, M., JORGENSEN, H., ROIX, J., MCQUEEN, P., MISTELI, T., MERKENSCHLAGER, M. & FISHER, A. G. (2006) Neural induction promotes large-scale chromatin reorganisation of the Mash1 locus. *J Cell Sci,* 119**,** 132-40.

YOSHINO, T. P., WU, X. J. & LIU, H. D. (1998) Transfection and heat-inducible expression of molluscan promoter-luciferase reporter gene constructs in the Biomphalaria glabrata embryonic snail cell line. *Am J Trop Med Hyg,* 59**,** 414-20.

ZINK, D., CREMER, T., SAFFRICH, R., FISCHER, R., TRENDELENBURG, M. F., ANSORGE, W. & STELZER, E. H. (1998) Structure and dynamics of human interphase chromosome territories in vivo. *Hum Genet,* 102**,** 241-51.

ZINNER, R., ALBIEZ, H., WALTER, J., PETERS, A. H., CREMER, T. & CREMER, M. (2006) Histone lysine methylation patterns in human cell types are arranged in distinct three-dimensional nuclear zones. *Histochem Cell Biol,* 125**,** 3-19.

Appendix

List of publications

- **Odoemelam, E,** Raghavan N, Ittiprasert W, Miller A, Bridger J, Knight M. (2010) FISH on chromosomes derived from the snail model organism *Biomphalaria glabrata*: Methods in molecular biology, chapter 29. Edited by E. Volpi and J M. Bridger, Humana press, New Jersey.

- **Odoemelam E**, Raghavan N, Miller A**,** Bridger J M and Knight, M. (2009) Revised karyotyping and gene mapping of the *Biomphalaria glabrata* embryonic (Bge) cell line. *Int J Parasitol,* 39, 675-81.

- Knight M, Bridger J M, Ittiprasert W, **Odoemelam E**, Masabanda J S, Miller A, and Raghavan N (2007) Endogenous retrotransposon sequences of the Schistosoma mansoni intermediate snail host, *Biomphalaria glabrata*, Landes bioscience.

Publications